FACULDADE DE CIÊNCIAS DA UNIVERSIDADE DO PORTO

BIOSENSORS FOR THE DETECTION AND QUANTIFICATION OF AQUATIC BACTERIAL CONTAMINATION IN WATERS FOR HUMAN USE

Raquel Barbosa Queirós

Departamento de Física e Astronomia da Faculdade de Ciências da Universidade do Porto

Porto 2013

This page was intentionally left blank

FACULDADE DE CIÊNCIAS DA UNIVERSIDADE DO PORTO

BIOSENSORS FOR THE DETECTION AND QUANTIFICATION OF AQUATIC BACTERIAL CONTAMINATION IN WATERS FOR HUMAN USE

Raquel Barbosa Queirós

Thesis submitted to Faculdade de Ciências da Universidade do Porto in partial fulfilment of the requirements for the degree of Doctor of Philosophy

This thesis was conducted under the supervision of
Professor Doctor Maria Goreti Ferreira Sales
Adjunct Professor in Chemical Engineering Department of Instituto Superior de Engenharia do Instituto Politécnico do Porto
and
Professor Doctor Paulo Vicente da Silva Marques
Assistant Professor in Physics and Astronomy Department of Faculdade de Ciências da Universidade do Porto

This page was intentionally left blank

Bolsa de investigação da Fundação para a Ciência e a Tecnologia com a referência SFRH/BD/49072/2008, financiada pelo POPH – QREN – Tipologia 4.1 – Formação Avançada, comparticipada pelo Fundo Social Europeu e por fundos nacionais do MCTES.

This page was intentionally left blank

To my deepest love, Miguel,

for his help, support and encouragement in every aspect of my life;

and

to my parents and sister Inês,

who raised me and trust me with their endless love.

This page was intentionally left blank

Acknowledgments

I would like to express the most sincere gratitude to my advisors Dr. Goreti Sales, Dr. João Paulo Noronha and Dr. Paulo Marques for giving me this opportunity to further my education and for the valuable lessons passed down over the last few years.

I would like to also extend my sincere thanks to Orlando Frazão, Pedro Jorge and Paulo Moreira for their support, technical discussions, and tips for the experimental work. I also thank Dr. Irineu Dias for his support and Prof. José Luís Santos for knowing when to give a word of encouragement at the right time.

A special thank goes to Susana Silva and Carlos Gouveia for all the knowledge shared regarding optical sensors, for all the help in experimental work, for the important discussions and for the help in the scientific writing.

To my colleagues and friends from UOSE, Joel Carvalho, Luís Coelho, Ricardo Silva, Jaime Viegas, Diana Viegas, Paulo Caldas, Hugo Martins, Kata Balogh and Ivo Nascimento for their many valuable discussions, support and mainly for your constant willingness and hilarious moments in coffee breaks.

A special thanks to Luísa Mendonça for being so kind, professional and helpful.

To Gerardo Aguilar for drafted the initial work plan. To Javier Cruz and Yonny Barcelay for the help and availability always demonstrated.

To all my coworkers of UOSE, thank you for helping me in one way or another.

To my colleagues from BioMark, Felismina Moreira, Sofia Almeida, Rafaela Guerreiro, Tânia Ribeiro, Liliana Truta and Gustavo Cabral for their support, help and for the fun moments shared.

I would like to acknowledge INESC TEC, BioMark, FCUP and ISEP for the facilities to support this work, without which this research would not be possible.

I would like to thank Dr. Noemí de-los-Santos-Álvarez for receiving me in GEUO (Grupo de Electroanálisis Universidad de Oviedo) and for all the knowledge shared in a new area of knowledge and to colleagues Eva, Elena, Goreti, Sonia and Daniel for all the help provided. I cannot forget Dr. Arturo Miranda-Ordieres for the valuable advises in electrochemical issues.

I would like to thank Dr. Janos Vörös from LBB (Laboratory of Biosensors and Bioelectronics, Institute for Biomedical Engineering, ETH Zurich) for receive me in LBB, for his accessibility, for providing all necessary resources for the implementation of my work but especially for guiding me in the right line of attack. To Kaori Sugihara for all the knowledge shared regarding OWLS system, for all the help in experimental work and for all the important discussion. And to all LBB members, Victoria, Sophie, Harald, Bernd, Pablo, Raphael G. and Raphael Z., Juliane, Alex L. and Alex T., Peter, Dario, Prayanka, Benjamin, Blandine, Chris, Leena, Rami, Gemma, Elsa, Jose, Norma, Mike, Tomaso, Esther and Bruno thanks for any help at lab work, for my integration into your group, and for the company and fun moments.

To my dearest friend, Paula Tafulo, for her restless help in my experimental work, assistance in technical writing and many valuable discussions that facilitated my research. For her encouragement, friendship and companion over the last 11 years in work but also in life.

To Pedro Serapicos for the unceasing encouragement, support and friendship and all the funny moments.

Finally, I would like to express my gratitude to all my friends and family that in many instances contributed with friendship, love, support and incentive for successfully complete this thesis.

"Most people say that is it is the intellect which makes a great scientist. They are wrong: it is character."

Albert Einstein

This page was intentionally left blank

Abstract

Water has long been considered of major importance to health and the well being of Humans. Water can however expose individuals to a variety of health hazards, through ingestion or direct contact with contaminated water. Water contamination may be of chemical or biological origin.

Cyanobacteria and *Escherichia coli* (*E. coli*) are water biological hazards of major concern. They produce toxins that may cause skin irritation, stomach cramps, vomiting, nausea, diarrhea, fever, urinary tract infections, respiratory illness and liver damage. The classic methods for detection and quantification of these bacteria are based on culture and counting methods, biochemical and immunologic assays, molecular based methods and separation techniques. These methods present some disadvantages being the most significant the cost of the required equipment and the long periods of analysis.

In order to prevent cyanobacteria and *E. coli* outbreaks and their subsequent effects in humans it is essential to have methods that are able to identify/quantify these pathogenic bacteria promptly. Therefore, the search for fast-screening methods for real-time and in situ control of bacteria is fundamental, accounting the need to develop low cost biosensor systems whith features of fast and sensitive detection.

This work reports systems that combine new biological elements of recognition for cyanobacteria and *E. coli* with physicochemical transduction units. The biological elements are of synthetic origin, made with non-biological materials or with nucleic acid oligostrutures. The transduction is of electrochemical (potentiometric or impedimetric) or optical (interferometric-based and fiber long period gratings-based) nature.

The biological elements of recognition for Microcystin-LR (MC-LR), a major toxin of Cyanobacteria, are designed by molecular imprintring (MI) techniques. The polymers were designed in sol-gel matrix or vinyl-based structures, having a carefully selected composition. The resulting sol-gel MI materials were coated on solid contact electrodes and optical fibres for potentiometric and interferometric monitoring, respectively. The vinyl-based molecularly-imprinted polymers (MIPs) were incorporated as ionophors in polyvinylchloride (PVC) selective membranes and then coated on solid contact electrodes for potentiometric transduction.

The biological recognition elements for *E. coli* are deoxyribonucleic acid (DNA) nucleotides; commonly know as aptamers (APTs). These elements carry a specific sequence to induce its interaction with the outer membrane proteins of *E. coli* (EcOMPs). The APTs are immobilized on gold electrodes and transduced by electrochemical impedance spectroscopy (EIS) or in optical fibres with inscribed long period gratings (LPGs) by means of evanescent field interaction.

In general, the reported devices introduce many technical innovations both in terms of assembly of recognition element and also in system configuration. Both APTs and MIPs are adequate synthetic recognition elements, providing a sensitive and selective recognition of the targeted analytes. Both, electrochemical and optical methods present advantages compared to previous conventional methods. They use low cost materials, are very simple to operate and require reduced operator intervention. Moreover, they provide a fast response and allow *in situ* monitoring. Thus, the proposed biosensors represent an advantageous alternative to standard methods currently used for the detection/quantification of Cyanobacteria and *E. coli* biological pathogens in water.

Key-words: Aptamers, Biosensor, *Escherichia coli*, Electrochemical Impedance Spectroscopy, Fabry-Perot, Long Period Gratings, Microcystin-LR, Molecular Imprinted Polymers, Potentiometry.

Resumo

A água tem sido considerada de grande importância para a saúde e bem-estar dos seres humanos. A água pode contudo expor os indivíduos a uma variedade de perigos para a saúde, quer através da sua ingestão quer pelo contato direto com água contaminada. A contaminação aquática pode ter origem química ou biológica.

As cianobactérias e a *E. coli* são patógenos de grande preocupação pois produzem toxinas que podem causar irritação na pele, dores de estômago, vómitos, náuseas, diarreia, febre, infeções do trato urinário, doenças respiratórias e danos graves ao nível do fígado. Os métodos clássicos para a deteção e quantificação destas bactérias são baseados em métodos de cultura e contagem, ensaios bioquímicos e imunológicos, métodos moleculares e em técnicas de separação. Estes métodos apresentam algumas desvantagens sendo as mais significativas o custo do equipamento necessário e os longos períodos de análise.

A fim de evitar surtos de cyanobactérias e *E. coli*, e os seus efeitos, é fundamental ter métodos capazes de identificar/quantificar estas bactérias patogénicas rapidamente. Por esse motivo, é necessária a procura de métodos rápidos de rastreio, que permitam a análise *in situ* e que proporcionem uma deteção rápida e sensível.

Este trabalho propõe dispositivos que combinam novos elementos de reconhecimento para cianobactérias e *E. coli* integrados em sistemas de transdução físico-quimica. O elemento biológico é de origem sintética, produzidos com materiais não biológicos, ou com oligo estruturas de ácidos nucleicos. A transdução é de natureza eléctrica (potenciométrica e impedimétrica) ou ótica (baseada em interferometrica e baseada em redes de período longo).

Os elementos de reconhecimento desenvolvidos para o reconhecimento da MC-LR, uma toxina produzida pelas cyanobactérias, foram concebidos através da técnica de impressão molecular. Estes polímeros foram produzidos em sol-gel ou em estruturas vinílicas, tendo uma constituição cuidadosamente selecionada. Os polímeros impressos em sol-gel foram depositados em electrodos de contacto sólido ou em fibras óticas para monitorização potenciométrica or interferométrica. Os polímeros impressos com estruturas de vinil foram incorporados, como iónoforos, em membranas selectivas de policloreto de vinil e depositadas em electrodos de contato sólido para monitorização potenciométrica.

Os elementos de reconhecimento biológico para a *E. coli* são nucleótidos de ácido desoxirribonucleico, usualmente conhecidos como aptámeros. Estes elementos têm uma sequência específica que induz a interacção com as proteínas da membrana externa da *E. coli*. Os aptámeros são imobilizados em eléctrodos de ouro ou em fibras ópticas com redes de período longo. A transdução do sinal é por espectroscopia de impedância electroquímica ou por interacção do campo evanescente.

No geral, os sistemas apresentados introduzem várias inovações quer em termos dos elementos de reconhecimento biológico quer em termos dos sistemas analíticos. Tanto os aptâmeros como os polímeros impressos são elementos de reconhecimento biológico adequados, fornecendo o reconhecimento sensível e selectivo dos anlitos. Os sistemas óticos e electroquímicos desenvolvidos apresentam vantagens quando comparados com os métodos convencionais. Utilizam materiais de baixo custo e são simples de operar, reduzindo a intervenção do operador. Além disso, proporcionam uma resposta rápida e permitem a monitorização *in situ*. Pode assim concluir-se que os biosensores propostos constituem uma alternativa viável aos métodos convencionais utilizados para a deteção/quantificação quer das cyanobactérias como da *E. coli* em águas.

Palavras-chave: Aptámeros, Biosensor, *Escherichia coli*, Espectroscopia de Impedância Electroquímica, Fabry-Perot, Redes de Período Longo, Microcistina-LR, Polímeros de Impressão Molecular, Potenciometria.

Table of Contents

List of Figures

List of Tables

List of Abbreviations

Ab	Antibody
Adda	3-Amino-9-methoxy-2,6,8-trimethyl-10-phenyldeca-4,6-dienoic acid
AFM	Atomic Force Microscopy
APHA	American Public Health Association
APT	Aptamer
APTES	(3-aminopropyl)triethoxysilane
APTMS	(3-aminopropyl)trimethoxysilane
AWWA	American Water Works Association
Borax	Sodium borate buffer
BPO	Benzoyl peroxide
BSA	Bovine serum albumin
CDC	Centers for Diseases Control and Prevention
C_{dl}	Double-layer capacitor
CE	Counter electrode
CFU	Colony forming unit
CNT	Carbon nanotubes
CPE	Capillary electrophoresis
CV	Cyclic voltammetry
DCE	Dichloroethylene
DMS	Dimethhyl sulfoxide
DNA	Deoxyribonucleic acid
DPDMS	Diphenyldimethoxysilane
DVB	Divinylbenzene

EC	European Commission
E. coli	*Escherichia coli*
EcOMP	*Escherichia coli* outer membrane protein
EDOT	3,4-ethylenedioxythiophene
EDS	Energy-dispersive X-ray spectroscopy
EDTA	Ethylenediamine tetraacetic acid
EEA	European Environmental Agency
EIA	Enzyme immunoassay
EIS	Electrochemical impedance spectroscopy
ELISA	Enzyme linked immunosorbent assay
Emf	Electromotive force
EPA	Environmental Protection Agency
EtOH	Ethanol
EU	European Union
FBG	Fibre Bragg Grating
FET	Field effect transistors
FFPI	Fibre Fabry-Perot interferometry
FRA	Frequency response analysis
FRET	Fluorescence Resonance Energy Transfer
FWHW	Full-width half-maximum
GUD	β-D-glucuronidase
HEPES	4-(2-hydroxyethyl)-1-piperazineethanesulfonic acid
HITM	Hospitality Institute of Technology and Management
HPA	Health Protection Agency
HPLC	High-performance liquid chromatography

IHP	Inner Helmholtz plane
ISE	Ion-selective electrode
ISG	Imprinted sol-gel
ISO	International Organization for Standardization
ITO	Indium tin oxide
IUPAC	International Union of Pure and Applied Chemistry
LC	Liquid chromatography
LOD	Limit of detection
LPG	Long period gratings
mAb	Monoclonal Ab
MCH	6-mercapto-1-hexanol
MC	Microcystin
MC-LR	Microcystin-LR
MC-RR	Microcystin-RR
MC-YR	Microcystin-YR
MeOH	Methanol
MI	Molecular imprinting
MI-CNT	Molecular imprinted carbon nanotubes
MIP	Molecularly-imprinted polymer
MPM	Matched-potential method
MPN	Most problable number
MS	Mass spectrometry
MUG	4-methylumbelliferone-β-D-glucuronide
MWCNT	Multi-walled carbon nanotubes
NI-CNT	Non-imprinted carbon nanotubes

NISG	Non-imprinted sol-gel
NMR	Nuclear magnetic resonance
OHP	Outer Helmholtz plane
ONPG	O-Nitrophenyl-β-D-galactopyranoside
oNPOE	O-Nitrophenyl octyl ether
OSA	Optical spectrum analyzer
pAb	Polyclonal Ab
PAH	Polyaromatic hydrocarbon
PBS	Phosphate buffered saline
PCR	Polymerase chain reaction
PDA	Photo díode array
PDMS	Poly(dimethyl siloxane)
PEG	Poly(ethylene glycol)
PIPES	Piperazine-*N,N'*-bis(2-ethanesulfonic acid)
PLL	Poly-L-lysine
PPI	Protein phosphatase inhibition
PP1	Protein phosphatase type 1
PP2A	Protein phosphatase type 2A
PVC	Polyvinyl chloride
QCM	Quartz crystal microbalance
RE	Reference electrode
R_{et}	Electron transfer resistor
RNA	Ribonucleic acid
R_s	Solution resistor
RT-PCR	Reverse transcriptase polymerase chain reaction

SAM	Self assembled monolayer
SELEX	Systematic evolution of ligands by exponential enrichment
SEM	Scanning electron microscopy
SH	Sensing head
SPE	Screen-printed electrode
SPR	Surface plasmon resonance
SRI	Surrouding refractive index
SWCNT	Single-walled carbon nanotubes
TCE	Trichloroethylene
TEOS	Tetraethoxysilane
THF	Tetrahydrofuran
THM	Trihalomethane
TKClPB	Potassium tetrakis(4-chlorophenyl)borate
TMVS	tris(2-methoxyethoxy)vinylsilane
TRIS	tris(hydroxymethyl)aminomethane
UV	Ultraviolet
VB	Vinylbenzene
VBate	vinylbenzoate
VBSate	sodium 4-vinylbenzenesulfonate
VBTMA	(vinylbenzyl)trimethylammonium chloride
WE	Working electrode
WHO	World Health Organization
Z_W	Warburg impedance

This page was intentionally left blank

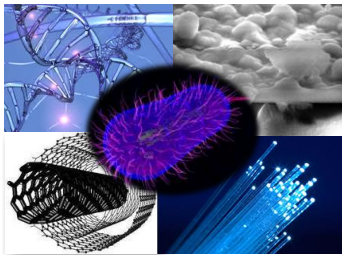

Chapter 1

Framework

1.1 Motivation

Freshwater is a finite resource and is essential for agriculture, industry and human subsistence. Freshwater of good quality is crucial for a sustainable socio-economic development (National Research Fund, 2005). Aquatic ecosystems are threatened on a world-wide scale by a variety of contaminants including a wide variety of chemicals, physical or sensory changes and pathogens.

The discharge of chemical contaminants (organic or inorganic) leads to disturbance of oxygen, enrichment of the water bodies with nutrients and algae growth with subsequent accelerated eutrophication. Great changes in physical (pH, temperature, electrical conductivity) and sensory (colour, smell, taste) water characteristics, must be controlled and regulated because they may have negative impacts on aquatic flora and fauna. Pathogens can produce waterborne diseases, illnesses caused by drinking water contaminated by human or animal faeces, which contain pathogenic microorganisms (Wolf, 2010). They can cause severe infectious diseases, allergic reactions and enteric illnesses.

WHO - World Health Organization states that every year more than 3.4 million people die as a result of water related diseases, making it the leading cause of disease and death around the world. Most of the victims are young children, the majority of whom die of illnesses caused by organisms that evolve in water sources contaminated by raw sewage.

“According to an assessment assigned by the United Nations, 4000 children die each day as a result of diseases caused by ingestion of unclean water.” Most cases of diarrheal illness are the result of poor hygiene and sanitation, including unsafe water, and are therefore preventable (WHO, 2009). Although major outbreaks of waterborne diseases still occur in developing countries when they occur in countries with highly developed water treatment processes a large population may be affected.

Bacteria such as *E. coli* and cyanobacteria are of major concern because of their potential for serious impact on human health. These pathogens produce toxins that may cause skin irritation, stomach cramps, vomiting, nausea, diarrhea, fever, blisters of the mouth, urinary tract infections, respiratory illness and liver damage (CDC - Centers for Diseases Control and Prevention, 2011; WHO, 1998). There are multiple routes for the transmission of such pathogens including direct ingestion of contaminated water or food, transmission through the faecal–oral or oral–oral route, through aerosols and also through dermal contact (Ford and Hamner, 2010).

The classic methods for detection and quantification of *E. coli* and cyanobacteria are based on the culture and counting methods, biochemical and immunologic assays, molecular based methods and separation techniques. These methods have several disadvantages such as the need of samples pre-treatment, animals use, highly qualified technicians to perform the analysis, expensive equipments and long periods of analysis. The normal period for result observations lies within 1 to 3 days and most of the times the answer comes too late to take effective measures. In order to prevent bacteria outbreaks, their spread and further complications, it is essential to be able to identify/quantify pathogenic bacteria quickly.

Therefore, large scientific efforts are being made to rapidly detect the presence of such bacteria in water. The search for fast-screening methods for real-time and *in situ* control has focused on the development of low cost sensor systems which provide a fast detection, selectivity and sensitivity, robustness, and the distinction between living and dead bacteria.

Biosensors, that combine a biological element of recognition with a physicochemical detector, can be employed for this purpose. They should offer high specificity and sensitivity, allowing the detection of a broad spectrum of analytes in simple or complex samples matrixes.

Their portability and low cost are other important features that enable the routine detection of pathogens anywhere and under any field condition.

Thus, the main goal of this research is to develop new biosensors that are capable to detect and quantify cyanobacteria and *E. coli* bacteria contamination in environmental waters at the limiting levels established by the competent institutions. The specific objectives are targeted for the detection/quantification of MC-LR, the most relevant Cyanobacteria toxin, and EcOMPs, proteins of the *E. co*li membrane, and include:

- Design and development of novel sensitive and selective biorecognition molecular elements*;*

    - ✓ Synthesis of new MIP for MC-LR by means of surface and bulk imprint, with vinyl-based or sol-gel matrixes;

- Integration of the recognition molecular elements into the biosensor devices;

    - ✓ Inclusion of surface imprinted materials for MC-LR in PVC selective membranes;
    - ✓ Application of these membranes on the transducer surface (solid contact electrodes);
    - ✓ Application of the bulk imprinted materials, made of sol-gel, on the transducer surface (solid contact electrodes and optical fibre);
    - ✓ Binding DNA APT for EcOMPs recognition on gold surface electrodes;
    - ✓ Binding DNA APT for EcOMPs detection/quantification on an optical fibre.

- Characterization of the biosensor devices by different transduction methods and their optimization;
    - ✓ Electrochemical evaluations by potentiometric and EIS methods;
    - ✓ Optical evaluations by interferometric-based and long-period gratings-based methods;

- Optimization of the most important parameters affecting the analytical response;
- Application of the biosensors displaying a suitable performance to spiked environmental waters.

1.2 Structure of the thesis

This thesis is organized in eight chapters.

Chapter 1 gives the motivation of the presented work, describes the structure and the framework of the thesis and lists the publications and communications associated with the PhD research program.

C**hapter 2** presents a brief literature review about the main components of biosensors, the target analytes, the recognition elements and the signal transducers, emphasizing those of special relevance to the present research work. It addresses for both targets, MC-LR and EcOMPs and the need of their control in environmental waters. Moreover, a general approach of the transducers used for target monitoring is also shown.

Chapters 3 to 7, present the development, characterization and application of optical and electrochemical biosensors selective to the targeted analytes, MC-LR and EcOMPs.

Chapter 3 reports new sensors for a direct determination of MC-LR in environmental waters, where the sensing layer consists of bulk imprinted sol-gel (ISG) materials. Sol–gel is a well-known process concerning the transition of a system from liquid ‘sol’ (the colloidal suspension of particles) into solid ‘gel’. After hydrolysation and condensation reactions an interconnected and porous material is obtained. When these reactions are carried out around a template, the resulting polymeric matrix is imprinted against this analyte and may respond selectively to this compound. The major parameters affecting the ISG bulk materials (water/alkoxide ratio, alcohol/alkoxide ratio, aging time, drying time and temperature) are studied and optimised.

ISG materials are futher applied directly onto solid-contact electrodes, with the resulting devices being optimized with regards to the effect of an ionic lipophilic additive, time of extraction of MC-LR from the sensitive layer and pH, in order to ensure suitable analytical features in the potentiometric transduction.

Moreover, different solid contact electrodes – carbon (C), titanium (Ti), aluminium (Al), copper (Cu), nickel/chromium (Ni/Cr) alloys - are tested to ascertain the best option in terms of conductivity and and electrical signal. Spiked solutions are tested with the most appropriate sensor.

This work is improved further in **Chapter 4** by employing a surface imprinting approach on nanosized materials of special electrical properties, the well known carbon nanotubes (CNTs). The use of surface imprinted polymers brings remarkable advantages such as the complete removal of templates, good accessibility to the target species, and low mass-transfer resistance. These advantageous features are due to the small dimension of the nanostructured imprinted materials with extremely high surface-to-volume ratio and also because template molecules are located at the surface of these materials. These new sensory materials for MC-LR were designed by with carefully selected monomers and introduced in a polymeric matrix and evaluated against potentiometric measurements. The stereochemical ability of the sensory material to detect MC-LR is checked by preparing blank materials where the imprinting stage is made without the template molecule. Selectivity of the sensors towards organic and inorganic compounds, cross-response to others microcystins (MCs) and analysis of spiked environmental water samples are tested. The sensors are further applied onto recycled chips, comprehending one site for the reference electrode and two sites for different selective membranes, in a biparametric approach for *in situ* analysis.

Potentiometry is a well-know analytical technique, simple and that allowing a fast response at a low cost. Still, there are some limitations deriving from possible unstability and potential drift resulting from small alterations affecting the outer surface of the selective membranes.

In **chapter 5** a new approach is studied to overcome these limitations. The optical fibre Fabry-Perot sensor presents a considerable potential for the measurement of physical parameters such as refractive index and is one of the preferred interferometric sensor configurations due to its versatility, simple configuration and fabrication, immunity to electromagnetic interference and low cost. These sensors also have high sensitivity, high resolution and enable multiplexing.

The Fabry–Perot sensing probe is based on an optical fibre tip coated with a thin film selective to MC-LR. Since the sol-gel is transparent in the wavelength region of interest, and compatible with an optical fibre and its interferometric measure, the selective membranes selected for this purpose are similar to those in chapter 3. These were applied at the end of the cleaved fibre by dip coating.

The Fabry–Perot interference is due to the Fresnel reflection at the distal end of the fibre probe and the other from the reflected light at the end of the sensitive membrane deposited in the fibre tip. Concentration dependence, stability, thermal-cross sensitivity and selectivity to other organic and inorganic compounds were tested for both ISG and non-imprinted sol-gel (NISG) materials. The sensors with best analytical features, appropriate for suitable interferometric transduction, were applied to environmental water samples.

Although MI has been applied, by large, to small organic molecules, only few sucessfull works report the development of MIPs for proteins. This is due to several technical difficulties associated to proteins, such as large numbers of competing binding sites in a flexible configuration; conformational sensitivity to temperature, pH, the nature of the solvent; and relatively large molecular sizes. For the successful application of MI technique in protein sensors, well-designed chemistry and extensive optimization procedures are essential. On the contrary, APTs are alternative materials to MIPs of well-established operation against proteins. Once the suitable nucleotide sequence ensuring its selective interaction with a target protein is identified, this oligonucleotide material may be efficiently immobilized on surfaces with high densities.

Chapter 6 describes the development of a rapid and sensitive DNA APT-based impedance biosensor for detection of EcOMPs. Two specific single stranded oligo-DNA sequences are tested as recognition elements and compared. The APT capture probes are immobilized, with or without an alkanethiol hydroxyl terminated on a gold electrode to study if the nonspecific effects are reduced with the application of a bilayer. Each step of the modification process was characterized by EIS. Silver/silver chloride (Ag/AgCl) and platinum are also present in the electrochemical system, acting as reference and counter electrodes. All these were used in conventional size. EIS results were obtained an electronic circuit based on the Randles theoretical model. This equivalent circuit includes the ohmic resistance of the electrolyte solution, R_s, the Warburg impedance, Z_W, resulting from the diffusion of the redox-probe, the double-layer capacitance, C_{dl}, and the electron-transfer resistance, R_{et}.

The self-assembly of the different monolayers during the integration of the recognition molecular elements onto the electrode surface increased R_{et} which resulted in a barrier for the interfacial electron transfer. Subsequently, the incubation of ECA with EcOMPs progressively increased R_{et} in the four modified surfaces tested.

The APT-based bioassay configuration adopted to transduce the bio-recognition event was of a single-site binding type, where the APTs bind to EcOMPs by a specific region of the proteins. The four modified sensor surfaces were tested against other water contaminants like MC-LR and the regeneration of the capture probes were also studied and compared. The developed biosensor was also applied to environmental water samples.

Chapter 7 describes the application of one capture probe tested in chapter 6 for the determination of EcOMPs in waters using a LPG as a refractometric platform for optical detection. Fiber optic refractometers are increasingly popular due to its versatility, relative ease of fabrication and high sensitivity of different evanescent wave configurations. Among the most popular fiber optic refractometric devices for label-free biosensing, LPGs preserves the physical integrity of the fiber and thus increases the robustness of the sensor to use and handling.

In this work a LPG was inscribed by arc-electric discharge in a single mode fibre optic to provide evanescent interaction with the fibre surrounding medium.

The APT used herein contains 36 nucleotides and was immobilized using two different methods of immobilization; electrostatic (using poly-L-lysine (PLL) as cationic polymer) and with covalent bonds (using an organofunctional alkoxysilane molecule). The functionalization of the bare LPG by these two different methods of immobilization originate two different sensing heads that are characterized by Scanning Electron Microscopy (SEM) and Atomic force Microscopy (AFM). The sensing heads are also tested against other water contaminants like MC-LR. The regeneration of these is possible (under low pH conditions) and applied to spiked environmental water samples.

Chapter 8 summarizes the main results obtained and presents guidelines for future research work.

1.3 List of Publications

1.3.1 Papers published in international scientific journals

Queirós, R.B.; de-los-Santos-Álvarez, N.; Noronha, J.P.; Marques, P.V.S.; Sales, M.G.F. (**2013)** A Rapid and Sensitive DNA Aptamer-based Impedance Biosensor for the Detection of *E. coli* OMPs. Sensors and Actuators B, in press. DOI: 10.1016/j.snb.2013.01.062

Queirós, R.B.; Noronha, J.P.; Marques, P.V.S.; Sales; M.G.F. (**2012)** Recycling old screen-printed electrodes with newly designed plastic antibodies on the wall of carbon nanotubes as sensory element for in-situ detection of bacterial toxins in water. Sensors and Actuators B, in press. DOI: 10.1016/j.snb.2012.11.112

Queirós, R.B.; Noronha, J.P.; Marques, P.V.S.; Fernandes, J.S.; Sales; M.G.F. (**2012)** Determination of Microcystin-LR in waters in the subnanomolar range by sol-gel imprinted polymers on solid contact electrodes. *Analyst 137*, 2437-2444. DOI: 10.1039/c2an35141b

Queirós, R.B.; Silva, S.; Noronha, J.P.; Frazão, O.; Jorge, P.; Aguilar, G.; Marques, P.; Sales, M.G.F. (**2011)** Microcystin-LR detection in water by the Fabry-Perot interferometer using an optical fibre coated with a sol-gel imprinted sensing membrane. *Biosensors and Bioelectronics 26*, 3932–3937. DOI: 10.1016/j.bios.2011.03.015

Queirós, R.B.; Noronha, J.P.; Sales, M.G.; Aguilar, G. (**2010)** Sensors for the Detection and Quantification of Bacterial Contamination in Water for Human Use. *Advanced Engineering Materials 12*(5), 175-178. DOI: 10.1002/adem.200980029

1.3.2 Book chapters published in international scientific books

Queirós, R.B.; Noronha, J.P.; Marques, P.V.S.; Sales, M.G.F. (**2012)** Emerging (bio)sensing Technology for Assessing and Monitoring Freshwater Contamination – Methods and Applications, in: Ecological Water Quality – Water Treatment and Reuse, InTech, Croatia. ISBN: 978-953-51-0508-4. DOI: 10.5772/32198

1.3.3 Conference Proceedings

Queirós, R.B.; Noronha, J.P.; Marques, P.V.S.; Sales, M.G.F. (**2012**) Label-free Detection of Microcystin-LR in Waters Using Real-Time Potentiometric Biosensors Based on Single-Walled Carbon Nanotubes Imprinted Polymers. Procedia Engineering 47, 758–761. DOI: 10.1016/j.proeng.2012.09.258.

Queirós, R.B.; Silva, S.O.; Sales, M.G.F.; Noronha, J.P.; Frazão, O.; Jorge, P.; Aguilar, G. (**2010**) Optical Cavity Fibre Sensor for Detection of Microcystin-LR in Water. *Proc. SPIE 7653*, ISSN 76531N. DOI:10.1117/12.865004

1.3.4 Communications presented in national and international scientific conferences

Queirós, R.B., Marques, P.V.S.; Noronha, J.P.; Sales, M.G.F. Label-Free Detection of Microcystin-LR in Waters Using Real-Time Potentiometric Biosensors Based on Single-Walled Carbon Nanotubes Imprinted Polymers, EUROSENSORS 2012, **2012**, Kraków, Poland (poster).

Queirós, R.B.; Noronha, J.P.; Marques, P.V.S.; Álvarez, N. de-los-Santos; Miranda-Ordieres, A.J.; Sales, M.G.F. Characterization of a DNA aptamer-based for *E. coli* OMPs detection in environmental water, MAP-fis PhD Research Conference, **2012**, Braga, Portugal (poster).

Queirós, R.B.; Marques, P.V.S.; Noronha, J.P.; Alvarez, N. de-los-Santos; Miranda-Ordieres, A.J.; Sales, M.G.F. Analytical Performance of a DNA Aptamer-based for *E. coli* Detection in Water, 2nd International Conference on Bio-Sensing Technology 2011, **2011**, Amsterdam, The Netherlands (poster).

Queirós, R.B.; Silva, S.O.; Sales, M.G.F.; Noronha, J.P.; Frazão, O.; Jorge, P.; Aguilar, G. Optical Cavity Fibre Sensor for Detection of Microcystin-LR in Water, EWOFS 2010 - Fourth European Workshop on Optical Fibre Sensors 2010, **2010**, Porto, Portugal (poster).

Queirós, R.B.; Silva, S.O.; Frazão, O.; Noronha, J.P.; Marques, P.V.S.; Sales, M.G.F. Sensor em Fibra Óptica para Detecção de Microcystin-LR, Física 2010, **2010**, Vila Real, Portugal (oral presentation).

Queirós, R.B.; Oliveira Silva, S.; Frazão, O.; Noronha, J.P.; Marques, P.V.S.; Sales, M.G.F. Fibre Optic Fabry-Perot Biosensor for detection of Microcystin-LR, SEON 2010 - Symposium on Enabling Optical Networks and Sensors 2010, **2010**, Porto, Portugal (poster).

Queirós, R.B.; Noronha, J.P.; Sales, M.G.F.; Aguilar, G. (Bio)Sensors for detection/quantification of aquatic bacterial contamination in waters for Human use, NN09 - 6th International Conference on Nanoscience and Nanotechnology 2009, **2009**, Thessaloniki, Greece (oral presentation).

Queirós, R.B.; Sales, M.G.F.; Noronha, J.P.; Aguilar, G. Supramolecular theoretical models for designing cyanotoxins sensors, CIC 2009 - I Congresso Ibérico de Cianotoxinas 2009, **2009**, Porto, Portugal (oral presentation).

Queirós, R.B.; Sales, M.G.F.; Noronha, J.P.; Aguilar, G. Sensors for detecting/quantifying cyanotoxins in water for human use, CIC 2009 - I Congresso Ibérico de Cianotoxinas 2009, **2009**, Porto, Portugal (poster).

References

Centers for Diseases Control and Prevention, National Center for Emerging and Zoonotic Infectious Diseases, Division of Foodborne, Waterborne, and Environmental Diseases. http://www.cdc.gov/ecoli/, accessed August 15th 2012.

Ford, T.; Hamner, S. 2010. Control of waterborne disease in developing countries, in: Mitchell, R.; Gu, J.-D. (Eds.). Environmental Microbiology. John Wiley & Sons Inc., 2nd ed., pp. 33-55.

National Research Fund. 2005. Sustainable management of water resources – report, Luxembourg, pp. 4-9.

World Health Organization. 1998. Drinking-water quality guidelines for parameters of concern in agricultural drainage water - Annex 3, Technical Report, Geneva, pp. 281–289.

World Health Organization. 2009. Vision 2030: The resilience of water supply and sanitation in the face of climate change. World Health Organization, Geneva, pp. 4-8.

Wolf, C. 2010. Structured Antibody Surfaces for Bio-Recognition and a Label-free Detection of Bacteria. PhD Thesis. Biology Department, University Johannes Gutenberg of Mainz, Germany.

This page was intentionally left blank

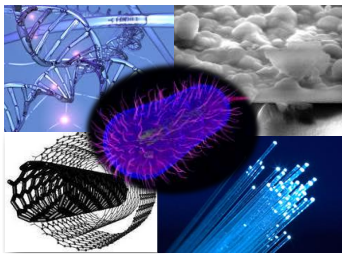

Chapter 2

Literature Review

2.1 Introduction

Water is life and its preservation is not only a moral obligation but also a legal requirement. By 2030, global demands will exceed more than 40 % the existing resources and more than a third of the world's population will have to deal with water shortages (EEA - European Environmental Agency, 2010). Climate change effects on water resources will not help. Efforts are being made throughout Europe towards a reduced and efficient water use and prevention of any further deterioration of the quality of water (Eurostat, EC - European Commission, 2010). The Water Framework Directive (EC, 2000) lays down provisions for monitoring, assessing and classifying water quality. Supporting this, drinking water sets standards for 48 microbiological and chemical parameters that must be monitored and tested regularly (EC, 1998). The Bathing Water Directive also sets concentration limits for microbiological pollutants in inland and coastal bathing waters (EC, 2006) and addresses risks from algae and cyanobacteria contamination and also risks from faecal contamination, requiring immediate action, including the provision of information to the public, to prevent exposure. With these directives, among others, the EU - European Union expects to offer its citizens, by 2015, fresh and coastal waters of good quality.

Freshwater quality is generally monitored with regard to chemical and microbiological parameters. Most regulated chemical parameters are monitored by more or less expensive but reliable techniques and some of which allow on-site analysis.

The ease of access to such analytical procedures is reflected on the large amount of chemical data given by the Water Information System for Europe (EEA, 2011). Microbial parametric data are, on the contrary, more difficult to obtain. Microorganisms may be defined as those organisms that are not readily visible to the naked eye. These have a size range (maximum linear dimension) up to 200 mm, and vary from viruses, through bacteria and archea, to micro-algae, fungi and protozoa (Sigee, 2005).

There are many different microorganisms that can pose serious risks to the environment and public health. In general, waterborne pathogens cause 10–20 million deaths and 200 million non-fatal infections each year (Leonard et al., 2003). They contribute to harmful effects: through the direct contact with the pathogen or by their metabolites like the toxic products excreted to water bodies. Some of these contaminants of microbiological origin are subject to limiting values in waters.

Legal requirements indicate culture-based methods to monitor cell activity or highly sophisticated and expensive instrumental-based methods for metabolite detection/quantification. In general, these methods are cumbersome and take too long to produce the desired response; within that time the contamination can move/spread out, while users of recreational waters and possible consumers are at risk of contracting serious infections. Regardless their sensitivity and selectivity, these methods also are unsuitable for routine and on-site applications (An and Carmichael, 1994; HPA - Health Protection Agency, 2005; ISO - International Organization for Standardization, 2005).

Novel technologies for assessing and monitoring microbial water contamination are now becoming available. Biosensors are of main interest in this context (Figure 2.1). They bear a capture-probe (or biorecognition element) on a standard transduction surface allowing on-site inexpensive determination. The biorecognition element (enzymes, cofactors, cells, antibodies, nucleic acids, or structured polymers) interacts with the target analyte, producing a physical-chemical change that is converted by the transducer into a detectable signal. This signal can be measured optically, mechanically, magnetically, thermally or electrically (Nayak et al., 2009; Su et al., 2011; Turner and Piletsky, 2005; Vo-Dinh, 2007).

Optical or radiant transducers can be classified according to mode or scattering. Classification by mode includes absorption, intensity, emission or combination thereof, including - absorbance or transmission in ultra-violet (UV), visible), or infra-red region of the spectrum, attenuated total reflectance, evanescent field, surface plasmon resonance (SPR), luminescence, and photoemission. Classification by scattering consists on phase change, polarization, absorption and opto-thermal effect, namely - Raman, ellipsometry, SPR and photo-acoustic effect. Mechanical transducers are often called frequency transducers and include surface acoustic wave, piezoelectric oscillators, and quartz crystal microbalance (QCM). Magnetic transducers are nuclear magnetic resonance (NMR) and mass spectrometry (MS) detection systems. Thermal transducers include calorimetric systems. Electrical transducers can be called electrochemical transducers when the electrical measure is evaluated in a solution. The classification of electrical transducers by mode can include voltage (potentiometric) or current transducers (amperometric), current-voltage transducers (voltammetric, field effect transistors (FET), metal oxide semiconductor, charge transfer and resistance transducers (coulometric, chemiresistors, ion mobility, and mass spectrometry) and dielectricity transducers (capacity systems) (Spichiger-Keller, 1998).

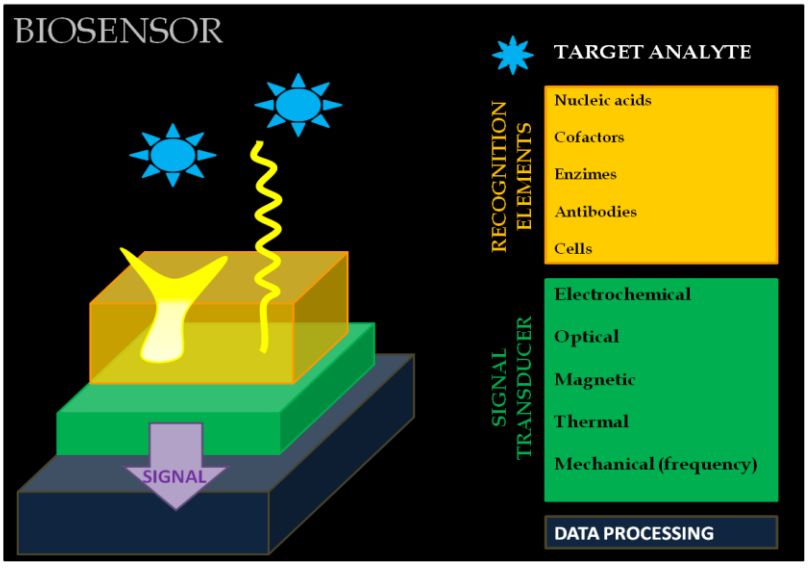

Figure 2.1 – General structure of a biosensor, with regard to recognition elements and signal transducers.

Biosensors must meet essential requirements for a successful application. First, the output signal must be of relevance. The biosensor must be accurate and sensitive, providing zero “false negatives” and few “false positives” and should be reproducible. Moreover the biosensor must be specific, discriminate between the target and other organisms. The response time of the biosensor must be inferior to the analytical reference methods, ideally provide a “real-time” response. Also, it must be physically robust and be insensitive to temperature, pH, and ionic strength changes as well as be indifferent to other environmental interferences. The assay should require minimal operator skills for routine detection. One of the most important criteria is the cost of manufacture, running and life cost. Finally, the biosensing assay must be accurate against standard techniques (Leonard et al. 2003).

Biosensors have been applied by now to the most important forms of microbial contamination. This chapter reviews emerging biosensing technology, methods and applications for assessing and monitoring bacterial water contamination.

It focuses the development of cost-effective on-site methods, based on biosensing devices that show the potential to complement both laboratory-based and field analytical methods.

The chapter is structured according to the biosensor components developed. Firstly, some considerations about the target analytes, cyanotoxin MC-LR and *E. coli*, are given. Secondly, the recognition elements used (MIPs and APTs) in the biosensing systems considered are described and compared. Next, the type of transducers and the measurement methods and techniques applied are presented and described. Finally, some recent emerging technologies development and published in literature for assessing and monitoring freshwater bacterial contamination are presented.

2.2 Target Analytes

2.2.1 Microcystin-LR

Every summer waters from rivers, fluvial beaches and other water sources for human use suffer from bacterial and algae contamination. Cyanobacteria, also known as blue-green algae, are very common in this context. Cyanobacteria are prokaryotes and photosynthetic. Their dominant nutritional mode is autotrophic - requiring water, carbon dioxide, inorganic substances and light (Msagati et al., 2006). Some species can also grow in the dark, in presence of some organic substrates (facultative heterotrophic) and others under anaerobic conditions, using sulphite as electron donor for photosynthesis. Some species of Cyanobacteria are also capable of capturing atmospheric nitrogen presenting the simplest nutritional form of all microorganisms (Msagati et al., 2006; Panosso et al., 2007).

Cyanobacteria exhibit a variety of shapes and arrangements, from unicellular cocci to bacilli and also filamentous and multicellular ramified filamentous. They don't have flagella but have sliding motion and can migrate through damp surfaces. Although each individual entity has microscopic dimensions, with cells ranging from 1 to100 µm, their occurance in water beacmes many times visible because their form scums, Figure 2.2, (Lorenzi, 2004).

Figure 2.2 – Microcystins blooms (Center of excellence for great lakes and Human health, 2011; Earth Project Management, 2012; Patau, 2008).

Cyanobacteria are able to grow in different conditions/mediums. They can be found in fresh, brackish or marine waters, also some species can survive in extreme environmental conditions, such as desert rocks, hotsprings and in some Arctic and Antarctic lakes (Mohamed, 2008). The presence of Cyanobacteria has been observed in salt or freshwaters, as free-living organisms or in association with others, and in terrestrial habitats, growing over rocks and soils, while playing an important role on ecosystem functional processes and on the nutrients recycling. Freshwaters are the most favourable for Cyanobacteria growth because most of Cyanobacteria species prefers neutral-alkaline waters (pH 6-9), temperature around 25 ºC, and high concentration of nutrients, specially nitrogen and phosphorus, (Lorenzi, 2004; Panosso et al., 2007; WHO, 1998).

Several species of Cyanobacteria produce toxins, which are classified, according to their mode of action into hepatotoxins, neurotoxins, skin irritants or other. Both hepatotoxins and neurotoxins are produced by Cyanobacteria commonly found in surface water and therefore are of relevance to water supplies (Carmichael, 1992; WHO, 1998, 1999). The hepatotoxins are produced by various species within the genera *Microcystis, Anabaena, Oscillatoria, Nodularia, Nostoc and Cylindrospermopsis*. Most hepatoxins belong to the chemical family of MCs. So far, more than 50 different MCs have been isolated and characterized (Sivonen and Jones, 1999) and among them, MC-LR is the most widespread hepatotoxic toxin (Chianella et al., 2003).

The chemical structure of MCs includes two variable amino acids and an unusual aromatic amino acid, 3-amino-9-methoxy-2,6,8-trimethyl-10-phenyldeca-4,6-dienoic acid (Adda), containing a substituted phenyldecadienoic acid (Botes et al., 1985; WHO, 1999). MC-LR is the first MC chemically identified being associated to most of the incidents of toxicity involving MCs in several countries (Fawell et al., 1993). MC-LR is a cyclic heptapeptide, Figure 2.3, consisting of two variable L-amino acids (leucine, X, and arginine, Y,), three D-amino acids (alanine, methylaspartic acid and glutamic acid) and two unusual amino acids (Adda and N-methyldehydroalanine) (Botes et al., 1985; Lindner et al., 2004).

The presence of MCs in water bodies has led to fatalities in wild and domestic animals worldwide, being also associated with episodes of human illness. Human beings are most likely to be exposed to MCs through consumption of contaminated drinking water or recreational activities such as swimming (Kuiper-Goodman et al., 1999).

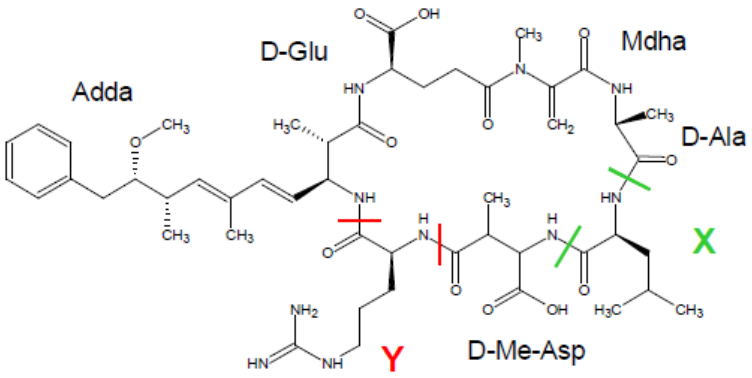

Figure 2.3 – Cyclic peptide structure of microcystin-LR; X: leucine; Y: arginine; D-ala: alanine; D-Me-Asp: methylaspartic acid; D-glu: glutamic acid; Adda: 3-amino-9-methoxy-2,6,8-trimethyl-10-phenyldeca-4,6-dienoic acid; Mdha: N-methyldehydroalanine (Dahlmann and Luckas, 2010).

The toxicity of MCs is associated with the inhibition of serine and threonine protein phosphatase 1 (PP1) and 2A (PP2A) responsible for the dephosphorylation of intracellular phosphoproteins. The acute effects of such inhibition leads to hepatocyte necrosis and hemorrhage (MacKintosh et al., 1990; Msagati et al., 2006).

Long exposure to low concentrations of MCs in drinking water can also cause chronic effects in mammals, due to their potent tumor promoting activity. Indeed, increased rates of primary liver cancer in some areas of China have been attributed to the contamination of drinking water with MCs (Falconer, 2001; Kuiper-Goodman et al., 1999; Yu, 1995). Documented incidences of animal and human fatalities caused by MCs have led WHO to introduce guideline values for MC-LR in drinking water, with a recommended limit of 1 µg L^{-1} (WHO, 1998).

2.2.1.1 Standard analytical methods for microcystin-LR detection

Amongst the wide range of standard techniques that may be employed for the determination of MCs in water, there is a requirement for sensitive, rapid, robust, reliable and non-expensive methods capable of detecting low concentrations of these toxins in a wide range of sample matrixes. Given these criteria, all methods reported so far have many limitations.

The standard methods for MCs detection can be divided into biological and biochemical methods and in physico-chemical methods. Table 2.1 summarizes and compares the existing analytical methods for the detection of MCs. Currently, the most suitable technique to detect and quantify MC-LR is the instrumental technique of high performance liquid chromatography (HPLC) with MS detection.

The mousse bioassays are used to determine the presence of hepatoxins in samples (Kuiper-Goodman et al., 1999). But these assays lack of sensitivity and specificity, and the use of animals to test toxins is not well accepted by the general public (Kuiper-Goodman et al., 1999; McElhiney and Lawson, 2005; Nicholson and Burch, 2001).

Protein phosphatase inhibition (PPI) assay is determined using ^{32}P radiolabelled substrates. This isotope has a short half-life (approximately 14 days), which requires the labelled proteins for the assay to be prepared on a regular basis. Another limitation is that the proteins require sophisticated procedures for their preparation. Furthermore, they use radioactive adenosine-5'-triphosphate and commercial enzymes in their preparation, most of which are expensive. In addition, many routine laboratories are not set-up to carry out radioactive determinations.

HPLC is a widely used method for the analysis of MCs. The good separation of the several MC variants in the same sample is largely dependent of the composition of mobile, and the stationary phases. MCs can be separated using both gradient and isocratic elutions. Most MCs have absorption maximum at 238 nm, for which this wavelength is most often set when UV detection is coupled to the HPLC. However, other components present in the matrix can also absorb at this wavelength. Another problem of this technique is that HPLC cannot differentiate between structural variants of cyanobacterial hepatoxins, as MCs variants (Ikawa et al., 1999; Lawton et al., 1994; Moollan et al., 1996).

An antibody (Ab) can be used in a wide range of formats for toxin detection, mostly associated with Enzyme-Linked ImmunoSorbent Assay (ELISA) assays. Accounting for the great selectivity of Abs, these assays are today widely used, available in commercial kits that employ monoclonal or polyclonal. These kits have proven to be useful in the screening of water and cyanobacterial samples, but often show poor cross-reactivity against different MC variants. The reason for this can be that most of these assays use Abs that have been obtained through animals that were infected with a specific MC variant, usually MC-LR.

Consequently, the strength of ELISA in routine sample screening is dependent on the ability of the Abs to recognize all variants of MCs present in sample (An and Carmichael, 1994; McElhiney and Lawton, 2005; Metcalf et al., 2000; Nagata et al., 1995).

MS coupled to HPLC is the best analytical method for the detection of cyanotoxins. The method enables the simultaneous separation by HPLC and subsquent identification of cyanotoxins in a mixture. From the mass spectrum, which acts as a fingerprint, toxins could be identified as long as a mass spectrum of an authentic standard is available. However, this technique is not suited for routine/local applications because it used non-portable very expensive equipment highly purified samples and highly skilled technicians (Lawton et al., 1994; Nicholson and Burch, 2001).

Table 2.1 - Comparison of analytical methods for the detection of microcystins.

Methods	Sensitivity (Mcyst-LR)	Specificity for MCs	Cross reactivity	Cost	Advantages	Disadvantages	References
Mousse assay	µg *	non-specific	all MCs	M	· useful toxicity assay	·requires animal license; ·poor sensitivity and selectivity; ·not suitable for in-situ monitoring	Kuiper-Goodman et al.,1999; Nicholson and Burch, 2001
PPI assay (radiometric, colorimetric and fluorometric)	pg	non-specific	all MCs	M-H	· very sensitive	·radiometric assay requires specialized facilities; ·expensive due the need of purified enzyme and radioactive ATP; ·not suitable for in-situ monitoring	Bouaïcha et al., 2002; Rapala et al., 2002; Xu et al., 2000
ELISA (mono and polyclonal)	pg	low specificity	variable	M-H	· very sensitive	·requires animal license; ·variable cross-reactivity consequently may underestimate concentration of MCs; ·difficult to maintain a reproducible source; ·cross reactivity depends on conjugation method	An and Carmichael, 1994; Metcalf et al., 2000; Nagata et al., 1995
HPLC (UV and PDA)	ng	specific	variable	M-H	· routine method (medium sensitivity, specificity and cost)	·Cannot differentiate between all structural variants of MCs; ·other components in the sample may have absorbance at the same wavelengths; ·not suitable for *in-situ* monitoring	Ikawa et al., 1999; Lawton et al., 1994; Moollan et al., 1996;

Methods	Sensitivity (Mcyst-LR)	Specificity for MCs	Cross reactivity	Cost	Advantages	Disadvantages	References
HPLC-MS	µg	very specific	very specific	H	· different interfaces (-ESI, MALDI-TOF, FAB, TSP); · gives mass confirmation (improved accuracy); · sensitive and specific	·not suitable for in-situ monitoring; · very expensive technique; ·requires highly skilled technicians; ·requires highly pure samples	Lawton et al., 1994; Robillot et al., 2000
CE	µg	non-specific	variable	M	· derivatization (fluorescence products) detection using a laser-induced fluorescence detector (more sensitive)	·poor sensitivity; ·not robust; ·not suitable for routine monitoring	Bateman et al., 1995; Li et al., 1999
NMR	µg	very specific	very specific	H	· very specific	·requires large amounts of sample; ·samples must be pure; ·very expensive technique	Harada et al., 1995

PPI: Protein Phosphate Inhibition; ELISA: Enzyme-Linked Immunosorbant Assay; HPLC: High Performance Liquid Chromatography; MS: Mass Spectometry; NMR: Nuclear Magnetic Ressonance; CPE: Capillary electrophoresis; PDA: PhotoDiode Array; MCs: Microcystins; L: low; M: medium; H: high; *IC_{50}: half maximal inhibitory concentration.

Capillary electrophoresis (CPE) is also employed for detection/quantification of MCs, but it has lower sensitivity when compared with HPLC procedures. It is also unsuitable for routine monitoring of water because it is not sufficiently robust to be used in a routine analytical laboratory. Sensitivity can be increased in CPE separation by derivatizing toxins to give fluorescent products that can be detected using a laser-induced fluorescent detector (Bateman et al., 1995; Li et al., 1999). However, this method requires further evaluation in terms of technologies which may increase flow cell volume which will enhance the detection limits (Msagati et al., 2006).

NMR experiments have been conducted for detecting isolated MCs, usually measured in deuterodimethylsulfoxide (Harada, 1995).The main drawbacks of such technique include the need of large amounts of sample (mg); of completely purified samples; and also the very expensive equipment.

Overall, all previous methods are expensive, time consuming and most of the times require lengthy sample processing to concentrate MCs and eliminate matrix contaminants. In recent years several techniques have been explored in order to improve the detection of MCs in biological and environment samples. Highly specific recognition molecules such as APTs and MIPs have been developed in the trace of MCs from waters and show great potential in the analysis of these kinds of samples. New biosensors technology are also becoming available, with the sufficient sensitivity and specificity to enable rapid *on-site* screening without the need for sample processing. More information about these screening methods will be addressed in point 2.3 of this chapter.

2.2.2 *Escherichia coli*

E. coli is a Gram negative, non-spore forming, rod-shaped bacterium and is about 2.0 µm long and 0.5 µm in diameter, with a cell volume of 0.6 – 0.7 μm^3 (CDC, 2012; HTIM - Hospitality Institute of Technology and Management, 1998; Kubitschek, 1990), Figure 2.4. It may have mobility or not, because there are strains that possess flagella and are able to move.

E. coli is a facultative anaerobe and ferments simple sugars such as glucose to form lactic, acetic, and formic acids. It is commonly found in the lower intestine of warm-blooded organisms (CDC, 2012; HITM, 1998).

Its growth occurs at 37°C, ranging from 7.2 to 45.5 ºC (CDC, 2012), but some strains can grow at temperatures up to 49°C (Fotadar et al., 2005). The optimum pH for growth is 6.0 to 8.0, however, growth can occur as low as pH 4.3 and as high as pH 9 to 10 (Banwart, 1989; Mitscherlich and Marth, 1984).

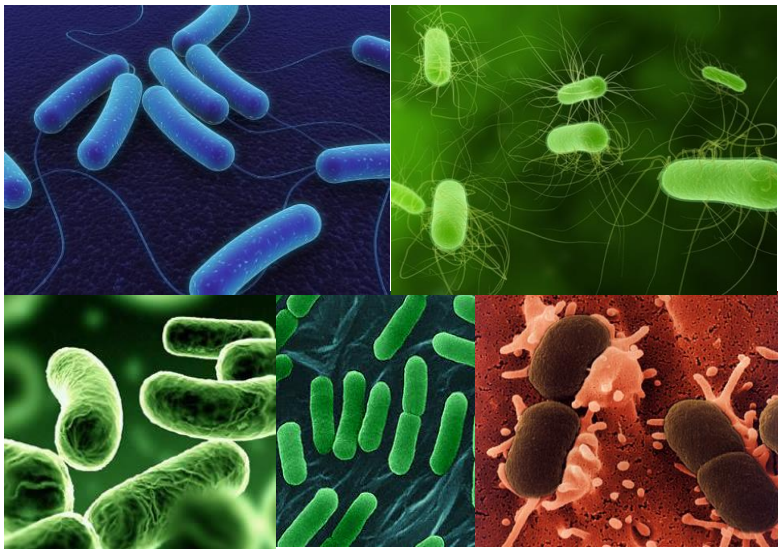

Figure 2.4 – *Escherichia coli* cells (Agricorner, 2012; Kunkel, 2012; Marler, 2010, 2011).

According to their phylogeny the specie *E. coli* can divided into six groups (A, B1, B2, D, E and *Shigella*) (Lukjancenko et al., 2010; Sims and Kim 2011). Most *E. coli* strains are harmless and may be found in the lower intestine of warm-blooded organisms (CDC, 2012; HITM, 1998), providing useful functions in the body by suppressing the growth of harmful bacteria (Hudault et al., 2001; Reid et al., 2001) and by synthesizing appreciable amounts of vitamins (vitamin K_2) (Bentley and Meganathan, 1982). The few pathogenic *E. coli* strains are however responsible for infection of the enteric, urinary, pulmonary and nervous systems, varying from enteropathogenic, enteroinvasive, enterotoxigenic and enterohemorrhagic effects.

Enteropathogenic *E. coli*, normally classified in D group, causes severe diarrhea in infants that can last for over 2 weeks and results in death in case of severe dehydration. In adults, the illness is characterized by severe diarrhea, nausea, vomiting, abdominal cramps, headache, fever, and chills. The time for onset of the illness is 17 to 72 hours; the duration of the illness is 6 hours to 3 days (HITM, 1998).

Enteroinvasive *E. coli*, included in B1 group, is similar to shigellosis and is caused by bacterial penetration and destruction of intestinal mucosa. Symptoms include: chills, fever, headache, muscle pain, abdominal cramps, and profuse diarrhea. The illness occurs 8 to 24 hours after ingestion of food or water containing this organism. The ingestion of a large number of cells (10^4 to 10^5 cells) is required to cause the illness (HITM, 1998). An outbreak of this type occurred in the United States in 1981, which was traced to imported French Brie and Camembert cheese.

Enterotoxigenic *E. coli*, also included in B1 group, include strains that produce enterotoxins when the organisms multiply in the intestine. These strains are commonly responsible for traveller's diarrhea, a problem for travellers from developed countries with good hygiene who visit countries with poor hygiene standards. The illness is characterized by severe diarrhea, which may lead to dehydration. The onset of the illness can occur 8 to 44 hours after ingestion. Infective dose, as determined by a human study, is 10^8 to 10^{10} microorganisms (HITM, 1998). In 1974, more than 2000 staff members and visitors at Crater Lake National Park in Oregon developed gastrointestinal illness due to this strain of *E. coli*, trace to the park's water supply, which had been contaminated with raw sewage.

Enterohemorrhagic *E. coli* (*E. coli* O157:H7), belonging to E group, is characterized by severe abdominal cramps usually, but not always, followed by bloody diarrhea (hemorrhagic colitis). Some individuals exhibit only watery diarrhea. The incubation period is usually about 3 to 9 days. This microorganism can also cause hemolytic uremic syndrome in children (HITM, 1998). In the summer of 1998, a large outbreak of *E. coli* O157:H7 infections occurred in Wyoming, USA, associated with drinking municipal water. The unchlorinated water supply had microbiologic evidence of fecal organisms and the potential for chronic contamination with surface water (Olsen et al., 2002). In another episode, a trailer park pool party lead to gastrointestinal illnesses, including one case of hemolytic-uremic syndrome and one culture-confirmed *E. coli* O157:H7 infection. Of the 51 party attendees and trailer park residents, 18 developed a gastrointestinal illness (Friedman et al., 1999).

A major outbreak with enteroaggregative hemorrhagic *E. coli* O104:H4, belonging to phylogenetic group B1 has also occurred, most recently, in Germany, in May 2011, involving 3842 cases of human infections.

The high proportion of adults affected in this outbreak and the unusually high number of patients that developed hemolytic uremic syndrome makes this outbreak the most dramatic since Enterohemorrhagic *E. coli* strains were first identified as agents of human disease.

Overall, the above infections are usually transmitted through consumption of contaminated water or food, such as undercooked meat products and milk. Although most patients recover in most cases, these infections may turn out life-threatening (WHO, 2007a, 2007b). Avoiding those large and widely dispersed outbreaks is only possible by controlling *E. coli* contaminants in food and water. The presence of *E. coli* in water has well established legal limits and is usually connected to the presence of faecal contamination. Conventional methods for their detection and identification mainly rely on specific microbiological and biochemical identification and serological characterizations (Ercole et al., 2003; Payment et al., 2003).

2.2.2.1 Standard analytical methods for *Escherichia coli* detection

The standard methods used for the detection of pathogens are culture and colony counting (counting of bacteria), immunology-based (antigen–Ab interactions) and polymerase chain reaction (PCR) method (Köster et al., 2003). While these methods can be sensitive, inexpensive and give both qualitative and quantitative information of the tested microorganisms, they are greatly restricted by assay time, quantity of sample needed and initial enrichment for the growth of the pathogens. In Table 2.2 the standard methods used for this pathogen detection are summarized.

The Colilert® method is based upon the sample turning yellow, indicating coliforms with β-galactosidase activity on the substrate O-nitrophenyl-β-D-galactopyranoside (ONPG), and fluorescence under long-wavelength UV light when the substrate 5-methylumbelliferyl-β-D-glucuronide (MUG) is metabolised by *E. coli* containing β-glucuronidase (GUD). The analytical method involves adding commercial dried indicator nutrients containing the two defined substrates to a 100 mL volume of water and incubation at 37 °C during 18 to 22 h.

The result is either presence/absence testing in the 100 ml volume or quantification in a proprietary tray (QuantiTray™) which separates the sample into a series of test wells and provides a most probable number per 100 ml of water (APHA - American Public Health Association, AWWA - American Water Works Association, and WEF - Water Environment Federation, 1998; HPA, 2005).

In the method most probable number (MPN) the sample is inoculated into a microplate well containing dehydrated culture medium. The microplates are observed under UV light (366 nm) in the dark after an incubation period of 36 to 72h at (44±0.5) °C. The presence of *E. coli* is indicated by a blue fluorescence resulting from the hydrolysis of MUG (APHA, AWWA, WEF 1998; HPA, 2005).

In membrane filtration method, the quantification of coliform bacteria, faecal coliforms and *E. coli* is based on filtering a specific volume of water sample, through a membrane with 0.45 μm of porosity. The filter is placed on a solid selective medium and incubated for 21 h at 44 ºC. The characteristic yellow colonies on the membrane (culture medium turning for yellow as well) are counted as lactose positive bacteria. For coliform bacteria and *E. coli* a subculture made of the characteristic colonies is prepared, for confirmation test. The number of coliform bacteria and *E. coli* present in the sample volume filtered are forward count (APHA, AWWA, WEF 1998; HPA, 2005).

Immunologic-based methods rely on antigen–Ab bindings and are widely used for determining waterborne pathogens. The different kind of available Abs types and formats (conventional and heavy chain Ab, pAb, mAb or recombinant Ab) allow different types of assays with different characteristics, sensitivities. For example, pAb can be raised quickly and cost effectively (Cahill et al., 1995), but are limited both in terms of their specificity and abundance (Leonard et al., 2003), while mAbs are often difficult to obtain but more useful for specific detection of a molecule than pAbs because they provide an indefinite supply of single Ab (Velusamy et al., 2010).

In Enzime Immunoassay (EIA) method, samples are collected and are enriched in a specific broth for 48 h at 42 ºC. Then a few mL are heated to 100°C in a water-bath for 15 min and then cooled to room temperature. A few μL of the sample is then transferred to a sample well and allowed to react for some minutes with a specific reagent. After samples are readed in an enzyme immunoanalyser.The sensitivity of the EIA method is higher than that of the conventional culture techniques but varied depending on the type of sample and enrichment broth (Borck et al., 2002).

In ELISA method, wells from well plates are previously modify with an specific Ab, then sample is added and let to reacted for 2h at room temperature. The results of ELISA were measured by a spectrophotometric microplate-reader. In this method none enrichment of the sample is needed (Abdel-Hamid et al., 1999).

In general, immunological-based methods are faster than culture and colony counting methods, more robust and have the ability to detect not only contaminating organisms but also their biotoxins that may not be expressed in the organism's genome; however they are less specific and sensitive than nucleic acid-based methods (Velusamy et al., 2010).

PCR is a method in which a chosen nucleic acid sequence - (DNA or ribonucleic acid, RNA) - is copied a number of times. This method can detect a single copy of a target DNA sequence, and thus, can be used to detect a single pathogenic bacterium in a sample. It is promising because it detects the organism by amplifying the target rather than the signal, and is therefore less susceptible to producing false-positives. A target DNA can be amplified 1-million-fold in less than an hour, with sensitivities in theory down to a single target pathogen. PCR has several advantages over culture and other standard methods for the detection of microbial pathogens and offers the advantages of specificity, sensitivity, rapidity, accuracy and capacity to detect small amounts of target nucleic acid in a sample (Velusamy et al., 2010). On the other hand, sample specific substances can interfere with the PCR reaction and may seriously affect the detection limit (Koster et al., 2003; Wilson, 1997). The design of primers and probes is a critical step in any molecular assay since it defines the specificity of the PCR reaction. Assay optimization for increasing sensitivity comprises adjusting the annealing temperature and the primer, probe, and magnesium concentration (Cupples et al., 2010; Koster et al., 2003). There are different PCR based methods used to detect pathogens; real-time PCR, multiplex PCR and reverse transcriptase PCR (RT-PCR). Compared to other PCR methods, multiplex PCR is very useful as it allows the simultaneous detection of several bacterial strains (Touron et al., 2005). Real-time PCR technologies have emerged, in recent years, as a leading technology for rapid identification of pathogens due to their speed and high degree of sensitivity and specificity, which also allows obtaining quicker results without excessively handling. Nonetheless, one of the main drawbacks of the PCR techniques previous described is that, the users cannot distinguish between viable and non-viable cells, since DNA is always present whether the cell is dead or alive.

Althougth this limitation can be overcome by using RT-PCR. Real-time RT-PCR detection eliminates some purification and concentration steps that are required for conventional PCR detection (Velusamy et al., 2010).

The conventional methods for detecting foodborne pathogens are often time-consuming thus there is a call for rapid, reliable, simple, specific and sensitive new methods and technologies. Moreover, the technique should be able for in situ real-time monitoring at a low cost. Recently, there has been a large extent in research aiming the development for new solutions of pathogen detection and identification (Ercole et al., 2003; Payment et al., 2003).

Table 2.2 - Comparison of analytical methods for *Escherichia coli* detection.

Method type	Method	Detection limit	Time of assay (h)	Sample volume	Advantages	Disadvantages	References
Culture and colony counting	Idexx Colibert 18	1MPN/100 mL	18	100 mL	·very sensitive; · fewer errors comparing to MPM and MF methods	· some strains of *E. coli* (β-glucuronidase negative) cannot be detected; · detection of a huge number of false positive because other bacteria also produce □-glucuronidase	HPA, 2005; ISO 8199:2005
	Miniaturized Method (Most Probable Number)	15 MPN/100 mL	36	100 mL	·aplication to all kind of samples; ·easy interpretation of test results; ·culture meia often inexpensive	· samples must contain inhibitors that affect pathogen growth; ·futher culture in a solid media require for pure cultures isolation; · time-consuming	ISO 9308-3:2000; ISO 8199:2005
	Membrane filtration	1 CFU/sample volume filtrate	36	0.1 - 250 mL	· flexible volume sample; · quantative results and good precision on CFU;	· not aplicable to turbid samples; · quality of membarnes variable; · time-consuming; · poor selectivity	ISO 9308-1:2000; ISO 8199:2005
Immunologic	EIA ELISA	50 cells/mL	0.5	0.1 - 250 mL	· rapid then culture methods;	·skilled technician and specialized growth apparatus for tissue culturing (mAb); · very expensive; · variable specificity;	Abdel-Hamid et al., 1999; Borck et al., 2002; Velusamy et al., 2010
PCR	PCR RT-PCR Multiplex-PCR	1 single cell	3	few µL	· high sensitivity and selective; · faster than culture and immunologic methods	· dead or inactivated bacteria can be detected; · false positive results (interference of some compounds present in samples); · samples must be concentrate	Batt, 2007; Cupples et al., 2010; Koster et al., 2003

CFU: Colony Form Unit; MPN: Most problable Number; EIA: Enzyme ImmunoAssay; ELISA: Enzyme-Linked Immunosorbent Assay; PCR: Polymerase Chain Reaction; RT-PCR: Reverse Transcriptase-Polymerase Chain Reaction; HPA: Health Protectiion Agency; ISO: International Organization for Standardization.

2.3 Recognition elements

Tailor-made artificial receptors, such as APTs and MIPs, bind target analytes in a similar way to Abs, by displaying molecular recognition phenomena of high affinity and selectivity. These binding features have made them appropriate for applications in life science and biotechnology in which selective recognition is necessary.

Over the last years, these affinity tools have gained an interest as potential alternatives in many applications, showing several advantages such as reduction of the molecular mass, improvement of the stability, and more efficient selection and screening system. An overview of the current state of APTs and MIPs, is presented next.

2.3.1 Molecularly Imprinted Polymers

MIPs are tailor-made polymers prepared in the presence of a template molecule (similar or equal to the target molecule), which is removed after polymerisation and leaves cavities with recognition elements capable of further rebinding. MIPs are totally synthetic affinity tools (without any biological basis). They are able to recognize a single target molecule, small molecules to proteins, or a group of structurally similar molecules based on their shape, size and chemical functionality (Donald, 1988; Giovannolli et al., 2008; Haupt and Mosbach, 2000; Mosbach, 1994).

2.3.1.1 General synthetic process

The MI process can be resumed in three main steps, complexation, polymerisation and extraction (Figure 2.5). In complexation the functional monomers became either strongly linked or interact with the template molecule by a covalent or non-covalent connection, respectively (Komiyama et al., 2003; Spégel et al., 2002; Wang et al., 1996). In polymerisation the template/monomer complex is polymerised in a three-dimensional network. And finally the template is extracted from the polymer, leaving behind the imprinted cavities. These cavities will be able to recognize analyse which share the same molecular groups with the template molecule (Komiyama et al., 2003; Spégel et al., 2002).

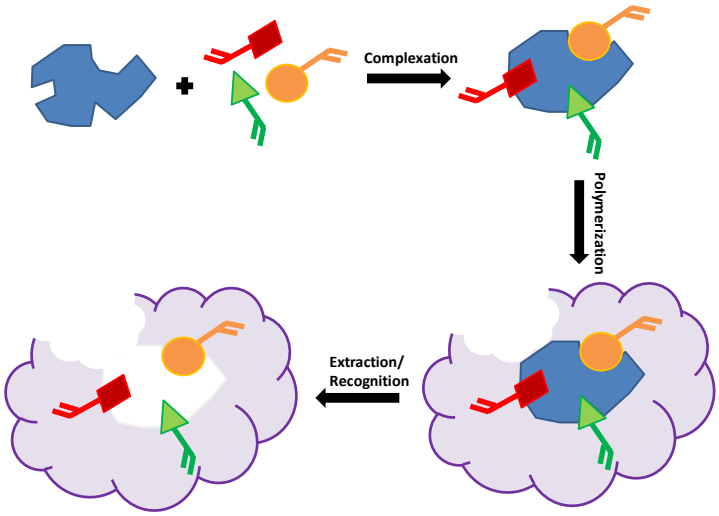

Figure 2.5 – Generic scheme of molecular imprinting process.

Covalent imprinting usually produces more homogeneous binding sites however the extraction of the template is more difficult. Non-covalent imprinting generally produces more heterogeneous binding sites, with a slightly wide affinity range for the target analytes different than the target compound. Currently, noncovalent imprinting is used most frequently mainly because the process is simple and a wide variety of monomers are accessible (Mosbach, 1994; Wang et al., 1996).

Many aspects can influence the final properties of the MIPs. The choice of template and functional monomers has great influence in the produced polymer, but the ratio of these molecules is of major importance, large amounts of analyte are as well required to create a huge number of cavities, increasing the sensibility of the imprinted material (Mosbach, 1994).

An excess of functional monomer is tipically required to shift the equilibrium in the first stage of MIPs production to the complex from, but this can lead also to the creation of nonspecific sites. The final porosity of MIP materials depends on the solvent and temperature used for polymerisation. This feature is important because pores that are too small limit flowthrough or make cavities inaccessible, while pores that are too large limit the overall binding capacity of the MIPs (Warsinke and Nagel, 2006).

2.3.1.2 Methods/formats of synthesis

In general, MIPs have been prepared via bulk polymerisation, which is an established technique for the production of polymer monoliths. This type of polymerisation requires, in the end of the process, the grinding and sieving of polymers to a desired particle size. The resulting polymeric particles are used for different purposes, being as the packin of stationary phases for HPLC columns (Anderson et al., 1990) their first application. More recently, they have been used in chemical/biological sensing (Merkoçi and Alegret, 2002), therapeutic drug delivery (Puoci et al., 2008) and catalysis (Li, W. and Li, S., 2007). Bulk polimerisation results in a very stable and inexpensive polymer matrixes, but this kind of process cannot be used for all desired functions, such as *in vivo* applications. Thus, alternative methods to produce new MIP structures have been developed by means of other polimerisation formats. These formats comprise MIP beads (Yoshimatsu et al., 2007; Zourob et al., 2006), monolayers (Lahav et al., 2001; Lotierzo et al., 2004), membranes (Sergeyeva et al., 2007; Yang et al., 2004) and surface imprinting (Moreira et al., 2011).

Regular MIP beads can be obtained using the precipitation polymerisation method. This technique allows the formation of imprinted beads with the same reaction mixture used in the bulk method but in this polymer chains continue to grow, precipitating only when become large enough to be insoluble in the reaction mixture. This technique is easy, less time consuming than bulk polimerisation and provides regular beads in good yields (Vasapollo et al., 2011).

MIP membranes are synthesized by the method of *in situ* polymerisation using the principle of synthesis of interpenetrating polymer networks. The low membrane permeability is still the main drawback for their application (Vasapollo et al., 2011; Yang et al., 2004).

MI monolayers are produced directly over the support surface of detection. This is an advantage of the process in terms of time synthesis of the MIP. Usually, MI monolayers are synthesized through the grafting method (Sergeyeva et al., 2007). Surface grafting on supports enables better accessibility to the specific binding sites (Sulizky et al., 2002). Compared with the traditional radical polymerization, this polymerization process can be well controlled by iniferter due to the avoidance of some adverse reactions such as radical coupling (Fairhurst et al., 2004).

In surface imprinting, molecules with nanoscale dimensions can be assembled on a surface, piece by piece, with high structural control, mimicking nature's modular approach to nanostructured materials. Eventually, most of the imprinted sites are near or in the surface, with most templates being removed from the highly cross-linked matrix. Template rebind produces electrical, optical, thermal or mass changes in the nanostructured surface, thus enabling its detection. Searching for a high number of effective imprinted sites, MIPs may be designed on top of nanostructured materials (Moreira et al., 2011). Their small dimension leads to extremely high surface to-volume ratio, favoring miniaturization and to a more homogeneous distribution of the recognition sites. However, the synthesis of these materials is less direct and requires specially adapted protocols, such as the orientation of the template molecule at its immobilization on the support.

The efficiency of the overall processes is however correlated to the kind of analyte that is being imprinted.

2.3.1.3 Target analytes

In terms of target analyte, the majority of the conventionally synthesized MIPs have been designed to selectively recognize small molecules in organic solvents. These include drugs (Puoci et al., 2007), polluants (Pichon and Chapuis-Hugon, 2008) and metal ions (Biju et al., 2003) and they mostly obtained by bulk approach, emplying typical monomers such as carboxylic acids (acrylic acid, methacrylic acid, vinylbenzoic acid), sulphonic acids (2-acrylamido-2-methylpropane sulphonic acid) and heteroaromatic bases (vinylpyridine, vinylimidazole) (Vasapollo et al., 2011). The resulting materials have been integrated in biosensors by means of by *in situ* polymerization, using a photochemical or thermal initiator (Henry, et al., 2008), or by surface grafting with chemical or UV initiation (Piletsky et al., 2000). These approaches are now well established for small moleculares and widely used in biosensing technology.

Today, there is however an emerging and strong need to create artificial receptors for peptides and proteins (Janiak and Kofinas, 2007). Special care must be taken in the imprinting of proteins due to the special nature of these biomolecules, whose biological activity demands a great flexibility and emplies in many cases conformational changes.

Polimerisation can only take place in the aqueous environment (because proteins are water-soluble and change their stereochemical shape in organic solvents); pH and temperature must also be controlled (because of the flexible structure and conformation of proteins) and should be close to physiological conditions.

According to the part of the molecule to be imprinted, proteins can be imprinted by three different approaches: bulk imprinting (imprint of whole protein), surface imprinting (imprint of a part of the surface of the protein) and epítope imprinting (imprint of a small, specific part of the protein) (Ruigrok et al., 2011). Surface imprinting of proteins is the most used strategy (Turner et al., 2006), requiring a smaller amount of template than conventional MIP approaches. It consists on placing the template on a surface and polymerizing around it, thus creating binding sites close to the surface. These binding sites are more accessible than in bulk-based approaches and template/polymer interactions are not hindered by diffusion (Mirsky et al., 1999). Overall, this decreases the equilibrium time and increases binding kinetics.

Overall, the imprinting of small molecules is today a well established technique while the imprinting of protein is still an emerging field of research. Small molecules may be successfully imprinted through many approaches, but proteins seem to require a surface imprinting technique. Although the more favourable details around this technique are yet to be discovered, surface imprinting is always made on a suitable receptor surface acting as support of the MIP material.

2.3.1.4 Supports in surface imprinting

Independent of the kind of template, one of the important aspects in surface imprinting is the material acting as support of the imprinted structure. Carbon materials have been previously used with success in surface molecular imprinting.

These includes several kinds of carbon at nanometer range, carbon powder (Fang et al., 2008), carbon nanostructured forms of fullerenes (buckyballs) (Shinkai and Takeuchi, 2004), graphene sheets (Pumera, 2010) and carbon nanotubes (Chen et al., 2012).

CNTs are especially attractive due to its many interesting properties. In particular, their large length-to-diameter aspect ratios provide high surface-to-volume ratios. CNTs also have an outstanding ability to mediate fast electron-transfer kinetics for a wide range of electroactive species. In addition, CNTs chemical functionalization can be used to attach almost any desired chemical species to them, thus widening their range of applications (Tasis et al., 2006).

CNTs may be assembled in single-walled (SWCNTs) or multi-walled (MWCNTs) nanotubes. SWCNTs consist in seamless cylinders rolled up from a piece of graphene, while MWCNTs are concentric cylinders of multiple layers of graphene. SWCNTs have typically 1nm of diameter while MWCNTs tend to have diameters between 2 and 100 nm (Yang W. et al., 2007) (Figure 2.6). They can be found in both oriented (vertically aligned) and non-oriented (random mixtures) configurations (Merkoçi et al., 2005).

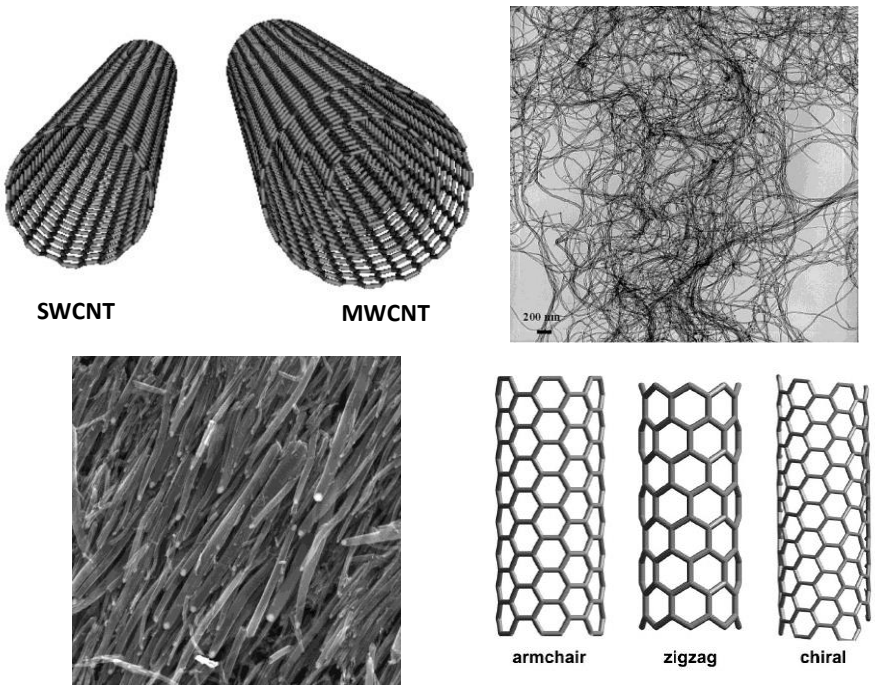

Figure 2.6 – Different arrangements for carbon nanotubes structures and scanning electron microscope images, adapted from (Grady, 2008; Graphistrenth, 2012; Tasis et al., 2006).

Two main approaches are considered for the surface modification of CNTs: noncovalent attachment of molecules and covalent attachment of functional groups to the walls of the nanotubes. The advantage of noncovalent attachment is that the perfect structure of the nanotube is not altered, thus its mechanical properties should not change. The main disadvantage is that the forces between the biomolecule and the nanotube might be weak and the efficiency of the load transfer might be low. The covalent attachment of functional groups to the surface of nanotubes can improve the efficiency of load transfer. But might introduce defects on the walls of the perfect structure of the nanotubes (Eitan et al., 2003).

The particular cylindrical form of CNTs is the principal aspect that provides the quantum confinement effect in the oriented 1D nanostructured materials (Ajayan, 1999). These characteristics provide the possibility to increase chemical reactivity and electronic properties of this particular carbon material, which becomes a crucial point for biosensing devices (Rivas, 2007).

MWCNTs form a special class of nanotubes because their morphology and properties are similar to those of SWNTs but their resistance to chemicals is significantly improved. This is especially important when functionalization is required to add new properties to the CNTs. In the case of SWNTs, covalent functionalization will break some C=C double bonds, leaving "holes" in the structure on the nanotube and, thus, modifying both their mechanical and electrical properties. In the case of MWCNTs, only the outer wall is modified (Flahaut et al., 2003)

One final issue that greatly affects the efficiency of the imprinting process is the nature of the polymeric material used to design the imprinted site.

2.3.1.5 Polymeric environment

The polymeric reticulated structure in MIP materials is usually formed from a sol-gel based chemistry or vinyl monomers polymerized by an addition reaction, following a chemical of photoinitiation.

The majority of molecular recognition by imprinting is carried out using radical polymerization of acrylic or vinylic type of polymers, thus these were the first to be tested for sensor applications and the most frequently used.

The most functional acrylic or vinylic types of monomers used are methacrylic acid, vinylpyridine and acrylamide derivatives.

Thermal polymerization tipically used 2,2'-azobis(isobutyronitrile) as initiator, whereas photochemical polymerization was undertaken with 2,2'-azobis(isobutyronitrile), benzophenones or acetophenone derivatives. In terms of porogenic solvents, dimethylformamide, is frequently used when the aim is to develop a sensor for aqueous applications, in order to minimize swelling effects (Piletsky et al., 1995; Sergeyeva et al., 1999). Conventional MI includes high crosslinker ratios (5:1 mole of functional monomer), which favor the formation of imprinted sites. But with as little as 20% of crosslinker, it was still possible to observe memory effects by using batch-binding assays (Yilmaz et al., 1999). The most used crosslinker agent is this type of polimerisation is ethylene glycol dimethylacrylate. In the case of polymeric films for sensors, it was observed in some cases that some degree of flexibility favors the binding of the template and improves the adherence to the electrode surface in optical devices (Jenkins et al., 1999), but only to some electrochemical sensors (Sergeyeva et al., 1999).

The only application, known so far, for the design of MIPs through radical polymerization of acrylic monomers for the analites in study is the two imprinted polymers for MC-LR that were synthesized using (i) the functional monomer 2-acrylamido-2-methyl-1-propanesulfonic acid and using (ii) metacrylic acid. MIP affinity for the template was performed using a competitive ELISA assay against MC-horseradish peroxidase analogues. It was found that the computationally designed MIP, prepared using the first monomer, had affinity and sensitivity comparable to those of pAbs. Although the affinity was still lower than that of mAbs, the synthetic MIPs showed superior chemical and thermal stabilities compared with those of biological Abs. The MIP also performed better than the antibodies in selectivity studies for MC-LR compared with other toxin analogues (Chianella et al., 2003).

Silane chemistry has also been used in the imprinting process for many years. Sol-gel materials have several characteristics that increase their interest in integrating biosensors (Mac-Craith et al., 1997).

First, these materials are transparent to UV-Vis spectra, allowing their integration in optical transducers, with the possibility of measuring different optical properties like absorption, reflection, fluorescence and luminescence (Jerónimo, 2005; Mujahid et al., 2010). Moreover, sol-gel materials are rigid, robust, electro-, photo- and chemically stable and are resistant to photo-, thermal- and bio-degradation (Díaz-García and Laíno, 2005; Monton et al., 2012).

The sol-gel technique may follow different approaches to the production of three-dimensional matrices, which allows the custom made of different configurations, such as monoliths, powders, fibers and thin films (Díaz-García and Laíno, 2005; Jerónimo, 2005; Monton et al., 2012; Moreira, 2005;).

The sol-gel process comprises different steps: mixing, gelation, aging, drying, stabilization and densification (Hench and West, 1990; Jerónimo, 2005; Moreira, 2005). The preparation of a sol-gel material starts with the mixing of an appropriate alkoxide with water and a mutual solvent to form the sol (liquid colloidal particles dispersion). Hydrolysis leads to the formation of silanol groups (Si—OH). Subsequent condensation reactions produce siloxane bonds (Si—O—Si). The hydrolysis and condensation reactions are regulated by several conditions, temperature, pH, catalysis, which determine the properties and the composition of the ultimate material (Díaz-García and Laíno, 2005; Klein, 2005; Moreira, 2005). Besides, the physical properties, pore size, shape and distribution of the gel depend on the process parameters and the method used for the preparation of the material, Figure 2.7 (Díaz-García and Laíno, 2005).

The sol substance can originate some of the final materials like thin films that can be achieved by heating the sol after their coating onto a surface and dense fibres by the extrusion of the sol at high temperatures (Brinker and Scherer, 1990). The continuos reaction and the formed gel lead to a rigid and porous three-dimensional network constituted by pores and polymeric chains (Brinker and Scherer, 1990). During the drying process, the solvent is removed and shrinks. The resulting material is known as a xerogel. After gelification, and when solvent removal occurs under supercritical conditions, the network does not shrink and a highly porous, low-density material known as an aerogel is produced. Heat treatment of a xerogel at elevated temperature produces viscous sintering and effectively transforms the porous gel into a monolith (ceramic material), see Figure 2.7 (Brinker and Scherer, 1990; Díaz-García and Laíno, 2005).

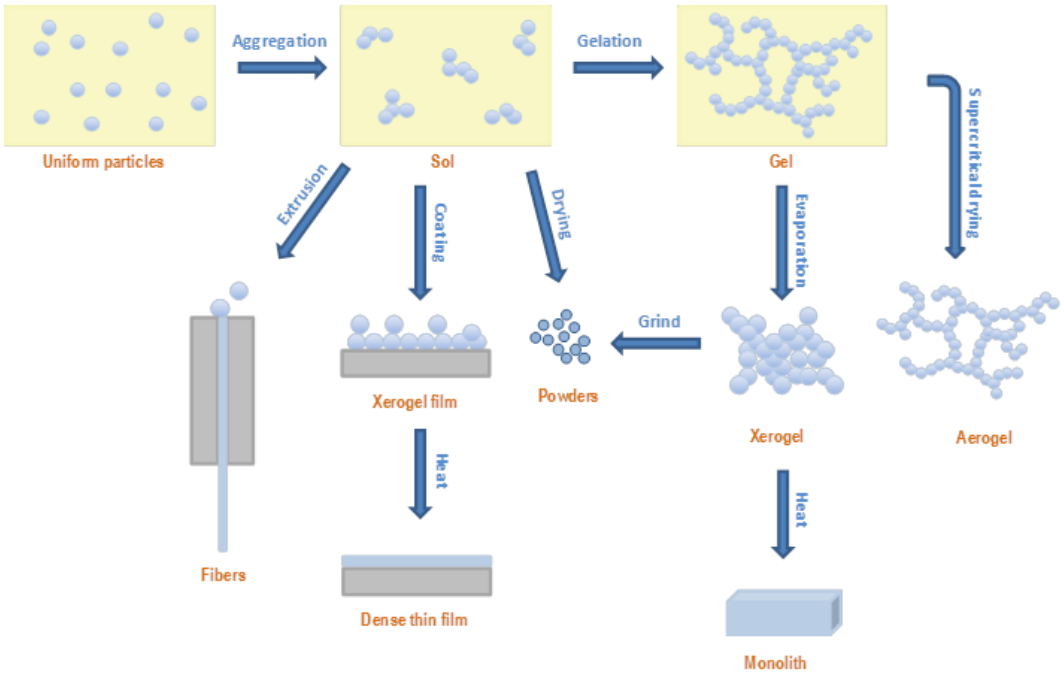

Figure 2.7 – General scheme of the sol-gel process with the different approaches to the production of three-dimensional matrices (adapted from Brinker and Scherer, 1990).

The imprinting with a sol-gel matrix is tipically carried out by introducing the template molecule to the functional alkoxide percursors sol and let stand for molecular pre-organization according to electrostatic interactions. As the precursors follow hydrolysis and polycondensation reactions, an interconnected 3-D porous network is formed around the template. Polymerization becomes solution increasingly thicker. The reaction is stopped taking into account the desired final product. The template is then removed leaving behind the recognition cavities with specific sites capable of binding the target molecule.

Overall, the entrapment of the biomolecules by a soft gel imprint promotes the protection of the leaching of the molecules but still allows the motions required for binding the substrate and exchanging small molecules like ions from buffer solutions and products of reaction (Gill, 2001; Mac-Craith et al., 1997; Monton et al., 2012). The matrix also acts like a barrier, which for one hand protect the sensing element from potentially deactivating components of the sample and on the other hand, protect the sample from direct exposure to the biomolecule, Figure 2.8 (Jerónimo, 2005).

The flexible design of the sol-gel process and the control of the processing conditions like pH and ionic strength, as well as the control of some properties like pore size and surface allows the adaptation to the desired biomolecule entrapment and the maximization of the sensing application (Mac-Craith et al., 1997).

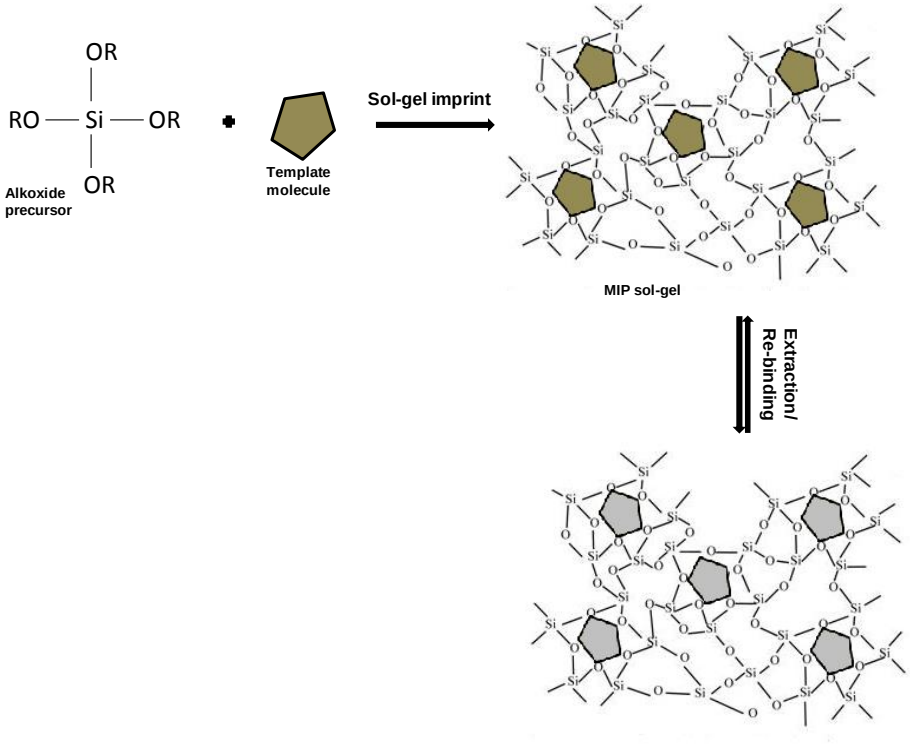

Figure 2.8 – Schematic representation of the sol-gel imprinting process (Díaz-García and Laíño, 2005).

The sol-gel imprint for target molecules of small size has been reported often, for simple organic chemical molecules (Makote and Collinson,1998), metal ions (He et al., 2001), pesticides (Graham et al., 2002), dyes (Glad et al., 1985), toxins (Lulka et al., 2000) and antibiotics (Fernández-González et al., 2004) among others. The sol-gel system used in the majority of these processes are metal (Ti, Si) alkoxides percursors and hydrophilic precursors (3-aminopropyl)triethoxysilane (APTES)). The conditions of the polimerisation incude water, acid and an organic solvent.

In terms of the imprint approach, these processes cover practically all types, since covalent to non-covalent, and using all kinds of formats, beads, membranes, monolayers and surface imprint (Fernández et al., 2004; Glad et al., 1985; Graham et al., 2002; He et al., 2001; Lulka et al., 2000; Makote and Collinson, 1998). Some are integrated in QCM, FETs or voltammetric devices, but the majority has not been yet evaluated as analytical materials (Díaz-García and Laíño, 2005).

The growth interest in organic–inorganic hybrid materials prepared by sol-gel chemistry along with the growing interest in MI may prompt the design of unique materials with controllable pore sizes, structural rigidities, thermal stabilities and enhanced recognition properties.

The major achievement in sol-gel sensor technology is the successful induction of several biological recognition elements such as enzymes (Li et al., 2013), bacteria (Premkumar et al., 2002), proteins (Zhang et al., 2006) and even whole cells (Cohen et al., 2010). Three-dimensional MI sol-gel materials can be synthesized in different configurations (thin films, porous materials, bulk structures) and two main approaches, non-covalent and covalent.

In the non-covalent approach, the template may be directly added to a sol-gel solution prior to acid-catalysed hydrolysis and condensation. By using a fairly polar solvent, such as ethanol, and a non-polar sol-gel precursor, imprinted sites are generated by van der Waals forces, π-stacking or electrostatic interactions between the template and the sol-gel network. As the solvent evaporated to yield a solid porous material, the imprinted sites could be formed by the template's affinity for the sol-gel matrix. The precursor should be carefully selected to provide the porosity necessary to facilitate diffusion of the template into and out of the sol-gel. Following the drying step, the gels should be extracted with an adequate solvent to remove the template (Díaz-García and Laíño, 2005).

In the covalent approach reversible covalent bonds are employed, usually involving a prior chemical synthesis step to link the precursors to the template. This conjugate is then polymerised using an excess of the metal alkoxide precursor. Once the sol-gel is formed, the template is chemically removed, leaving a cavity that should have the ability to bind molecules of the appropriate size and shape (Díaz-García and Laíño, 2005).

No MI sol-gel polymer was yet synthetized for MC-LR and only few were synthethise for *E. coli* (Armon et al., 2000; Cohen et al., 2010; Premkumar et al., 2002). Although none was integrated in a biosensor.

Materials with tailor-made pore sizes and shapes have attracted much attention for their potential applications in biosensing. There are several advantages associated with using sol-gel materials over other polymers. The control of the thickness, porosity and surface area is easier. Also, they can be easily synthetise in a variety of geometric configurations, such as monoliths, powders, thin films, fibers and arrays, offering flexibility to the design of the sensor. The matrix provides a steric barrier, protecting the sensing element from potentially interfering components of the sample (Monton et al., 2012). On the other hand, selectivity and diffusion are comparable between the two techniques. One of the major drawbacks of the sol-gel materials is the cracking of the polymer that appears after several applications of the polymers in aqueous medium.

2.3.1.6 Applications in biosensors

The application of MIP materials in the development of biosensors, has emerged mostly in the late 90s and increased over this past deade. This great increase is a resut of the many advantages of MIP materials compared to Abs, such as high stability, low cost and easy preparation. The application of MIPs for the recognition of biomolecules of bacterial origin in a biosensor unit has also been growing over the past decade.

The only reported biosensor for detection of MC-LR was produced by Chianella and co-workers in 2003, where an artificial receptor for MC-LR using a conventional MIP approach and bulk polimerisation were employed. The synthesised polymer was used both as a material for solid-phase extraction and as a sensing element in a piezoelectric sensor (Chianella et al., 2003). The analytical features of the resulting device include detection limit of 0.35 nM.

About *E. coli,* a few more MI-based biosensors were reported so far. Artificial receptors based on surface imprinted polymers were designed for detection of *E. coli*. Surface-imprinted polyurethanes optimized to selectively recognize *E. coli* showed ten times higher sensor responses on QCM than the respective non-imprinted polymers. Detection limits of these sensors turned out to be in the range of 0.1 mg/ml *E. coli* in aqueous solution (Findeisen et al., 2012).

In another work, recombinant fluorescent *E. coli* cells are encapsulated in sol-gel derived silicate films. The effect of the preparation protocol on the viability of the encapsulated cells and their ability to express the fluorescent proteins in response to genotoxicity stress were evaluated. The implications of these observations for dual sensing and multistep biosynthesis and biodegradation are discussed (Premkumar et al., 2002).

Overall, there is already a MIP material integrated in a biosensor platform for MC-LR detection in water, but it should be improved with regard to pre-concentration of samples and the integration of the MIPs in cartidges in order to be useful for tracking Cyanobacteria in water. Furthermore, the transducers used, QCM requires a stabilisation of at least 3 hours to reach a steady resonant frequency. Regarding the direct bacterial detection in (Premkumar et al., 2002), the already described MIP materials do not show suitable features for a practical application in detection of the *E. coli* bacterium in water. This is mostly due to specificity of the imprint, which permits the detection of similar bacteria (same shape). The design of a sucessfull imprint targeted for the proteins that exist in the outer surface of these bacteria could be an alternative approach. However, this is yet an emerging field, with many variables requiring intensive study in order to reach a sucessfull MIP design. Alternative approaches may be found in the literature for this purpose, namely the use of APTs as biorecognition elements for proteins.

2.3.2 Aptamers

2.3.2.1 Definition and main characteristics

APTs are short, single-stranded DNA or RNA oligonucleotides, which can interact with high specificity and affinity to their targets (Ellington and Szostak, 1990; Tombelli et al., 2005). The term ‘aptamer’ is derived from the Latin word ‘aptus’ (to fit) and the Greek word ‘meros’ (part or section) (Ruigrok et al., 2011), and their affinity to different targets results from the ability to fold into numerous tertiary conformations (de-los-Santos-Álvarez et al., 2008), Figure 2.9.

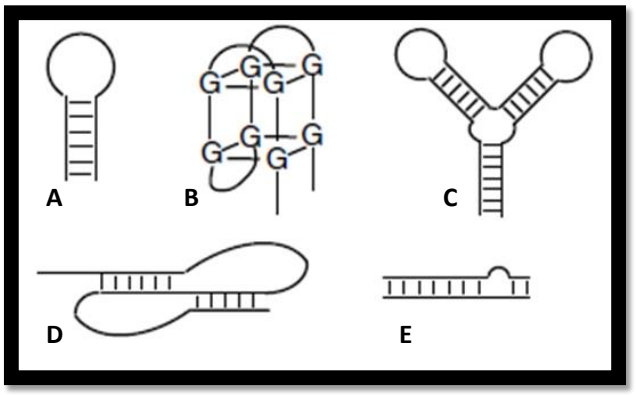

Figure 2.9 – Different tertiary conformations adopted by aptamers, hairpin (A); G-quarter (B); T-junction (C), pseudoknot (D) and stem-bulge (E), adapted from (de-los-Santos-Álvarez et al., 2008).

APTs are very resistant to denaturation and degradation, especially those of DNA, and their binding affinities and specificities can easily be handled and improved by rational design or molecular evolution techniques. They, can also be synthesized by using standard chemical nucleic acid synthesis and covalently immobilized on many surfaces (using different functional groups), that in many cases are expected to result in highly ordered receptor layers (Stadtherr et al., 2005; Strehlitz et al., 2008). Moreover, DNA APTs are temperature stable, and also reversibly denatured, converting them into ideal capture molecules in biosensor devices.

Theoretically, APTs can be generated for any target by a combinatorial procedure called systematic evolution of ligands by exponential enrichment (SELEX) (Tuerk and Gold, 1990) and synthesized in a large quantity in vitro in a very reproducible way (Stoltenburg et al., 2007; Mok and Li, 2008).

2.3.2.2 Systematic Evolution of Ligands by Exponential Enrichment process

In SELEX process, Figure 2.10, a random library of oligonucleotides is incubated with the target of interest in a buffer at a given temperature. In the initial cycles of selection, a tiny percentage (0.1–0.5%) of individual sequences interacts with the target. These sequences are separated from the rest of the library by using selection techniques such as affinity chromatography (O'Sullivan, 2002; Warsinke and Nagel, 2006).

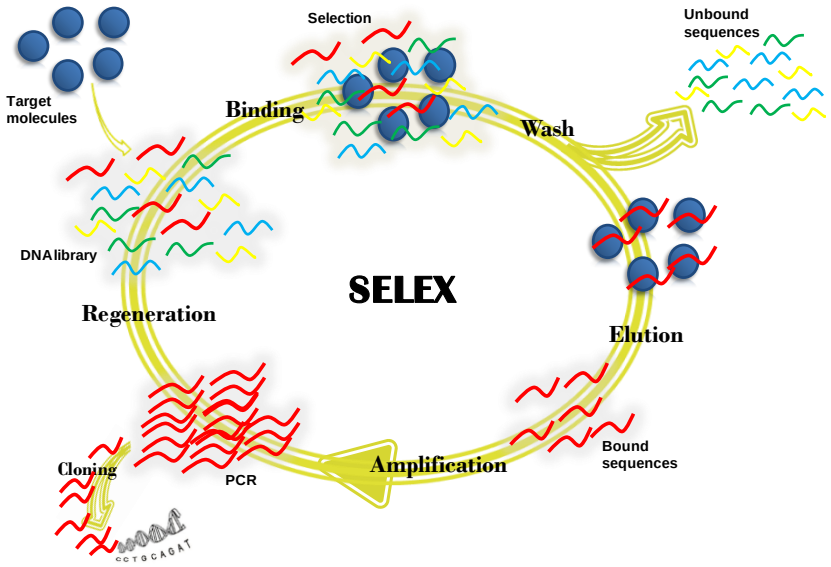

Figure 2.10 – General scheme of the Systematic Evolution of Ligands by EXponential enrichment process adapted from (Stoltenburg et al., 2007).

The obtained sequences are amplified to find an enriched library for further used in the selection/amplification process cycle. After 8–15 cycles, APTs are obtained. The enriched library is cloned and sequenced and individual sequences investigated for their ability to bind to the target. A typical SELEX experiment that includes cloning and sequencing may take 2–3 months. Full-length APTs are generally 40 – 80 nucleotides long but can be shortened for the elimination of the nucleotides that are not necessary for target binding (O'Sullivan, 2002; Warsinke and Nagel, 2006). Once a suitable APT for a specific target analyte is identified and produced, it must be integrated in a biosensor device in order to act as a biorecognition element.

The main advantages and disadvantages of this selection technology are summarized below. The SELEX process is applicable to different classes of targets, single or complex target structures or mixtures without proper knowledge of their composition. The affinities are often comparable to those observed for antibodies. In contrast to antibodies, aptamers are selected by an in vitro process independent of animals or cell lines. Thus, the SELEX process is also applicable under non-physiological conditions. The selection of aptamers for toxic target molecules or for molecules with no or low immunogenicity is possible (Stoltenburg et al., 2007).

Various modifications can be introduced in the basic SELEX process to direct the selection to desired aptamer features or to intended applications of the aptamers. Several methods were developed to modify aptamers after their selection, mostly to enhance their stability or to permit the quantification and immobilization of the aptamers

Denatured aptamers can be regenerated easily within minutes, which is important for many applications. The small size relative to antibodies makes aptamers easier to be synthesized and chemically modified, and enables them to access protein epitopes that might otherwise be blocked or hidden (Lee et al., 2006). Aptamers display low to no immunogenicity, which is important for animal or human therapeutic applications (Stoltenburg et al., 2007).

Paper published on aptamer also reveal several limitations of aptamers and their selection technology. Such experiences are valuable for starting new SELEX experiments, because some limitations can be overcome by modifying the SELEX conditions. In reality, not any target molecule is suitable for an aptamer selection. There is no standardized SELEX protocol applicable for any kind of target. The selection conditions have to be adapted to the current situations (target, desired features of the aptamers, applications). The majority of the published aptamers were manually selected. Thus, the whole process to get high affinity and specific aptamers is time consuming (Stoltenburg et al., 2007).

Aptamers are relatively unstable in biological fluids and so different strategies such as chemical modifications are being developed to overcome this difficult. They may be susceptible to non-specific binding in complex biological samples, which makes it difficult to quantify the target by use of aptamer based assays, and may necessitate sample pre-treatment.

2.3.2.3. Integration in biosensing devices

The integration of APTs in biosensors involves typically a covalent or non-covalent bond to a solid surface. The selection of the most suitable approach depends on the analytical purposes of such device and on the prompt availability of a commercial APT bearing the desired chemical function.

When a covalent bond is originated, the link of the APT to the support is rather stable, but requires previous a chemical modification in any of the two terminals of the oligonucleotide. Standard modifications are thiol, amine and biotin. Gold surfaces are used for many electrochemical measurements and thus, the direct attachment of aptamers to gold could be achieved by using a thiol-alkane linked to the aptamer sequence. The avidin-biotin complex is widely used due to the good results regarding sensitivity compared to other immobilization strategies (Hianik et al, 2007). Strepavidin can be physically adsorbed or covalently immobilized onto the support and the method mainly requires incubation of the biotin-tethered aptamer with the modified substrate (Velasco-Garcia and Missailidis, 2009).

Although, almost any surface could be functionalized and the type of chemistry selected is dependent on what type of terminal functional group is linked to the aptamers.

The most common groups employed for surface attachment are hydroxyl, amine, and carboxylic acid surface functional groups. Hydroxylated surfaces can be modified to form a stable carbamate bond to an aminoterminated aptamer group (Liss et al., 2002). Amine-terminated surfaces provide several options for aptamer attachment. A surface amine group can be modified with a symmetric bifunctional dialdehyde linker, which forms an imine bond with an aldehyde, leaving the other aldehyde free for repeating this chemistry with an amino-terminated aptamer group (Stadtherr et al., 2005). Symmetrical diisothiocyanates have also been used as bifunctional linkers for attachment of amine-functionalized surfaces to either thiol-terminated or amine-terminated aptamers (Zhu et al., 2006).

Surface immobilization of APTs is also possible via physisorption, which involves non-covalent interactions between molecules such as electrostatic interactions. Some biological polymers such as polyethyleneimine or poly-L-lysine (PLL) which have positively charged amino-groups in the side chain that can bind to the negatively charged surface (Balamurugan et al., 2008; Choi et al., 1998).

The different analytical methods used for the immobilization of APTs require different substrates (gold, silica, metal oxides, carbon nanotubes, polymers and nanoparticles) due to the read out of the transducers or its application area and thus different immobilization approaches are required.

This step could determine the specificity of a biosensor in detecting any analyte of interest and thus indicating the importance of the optimisation of this step.

2.3.2.4. Assay configuration/format

APTs bioassays can adopt different configurations to transduce bio-recognition events. As APTs have been selected to bind very different targets, ranging from small molecules to macromolecules, various assay configurations can be designed. However, the majority of these configurations are (i) single-site binding and (ii) dual-site binding. In single-site binding of small molecules, the target molecule are inserted in the binding pockets of APTs, leaving almost no space for the interaction of the APT with a second target molecule. In the case of macromolecules, like proteins, their can interact with the APTs through some points, thus the configuration of these assay can be of single ou dual type. In the dual-site binding configuration, a “sandwich” is made using two APTs or one APT and one other affinity molecule, such as an Ab (Song et al., 2008). Futhermore, APT assays can have different formats also according to the method of collecting signal used in the biosensor and the tertiary structures adopted after binding to their target molecules.

2.3.2.5 Applications in Biosensors

APTs can be selected for a wide variety of targets such as proteins, small molecules, cells, antibiotics, and viruses (Stoltenburg et al., 2007), in various types of biodetection approaches from label-free (de-los-Santos-Álvarez et al., 2008) to self-reporting or labelling strategies (Miranda-Castro et al. 2009) using a variety of assay formats (Mascini et al., 2012).

In terms of the analytes in study, specific RNA APTs have been already developed by Gu and Famulok, and four clone RNAs were identified with relatively high affinity for the identification of MC-LR (Gu and Famulok, 2004).

The identification of APTs against bacteria in biosensors is still an emerging field. Unlike conventional SELEX, the specific target is not usually known and a pool of APTs against different targets is often found.

This obliges to carry out further experiments in order to know the exact nature of the final target a step that may be avoided by increasing the expression of the desired protein by genetic modification of the bacteria (Torres-Chavolla and Alocilja 2009).

Until now, eigth APTs have been raised against *E. coli* bacteria. Three of them are RNA molecules against release factor 1 (Sando et al., 2007), O157:H7 specific lipopolysaccharide (Lee et al., 2012a) and unidentified target (So et al., 2008). The latter was used in a reverse transcription PCR amplified immunomagnetic sandwich assay as a detection recognition element (Lee et al., 2009) and a real-time potentiometric assay (Zelada-Guillen et al., 2010). However, these RNA APTs must be handled with extreme care, especially to prevent the attack of ubiquitous endonucleases that degrade it in a few minutes.

Bruno et al. have recently evolved two DNA APTs; one against *E. coli* O111 lipopolysaccharides (Bruno et al., 2008) that was employed in a displacement voltammetric assay (Luo, C. et al., 2012) and the other against EcOMPs (Bruno et al., 2010). These were not integrated in biosensors.

2.3.3 Aptamers versus and Molecular Imprinted Polymers

After presenting the most relevant features of APTs and MIPs aroud biosensors, is it still difficult to know which would be the most suitable biorecognition material for bacterial detection or their toxins. The fact is there is not, yet, a single affinity tool that fits all of the requirements under the present work. Each of the two affinity tools mentioned has its own specific characteristics (Table 2.3) and, depending on the intended application, one tool has more potential than another.

Table 2.3 – Comparison between aptamers and molecular imprinted polymers.

Characteristics	Apatmers	Molecular Imprinted Polymers
Selection	*in vitro*	*in vitro*
Production	synthetic	synthetic (at large scale low cost)
Post-selection modifications	wide variety of options (on sugars, on bases or phosphate groups, on 5' or 3' ends)	possible (must be taken into account during imprint)
Storage	DNA: years at room temperature RNA: several months at -80 ºC	years at room temperature
Binding site	homogeneous	homogeneous or heterogeneous (depending on imprint strategy)
Target molecules	Few low-molecular-mass, mainly macromolecules and whole cells	mainly low-molecular-mass molecules, few macromolecules
Application conditions	physiological, aqueous solution and organic sovents	mainly organic solvents, some aqueous solutions

2.4 Transducers

2.4.1 Electrochemical

The electroanalytical methods provide chemical information about the test solution by measuring a property of electrical nature in an electrochemical cell. These methods offer some advantages over others instrumental methods: (i) allow obtaining rapidly quantitative information from small amounts of analyte; (ii) use low cost equipment and easy to miniaturize, which enhances portability and field analysis; (iii) can provide information about the stoichiometry and equilibrium constants, mass transfer processes, velocity and reversible of reactions; (iv) and do not need complex sample preparation processes. The field of electrochemical biosensors continues to expand based on affordable, simple, and highly selective and sensitive detection inherent with biological binding. Research in this field remains focused on novel sensing strategies with specific attention to the enhancement of selectivity, limits of detection, and response time as well as portability and miniaturization. There are several instrumental strategies in the electroanalytical field, resulting in multiple techniques, such as potentiometric, voltammetry, amperometry, among others. The most disseminated technique along times is Potentiometry, available in any laboratory with a pH meter.

2.4.1.1 Potentiometry

Potentiometry is the field of electroanalytical chemistry in which potential is measured under the conditions of (almost) no current flow. The measured potential may then be used to determine the analytical quantity of interest, generally the concentration of some component of the analyte solution (Brett A. and Brett C., 1993).The potential that develops in the electrochemical cell is the result of the free energy change (ΔG) that would occur if the chemical phenomena were to proceed until the equilibrium condition (equation 2.1) has been satisfied.

$$\Delta G = -nFE, \tag{2.1}$$

in which E is the maximum potential between two electrodes, F is Faraday's constant (1F = 96,485 C mol^{-1}) and *n* is the number of electrons exchanged.

For electrochemical cells that contain and anode and a cathode, the potential difference between the cathode electrode potential and the anode electrode potential is the potential of the electrochemical cell. If the reaction is conducted under standard state conditions, this equation allows the calculation of the standard cell potential.

When the reaction conditions are not standard state the Nernst equation (equation 2.2) to determine the cell potential should be used.

$$E_{cell} = E^{\circ} - \frac{RT}{nF} \ln K_{eq}\ , \tag{2.2}$$

where E^0 is the cell potential at standard conditions, R is the universal gas constant (8.314 J/(Kmol)), T is the temperature in kelvins, *n* is the charge of the ion or number of electrons participating in the reaction and K_{eq} is the equilibrium constant.

Physical phenomena which do not involve explicit redox reactions, but whose initial conditions have a non-zero free energy, also generate potential change. An example of this would be ion concentration gradients across a semi-permeable membrane. This can also be potentiometric phenomena, and is the basis of measurements that use ion-selective electrodes (ISEs) (Buck and Lindner, 1994; Ciobanu et al., 2007).

ISEs are characteristically electrodes that exhibit high selectivity to a particular ion by membranes that incorporate ions by complexation, crystallization or ion exchange processes.

They provide a stable potential at the interface electrode/solution and should be combined with a reference electrode to form an electrochemical cell, Figure 2.11. The need for a reference electrode comes from the inability to measure directly the potential of a single electrode. The indicator electrode immersed in the test solution is linked through a salt bridge, to the reference, in order to measure the electromotive force (emf) of the cell.

The emf of the cell is thus the algebraic difference of the potentials of the two electrodes. The potential of the reference electrode must remain constant, unvarying for the duration of an experiment, in order to provide a stable potential that is not affected by the solution environment. The reference electrode potential should be reversible, permitting a potential to be calculated from the Nernst equation, as well as have the capability to recover its potential after stress. The Ag/AgCl reference electrode is the most regularly used reference electrode due to its simplicity and inexpensive design. The Ag/AgCl reference electrode is constituted by a silver wire with an electrolytic coating of a thin layer of silver chloride. The wire is immersed in a solution of potassium chloride of known concentration, saturated with AgCl; see Figure 2.11, (Smith and Stevenson, 2007).

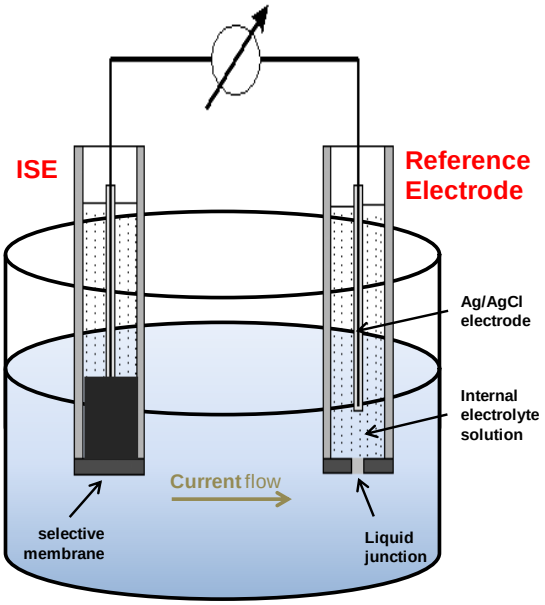

Figure 2.11 – Electrochemical cell constituted by an ion selective electrode and a silver/silver chloride reference electrode.

ISEs offer high signal stability over time and respond over a wide range of concentrations. Moreover, they are sufficiently selective and easy to operate and can easily be constructed in the laboratory. It should also be noted the low cost of the detectors and the equipment involved. Thus, the time and cost of each analytical determination with ISEs are currently quite low.

The membranes of ISEs must have low solubility, electrical conductivity and selective reactions with the target analyte (Buck and Lindner, 1994; Gründler, 2007). Membranes with mobile local exchangers are named non-crystalline and consist of three basic components: an ion exchanger, a mediator solvent and an incorporation matrix. The exchanger is the material responsible for the electrochemical response of the electrode and can be positive or negatively charged or neutral. The incorporation matrix is based on polymer that should have rubbery properties at room temperature, usually in result of the presence of a mediator plasticizer solvent (Stefan and Aboul-Einen, 1999).

The selective membranes are used since the beginning of ISEs as a physical separation between two compartments: one with the sample solution and the other an inner reference solution. The resulting ISE is of conventional configuration and is said to have an internal reference solution. In alternative, the selective membrane may be applied over a solid contact of low electrical resistance (Amemiya, 2007). This contact may be of metal or carbon. The solid support for the selective membrane gives ISEs of more compact configuration and easy construction. They are also of easy handling and longer lifetimes.

In this work, the selective membrane was applied over a solid contact made of a carbon (comprising a mixture of graphite with non-conductive epoxy). The solid support was introduced in a Perspex tube over a copper contact connected to an electrical wire, Figure 2.12. The selective membrane is than applied over the solid carbon support.

Compared to internal standard solution ISEs, the solid contact electrodes have a higher mechanical stability and longer lifetimes. The absence of the internal standard solution also simplifies handling the electrode and allows the recovery of electrode body for other applications, after complete removal of the former membrane. Also, these electrodes used small amounts of selective membrane.

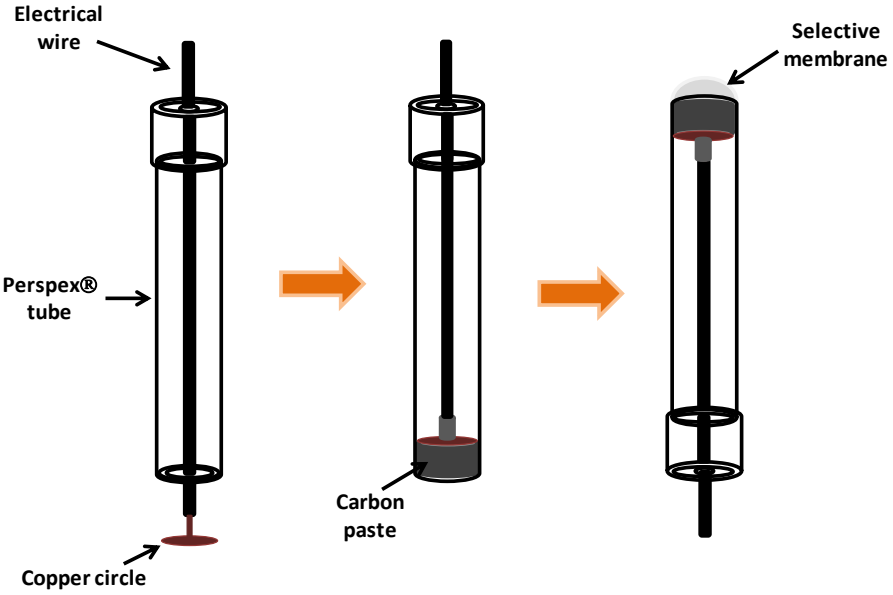

Figure 2.12 – Scheme of the ion selective electrode construction used in this work.

Other kinds of ISE's exist, including the electrochemical materials in crystalline or rubber-based membranes, built in homogeneous or heterogeneous environment (Moreira, 2009).

The indicator electrodes can also be metallic, being classified as inert, first or second class, according to the type of metal and its coatings. Inert indicator electrodes are made of gold or platinum. First class electrodes consist of a metal immersed in a solution containing ions of the same kind, and are used to measure the activity of the metal ion in the solution. Only silver and mercury electrodes are first class. Second class electrodes consist of a metal coated with a poorly soluble salt or a complex of the metal immersed in a solution containing an ion that forms a salt or a complex. These are used to measure the activity of the ligand or anion, being use of Ag/AgCl to determine Cl^- a classical example (Godinho, 2005).

Overall, ISEs most often used rely on selective PVC membranes that include a suitable ionophore for analyte recognition, being this material at the core of the electrode performance.

2.4.1.2 Electrochemical impedance spectroscopy

EIS is an electroanalytical technique used in the analysis of electrochemical processes that occur at the interface electrode/solution. This method allows the identification and determination of parameters of an elaborated model based on the frequency response of the electrochemical system in study.

In EIS, a small amplitude sinusoidal voltage signal is applied to an electrochemical cell and as a result a measurable current response is obtained. The changes that occur at the electrodes are exhibit as the resistive or capacitive properties of materials, also called as impedance (Park and Yoo, 2003). Impedance is calculated as the ratio of the system voltage phasor, U (jω), and the current phasor, I (jω), generated by a frequency analyzer that is connected to a potentiostat (equation 2.3).

$$Z(j\omega) = \frac{U(j\omega)}{I(j\omega)} = Z_{real}(\omega) + j\, Z_{imagine}(\omega), \quad (2.3)$$

where j= $(-1)^{1/2}$, w= 2πf (rad s^{-1}) and f is the frequency (Hz). Faradaic impedance is generally conducted in the presence of a redox probe.

Representations of the electrified interface model (first proposed by Helmholtz) can be described as an equivalent circuit, also called a Randles circuit (Randles, 1948), constituted by a double-layer capacitor (C_{dl}) in parallel with a charge transfer resistor (R_{et}) and a Warburg impedance (Z_W), connected in series with a resistor that measures the resistance of the electrolyte solution (R_s), Figure 2.13. The Faradaic impedance is composed of Z_w which represents the diffusion of the redox probes in solution while R_{et} is the interfacial electron transfer resistance. In the presence of a redox probe, the dielectric and insulating features resulting from biomolecular interactions at electrode/electrolyte are represented by C_{dl} and R_{et} components. Depending on the types of electrochemical reactions involved at the interface, the equivalent circuit can take other configurations (Katz and Willner, 2003; K'Owino and Sadik, 2005; Park and Yoo, 2003).

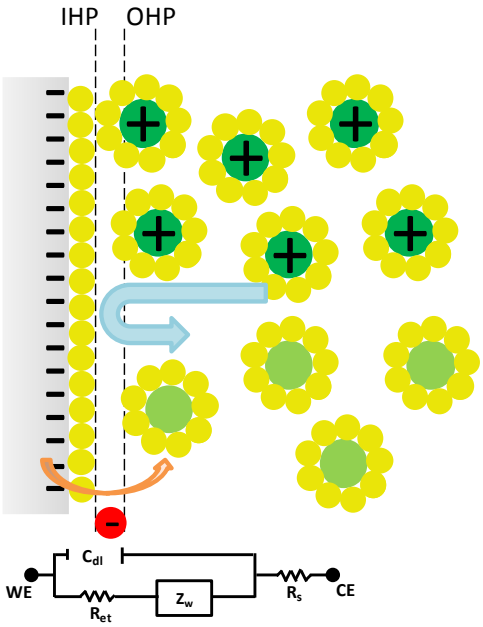

Figure 2.13 – Randles equivalent circuit representation with the electrified interface. WE: working electrode; CE: counter electrode; R_s: solution resistor; R_{et}: electron transfer resistor; C_{dl}: double layer capacitor; Z_W: Warburg impedance; IHP and OHP are inner and outer Helmholtz planes, adapted from (Park and Yoo, 2003).

Impedance changes may be quantified through C_{dl}. C_{dl} is the product of the dielectric constant (ε), the permittivity of free space (ε_0) and the ratio between the electrode area (A) and the monolayer thickness (δ). The capacitance of the modified electrode is inversely proportional to the thickness of the dielectric distance. A change in thickness of the electrode material manifests as a corresponding change in capacitance.

These changes may equally be reflected by increases in R_{et}. while R_{et} controls electron transfer characteristics of the redox probe at the electrode surface, the formation of an insulating layer resulting from the interactions of a macromolecule with the binding associate will retard the flow of electrons to the electrode surface and provide increased electron transfer resistance (Katz and Willner, 2003; K'Owino and Sadik, 2005; Park and Yoo, 2003). A schematic illustration of Faradaic impedance spectra in the form of Nyquist (A) and Bode (B) plots are presented in Figure 2.14.

The Nyquist plot has a semicircle segment, observed at high frequencies, that corresponds to electron-transfer limited process and a straight-line segment that represents diffusion limited electron transfer process at low frequencies.

In Nyquist plot of Figure 2.14 (a) represents a modified electrode with minimum R_{et} and where diffusion of redox probe molecules to the electrode surface is more prominent, (b) represents modified electrode whose impedance is controlled by the diffusion of redox molecules to the electrode surface and (c) represents a modified electrode with a dense layer of insulating material limiting the diffusion of redox probes to the electrode surface.

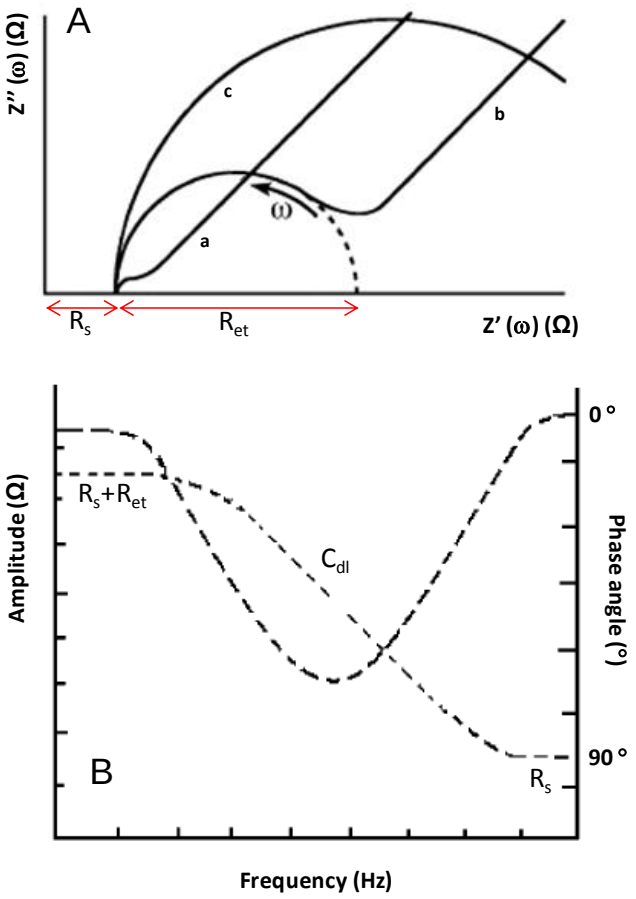

Figure 2.14 – Representation of Nyquist (A) and Bode (B) plots. R_s: solution resistor; R_{et}: electron transfer resistor; C_{dl}: double layer capacitor; adapted from (Katz and Willner, 2003).

The impedance at the electrode surface is controlled by the R_{et} (Katz and Willner, 2003; K'Owino and Sadik, 2005; Park and Yoo, 2003). R_s and R_s+R_{et} can be extracted from the intercept of the semicircle with the Z'(ω) axis at the respective high and low frequency regions of the curve. Thus, the diameter of the semicircle corresponds to R_{et} and its size increases with the thickness of the dielectric layer (δ) and can be used to evaluate the kinetics of biolayer formation.

On the other hand, R_s remains constant in spite of the changes occurring at the electrode surface. Impedance data could also be represented as Bode plots in which the absolute values of amplitude and phase angle are plotted against the frequency (Katz and Willner, 2003; K'Owino and Sadik, 2005; Park and Yoo, 2003).

The superiority of EIS over other electroanalytical techniques is the use of very small amplitude voltage signals without significantly disturbing the properties being measured. A small alternating current voltage perturbations cause variations in impedance in a way that is related to the properties of the liquid or solid under investigation. This may be due to the physical structure of the material, chemical processes within it or to a combination of both. Consequently, EIS is constantly used as a non-destructive technique for providing accurate and repeatable measurements regarding surface conditions such as adsorption and desorption processes at electrode surfaces.

2.4.2 Optical

The general structure of a classical, cylindrically symmetric, glass-based optical fibre comprises a core, a cladding and a jacket. Light propagates mainly in the core, due to the refractive index difference between core and cladding, see Figure 2.15.

The jacket (usually acrylate) has two main functions: (i) to absorb all cladding light, which is not properly guided; and (ii) to protect the otherwise naked glass from atmospheric interactions, which can compromise the mechanical strength of the fibre. (Culshaw and Dakin, 1997; Lopez-Higuera, 2002; Snyder and Love, 1983).

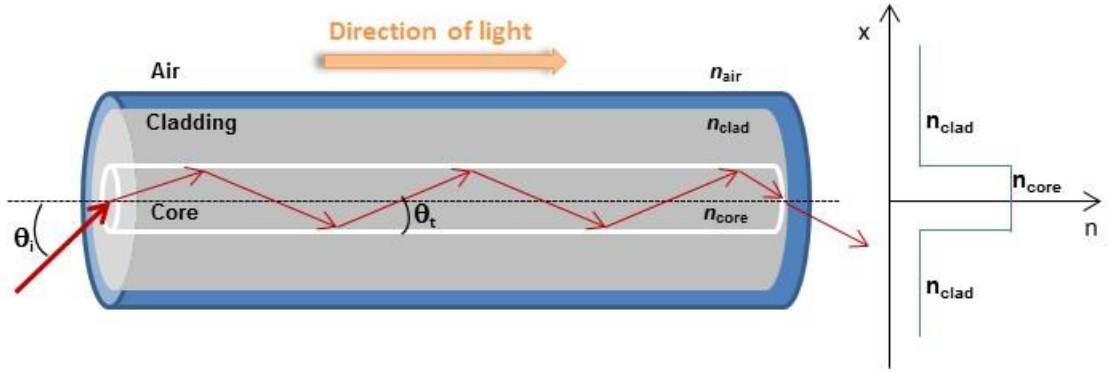

Figure 2.15 - Basic structure and refractive-index profile of a step index optical fiber. θi: incidence angle; θt: transmitted angle; n: refractive index.

Propagation of light in optical fibres can be described using geometrical optics. Consider a meridional light ray (a ray that crosses the axis of symmetry of the cylindrical fibre) which forms an incident angle (θ_i) with the core/cladding interface and that the cladding refractive index is lower than core ($n_{clad} < n_{core}$), see Figure 2.15, light guidance along the fibre core must satisfy the condition for total internal reflection in the core/cladding interface. Below this value no total internal reflection is obtained (Hecht, 2003). Critical angle can be calculated by equation 2.4.

$$\theta_c = arcsin(\frac{n_{clad}}{n_{core}}) \quad (2.4)$$

The light beams whose incidence angle θ_i satisfy the condition ($\theta_c < \theta_i < \pi/2$) are called guided modes. When $\theta_i < \theta_c$, the light beams are not confined and are called radiation modes. However, phase considerations dictate the only a few discrete angles can endure long distance propagation. These solutions correspond to the fibre propagation modes.

The number of guided modes and transverse amplitude profiles depend on the details of the fibre structure (guide geometry) as well as on the transmitted light wavelength and on the variation of the core refractive index (Okamoto, 2006). Single mode fibres are usually based on a silica cladding and a Ge-doped silica core and support only one guided mode (Boudrioua, 2009). This type of fibre has very small core – typically dimensions are 8 μm and 125 μm for core and cladding diameters, respectively.

Optical fibre sensors offers numerous operational benefits as they can operate in high and variable electric field environments, are chemically and biologically inert and its packaging is relatively easy due to the small size and weight.

Optical fibre biological sensing is based on the specific binding between biorecognition molecules immobilized on the sensor surface and the targeted biological species, which causes a change in the effective thickness or density of the surface of fiber and consequently a change (intensity, wavelength, polarization, and phase) parameter on the optical signal. Light modulation must be processed into an optical intensity signal at the receiver, which subsequently performs a conversion into an electric signal. Moreover, optical fibre sensors can be operated over very long transmission lengths, so that the sensor can easily be placed kilometres away from the monitoring local and data can be reliable transmitted between the two.

Adding to this, it is also possible to perform multiplexed measurements using large arrays of remote sensors, operated from a single optical source and detection unit, with no active optoelectronic components located in the measurement area, thereby retaining electromagnetic passiveness and environmental resistance (Culshaw and Dakin, 1997; Lopez-Higuera, 2002).

Optical biosensing typically requires that radiation interacts with the external media, either directly with a given analyte (label-free) or by means of an auxiliary indicator dye (labeling-based detection).

In this last procedure, either target molecules or biorecognition molecules are labeled with either fluorescence or light absorbing markers in order to detect and quantify the presence of a specific sample molecule of interest. In the label-free procedure, the target molecules are not labeled or modified, and their presence is revealed by methods such as refractometry. Label-free techniques are very attractive because target molecules are not labeled or altered, being detected in its natural form. Also, this technique is relatively easy and cheap to perform, and allows quantitative measurement of molecular interaction. Label-free methods require the design of sensing layers that measures refractive index changes induced by molecular interactions, which is related to the sample concentration or surface density. This can be achieved by using biomolecules with a natural affinity to the target, or chemical species having analyte specific ligands (Fan et al., 2008; Jorge, 2010).

Due to all these favourable characteristics, fibre sensing has been the focus of substantial research and development along the years and many solutions for biosensing field applications are becoming available.

In the following sections, two of the most relevant fiber refractometric platforms based on evanescent field interactions and capable for label free biochemical sensing will be presented.

2.4.2.1 Fibre Fabry-Perot Interferometry

The Fabry-Perot interferometer is based on the interference of multiple reflected beams and is a key element of considerable importance in nowadays optics (Hecht, 2003). Despite its simple configuration, it has been shown that it is a powerful tool in many applications. It is used in precise measurements of wavelength, analysis of ultra-narrow spectral lines, determination of the refractive index of glasses and metric calibrations.

Besides playing an important role in spectroscopy with high spectral resolution, it is also the base configuration for various laser cavities (Zheng et al., 2009).

A Fabry-Perot interferometer consists of a pair of identical plane surfaces, with plane-parallel internal faces of reflectivity, separated by a uniform spacing (Figure 2.16). Surfaces are based in semi-transparent mirrors, quartz plates or even optical fibres with cuts perpendicular to the longitudinal direction of propagation. The surfaces can also have high reflecting coatings, which are normally fabricated by thin-film deposition processes (Elderin et al., 1991; Hecht, 2003).

The distance, d, between surfaces may vary from some microns to some centimeters, but it can have several meters when used as a resonant cavity of a laser. Normally, the medium between reflectors is air; however, in the general case, the medium have a refractive index *n*. The internal faces of the reflectors are responsible for the interference of multiple beams inside the cavity, while the external faces are normally built with a very small angle relative to the internal parallel face. Thus, it is possible to eliminate interferences that might appear between reflected beams in both external and internal surfaces (Hecht, 2003).

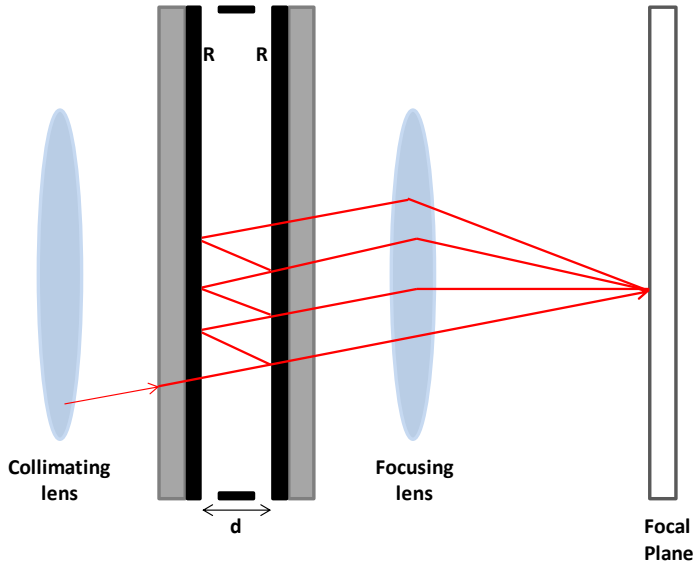

Figure 2.16 – Fibre Fabry-Perot interferometer scheme. R: parallel internal faces of reflectivity; d: distance between mirrows.

A fibre Fabry-Perot Interferometer (FFPI) have been formed in a variety of fibre optic configurations due to the relative ease of fabrication. FFPI sensors can be classified as extrinsic or intrinsic optical fibre sensors. An extrinsic sensor, in its most simple way, uses an air cavity between two optical fibres with cleaved ends (Lee et al., 2012b).

The air cavity is the sensing medium and the input fibre serves only as an optical channel that guides the light and back-reflects the encoded information to the detector. Alternately, in the intrinsic sensor type, the parameter aimed for measurement interacts directly with the fibre, by changing the optical properties of the guided light, i.e., the sensing element is the optical fibre itself. Typical examples of intrinsic FFPIs make use of a pair of splices (Lee and Taylor, 1988), a pair of tapers (Brophy et al., 1993) or two consecutive identical fibre Bragg grating structures (Du et al, 1999).

Another possible configuration of a FFPI sensor is to coat a fibre tip with a thin film. In this case, a Fabry-Perot cavity is formed by the film, and the cavity length is the thickness of the film. The working principle relies on the on two-wave interference based on the fibre tip interaction concept. When light travels along the sensor head, part is back-reflected on the fibre/film interface (R1); the remaining light propagates through the film (L) and a second reflection occurs at the film/external medium interface (R2) – Fresnel reflection.

R1 is the reference reflection while R2 is the sensing reflection. These two light waves interfere constructively or destructively based on the path length traversed by the sensing reflection, and travel back to the detector, see Figure 2.17.

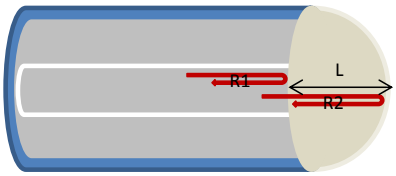

Figure 2.17 – Scheme of the fibre Fabry-Perot interferometer sensing head used in this work. R1 and R2: reflected waves; L: cavity length.

For an FFPI with a cavity length L, the constructive interference condition is given by

$$\lambda = 2nL\cos\theta_t \tag{2.6}$$

The fringe spacing of the Fabry-Perot channelled spectrum is given by

$$\Delta\lambda = \frac{\lambda^2}{2nL}, \tag{2.7}$$

where λ is the operating central wavelength and *n* is the refractive index.

The advantages of FFPI sensors include high sensitivity, ease of fabrication, localization and lead insensitivity since light is transmitted to and from the sensor through the same fibre. Based on phase modulation, FFPI sensors are immune to optical power fluctuations.

Fringe patterns from a Fabry-Perot cavity are modulated by environmental factors such as temperature, pressure, humidity, vibration, position and others. Monitoring the changes in the optical cavity allows measurands to be investigated with high accuracy and resolution.

2.4.2.2 Long-period gratings

LPGs are one of the most popular fibre optic refractive index sensor and it has been widely used for chemical and biological sensing. LPGs are diffraction structures where the refractive index of the fibre core is modulated, with a period between 100 μm to 1000 μm that is induced in the optical fiber using different techniques such as UV laser irradiation, CO_2 laser irradiation, electric-arc discharge, mechanical processes and periodic etching (James and Tatam, 2003). This periodic perturbation satisfies the phase matching condition between the fundamental core mode and a forward propagating cladding mode of an optical fibre. Thereby, in LPGs, the core mode couples into the cladding modes of the fibre, resulting in several attenuation bands centered at discrete wavelengths in the transmitted spectrum, where each attenuation band corresponds to coupling to a different cladding mode. The spectral width of the resonant dip varies from few nanometers up to tens of nanometers depending on the physical length of the grating.

LPGs are intrinsically sensitive to external refractive index, exhibiting changes in the position of the resonance wavelength (λ_R). The resonant coupling of light to a particular cladding mode is given by the phase matching condition (Erdogan, 1997).

$$\lambda_R^m = (n_{eff,core} - n_{eff,clad}^m)\Lambda \,, \tag{2.8}$$

where Λ is the grating period, and $n_{eff,core}$ and $n_{eff,clad}$ are the effective indexes of the guided modes and m^{th}-cladding mode, respectively. Following the phase matching condition, a change in the surrounding refractive index (SRI) will induce a shift in the resonance wavelength due to the variation of the $n^m_{eff,clad}$ which is dependent on the external refractive index. Figure 2.18 illustrates the principle of operation of LPGs.

In LPGs, the core guided mode couples into the cladding modes of the fibre, resulting in attenuation bands centred at specific wavelengths in the transmitted spectrum. A small fraction of the cladding mode, also known as evanescent field, travels outside of the optical fibre, interacting with the external medium; any variations in the refractive index of the outer region will affect the effective refractive index of the cladding modes and, thus, will change λ_R.

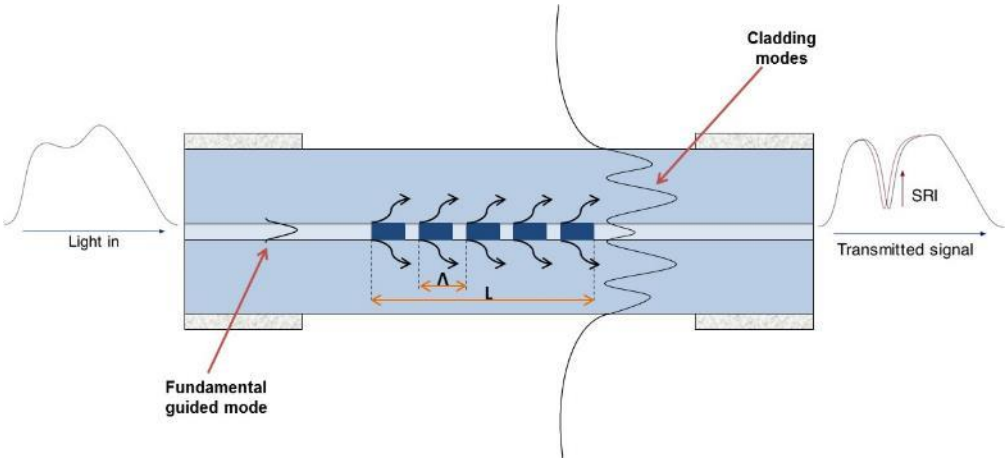

Figure 2.18 – Scheme of fibre long period grating with the representation of the fundamental and cladding modes, the input and output signal and the period (Λ) and the length (L) of the long period grating. SRI: surrounding refractive index.

Fiber optic biochemical sensors based on evanescent field configuration rely on the use of sensing layers deposited on the sensitive surface that experience a refractive index change in presence of an analyte. This can be achieved by using biomolecules with a natural affinity to the target, or chemical species having analyte specific ligands. When exposed to an analyte, a chemical/biochemical interaction takes place within this layer or on its surface. In this case, only a portion of the optical radiation which comes out of the sensor (evanescent field) is modulated, depending on the optical thickness of the interaction region.

LPGs show great sensitivity to the SRI, but at the same time to temperature. The measurement of the refractive index is strongly dependent of the temperature due to thermo-optic coefficient. Thus, measurement and compensation of this parameter is an important issue for this kind of platforms. This could be appointed as the main disadvantage of this devices. A number of techniques have been proposed in order to eliminate temperature cross-sensitivity mainly based on the use of a second grating sensitive only to temperature (Baldini et al., 2012; Jesus et al., 2012).

LPGs has been widely used for biosensing; several works were reported regarding antibody-antigen interaction (Pilla et al., 2009; Kim et al., 2005; Yang et al., 2007; Wang et al., 2009), DNA hybridization (Cooper et al., 2011; Chen et al., 2007; Jang et al., 2009; Hine et al., 2009) and specific bacteria detection (Smietana et al., 2011).

2.5 Applications

2.5.1 *Escherichia coli* emerging (bio)sensing technology

Pathogens transmitted via water are mostly of faecal source (Ashbolt, 2004). Pathogenic *E. coli* strains are responsible for infection of the enteric, urinary, pulmonary and nervous systems. *E. coli* infection is usually transmitted through consumption of contaminated water or food. The routine detection methods for these microorganisms are based on colony forming unit (CFU) count requiring selective culture, or biochemical and serological characterizations. Although bacterial detection by these methods is sensitive and selective, days are needed to get a result. Besides, these methods are costly and time consuming.

Because of its great importance as faecal contaminant indicator in waters, the development of biosensors to detect and quantify *E. coli* has been extensible studied and there are a very large number of new methods and improvements to reference methods (Choi et al., 2007; Deobagkar et al., 2005; Gau et al., 2001; Liu & Li, 2002; Simpson & Lim 2005; Tang et al., 2006; Yáñez et al., 2006; Yoo et al., 2007; Yu et al., 2009). Table 2.4 described the most recent emerging technologies for the *E. coli* monitoring in waters with emphasis to the capture and transduction methods used, linear range and limit of detection found.

The immunological methods are the most widely used as recognition method, but nucleic acid capture probe are starting to gain some importance in the field. The use of APTs instead of Abs as capture probes are increasing due to the advantages they present against Abs. Despite its high specificity and affinity, aptamers offer higher chemically stability and can be selected in vitro for a specific target, ranging from small molecules to large proteins and even cells. Moreover, once selected, APTs can be synthesized with high reproducibility and purity from commercial sources.

Table 2.4 – Latest emerging techniques for the detection of *Escherichia coli* in waters.

***E. coli* Strain**	**Methods**		**LOD**	**Detection range**	**References**
	Capture	**Transduction**			
O157:H7	Immunological	Electrochemical	10^2 CFU mL^{-1}	10^2 - 10^5 CFU mL^{-1}	Yu et al., 2009
O157:H7	Immuno-nucleic acid sandwich	Electrochemical	0.5 nmol L^{-1}	-	Wang et al., 2009
ATCC 8739	Nucleic acid	Optical	30 CFU mL^{-1}	30 - $3x10^4$ CFU mL^{-1}	Bruno et al., 2010
unspecified	Nucleic acid	Electrochemical	50 cells mL^{-1}	$1.0x10^2$ - $2.0x10^3$ cells mL^{-1}	Geng et al., 2011
K12	Immunological	Optical	10^4 CFU mL^{-1}	10^2 - 10^6 CFU mL^{-1}	Duplan et al., 2011
O157:H7	Immunological	Electrical	61 CFU mL^{-1}	0 - 10^4 CFU mL^{-1}	Luo et al., 2010
O157:H7	Nucleic acid	Mechanical	$1.2x10^2$ CFU mL^{-1}	10^2 - 10^6 CFU mL^{-1}	Chen et al., 2008
ATCC 15597	Immunological	Optical	10 CFU mL^{-1}	10 - 10^7 CFU mL-1	Yoon et al., 2009
unspecified	Immunological	Optical	8 CFU mL^{-1}	10^1 – 10^4 CFU mL-1	Guven et al., 2011
several	Nucleic acid	Optical	15 culturable *E. coli* $(100\ mL)^{-1}$	3·5 and 14·5 viable E. coli $(100\ mL)^{-1}$	Baudart & Lebaron, 2010
DSM 30083	Enzimatic	Optical	7 CFU mL^{-1}	100 – 10^8 CFU mL^{-1}	Wildeboer et al., 2010
ACTT 25922	Nucleic acid	Mechanical	8 Cells $(800\ mL)^{-1}$	-	Sun et al., 2009

E. coli Strain	Methods		LOD	Detection range	References
	Capture	Transduction			
K12	Immunological	Optical	100 CFU mL^{-1} (33% Ab coverage) 10 CFU mL^{-1} (50% and 100 % AB coverage)	-	Kwon et al., 2010
BD2399	Immunological	Mechanical	10^5 CFU mL^{-1}	$5x10^4$ - $5x10^9$ CFU mL^{-1}	Fu et al., 2010
DH5α	Nucleic acid	Electrochemical	5 CFU mL-1	$1x10^3$ - $5x10^5$ CFU mL^{-1}	Li et al., 2011
ATCC 35218	Immunological	Optical	< 1000 CFU mL-1	10^1 – 10^8 CFU mL^{-1}	Bharadwaj et al., 2011
unspecified	TGA	Optical	10^2 CFU mL^{-1}	10^2 – 10^7 CFU mL^{-1}	Xue et al., 2009
O157:H7	Immunological	Optical	$1.8x10^3$ CFU mL^{-1}	$1.8x10^3$ – $1.8x10^8$ CFU mL^{-1}	Park et al., 2008
O157:H7	Immunological	Optical	$1x10^4$ cells mL^{-1} (single) $3x10^3$ cells mL^{-1} (multi)	$1x10^4$ - $1x10^6$ cells mL^{-1} (single) $3x10^4$ - $3x10^6$ cells mL^{-1} (multi)	Wolter et al., 2008
O157:H7	Immunological	Optical	$1.8x10^4$ cells mL^{-1}	$8.5x10^4$-$3.7x10^6$ cells mL^{-1}	Karsunke et al., 2009
O157:H7	Polymeric	Mechanical	$2x10^2$ cells mL^{-1}	$2x10^2$ - $3x10^6$ cells ml^{-2}	Huang et al., 2008
O157	Nucleic acid	Electrical	1 pg μL^{-1} DNA molecules	1 - 10 pg μL^{-1}	Subramanian et al., 2012
O157:H7	Immunological	Electrical	67 CFU mL^{-1}	10^1 –10^4 CFU/mL	Luo Y. et al., 2012
O111	Nucleic acid	Electrochemical	112 CFU mL^{-1}	10^2 -10^6 CFU mL^{-1}	Luo C. et al., 2012
K12 ER2925	Immunological	Electrical	10 CFU mL^{-1}	0 - 10^5 cfu mL^{-1}	Huang et al., 2010

CFU: Colony Form Units

Furthermore, APTs often undergo significant conformational changes upon target binding. This offers great flexibility in design of novel biosensors with high detection sensitivity and selectivity (Song et al., 2008).

Bruno et al. described a fluorescence resonance energy transfer (FRET)-APTs assay applied to *E. coli* detection. In this assay 25 reverse and 25 forward aptamer candidate sequences against *E. coli* were tested and compared in order to select the most sensitive to SPR and competitive-FRET analysis (Bruno et al., 2010). An iron oxide (Fe_2O_3) Au core/shell nanoparticle-based electrochemical DNA biosensor was developed for the amperometric detection *E. coli* by Li et al.. The assay doesn't require any amplification step and the lowest detection value found was 5 CFU mL^{-1} of *E. coli* after 4.0 h of incubation (Li et al., 2011). Another aptamer-based biosensor using magnetic particles was reported by (Geng et al., 2011). This work included cobalt NPs and an enrichment process was necessary to found 10 *E. coli* cells mL^{-1} in real water samples by differential pulse voltammetry.

A flow piezoelectric biosensor, based on synthesized thiolated probe specific to *E. coli* O157:H7 eaeA gene was immobilized onto the piezoelectric biosensor surface. Then, DNA hybridization was induced by exposing the immobilized probe to the *E. coli* O157:H7 eaeA gene fragment, resulting in a mass change and a consequent frequency shift of the piezoelectric biosensor. A second thiolated probe complementary to the target sequence was conjugated to the gold nanoparticles to amplify the frequency change of the piezoelectric biosensor. The products amplified from concentrations of 1.2×10^2 CFU mL^{-1} of *E. coli* O157:H7 were detectable by the piezoelectric biosensor (Chen et al., 2008).

Sun et al. described a nano silver indium tin oxide (ITO)-coated piezoelectric quartz crystal electrode using DNA hybridization to detect *E. coli* cells. Neutravidin and a biotinylated probe were loaded at nano silver ITO-coated piezoelectric quartz crystal and binding ratio was assessed.

The binding ratio between the neutravidin and biotinylated DNA probe is increased from 1.00:1.76 of normal piezoelectric quartz crystal to 1.00:3.01 using the nano-Ag-modified electrode, leading to an increase of more than 71% of the binding capacity of neutravidin to biotinylated DNA probes and an enhancement of 3.3 times for binding complementary DNA onto the nano-Ag-modified neutravidin/biotinylated DNA piezoelectric quartz crystal biosensor.

Under the optimized conditions, the detection limit was 0.4 ng/L for DNA PCR products or 8 *E. coli* cells in 800 mL in order to detect a single *E. coli* (Sun et al., 2009).

Magnetoelastic biosensors are based on the principle of change in the frequency of magnetoelastic materials (Nayak et al., 2009). Fu et al. developed a magnetostrictive microcantilever using physical absorption as detection system and an Ab against *E. coli* immobilized onto the surface of the microcantilever to form a biosensor. It was found a detection limit of 10^5 CFU mL^{-1} for a microcantilever with the size of 1.5 mm×0.8mm×35µm (Fu et al., 2010).

Immuno-optical biosensors are largely the most detection systems used and many different approaches are developed. A poly(ethylene glycol) (PEG) hydrogel based microchip with patterned nanoporous aluminum oxide membrane for bacteria fast patterning and detection with low frequency impedance spectrum was reported by Yu et al.. The PEG hydrogel micropatterns on the saline-modified nanoporous alumina surface created controlled spatial distribution of hydrophobic and hydrophilic regions. These microwell arrays were composed of hydrophilic PEG sidewalls and hydrophobic silane-modified aluminum oxide membrane in the bottom. Abs against *E. coli* were added and washed to form the patterns in the microwells. Then, the target bacteria was successfully patterned and captured inside the microwells. The microchip was able to detect bacteria concentrations of 10^2 CFU mL^{-1} (Yu et al., 2009).

Luo et al., 2010 developed a nitrocellulose nanofibers surface functionalized with anti-*E. coli* Abs on the top of silver electrodes Another Ab were coupled with conductive magnetic NPs and incubated with the test sample for target conjugation. After, the purified sample with the conductive label was dispensed on the application pad (a conductometric lateral flow biosensor). After capillary flow equilibrium, the direct-charge transfer between the electrodes was proportional to captured sandwich complex, which could be used to determine the pathogen concentration. The detection time of the biosensor was 8 min, and the detection limit 61 CFU mL^{-1} (Luo et al., 2010).

A microfluidic device with a portable spectrometer and UV to identify the signal intensity at 375 nm was developed by (Know et al., 2010; Yoon et al., 2009). The device fabricated by Kwon et al. was constructed in acrylic using an industrial-grade milling machine eliminating the need for photolithography and internal or external pumping, while the microdevice developed by Yoon was fabricated by standard soft lithography with the poly(dimethyl siloxane) (PDMS).

A hole was made through the PDMS to make a view cell. Two cover glass slides were bonded to the top and bottom slides of a view cell using oxygen plasma asher (Know et al., 2010; Yoon et al., 2009). Two inlets and one outlet were then connected to Teflon tubing. A syringe pump was used to inject anti-*E. coli* conjugated latex particles and *E. coli* target solutions into the microchannel device (Yoon et al., 2009). Both devices presented 10 CFU mL^{-1} as detection limit.

A label-free technique based on evanescent wave absorbance changes at 280 nm from a U-bent optical fiber sensor was reported by Bharadwaj. Bending a decladded fiber into a U-shaped structure enhanced the penetration depth of evanescent waves and hence the sensitivity of the probe. A portable optical set-up with a UV light-emitting diode, a spectrometer and U-bent optical fiber probe of 200µm diameter, 0.75mm bend radius and effective probe length of 1 cm demonstrated an ability to detect less than 1000 CFU mL^{-1} (Bharadwaj et al., 2011).

A method combining immunomagnetic separation and surface enhanced Raman spectroscopy was developed by (Guven et al., 2011). Au-coated magnetic spherical nanoparticles were prepared by immobilizing biotin-labeled anti-*E. coli* Abs onto avidin-coated magnetic nanoparticles and used in the separation and concentration of the *E. coli* cells. Raman labels have been constructed using rod shaped gold nanoparticles coated with 5,5-dithiobis-(2-nitrobenzoic acid) and subsequently with a molecular recognizer. Then 5,5-dithiobis-(2-nitrobenzoic acid)-labeled gold nanorods interacted with the gold-coated magnetic spherical nanoparticle-Ab-*E. coli* complex. The limit of detection value of this method was 8 CFU mL^{-1}.

The enzyme GUD is a specific marker for *E. coli* and MUG a sensitive substrate for determining the presence of *E. coli* in a sample. Wildeboer et al., 2010 described a novel hand-held fluorimeter to directly analyse real samples for the presence of *E. coli*. The miniaturized fluorescence detector reduced the incubation time to 30 min and detects *E. coli* as low as 7 CFU mL^{-1} in river water samples (Wildeboer et al., 2010).

The use of carbon allotropes like graphene is of a great potential in biosensing due to their extraordinary electrical, physical and optical properties. Huang et al. reported a graphene based biosensor to electrically detect *E. coli* bacteria with high sensitivity and specificity. The device has a graphene film immobilized with Abs against *E. coli* and a passivation layer. After exposure to *E. coli* bacteria, the graphene device conductance increased significantly.

The lowest concentration detected was 10 CFU mL^{-1}. The sensor also detected glucose induced metabolic activities of the bound *E. coli* bacteria in real time (Huang et al., 2011).

Some authors used synthetic materials as recognition materials (Huang et al., 2008; Xue et al., 2009). Xue et al. described a thioglycol acid coupled with water-soluble quantum dots as a fluorescence marker for *E. coli* total count. thioglycol acid covalently bound to membrane protein of bacteria cells and after 30 min. fluorescence signal are clean seen at a fluorescent microscope (Xue et al., 2009). Huang et al. also reported a synthetic biosensor with polyurethane as capture probe of *E. coli* cells and a remote-query magnetoelastic system. The resonance frequency of a liquid immersed magnetoelastic sensor, measured through magnetic field telemetry, changed mainly in response to bacteria adhesion to the sensor and the liquid properties of the culture medium. During its growth and reproduction, *E. coli* consumed nutrients from a liquid culture medium that decreased the solution viscosity, and in turn changed the resonance frequency of the medium-immersed magnetoelastic sensor (Huang et al., 2008).

2.5.2 Microcystin-LR emerging (bio)sensing technology

Current standard methods to monitor MC-LR require sophisticated and expensive procedures and specific laboratorial conditions that take long time to reach the intend result. Within that time the contamination can move/spread out, while users of recreational waters and possible consumers are at risk of contracting serious infections. A huge number of novel methods and techniques have been developed recently for MC-LR monitoring in water. They are presented in Table 2.5.

Optical immuno-based techniques are by large the most widely techniques that have been developed for the detection of MCs.

The chemiluminescence sensing technique used in microbial biosensors relies on the generation of electromagnetic radiation as light by the release of energy from a chemical reaction using synthetic compounds (highly oxidized species) which respond to the target analyte in a dose-dependent manner (Hu et al., 2008; Lindner et al., 2009; Su et al., 2011). Lindner et al. reported a rapid immunoassay for sensitive detection of MC-LR using a portable chemiluminescence multichannel immunosensor.

Table 2.5 - Latest emerging techniques for the detection of microcystin-LR in waters.

Methods		Microcystins	LOD ($\mu g\ L^{-1}$)	Detection range ($\mu g\ L^{-1}$)	References
Capture	**Transduction**				
Immunological	Electrochemical	-LR	0.6	up to 10	Wang. et al., 2009
Immunological	Optical	-LR	0.03	0.1-10	Long et al., 2009
Immunological	Optical	-LR -RR	down to 0.1	0.001-30	Sheng et al., 2007
Immunological	Piezoelectric	-LR	0.1 (river) $1.00E^{-3}$ (tap)	1-100	Ding & Mutharasan, 2010
Immunological	Optical	Any	0.024	0.05–10	Hu et al., 2008
Enzimatic	Optical	-LR	1.00E-02	0-100	Almeida et al., 2006
Immunological	Optical	-LR	1.50E-01	0.150-1.6	Pyo & Jin, 2007
Immunological	Electrochemical	-LR	0.10 (MAb) 1.73 (PAb)	10^{-4}-10^{2} (MAb) 10^{-1}-10^{2} (PAb)	Campàs & Marty, 2007
Immunological	Mechanical	-LR	1	1-1000	Xia et al., 2011
Enzimatic	Optical	-LR	1	0-1000	Allum et al., 2008
Immunological	Optical	-LR	0.2	0-10	Lindner et al., 2009
Immuno-Nucleic acid sandwich	Optical	-LR -RR	0.5 0.3	10^{-4} - 2.5	Shi et al., 2012

Methods		Microcystins	LOD (μg L^{-1})	Detection range (μg L^{-1})	References
Capture	**Transduction**				
Enzimatic	Electrochemical Optical	Any	37 2	37-188 -	Campàs et al., 2007
Immunological	Electrochemical	-LR	0.1	0.01-3.16	Zhang et al., 2007
Immunological	Electrochemical	-LR	7.00E-06	$10E^{-6}$-1	Loypraserta et al., 2008
Immunological	Optical	-LR	1	1-100	Xia et al., 2010
Immunological	Optical	-LR	0.05	0.05-1.2	Pyo et al., 2005
Immunological	Optical	-LR	0.05	0-1.6	Pyo et al., 2006
Immunological	Optical	-LR	0.04	0-1000	Long et al., 2010
Immunological	Electrochemical	-LR	1.00E-06	$1.00E^{-6}$-$1.00E^{-4}$	Dawan et al., 2011

The sensor device is based on a capillary ELISA technique in combination with a miniaturized fluidics system and uses chemiluminescence as the detection principle. Minimum concentrations of 0.2 μg L^{-1} MC-LR could be measured in spiked buffer as well as in spiked water samples (Wang et al., 2009a). Hu et al. also presented a chemiluminescence immunosensor based on gold nanoparticles. The immunoassay included three main steps: indirect competitive immunoreaction, oxidative dissolution of gold nanoparticles, and indirect determination for MCs with Au^{3+}-catalysed luminol chemiluminesent system. The method has an extensive working range of 0.05–10 μg L^{-1}, and a limit of detection of 0.024 μg L^{-1} (Hu et al., 2008).

Evanescent wave fiber optic immunosensors have been developed to determine numerous target compounds based on the principle of immunoreaction and total internal reflect fluorescent. They also show potential advantages such as miniaturization, sensitivity, cost-effectiveness, and capability of real-time rapid measurements (Long et al., 2009). A portable trace organic pollutant analyzer based on the principle of immunoassay and total internal reflection fluorescence was developed by Long et al.. The reusable fiber optic probe surface was produced by covalently immobilizing a MC-LR-ovalbumin conjugate onto a self-assembled thiol-silane monolayer of fiber optic probe through a heterobifunctional reagent. The recovery of MC-LR added to water samples at different concentrations ranged from 80 to 110% with relative standard deviation values less than 5% (Long et al., 2009).

Pyo et al. developed a few number of optical immuno-based assays to detect MC-LR: a gold colloidal immunochromatographic strip, a fluorescence immunochromatographic strip and cartridge and a PDMS microchip using a liquid-cord waveguide as optical detectors and a mAb against MC-LR as recognition element. The detection limits found were 0.05 μg L^{-1}, 0.15 μg L^{-1} and 0.05 μg L^{-1}, respectively (Pyo et al., 2005, 2006; Pyo & Jin, 2007).

Optical sensing techniques, and specially integrated in immunoarrays, are particularly powerful tools in high throughput screening to monitoring multiple analytes simultaneously (Long et al., 2010; Su et al., 2011). Long et al. developed an optical fiber-based immunoarray biosensor for the detection of multiple small analytes (MC-LR and trinitrotoluene). These compounds can be detected simultaneously and specifically within an analysis time of about 10 min for each assay cycle.

The limit of detection for MC-LR was 0.04 μg L^{-1}. This compact and portable immunoarray shows good regeneration performance and binding properties, robustness of the sensor surface, and accuracy in the measurement of small analytes which can be considered an excellent multiple assay platforms for clinical and environmental samples (Long et al., 2010).

A suitable disposable type biosensor for on-site monitoring of MC-LR in environmental waters was described by (Zhang et al. 2007). They reported a competitive binding non-separation electrochemical enzyme immunoassay, using a double-sided microporous gold electrode in cartridge-type cells. Mean recovery of MC-LR added to tap water was 93.5%, with a coefficient of variation of 6.6% (Zhang et al., 2007).

Electrochemical detection methods are also commonly used. Campàs et al. developed a highly sensitive using both mAb and pAb against MC-LR. This amperometric immunosensor was compared with colorimetric immunoassay, PPI assay and HPLC. The amperometric immunosensor simplifies the analysis, and offer faster and cheaper procedures than others assays.

Wang et al. described a simple, rapid, sensitive, and versatile ELISA-SWCNT-paper based sensor for detection of MC-LR in waters. This paper described the use of paper saturated with SWCNT embebed in a poly(sodium 4-styrenesulfonate) solution where the Abs are after immobilized. The chronoamperometric detection system was tested and performed a limit of detection (LOD) of 0.6 μg L^{-1} with a linear range up to 10 μg L^{-1} (Wang et al., 2009a).

The use of electrochemical capacitance systems as detection methods in biosensors allows obtaining exceptionally low limits of detection. Loypraserta et al. and Dawan et al. described a label-free immunosensor based on a modified gold electrode incorporated with silver nanoparticles to enhance the capacitive response to MC-LR has been developed. Anti-MC-LR was immobilized on silver nanoparticles bound to a self-assembled thiourea monolayer, and compared with an electrode bare without the modified silver nanoparticles (Dawan et al., 2011; Loypraseta et al., 2008). MC-LR could be determined with a detection limit of 7.0×10^{-6} and 1.0×10^{-6} μg L^{-1} for (Loypraseta et al., 2008) and (Dawan et al., 2011), respectively. Compared with the modified electrode without silver nanoparticles, this assay presented higher sensitivity and lower limit of detection.

The Adda group of MCs is responsible by the infiltration of toxins in the liver cells where MCs irreversibly bind to serine/threonine PP2A and PP1, inhibiting their enzymatic activity (Almeida et al., 2006; Campàs et al., 2007). These enzymes are involved on the dephosphorylation of proteins. Consequently, their inhibition results in hyperphosphorylation and reorganisation of the microfilaments, promoting tumours and liver cancer (Almeida et al., 2006; Campàs et al., 2007). Almeida et al., Allum et al. and Campàs et al. developed enzymatic-based capture probes based on PP1 and PP2A inhibition. Almeida et al. and Allum et al. presented a simple, rapid and reproducible PP1 inhibition colorimetric test, with the first one presenting a detection limit of 1.00×10^{-2} μg L^{-1}. Allum et al. showed an optical fluorometric biosensor based on protein phosphate for the detection of MC-LR or diarrhetic shellfish toxins. The immobilised format described was used to evaluate the potential to translate protein phosphate into a prototype biosensor suitable as a regulatory assay allowing faster throughput than a solution assay and in particular, in assessments of sensitivity and reusability (Allum et al., 2008).

A chronoamperometric biosensor was developed by Campàs et al. also based on the inhibition of the PP2A. The enzyme was immobilized by the use of poly(vinyl alcohol) azide-unit pendant water-soluble photopolymer. The standard inhibition curve has provided a 50% inhibition coefficient (IC50) of 83 μg L^{-1}, which corresponds to a limit of detection of 37 μg L^{-1} (35% inhibition). Real samples were analysed using the developed amperometric biosensor and compared to those obtained by a conventional colorimetric PPI assay and HPLC. The results demonstrated that the developed amperometric biosensor must be used as screening method for MCs detection (Campàs et al., 2007).

A dendritic surfactant for MC-LR detection by double amplification in a QCM biosensor was presented by Xia et al.. For primary amplification, an innovative interface on the QCM was obtained as a matrix by the vesicle layer formed by a synthetic dendritic surfactant. The vesicle matrix was functionalized by a mAb against MC-LR to detect the analyte. The results showed that a detection limit of 100 μg L^{-1} was achieved by the first amplification. A secondary amplification was implemented with anti-MC-LR gold nanoparticles conjugates as probes, which lowered the detection limit for MC-LR to 1 μg L^{-1} (Xia et al., 2011).

A piezoelectric-excited millimeter-sized cantilever sensor was developed by Ding et al. for the sensitive detection of MC-LR in a flow format using mAb and pAb that bind specifically to MC-LR. mAb against MC-LR was immobilized on the sensor surface via amine coupling. As the toxin in the sample water bound to the Ab, resonant frequency decreased proportional to toxin concentration. Positive verification of MC-LR detection was confirmed by a sandwich binding on the sensor with a second Ab binding to MC-LR on the sensor which caused a further resonant frequency decrease (Ding and Mutharasan, 2010).

2.6 Final considerations

This chapter presents a brief review of the existing methods and technologies applied for the assessment of both target analytes in study. A description of the recognition elements used for the new design of biosensors was presented and compared. Several configurations of optical and electrochemical systems were also reviewed with emphasis on the desired characteristic that biosensors should exhibint. Finally a survey of the emerging technologies for the monitoring of MC-LR and *E. coli* was carried out. Of the different approaches described in this chapter, this thesis focused on the design and studied of combined systems of recognition elements and transducers that can be suitable for the routine screening of the desired targets.

References

Abdel-Hamid, I.; Ivnitski, D.; Atanasov, P.; Wilkins, E. 1999. Biosens. Bioelectron. 14, 309–316.

Agriculture Corner. http://www.agricorner.com/e-coli-outbreak-german-farm-in-uelzen-likely-source/, accessed August 20th 2012.

Ajayan, P.M. 1999. Chem. Rev. 99(7), 1787–1800.

Allum, L.L.; Mountfort, D.O.; Gooneratne, R.; Pasco, N.; Goussaind G.; Halle, E.A.H. 2008. Toxicon 52(7), 745-753.

Almeida, V.; Cogo, K.; Tsai, S.M.; Moon, D.H. 2006. Braz. J. Microb. 37, 192-198.

Amemiya, S. 2007. Potentiometric Ion-Selective Electrodes, in: Zoski, C.G. (Ed.). Handbook of Electrochemistry. Elsevier Science, Amsterdam, The Netherlands, pp. 261-292.

American Public Health Association, American Water Works Association, Water Environment Federation. 1998. Standard Methods for the Examination of Water and Wastewaters, 20th Ed., American Public Health Association, Washington, DC.

An, J.; Carmichael, W.W. 1994. Toxicon 32, 1495-1507.

Anderson, L.I.; O'Shannessy, D.J.; Mosbach, K. 1990. J. Chromatogr. A 513, 167–179.

Armon, R.; Starosvetsky, J.; Saadi, I. 2000. J. Sol-Gel Sci. Technol. 19, 289–292.

Ashbolt, N.J. 2004. Toxicology 198, 229-238.

Balamurugan, S.; Obubuafo, A., Soper, S.A.; Spivak, D.A. 2008. Anal. Bioanal. Chem. 390, 1009–1021.

Baldini, F.; Brenci, M., Chiavaioli, F.; Giannetti, A.; Trono, C. 2012. Anal. Bioanal. Chem. 402(1), 109-116.

Banwart, G.J. 1989. Basic Food Microbiology, 2nd Ed., Van Nostrand Reinhold, New York, NY.

Bateman, K.P.; Thibault, P.; Douglas, D.J.; White, R.L. 1995. J. Chromatogr. A 712, 253–268.

Batt, CA. 2007. Science 316, 1579–80.

Baudart, J.; Lebaron, P. 2010. J. Appl. Microbiol. 109(4), 1253–1264.

Bentley, R.; Meganathan, R. 1982. Microbiol. Rev. 46(3), 241–80.

Bharadwaj, R.; Sai, V.V.R.; Thakare, K.; Dhawangale, A.; Kundu, T.; Titus, S.; Verma, P.K.; Mukherji, S. 2011. Biosens. Bioelectron. 26, 3367–3370.

Biju, V.M.; Gladis, J.M.; Rao, T.P. 2003. Analytica Chimica Acta 478, 43–51.

Borck, B.; Stryhn, H.; Ersboll, A.K.; Pedersen, K. 2002. J. Appl. Microbiol. 92, 574–82.

Botes, D.P.; Wessels, P.L.; Kruger, H. 1985. Chem. Soc. Perkin Trans. 1, 2747–2748.

Bouaïcha, N.; Maatouk, I.; Vincent, G.; Levi, Y. 2002. Food Chem. Toxicol. 40, 1677–1683.

Boudrioua, A. 2009. Photonic Waveguides - Theory and Applications, Pierre-Noël Favennec (Ed.), ISTE Ltd and John Wiley & Sons, Inc.

Brett, A.M.O.; Brett, C. 1993. Electrochemistry - Principles, Methods, and Applications. Oxford University Press, New York, USA.

Brinker, C.J.; Scherer, G.W. 1990. Sol-Gel Science, the physics and chemistry of sol-gel processing. Academic Press, San Diego, California, USA.

Brophy, T.J.; Bobb, L.C.; Shankar, P.M. 1993. Elect. Lett. 29(14), 1276–1277.

Bruno, J.G.; Carrillo, M.P.; Phillips, T.; Andrews, C.J. 2010. J. Fluoresc. 20, 1211–1223.

Bruno, J.G.; Carrillo, M.P.; Phillips, T. 2008. Folia Microbiol. (Praha) 53(4), 295-302.

Buck, R.P.; Lindner, E. 1994. International Union of Pure and Applied Chemistry (IUPAC), Pure Appl. Chem. 66(12), 2527-2536.

Cahill, D.; Roben, P.; Quinlan, N.; O'Kennedy, R. 1995. In: Townsend A. (Eds.). Production of antibodies. Encyclopedia analytical science. Academic Press, New York, pp. 2057–66.

Campàs, M.; Marty, J.-L. 2007. Biosens. Bioelectron. 22, 1034–1040.

Campàs, M.; Szydłowska, D.; Trojanowicz, M.; Marty, J.-L. 2007. Talanta 72(1), 179-186.

Carmichael, W.W. 1992. J. Appl. Bacteriol. 72, 445-459.

Centers for Diseases Control and Prevention, National Center for Emerging and Zoonotic Infectious Diseases, Division of Foodborne, Waterborne, and Environmental Diseases. http://www.cdc.gov/ecoli/, accessed August 15th 2012.

Center of excellence for great lakes and Human health. 2011. http://www.glerl.noaa.gov/res/Centers/HABS/western_lake_erie_archive.html, accessed August 14th 2012.

Chen, S.-H.; Wu, V.C.H.; Chuang, Y.-C.; Lin, C.-S. 2008. J. Microbiol. Meth. 73, 7–17.

Chen, X.; Zhang, L.; Zhou, K.; Davies, E.; Sugden, K.; Bennion, I.; Hughes, M.; Hine, A. 2007. Opt. Letters 32, 2541.

Chen, H.-J.; Zhang, Z.-H.; Xie, D.; Cai, R.; Chen, X.; Liu, Y.-N.; Yao, S.-Z. 2012. Electroanal. 24, 2109–2116.

Chianella, I.; Piletsky, S.A.; Tothill, I.E.; Chen, B.; Turner, A.P.F. 2003. Biosens. Bioelectron. 18, 119-127;

Choi, J.W.; Lee, W.; Lee, D.B.; Park, C.H.; Kim, J.S.; Jang, Y.H.; Kim, Y. 2007. Environ. Monit. Assess. 129, 37–42.

Choi, Y.H.; Liu, F.; Kim, J.-S.; Choi, Y.K.; Park, J.S.; Kim, S.W. 1998. J. Control. Release 54, 39–48.

Ciobanu, M.; Wilburn, J.P.; Krim, M.L.; Cliffel, D.E. 2007. Fundamentals, in: Cynthia G. Zoski (Ed.). Handbook of Electrochemistry. Elsevier, Amsterdam, pp. 1-28.

Cooper, K.L.; Bandara, A.B.; Wang, Y.; Wang, A.; Inzana, T.J. 2011. Sensors 11(3), 3004-3019.

Cohen, T.; Starosvetsky, J.; Cheruti, U.; Armon, R. 2010. Int. J. Mol. Sci. 11, 1236-1252.

Culshaw, B.; Dakin, J. 1997. Optical fiber sensors, Artech House, vol. 4.

Cupples, A.; Xagoraraki, I.; Rose, J.B. 2010. New Molecular Methods for Detection of Waterborne Pathogens, in: R. and J.-D. Gu (Eds.). Environmental Microbiology. Mitchell, John Wiley & Sons Inc., 2nd Ed., pp. 57-94.

Dahlmann, J.; Luckas, B. 2010. Food and environment, AB SCIEX, 1830410-01.

Dawan, S.; Kanatharana, P.; Wongkittisuksa, B.; Limbut, W.; Numnuam, A.; Limsakul, C.; Thavarungkul, P. 2011. Anal. Chim. Acta 699(2), 232-241.

de-los-Santos-Álvarez, N.; Lobo-Castañón, M.J.; Miranda-Ordieres, A.J.; Tuñón-Blanco, P. 2008. TrAC- Trend. Anal. Chem. 27(5), 437-446.

Deobagkar, D.D.; Limaye, V.; Sinha, S.; Yadava, R.D.S. 2005. Sensor. Actuator. B 104, pp. 85–89.

Díaz-García, M.E.; Laíno, R.B. 2005. Microchim. Acta 149, 19-36.

Ding, Y.; Mutharasan, R. 2010. Environ. Sci.Technol. 45(4), 1490-1496.

Donald, J.C. 1988. Angew. Chem. Int. Ed. in Engl. 27(8), 1009–20.

Du, W.C.; Tao, X.M.; Tam, H.Y. 1999. Technol. Lett. 11(1), 105–107.

Duplan, V.; Frost, E.; Dubowski, J.J. 2011. Sensor. Actuator. B-Chem. 160, 46– 51.

Earth Project Management. http://www.earthpm.com/tag/cyanobacteria/, accessed August 14th 2012.

Eitan, A.; Jiang, K.; Dukes, D.; Andrews, R.; Schadler, L.S. 2003. Chem. Mater. 15, 3198-3201.

Elderin, C.A.; Knoesen, A.; Kowel, S.T. 1991. J. Appl. Phys. 69(6), 3676- 3680.

Ellington, A.D.; Szostak, J.W. 1990. Nature 346, 818–822.

Ercole, C.; Del Gallo, M.; Mosiello, L.; Baccella, S.; Lepidi, A. 2003. Sens. Actuat. B-Chem. 91, 163–8.

Erdogan, T. 1997. J. Opt. Soc. Am. A 14(8), 1760-1773.

European Comission, Council Directive 98/83/EC of 1998, November 3rd. On the quality of water intended for human consumption, In: Official Journal of the European Communities L330, pp. 32-54.

European Comission, Directive 2000/60/CE of 2000, October 23th. Water Frame Directive, In: Official Journal of European Commission L327/1.

European Comission, Directive 2006/7/EC of the European Parliament and of the Council of 2006, February 15th, Concerning the management of bathing water quality and repealing Directive 76/160/EEC, In: Official Journal of the European Communities L64, pp. 37-51.

European Environmental Agency. 2010. The European environment, State and outlook 2010, Water resources: quantity and flows, In: Publications Office of the European Union, Luxembourg, (ISBN 978 92 9213 162 3).

European Environmental Agency. 2011, February 18th. Wise TCM hazardous substances. Available from: http://www.eea.europa.eu/themes/water/interactive/tcm-hs, accessed August 18th 2011.

Eurostat, European Comission. 2010. Environmental statistics and accounts in Europe, In: Eurostat Statistical Book. ISBN 978-92-79-15701-1. Luxembourg.

Fairhurst, R.E.; Chassaing, C.; Venn, R.F.; Mayes, A.G. 2004. Biosens. Bioelectron. 20, 1098-1105.

Falconer, I.R. 2001. Phycologia 40, 228–233.

Fan, X.; White, I.M.; Shopova, S.I.; Zhu, H.; Suter, J.D.; Sun Y. 2008. Anal. Chim. Acta 620, 8–26.

Fang, B.; Kim, J.H.; Yu, J.S. 2008. Electrochem. Commun. 10(4), 659–662.

Fawell, J.K.; Hart, J.; James, H.A.; Parr, W. 1993. Water supp. 11, 109-121.

Fernández-González, A.; Badía, R., Díaz-García, M.E.; Guardia, L., Viale, A. 2004. J. Chromatogr. B 804, 247-254.

Findeisen, A.; Wackerlig, J.; Samardzic, R.; Pitkänen, J.; Anttalainen, O.; Dickert, FL.; Lieberzeit, P.A. 2012. Sensor. Actuat. B-Chem. 170, 196-200.

Flahaut, E.; Bacsa, R.; Peigney, A.; Laurent, C. 2003. Chem. Comm. 12, 1442–1443.

Fotadar, U.; Zaveloff, P.; Terracio, L. 2005. J. Basic Microbiol. 45(5), 403–4.

Friedman, M.S.; Roels, T.; Koehler, J.E.; Feldman, L.; Bibb, W.F.; Blake, P. 1999. Clin. Infect. Dis. 29, 298 –303.

Fu, L.; Zhang, K.; Li, S.; Wang, Y.; Huang, T.-S.; Zhang, A.; Cheng, Z.-Y. 2010. Sensor. Actuator. B-Chem 150, 220–225.

Gau J.-J.; Lan E.H.; Dunn B.; Ho C.-M.; Woo J.C.S. 2001. Biosens. Bioelectron. 16, 745–755.

Geng, P.; Zhang, X.; Teng, Y.; Fu, Y.; Xu, L.; Xu, M.; Jin, L.; Zhang, W. 2011. Biosens. Bioelectron. 26, 3325–3330.

Gill, I. 2001. Chem. Mater. 13, 3404-3421.

Giovannoli, C.; Baggiani, C.; Anfossi, L.; Giraudi, G.; 2008. Electrophoresis 29, 3349–3365.

Glad, T.; Glad, M.; Norrlöw, S.; Sellergren, B.; Siegbahn, N.; Mosbach, K. 1985. J. Chromatogr. 347(2), 11–23.

Godinho, M.I. 2005. Análise Instrumental II – Apontamentos teóricos. Departamento de Engenharia Química, Instituto Superior de Engenharia de Lisboa, pp. 26-55.

Grady, B. 2008. http://coecs.ou.edu/Brian.P.Grady/index.html, accessed 27th August 2012.

Graham, A.L., Carlson, C.A.; Edmiston, P.L. 2002. Anal. Chem. 74, 458-467.

Graphistrenth. http://www.graphistrength.com/sites/group/en/products/detailed_sheets/multi_wall_carbon_nanotubes_graphistrength/products_and_manufacture.page, accessed 27th August 2012.

Gründler, P. 2007. Chemical sensors. Springer-Verlag Berlin Heidelberg, Germany.

Gu, K.D.; Famulok, M. 2004. Zhonghua Yu Fang Yi Xue Za Zhi. 38(6), 369-73.

Guven, B.; Basaran-Akgul, N.; Temur, E.; Tamer, U.; Boyac, I.H. 2011. Analyst 136, 740–748.

Harada, K.; Fujii, K.; Shimada, T.; Suzuki, M.; Sano, H.; Adachi, K.; Carmichael, W.W. 1995. Tetrahedron Lett. 36, 1511–1514.

Haupt, K.; Mosbach, K. 2000. Chem. Rev. 100, 2495-2504.

He, J.; Ichinose, I.; Kunitake, T. 2001. Chem. Lett. 9, 850-851.

Health Protection Agency. 2005. Enumeration of coliforms and Escherichia coli by Idexx (colilert 18) Quanti-trayTM. National Standard Method W 18. <http://www.hpastandardmethods.org.uk/pdf_sops.asp., accessed 13th August 2012.

Hecht, E. 2003. Optics, 4th Ed., Pearson Education.

Hench, L.; West, J. 1990. Chem. Rev. 90, 33-72.

Henry, O.Y.F.; Piletsky, S.A.; Cullen, D.C. 2008. Biosens. Bioelectron. 23, 1769–1775.

Hianik, T., Ostatna, V., Sonlajtnerova, M.; Grman, I. 2007. Bioelectroch. 70, 127-133.

Hine, A.V.; Chen, X.; Hughes, M.D.; Zhou, K.; Davies, E.; Sugden, K., Bennion, I., Zhang, L. 2009. Biochem Soc. Trans. 37, 445-449.

Hospitality Institute of Technology and Management. 1998. *Escherichia coli* O157:H7 and other Pathogenic strains of *E. coli*, Food illness information. http://www.hi-tm.com/Documents/Ecoli98.html, accessed August 15th, 2012.

Hu C.; Gan N.; He Z.; Song L. 2008. Intern. J. Environ. Anal. Chem. 88, 267–277.

Huang, S.; Pang, P.; Xiao, X.; He, L.; Cai, Q.; Grimes, C.A. 2008. Sensor. Actuat. B-Chem. 131, 489–495.

Huang, Y.; Dong, X.; Liu, Y.; Lic, L.-J.; Chen, P. 2011. J. Mater. Chem. 21, 12358-12362.

Hudault, S.; Guignot, J.; Servin, A.L. 2001. Gut 49(1), 47–55.

Ikawa, M.; Phillips, N.; Haney, J.F.; Sasner, J.J. 1999. Toxicon 37, 923–929.

International Organization for Standardization. 2000. ISO 9308-1, Water quality – Detection and enumeration of Escherichia coli and coliform bacteria. Part 1: Membrane filtration method.

International Organization for Standardization. 2000. ISO 9308-3, Water quality – Detection and enumeration of *E. coli* and coliform bacteria - Part 3: Miniaturized method (Most Probable Number) for the detection and enumeration of *E. coli* in surface and waste water.

International Organization for Standardization. 2005. ISO 8199:2005, Water quality – General Guidance on the enumeration of microorganisms by culture.

James, S.; Tatam, R. 2003. Meas. Sci. Technol. 14(5), R49-R61.

Jang, H.S.; Park, K.N.; Kim, J.P.; Sim, S.J.; Kwon, O.J.; Han, Y.-G.; Lee, K.S. 2009. Opt. Express 17(5), 3855.

Janiak, D.S.; Kofinas, P. 2007. Anal. Bioanal. Chem. 389, 399–404.

Jenkins, A.; Uy, O.M.; Murray, G.M. 1999. Anal. Chem. 71, 373-378.

Jerónimo, P.C. 2005. Sensores ópticos de matriz sol-gel com interesse na análise farmacêutica e clínica. PhD thesis. Faculdade de Fármacia da Universidade do Porto, Portugal, pp. 63-126.

Jesus, C.; Caldas, P., Frazao, O.; Santos, J.L.; Jorge, P.A.S.; Baptista, J.M. 2009. Fiber Integrated Opt. 28(6), 440-449.

Jorge, P. 2010. Proc. 3rd WSEAS Intern. Conf. Advances in Sensors, Signals and Materials, ISBN: 978-960-474-248-6, 174-178.

Karsunke, X.Y.Z.; Niessner, R.; Seidel, M. 2009. Anal. Bioanal. Chem. 395, 1623–1630.

Katz, E.; Willner, I. 2003. Electroanal. 15(11), 913- 947.

Kim, D.; Zhang, Y.; Cooper, K.; Wang, A. 2005. Appl. Optics 44(26), 5368-5373.

Klein, L.C. 2005. Coatings Technology Handbook, CRC Press, New Jersey.

Kwon, H.-J.; Dean, Z.S.; Angus S.V.; Yoon, J.-Y. 2010. JALA 15, 216-223.

Komiyama, M.; Takeuchi, T.; Mukawa, T.; Asanuma, H. 2003. Molecular Imprinting – Fundamentals to Applications, Wiley-VCH Verlag GmbH & Co. KGaA; Weinheim, Germany.

Köster, W.; Egli, T.; Ashbolt, N.; Botzenhart, K.; Burlion, N.; Endo, T.; Grimont, P.; Guillot, E.; Mabilat, C.; Newport, L.; Niemi, M.; Payment, P.; Prescott, A.; Renaud, P.; Rust, A. 2003. Analytical Methods for Microbiological Water Quality Testing, in: Dufour, Snozzi, M.; Koster, W.; Bartram, J.; Ronchi, E.; Fewtrell, L. (Eds.). Assessing Microbial Safety of Drinking Water Improving Methods and Approaches. OECD, Paris, pp. 237-292.

K'Owino, I.O.; Sadik, O.A. 2005. Electroanal. 17(23), 2101–2113.

Kubitschek, H.E. 1990. J. Bacteriol. 172(1), 94–101.

Kuiper-Goodman, T.; Falconer, I.R.; Fitzgerald, J. 1999. Human Health Aspects, in: Chorus, I., Bartram, J. (Eds.). Toxic cyanobacteria in water, E. and F.N. Spon, London, pp. 113-153.

Kunkel, D. Dennis Kunkel Microscopy, INC., http://www.denniskunkel.com/index.php?module=media&pId=100&category=gallery/bacteria, accessed August 20th 2012.

Kwon, H.-J.; Dean, Z.S.; Angus S.V.; Yoon, J.-Y. 2010. JALA 15, 216-223.

Labib, M.; Zamay, A.S.; Muharemagic, D.; Chechik, A.V.; Bell, J.C.; Berezovski, M.V. 2012. Anal. Chem. 84(5), 2548-56.

Lahav, M.; Katz, E.; Willner, I. 2001. Langmuir 17, 7387–7395.

Lawton, L.A.; Edwards, C.; Cood G.A. 1994. Analysis 119, 1525-1530.

Lee, B.H.; Kim, Y.H.; Park, K.S.; Eom, J.B.; Kim, M.J.; Rho, B.S.; Choi, H.Y.; 2012b. Sensors 12, 2467-2486.

Lee, C.E.; Taylor, H.F. 1988. Electron. Lett. 24(4), 193-194.

Lee, H.J.; Kim, B.C.; Kim, K.W.; Kim, Y.K.; Kim, J.; Oh, M.K. 2009. Biosens. Bioelectron. 24(12), 3550-3555.

Lee, J.F.; Stovall, G.M.; Ellington, A.D.; 2006. Curr. Opin. Chem. Biol. 10, 282–289.

Lee, Y.J.; Han, S.R.; Maeng, J.S.; Cho, Y.J.; Lee, S.W. 2012a. Biochem. Biophys. Res. Commun. 417(1), 414-420.

Leonard, P.; Hearty, S.; Brennan, J.; Dunne, L.; Quinn, J.; Chakraborty, T.; O'Kennedy, R. 2003. Enzyme Microb. Tech. 32, 3–13.

Li, K.; Lai, Y.; Zhang, W.; Jin, L. 2011. Talanta 84, 607–613.

Li, P.C.H.; Hu, S.; Lam, P.K.S. 1999. Mar. Pollut. Bull. 39, 250–254.

Li, W.; Li, S. 2007. Adv. Polym. Sci. 206, 191–210.

Li, Y.; Li, Y.; Huang, L.; Bin, Q.; Lin, Z.; Yang, H.; Cai, Z.; Chen, G. 2013. J. Mater. Chem. B (Advance Article) DOI: 10.1039/C2TB00398H.

Lindner, P.; Moltz, R.; Yacoub-George, E.; Dürkop, A.; Wolf, H. 2004. Anal. Chim. Acta 512, 37-44.

Lindner, P.; Molz, R.; Yacoub-George, E.; Wolf, H. 2009. Anal.Chim. Acta 636(2), 218-223.

Liu Y.; Li Y. 2002. J. Microbiol. Methods 51, 369– 377.

Long, F.; He, M.; Zhu, A.N., Shi, H.C. 2009. Biosens. Bioelectron. 24, pp. 2346–2351.

Long, F.; He, M.; Zhu, A., Song, B.; Sheng, J.; Shi, H. 2010. Biosens. Bioelectron. 26(1), 16-22.

Lopez-Higuera, J.M. 2002. Handbook of Optical Fiber Sensing Technology, Wiley Blackwell.

Lorenzi, A.S. 2004. Abordagens moleculares para detectar cianobactérias e seus genótipos produtores de microcistinas presentes nas represas Billings e Guarapiranga. São Paulo, Brasil. M.Sc. thesis, Centro de Energia Nuclear na Agricultura, Universidade de São Paulo, São Paulo, Brasil.

Lotierzo, M.; Henry, O.Y.F.; Piletsky, S.; Tothill, I.; Cullen, D.; Kania, M.; Hock, B.; Turner, A.P.F. 2004. Biosens. Bioelectron. 20, 145–152.

Loypraserta, S.; Thavarungkul, P.; Asawatreratanakul, P.; Wongkittisuksa, B.; Limsakul, C.; Kanatharana, P. 2008. Biosens. Bioelectron. 24(1), 78-86.

Liss, M.; Petersen, B. Wolf, H., Prohaska, E. 2002. Anal. Chem. 74, 4488–4495.

Lukjancenko, O.; Wassenaar, T.M.; Ussery, D.W. 2010. Microb. Ecol. 60(4), 708–720.

Lulka, M.F.; Iqbal, S.S.; Chambers, J.P.; Valdes, E.R.; Thompson, R.G.; Goode, M.T.; Valdes, J.J. 2000. Mat. Sci. Engineer. C 11, 101-105.

Luo, C.; Yaning, L.; Li, Y.; Tianxiao, Y.; Qing, L.; Decai, Z.; Shijia, D.; Huangxian, J. 2012. Electroanal. 24(5), 1186 – 1191.

Luo, Y.; Nartker, S.; Miller, H.; Hochhalter, D.; Wiederoder, M.; Wiederoder, S.; Setterington, E.; Drzal, L.T.; Alocilja, E.C. 2010. Biosens. Bioelectron. 26, 1612–1617.

Luo, Y.; Nartker, S.; Wiederoder, M.; Miller, H.; Hochhalter, D.; Drzal, L.T.; Alocilja, E.C.; 2012. IEEE Trans. Nanotechnol. 11(4), 676-681.

Mac-Craith, B.D.; Mc Donagh, C.; Mcevoy, A.K.; Butler, T.; O' Keeffe, G.; Murphhy, V. 1997. J. Sol-Gel Sci. Technol. 8, 1053-1061.

MacKintosh, C.; Beattie, K.A.; Klumpp, S.; Cohen, P.; Codd, G.A. 1990. FEBS Lett. 264, 187-192.

Makote, R.; Collinson, M.M. 1998. Chem. Mater. 10, 2440-2445.

Marler, B. 2011. In: Food poisoning information. http://www.marlerblog.com/articles/e-coli-information/#.UQWZFL-Exzs, accessed August 20th 2012.

Marler, B. 2010. In: Legal cases. http://www.marlerblog.com/e-coli-information/e-coli-o157h7/#.UQWZSL-Exzs, accessed August 20th 2012.

Mascini, M.; Palchetti, I.; Tombelli, S. 2012. Angew. Chem. Int. Ed. 51, 1316 – 1332.

McElhiney, J.; Lawton, L.A. 2005. Toxicol. Appl. Pharm. 203, 219-230.

Merkoçi, A.; Alegret, S. 2002. TrAC – Trend. Anal. Chem. 21(11), 717-725.

Merkoçi¸ A.; Pumera, M.; Llopis, X.; Pérez, B.; del Valle, M.; Alegret, S.; 2005. TrAC - TrAC – Trend. Anal. Chem. 24, 826-838.

Metcalf, J.S.; Bell, S.G.; Codd, G.A. 2000. Water Res. 34, 2761–2769.

Miranda-Castro, R.; de-los-Santos-Álvarez, N.; Lobo-Castañón, M.J.; Miranda-Ordieres, A.J.; Tuñón-Blanco, P. 2009. Electroanal. 21(19), 2077-2090.

Mirsky, V.M.; Hirsch, T.; Piletsky, S.A.; Wolfbeis, O.S. 1999. Angew. Chem. Int. Ed. 38(8), 1108–1110.

Mitcherlich, E.; Marth, E.H. 1984. Microbial Survival in the Environment. Bacteria and Rickettsiae important in human and animal health, in: Schau, H.-P.; (Ed.). Journal of Basic Microbiology. Springer Verlag, New York, pp. 709.

Mohamed, Z.A. 2008. Toxicon 51, 17–27.

Mok, W.; Li, Y. 2008. Sensors 8, 7050-7084.

Monton, M.R.N.; Forsberg, E.M.; Brennan, J.D. 2012. Chem. Mater. 24(5), 796-811.

Moollan, R.W.; Rae, B., Verbeek, A. 1996. Analyst 121, 233–238.

Moreira, F. 2009. Determinação de Norfloxacina em Aquacultura. Msc thesis, Faculdade de Ciências da Universidade do Porto, Portugal, pp. 29-41.

Moreira, F.; Dutra, R.; Noronha, J.P.; Cunha, A.L.; Sales, M.G.F. 2011. Biosens. Bioelectron. 28, 243– 250.

Moreira, P. 2005. Óptica Integrada em Tecnologia Sol-Gel Híbrido. PhD thesis, Faculdade de Ciências da Universidade do Porto, Portugal, pp. 43-69.

Mosbach, K. 1994. Trend. Biochem. Sci. 19(1), 9–14.

Msagati, T.A.M.; Siame, B.A.; Shushu, D.D. 2006. Aquat. Toxicol. 78, 382-397.

Mujahid, A.; Lieberzeit, P.A.; Dickert, F.L. 2010. Materials 3, 2196-2217.

Nagata, S.; Soutome, H.; Tsutsumi, T.; Hasegawa, A.; Sekijima, M.; Sugamata, M.; Harada, K.-I.; Suganuma, M.; Ueno, Y. 1995. Nat. Toxins 3, 78–86.

Nayak, M.; Kotian, A.; Marathe, S.; Chakravortty, D. 2009. Biosens. Bioelectron. 25, 661-667.

Nicholson, B.C.; Burch, M.D. 2001. Evaluation of Analytical Methods for Detection and Quantification of Cyanotoxins in Relation to Australian Drinking Water Guidelines, a report to the National Health Authority. Endorsed, Commonwealth of Australia.

Okamoto, K. 2006. Fundamentals of Optical Waveguides, 2nd Ed., Elsevier.

Olsen, S.J.; Miller, G.; Breuer, T.; Kennedy, M.; Higgins, C.; Walford, J.; McKee, G.; Fox, K.; Bibb, W.; Mead, P. 2002. Emerg. Infect. Dis. 8(4), 370–375.

O'Sullivan, C.K. 2002. Anal. Bioanal. Chem. 372, 44–48.

Panosso, R.; Costa, I.A.S.; Souza, N.R.; Attayde, J.L.; Cunha, S.R.S.; Gomes, F.C.F 2007. Oecol. Bras. 11, 337–356.

Park, S.; Kim, H.; Paek, S.-H.; Hong, J.W.; Kim, Y.-K. 2008. Ultramicroscopy 108, 1348– 1351.

Park, S.-M.; Yoo, J.-S. 2003. Anal. Chem. 75(21), 455-461.

Patau, P. 2008. The beautiful green toxic cyanobacterial pond scum at Madison's B.B. Clarke Beach, http://www.peterpatau.com/2008/06/beautiful-green-toxic-cyanobacterial.html, accessed August 14th 2012.

Payment, P.; Waite, M.; Dufour, A. 2003. In: Assessing Microbial Safety of Drinking Water Improving Methods and Approaches. OECD, Paris, pp. 47–77.

Pichon, V.; Chapuis-Hugon, F. 2008. Anal. Chim. Acta 622, 48–61.

Piletsky, S.A.; Piletskaya, E.V.; Elgersma, A.V.; Yano, K.; Karube, I.; Parhometz, Y.P.; El'skaya, A.V. 1995. Biosens. Bioelectron. 10, 959-964.

Piletsky, S.A.; Piletska, E.V.; Chen, B.; Karim, K.; Weston, D.; Barrett, G.; Lowe, P.; Turner, A.P.F. 2000. Anal. Chem. 72, 4381–4385.

Pilla, P.; Manzillo, P.F.; Malachovska, V.; Buosciolo, A.; Campopiano, S.; Cutolo, A.; Ambrosio, L.; Giordano, M.; Cusano, A. 2009. Opt. Express 17(22), 20039-20050.

Premkumar, J.R.; Sagi, E.; Rozen, R.; Belkin, S.; Modestov, A.D.; Lev, O. 2002. Chem. Mater. 14, 2676-2686.

Pumera, M. 2010. Chem. Soc. Rev. 39(11), 4146–4157.

Puoci, F.; Cirillo, G.; Curcio, M.; Iemma, F.; Spizzirri, U.G.; Picci, N. 2007. Anal. Chim. Acta 593, 164–170.

Puoci, F.; Iemma, F.; Picci, N. 2008. Curr. Drug Deliv. 5, 85–96.

Pyo, D.; Jin, J. 2007. Bull. Korean Chem. Soc. 28(5), 800-804.

Pyo, D.; Choi, J.; Hong, J.; Oo, H.H. 2006. J. Immunoass. Immunoch. 27, 291–302.

Pyo, D.; Huang, Y.; Kim, Y.; Hahn, J.H. 2005. Bull. Korean Chem. Soc. 26(6), 939-942.

Randles, J.E.B. 1948. Trans. Faraday Soc. 44, 322-327.

Rapala, J.; Erkomaa, K.; Kukkonen, J.; Sivonen, K.; Lahti, K. 2002. Anal. Chim. Acta 466, 213–231.

Reid, G.; Howard, J.; Gan, B.S. 2001. Trend. Microbiol. 9(9), 424–428.

Rivas, G.A.; Rubianes, M.D.; Rodríguez, M.C.; Ferreyra, N.F.; Luque, G.L.; Pedano, M.L.; Miscoria, S.A.; Parrado, C. 2007. Talanta 74(3), 291–307.

Robillot, C.; Vinh, J.; Puiseux-Dao, S.; Hennion, M.C. 2000. Environ. Sci. Technol. 34, 3372–3378.

Ruigrok, V.J.B.; Levisson, M.; Eppink, M.H.M.; Smidt, H.; Van Der Oost, J. 2011. Biochem. J. 436, 1–13.

Sando, S.; Ogawa, A.; Nishi, T.; Hayami, M.; Aoyama, Y. 2007. Bioorg. Med. Chem. Lett. 17(5), 1216–1220.

Sergeyeva, T.A.; Piletsky, S.A.; Brovko, A.A.; Slichenko, E.A.; Sergeeva, L.M.; Panasyuk, T.L.; El'skaya, A.V. 1999. Analyst 124, 331-334.

Sergeyeva, T.A.; Brovko, O.O.; Piletska, E.V.; Piletsky, S.A.; Goncharova, L.A.; Karabanova, L.V.; Sergeyeva, L.M.; El'skaya, A.V. 2007. Anal. Chim. Acta 2007, 582, 311–319.

Sheng, J.; He, M.; Yu, S.; Shi, H.; Qian, Y. 2007. Front. Environ. Sci. Engin. China 1(3), 329–333.

Sigee, D.C. 2005. Freshwater Microbiology. John Wiley and Sons, LTD, Manchester, UK.

Shi, Y.; Wu, J.; Sun, Y.; Zhang, Y.; Wen, Z.; Dai, H.; Wang, H.; Li, Z. 2012. Biosens. Bioelectron. 38(1), 31-36.

Shinkai, S.; Takeuchi, M. 2004. Biosens. Bioelectron. 20, 1250–1259.

Simpson, J.M.; Lim, D.V. 2005. Biosens. Bioelectron. 21, 881–887.

Sivonen, K.; Jones, G. 1999. Cyanobacterial Toxins, in: I., Bartram, J. (Eds.). Toxic Cyanobacteria in Water. A Guide to Public Health Consequences, Monitoring and Management. Chorus, E & FN Spon, London, pp. 41–111.

Smietana, M.; Bock, W.J.; Mikulic, P.; Ng, A.; Chinnappan, R.; Zourob, M. 2011. Opt. Express 19(9), 7971.

Smith, T.J.; Stevenson, K.J. 2007. Reference Electrodes, in: Cynthia G. Zoski (Ed.). Handbook of Electrochemistry. Elsevier, Amsterdam, pp. 1-28.Sims, G. E.; Kim, S.-H. 2011. Proc. Natl. Acad. Sci. 108(20), 73-107.

Snyder, A.W.; Love, J.D. 1983. Optical waveguide theory, Chapman and Hall, London.

So, H.M.; Park, D.M.; Jeon, E.K.; Kim, Y.H.; Kim, B.S.; Lee, C.K.; Choi, S.Y.; Kim, S.C.; Chang, H.; Lee, J.O. 2008. Small 4(2), 197–201.

Song, S.; Wang, L.; Li, J.; Zhao, J.; Fan, C. 2008. Trend. Anal. Chem. 27, 108-117.

Spégel, P.; Schweitz, L.; Nilsson, S. 2002. Anal. Bioanal. Chem. 372, 37–38.

Spichiger-Keller U.E. 1998. Chemical Sensors and Biosensors for Medical and Biological Applications, Weinheim, WCH-Wiley.

Stadtherr, K.; Wolf, H.; Lindner, P. 2005. Anal. Chem. 77, 3437-3443.

Stefan, R.-I.; Aboul-Einen, H.Y. 1999. Instrum. Sci. Technol. 27(2), 105-110.

Stoltenburg, R.; Reinemann, C.; Strehlitz, B. 2007. Biomol. Eng. 24, 381–403.

Strehlitz, B.; Nikolaus, N.; Stoltenburg, R. 2008. Sensors 8, 4296-4307.

Su, L.; Jia, W.; Hou, C.; Lei, Y. 2011. Biosens. Bioelectron. 26, 1788-1799.

Subramanian, S.; Aschenbach, K.H.; Evangelista, J.P.; Najjar, M.B.; Song, W.; Gomez, R.D. 2012. Biosens. Bioelectron. 32, 69–75.

Sulizky, C.; Rueckert, B.; Hall, A.J.; Lanza, F.; Unger, K.; Sellergren, B. 2002. Macromolecules 35, 79-91.

Sun, H.; Choy, T.S.; Zhu, D.R.; Yam, W.C.; Fung, Y.S. 2009. Biosens. Bioelectron. 24, 1405–1410.

Tang, H.; Zhang, W.; Geng, P.; Wang, Q.; Jin, L.; Wu, Z.; Lou, M. 2006. Anal. Chim. Acta 562, 190–196.

Tasis, D.; Tagmatarchis, N.; Bianco, A.; Prato, M. 2006. Chem. Rev. 106(3), 1105-1136.

Tombelli, S.; Minunni, M.; Mascini, M. 2005. Biosens. Bioelectron. 20, 2424-2434.

Torres-Chavolla, E.; Alocilja, E.C. 2009. Biosens. Bioelectron. 24(11), 3175-3182.

Touron, A.; Berthe, T.; Pawlak B.; Petit, F. 2005. Res. Microbiol. 156, 541–53.

Tuerk, C.; Gold, L. 1990. Science 249, 505-510.

Turner, A.P.F.; Piletsky S. 2005. Biosensors and Biomimetic Sensors for the Detection of Drugs, Toxins and Biological Agents, in: Morrison, D. et al, (Eds.). Defense against Bioterror - NATO Security through Science Series. Springer Ed., Vol. 1, pp. 261-272.

Turner, N.W.; Jeans, C.W.; Brain, K.R.; Allender, C.J.; Hlady, V.; Britt, D.W. 2006. Biotechnol Prog. 22(6), 1474–1489.

Vasapollo, G.; Del Sole, R.; Mergola, L.; Lazzoi, M.R.; Scardino, A.; Scorrano, S.; Mele, G. 2011. Int. J. Mol. Sci. 12, 5908-5945.

Velasco-Garcia, M.N.; Missailidis, S. 2009. Gene Ther. Mol. Biol. 13, 1-9.

Velusamy, V.; Arshak, K.; Korostynska, O.; Oliwa, K., Adley, C. 2010. Biotechnol. Adv. 28, 232–254.

Vo-Dinh, T. 2007. Biosensors and biochips, In: Bashir, R.; Wereley, S. (Eds.). Biomolecular sensing, processing and analysis, Volume I, pp. 3-20.

Wang, L.; Chen, W.; Xu, D.; Shim, B.S.; Zhu, Y.; Sun, F.; Liu, L.; Peng, C.; Jin, Z.; Xu C.; Kotov, N.A. 2009a. Nano Letters 9(12), 4147-4152.

Wang, L.; Liu, Q.; Hu, Z.; Zhang, Y.; Wu, C.; Yang, M.; Wang, P. 2009b. Talanta 78, 647–652.

Wang, H.Y.; Kobayashi, T.; Fujii, N. 1996. Langmuir 12(20), 4850–4856.

Wang, Z.; Heflin, J.R.; Van Cott, K.; Stolen, R.H.; Ramachandran, S.; Ghalmi, S. 2009. Sensor Actuat B -Chem 139(2), 618-623.

Warsinke, A.; Nagel, B. 2006. Anal. Lett. 39(13), 2507-2556.

World Health Organization. 1998. Drinking-water quality guidelines for parameters of concern in agricultural drainage water - Annex 3, Technical Report, Geneva, pp. 281–289.

World Health Organization. 1999. Toxic Cyanobacteria in Water: A guide to their public health consequences, monitoring and management. E & FN Spon, London.

World Health Organization. 2007a. Food safety & food-borne illness, fact sheet 237 (reviewed March 2007), Geneva.

World Health Organization. 2007b. In: Global public health security in the 21st century – report. Geneva.

Wildeboer, D.; Amirat, L.; Price, R.G.; Abuknesha, R.A. 2010. Water Res. 44, 2621–2628.

Wilson, I.G. 1997. Appl. Environ. Microbiol. 63, 3741-3751.

Wolter, A.; Niessner, R.; Seidel, M. 2008. Anal. Chem. 80, 5854–5863.

Xia, Y.; Deng, J.; Jiang, L. 2010. Sensor. Actuator. B-Chem. 145(2), 713-719.

Xia, Y.; Zhanga, J.; Jiang, L. 2011. Colloid. Surface. 86(1), 81-86.

Xu, L.H.; Lam, P.K.S.; Chen, J.P.; Xu, J.M.; Wong, B.S.F.; Zhang, Y.Y.; Wu, R.S.S. Harada, K.I. 2000. Chemosphere 41, 53-58.

Xue, X.; Pan, J.; Xie, H.; Wang, J.; Zhang, S. 2009. Talanta 77, 1808–1813.

Yáñez, M.A.; Valor, C.; Catalán, V. 2006. J. Microbiol. Meth. 65, 608–611.

Yang, H.-H.; Zhang, S.-Q.; Yang, W.; Chen, X.-L.; Zhuang, Z.-X.; Xu, J.-G.; Wang, X.-R. 2004. J. Am. Chem. Soc. 126, 4054–4055.

Yang, J.; Sandhu, P.; Liang, W.; Xu, C.Q.; Li, Y. 2007. IEEE J. of Selected Topics in Quantum Electronics 13(6), 1691-1696.

Yang, W.; Thordarson, P.; Gooding, J.J.; Ringer, S.P.; Braet, F. 2007. Nanotechnol. 18, 412001 (12pp).

Yilmaz, E.; Mosbach, K.; Haupt, K. 1999. Anal. Commun. 36, 167-170.

Yoo, S.K.; Lee, J.H.; Yun, S.-S.; Gu, M.B.; Lee, J.H. 2007. Biosens. Bioelectron. 22, 1586–1592.

Yoon, J.-Y.; Han, J.-H.; Choi, C.Y.; Bui, M.; Sinclair, R.G. 2009. Trans. ASABE, 52(3), 1031-1039.

Yoshimatsu, K.; Reimhult, K.; Krozer, A.; Mosbach, K.; Sode, K.; Ye, L. 2007. Anal. Chim. Acta 584, 112–121.

Yu, J.; Liu, Z.; Liu, Q.; Yuen, K.T.; Mak, A.F.T.; Yang, M.; Leung, P. 2009. Sensor. Actuator. A-Phys. 154, 288–294.

Yu, S.-Z. 1995. J. Gastroenterol. Hepatol. 10, 674-682.

Zelada-Guillen, G.A.; Bhosale, S.V.; Riu, J.; Rius, F.X.; 2010. Anal. Chem. 82(22), 9254-9260.

Zhang, F.; Yang, S.H.; Kang, T.Y.; Cha, G.S.; Nam, H.; Meyerhoff, M.E. 2007. Biosens. Bioelectron. 22(7), 1419-1425.

Zhang, Z.; Long, Y.; Nie, L.; Yao, S. 2006. Biosens. Bioelectron. 21, 1244–1251.

Zheng, N.; Hagen, N.; John, R.; Brady, D.J. 2009. Proc. of SPIE-IS&T Electronic Imaging, SPIE Vol. 7249, 72490Z-1-8.

Zourob, M.; Mohr, S.; Mayes, A.G.; Macaskill, A.; Pérez-Moral, N.; Fielden, P.R.; Goddard, N.J. 2006. Lab Chip 6, 296–301.

Zhu, H.; Suter, J.D.; White, I.M.; Fan, X. 2006. Sensors 6, 785–795.

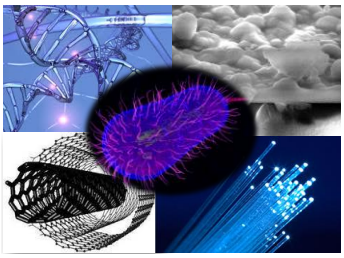

Chapter 3

Development of a biosensor for the detection of the microcystin-LR in waters with potentiometric detection using a sol-gel imprinted polymer in solid contact electrodes

3.1 Introduction

The occurrence of cyanobacteria blooms may be potential disseminators of hazardous cyanotoxins (Campàs and Marty, 2007; Lindner et al., 2004; Panosso et al., 2007). MC-LR is one of the most frequent and toxic MCs congeners. On account of this, some international organizations, like WHO, recommended for cyanotoxin MC-LR a limiting value of 1 $\mu g\ L^{-1}$ in drinking waters (WHO, 1998).

In the last decade, many efforts were undertaken to detect MC-LR by means of rapid tests (Campàs and Marty, 2007; Li et al., 2008). Still, a simple, low cost, portable and selective method is necessary for MC-LR determination in locus. ISEs with suitable membranes and potentiometric transduction may suit this purpose. They offer high precision and rapidity, low cost of analysis, and enhanced selectivity over a wide range of concentrations (Amemiya, 2007). Their selectivity may be enhanced by designing sensory materials targeted for a specific compound by means of MI. Different routes may be taken for this purpose.

Considering that MC-LR is a complex biological structure, it should be imprinted in mild conditions such as those from sol–gel techniques. Sol–gel materials with MI can be prepared as indicated in Figure 3.1. An organic solution containing the functional sol–gel precursors and the template molecule (MC-LR) is allowed to interact for molecular pre-organization according to electrostatic interactions. As the precursors follow hydrolysis and polycondensation reactions, an interconnected 3D porous network is formed around the template. Template removal leaves behind free sites able to rebind MC-LR molecules.

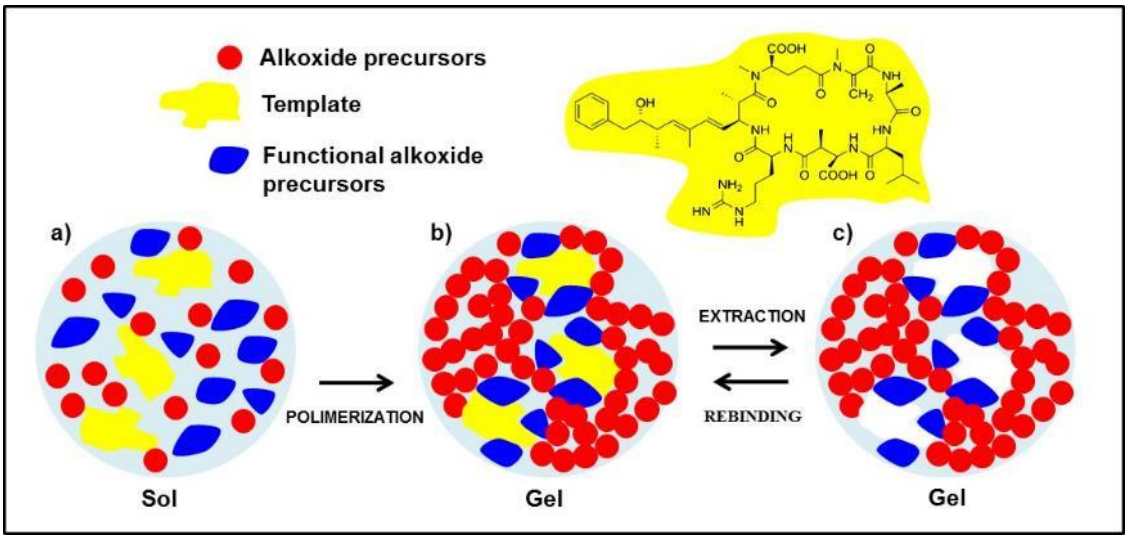

Figure 3.1- Process of sol–gel molecular imprinting. (a) template molecule and the functional precursor were mixed in the solvent (Sol) (b) the polimerisation of the complex template/monomer is formed and the solution becomes increasingly thick; (c) the microcystin-LR extraction leaves behind the recognition cavities, containing the specific sites capable of binding the target molecule when in his presence.

The present work describes the selection of a suitable (i) sol–gel MI composition for MC-LR (effects of ionic lipophilic additive, time of sol–gel polimerisation, ratio of water/alkoxide and solvent/alkoxide, polimerisation temperature and pH are studied) and (ii) solid-contact used for potentiometric transduction (carbon, metal or alloy).

Only electrodes of solid contact are considered because they are easily adapted to chip-based devices (highly desired in local monitoring operations) by coating a solid conductive layer with the selective membrane (Nagy G. and Nagy L., 2007; Trebbe et al., 2001).

All prepared sensors are evaluated and characterized and applied for real measurements.

3.2 Materials and methods

3.2.1 Apparatus

All potential measurements were made by a Crison pH-meter GLP 21 (±0.1 mV sensitivity), at room temperature under constant stirring. The signal was connected to six ISEs by a homemade switchbox. The assembly of the potentiometric cell (see Figure 2.11) was as follows: conductive graphite or metal | MC-LR selective membrane | buffered sample solution || electrolyte solution, potassium clhoride (KCl) |AgCl(s) | Ag. The reference electrode was a Crison 5240 Ag/AgCl double-junction. The carbon-based selective electrodes had an epoxy–graphite mixture as the solid contact. The metal-based electrodes were constructed with 5 different metals: Al, Ti, Cu, and two alloys of Ni/Cr (90:10) and (80:20). The temperature curing condition was annealed for Ti, Ni/Cr (90:10), Al and Cu and was hard for Ni/Cr (80:20). Voltammetric and electrochemical impedance spectroscopy measurements were carried out with a Potentiostat Autolab PGSTAT128N with Frequency Response Analysis (FRA) module. Reference and auxiliary electrodes were of Ag/AgCl (Crison 5240) and platinum (BASi MW-1032 mm, 7.5 cm length). N_2 of 6.0 quality grade (≥ 99.9999%, Air Liquide) was used for degassing. SEM images were collected by a FEI Quanta 400FEG ESEM/EDAX Genesis X4M microscope.

3.2.2 Reagents

Deionized water was used throughout. All reagents were pro-analysis grade and used without further purification. MC-LR, potassium tetrakis(4-chlorophenyl)borate (TKClPB) and APTES were purchased from Fluka. Diphenyldimethoxysilane (DPDMS) and Tetraethyl orthosilicate (TEOS) were purchased from ABCR. Hydrochloric acid (HCl) and methanol (MeOH) were from Merck. Ethanol (EtOH) was purchased from Panreac.

Buffer solutions were 1×10^{-3} M piperazine-*N,N'*-bis(2-ethanesulfonic acid) (PIPES) pH 6.6, 1×10^{-1} M phosphate buffered saline (PBS) pH 7.4 and 0.01 M sodium borate (Borax) pH 9.4. These were prepared in deionized water. The pH values were adjusted by adding the appropriate volumes of either concentrated HCl or orthophosphoric acid, or saturated sodium hydroxide (NaOH) solution, freshly prepared. A stock solution of 2.00 μg L^{-1} MC-LR was prepared in buffer by rigorous dilution of the commercial solution (10.025 μg mL^{-1} in EtOH). Less concentrated solutions were prepared by rigorous dilution of this one in a buffer.

3.2.3 Preparation of sensing membranes

The MC-LR ISG membrane was prepared from a reagent mixture of 10 μL of the MC-LR commercial solution, 3 mL of APTES, 3 mL of DPDMS, 10 mL of MeOH and 2.78 to 11.1 mL of TKClPB 3.63×10^{-4} M. This mixture was stirred for 30 minutes at 60 ºC. The resulting solution was then slowly hydrolyzed with 1 mL TEOS; 500 mL HCl 0.1 M; 5 mL EtOH; and 1.5 mL deionised water for 30–240 minutes, also at 60 ºC. The mixture was deposited on the solid contact by drop (carbon based electrodes) or dip-coating (metal-based electrodes) and then cured at 60 ºC for 12 h in a moisture atmosphere. The template was removed by washing the polymer in deionised water for 3 h (2×1.5 h). The NISG was also synthesized similarly, replacing the template MC-LR by the same volume in EtOH.

3.2.4 Potentiometric measurements

All potentiometric measurements were carried out at room temperature. Emf values of each electrode were measured in solutions of fixed pH and ionic strength. Calibrations were made by decreasing the initial concentration of MC-LR because the total reagent spent in each procedure is much less than for increasing concentrations. This was done by dipping the electrodes in 5 mL of a 2.0 μg L^{-1} MC-LR solution and adding consecutively increasing amounts of buffer (from 1 to 5 mL). The obtained MC-LR concentrations ranged from 0.37 to 2.0 μg L^{-1}. Potential readings were recorded after 2 min and emf was plotted as a function of log MC-LR molar concentration.

3.2.5 Procedures for selectivity assays

The potentiometric selectivity coefficients ($K^{pot}_{MC\text{-}LR,J}$) were assessed by the Matched-Potential Method (MPM). For this purpose, the change in emf caused by the principal ion was measured for a MC-LR rise in concentration from 1 to 5 μg L^{-1}. Similarly, the emf of a 1 μg L^{-1} MC-LR solution was measured and a solution of interfering species added until the previous potential change was reached. Solutions of 200 μg L^{-1} Al^{3+}, 500 μg L^{-1} NH_4^+, 250 mg L^{-1} Cl^-, 50 μg L^{-1} Mg^{2+}, 50 mg L^{-1} Mn^{2+}, 200 mg L^{-1} Na^+ and 250 mg L^{-1} SO_4^{2-}, were tested for this purpose. All these were prepared in a buffer.

3.2.6 Electrochemical measurements

Cyclic voltammetry (CV) and EIS assays were carried out at room temperature. The reference and counter electrodes were Ag/AgCl (3 M in KCl) and platinum, respectively. The measuring solution was a 1×10^{-3} M PIPES buffer (pH 6.5) with 5 mM of $[Fe(CN)_6]^{3-/4-}$, degassed by bubbling for ~30 seconds with N_2. CV measurements were performed at potential range between -1.5 V and 1.5 V, with 0.10 V s^{-1} scan rate, 0.0025 V step and 10 mA current range. EIS frequency ranges were between 0.1 and 10 000 Hz with amplitude of 0.005 V. The standard potential (indicated by CV assays) was -0.0979 V, 0.861 V, 0.176 V, 0.795 V, 0.410 V, and 0.400 V for carbon, Ti, Al, Cu, Ni/Cr (90:10) and (80:20) alloys, respectively.

3.2.7 Segment sandwich membrane method

The segmented sandwich membrane method is based on direct potential measurements arising from ligand–ion complexation (Mi and Bakker, 1999). The electrode was prepared by coating the carbon conductive support with the NISG material. An additional layer of ISG material was deposited on top of it after drying. The electrode was tested in PIPES buffer at pH 6.5 with a MC-LR concentration of 1 μg L^{-1}. Emf was measured every 5 min during 155 min (remained constant after this time).

3.3 Results and discussion

3.3.1 Microcystin sol–gel membrane on solid contact carbon electrodes

MC-LR ISG selective membranes on a carbon solid contact prepared with APTES, DPDMS and TEOS presented mostly super-Nernstian responses and positive slopes, although a few negative slopes were observed. This behaviour was attributed to the polyionic nature of MC-LR. It has three ionisable groups out of the cyclic peptide structure (Figure 3.1). Following Nernst equation, equilibrium partitioning between the membrane and aqueous phases would result in very small potential changes. However, a non-equilibrium ion-exchange process between a polyion in the aqueous phase and a counter ion of the ion exchanger sites in the membrane phase may cause a large potential change, resulting in a non-equilibrium super-Nernstian response (Amemiya, 2007). This possible change of sign was controlled by including in the membranes an anionic lipophilic additive (TKClPB), thus forcing the electrode to respond preferentially to positively charged species of MC-LR. In addition, these anionic sites improve the permselectivity of the membranes for cations in carrier-free membranes and enhance the performance of solid contact ISEs (Schaller et al, 1994). The time given for hydrolysis/polycondensation and template leaching of the sol–gel matrix was also optimized.

3.3.1.1 Effect of additive

Membranes with 8, 30 and 120 μmol of TKClPB in a sol–gel matrix were prepared and evaluated with regard to their potentiometric performance. The corresponding sensors displayed different sensitivities and detection limits. They showed linear responses in the concentration ranges 0.77–2.00, 0.77–2.00, and 0.77–1.67 μg L^{-1}, with slopes of 169.5, 180.7, and 126.0 mV per decade and detection limits of 0.77, 0.77 and 0.67 μg L^{-1}, respectively. These results pointed out that a minimal amount of TKClPB was enough to control the net ionic charge sensed by the membrane. Thus, the amount of additive was set to 8 μmol.

3.3.1.2 Hydrolysis/Condensation time

The time given for sol–gel hydrolysis/polycondensation affects the overall physical properties of the membrane, including hardness, porosity and integrity. These, in turn, affect with significance the potentiometric response. For a suitable transduction signal, the outer membrane must hydrate, keep its integrity and have the suitable porosity to enable (re)binding of MC-LR on the sensing layer. Furthermore, a good adhesion between the conductive support and the sol–gel membrane must be ensured to avoid water permeation into this internal layer. The time required to obtain a suitable sol–gel matrix was selected by letting the reaction take place for 30–240 minutes. The sensors prepared with 30 and 60 minutes presented cracked membranes that could be easily detached from the solid-contact. The membrane obtained by 120 minutes reaction period did not crack but dissolved in water while the template was being extracted, indicating that the hydrolysis was incomplete. After 240 minutes the membrane glazed and coating the electrode was impossible. Only membranes prepared after 180 minutes were crack free and water resistant. The corresponding ISE sensors showed linear responses from 0.67 to 1.67 μg L^{-1} of MC-LR, slopes of 140.5 mV per decade and detection limits of 0.67 μg L^{-1}. Thus, this time was considered as optimal for preparing MC-LR sol–gel membranes.

3.3.1.3 Template extraction

ISG membranes carry template molecules (MC-LR) that should be leached before conducting the potentiometric assays. This procedure ensures that the sites to which MC-LR species in the sample should bond are vacant. MC-LR presents enough solubility in water to be extracted by it from the sol–gel matrix. This is an inexpensive and innocuous material while the use of another solvent could lead to an irreversible damage/alteration of the sensing layer. Different washout times were tested aiming to extract the maximum amount of MC-LR while ensuring the integrity of the membrane. The extraction of MC-LR from the ISG outer layer was studied for 3 or 6 consecutive hours. The water phase was changed each 1.5 hours to avoid its saturation with MC-LR and enhance the extraction efficiency. After washing out MC-LR for 3 hours, the corresponding ISEs displayed linear responses in the range of 0.77–1.67 μg L^{-1} of MC-LR, average slopes of 180.0 mV per decade, and detection limits of 0.77 μg L^{-1}.

When these exact electrodes were subjected to an additional 3 hours washout period, the membranes became opaque (previously transparent) and the electrodes useless. The same result was observed for a 6 hours template extraction period and it became unsuitable to conduct further potentiometric analysis. Thus, the extraction time was set to 3 hours.

3.3.2 Scanning Electron Microscopy analysis

SEM analysis of ISG and NISG are presented in Figure 3.2. Nanostructures with variable dimensions (≈ 40-80 nm) are observed. The thickness of the sensing layer, the dimensions of the agglomerates and the size of the channels are very important because thin sensing layers mean short distances between the recognition sites and the electrodes, so that just a few target molecules can cause a noticeable perturbation on the electrode. On the other hand, very large channels allow the diffusion of molecules of sizes greater that that of the molecule of interest, diminishing the selectivity of the sensor. In the case of the ISG, the grain size seem to be smaller than the grain size of the NISG, this could be a consequence of differences in the sol-gel reaction velocity. More nominal differences between ISG and NISG membranes are very difficult to observe under electron microscopy evaluations, due to the non-conductivity of samples.

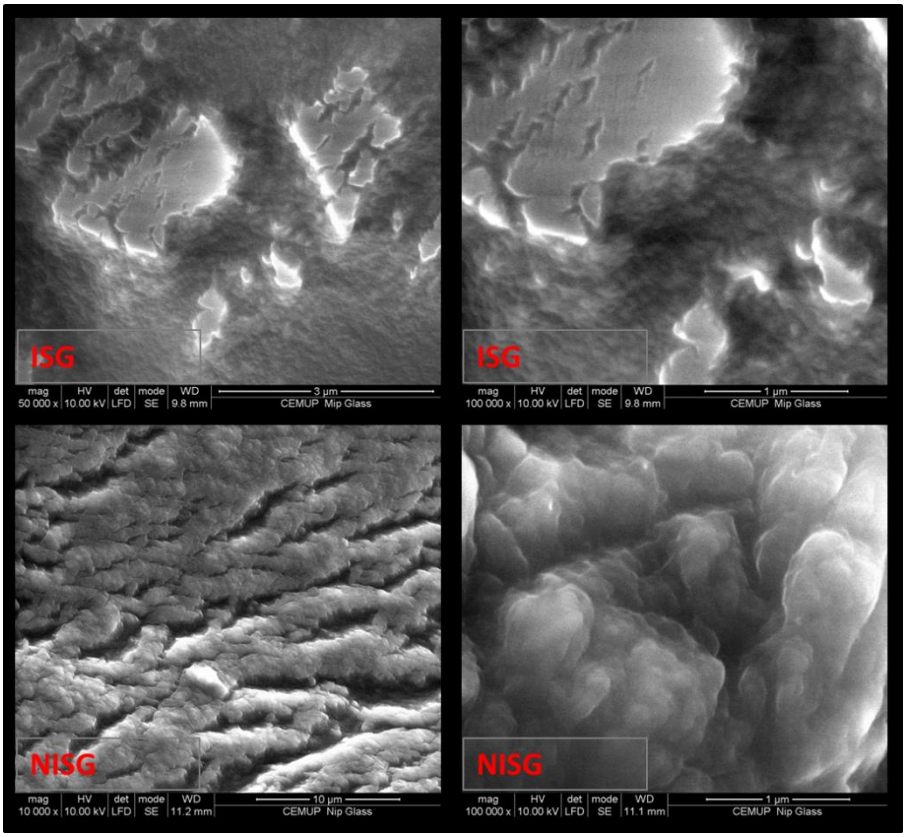

Figure 3.2 – Scanning electron microscopy analysis of imprinted sol-gel (ISG) and non-imprinted (NISG) membranes.

3.3.3 Effects of pH

The effect of pH in a sol–gel potentiometric sensor is a crucial aspect to consider. It affects both the sensing sol–gel layer and the MC-LR ionic structure. Furthermore, the dominant MC-LR species in highly acidic media is cationic while in alkaline media is anionic. This study was carried out by testing three different buffer solutions with pHs ranging from 6.5 to 9.4, the pH range in environmental waters (Law-Decree 307/2007). Different buffers were selected for this purpose, meaning that the performance of the electrodes was connected to both pH and nature of the buffer. The obtained analytical features were indicated in Table 3.1.

The best analytical features were found for pH 6.5 (PIPES buffer). As may be seen in Figure 3.3, a slight pH change to 7.4 increased the lower limit of linear range and the LOD but extended the linear behaviour. Further increase to pH 9.4 gave no emf changes (Figure 3.3).

Table 3.1 - Characteristics of membrane/solid contact tested for microcystin-LR selective readings in solutions of different pHs, along with the corresponding analytical features (*n* = 2)

Sensor	Membrane	Solid Contact	Buffer, pH	Linear range ($\mu g\ L^{-1}$)	Slope ($mV\ decade^{-1}$)	Detection limit ($\mu g\ L^{-1}$)	r^2
I	ISG	Carbon	PIPES, 6.5	0.77-1.67	211.3	0.73	0.993
II	NISG	Carbon	PIPES, 6.5	0.77-1.67	179.7	0.75	0.992
III	ISG	Carbon	PBS, 7.4	0.91-2.00	58.2	0.91	0.988
IV	NISG	Carbon	PBS, 7.4	0.91-2.00	59.3	0.91	0.995
V	ISG	Carbon	Borax, 9.4	—	—	—	—
VI	NISG	Carbon	Borax, 9.4	—	—	—	—
VII	ISG	Aluminium	PIPES, 6.5	0.77-1.00	594.3	0.77	0.983
VII	NISG	Aluminium	PIPES, 6.5	0.77-0.91	740.8	0.77	0.963
IX	ISG	Titanium	PIPES, 6.5	0.91-1.67	-103.0	0.91	0.997
X	NISG	Titanium	PIPES, 6.5	1.00-2.00	75.7	1.00	0.985
XI	ISG	Copper	PIPES, 6.5	0.77-1.00	-1019.3	0.77	0.986
XII	NISG	Copper	PIPES, 6.5	0.77-1.25	-560.2	0.77	0.971
XIII	ISG	alloy Ni90/Cr10	PIPES, 6.5	0.77-2.00	220.6	0.75	0.991
XIV	NISG	alloy Ni90/Cr10	PIPES, 6.5	0.84-2.00	132.0	0.77	0.993
XV	ISG	alloy Ni80/Cr20	PIPES, 6.5	0.91-1.67	173.0	0.84	0.996
XVI	NISG	alloy Ni80/Cr20	PIPES, 6.5	0.77-1.43	142.0	0.84	0.997

ISG: imprinted sol-gel membrane; NISG: non-imprinted sol-gel membrane.

The predominant form of MC-LR in this pH is anionic, thus hindering its interaction with a membrane that carried an anionic lipophilic additive (also playing as an anionic excluder). The similarity between ISG and NISG membranes obtained in pH 7.4 indicated, however, that the recognition of the template was made by means of general electrostatic interactions instead of stereo-chemical effects. Increased specific detection of MC-LR was achieved by decreasing the pH down to 6.5.

Under this condition, the average slope of the ISG biosensors was ~20% higher than that of the NISG. The limit of detection was also enhanced, decreasing in 20%. For this reason, the pH 6.5 was used in subsequent experiments. The overall differences between ISG and NISG were small and attributed to the stereochemical recognition of the analyte by the imprinted sites. Therefore, major response of the electrode resulted from non-specific electrostatic interactions between the sol–gel matrix and the target analyte.

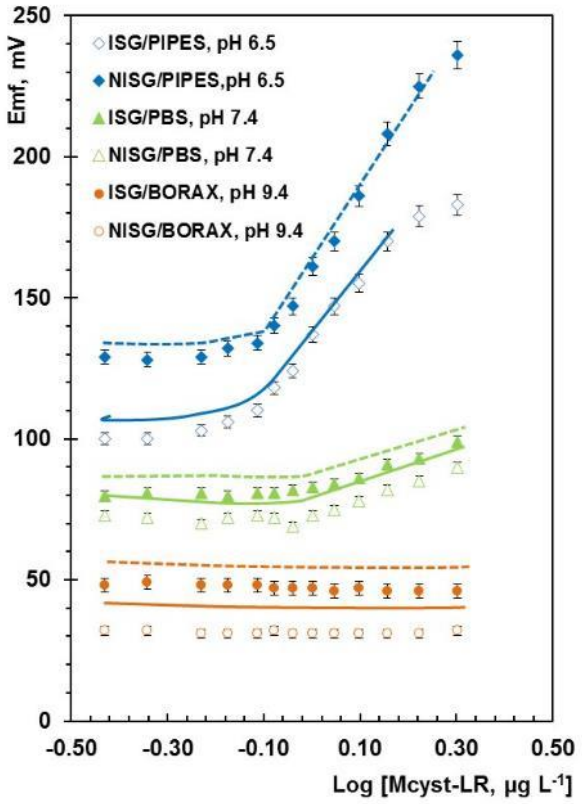

Figure 3.3 - Calibrations of ion selective electrodes were made in different buffers/pHs, ranging from 0.37 to 2.0 µg $L^{-1}$of Microcystin-LR. Potential readings were recorded after 2 min and emf was plotted as a function of log Microcystin-LR molar concentration.

Overall, these materials were found suitable for potentiometric ionophores, with the imprinted ones displaying higher slopes. Their ability to discriminate selectively MC-LR among other ionic species is evaluated by selectivity studies, addressed later in the manuscript.

3.3.4 Carbon *versus* metal solid contact

The material of the solid contact is important because it reflects the membrane occurring events. Mostly, they should be inert and offer high conductivity. A good adhesion to the membrane should also be observed, preventing the sample from permeating and contacting the conductive material directly. In this study, 5 different metals were coated with the same ISG or NISG composition (ISEs VII to XVI) and compared to the carbon-contact electrodes (I and II). All these measurements were conducted in PIPES buffer of pH 6.5.

As may be seen in Figure 3.4, most of the ISG membranes applied on metals did not show a suitable potentiometric performance. In addition, negative slopes were observed for ISEs IX, XI and XII, despite the negative anionic additive in the membrane and the pH of the test solution. The best general behaviour was recorded for carbon and Ni/Cr (90:10) (Table 3.1).

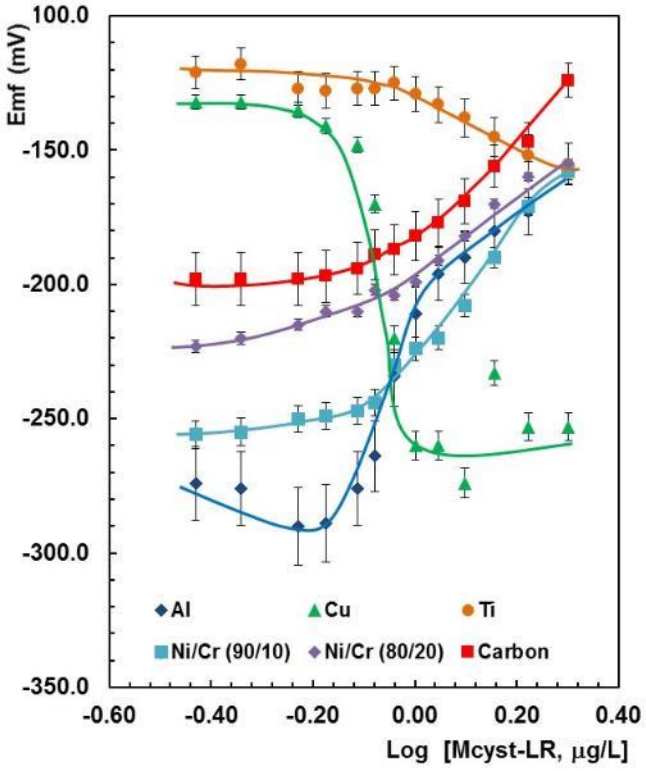

Figure 3.4 - Calibrations of ion selective electrodes with a microcystin-LR selective membrane on different conductive supports (emf was recorded after 2 min for microcystin-LR standards, ranging from 0.37 to 2.0 µg L^{-1}, in PIPES buffer, pH 6.5).

To justify the obtained results, the solid-contact electrodes were tested by CV and EIS, in order to assess their chemical stability and conductivity patterns. The results obtained are shown in Figure 3.5. Copper and titanium contacts resulted in sensors of negative slopes, with copper-based electrodes showing huge hyper-Nernstian behaviour. Despite this similar negative slope, they exhibited opposite features in terms of conductivity and chemical inertia. Titanium showed high resistance to charge transfer because it displayed very small currents when oxidizing or reducing of Fe(II) or Fe(III), respectively, by means of CV studies (Figure 3.5).

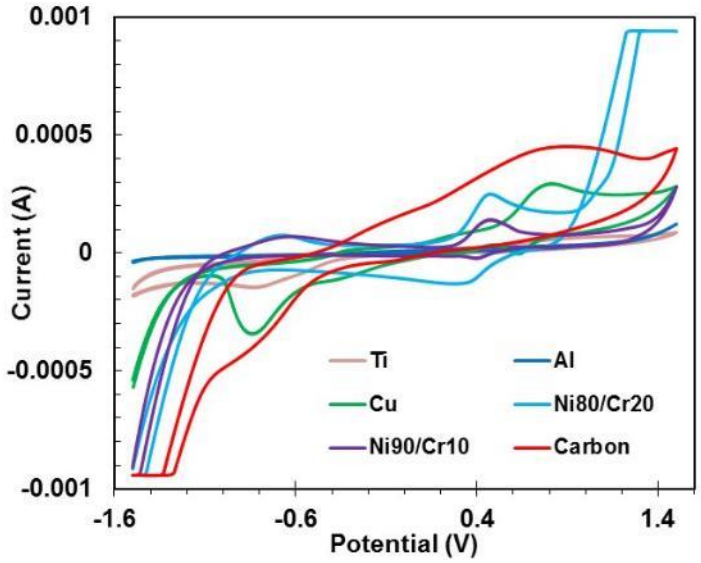

Figure 3.5 – Cyclic voltammetry for different conductive supports, in 10^{-3} M of PIPES buffer (pH 6.5) with 5 mM $[Fe(CN)_6]^{3-/4-}$.

The subsequent EIS studies were consistent with this observation. The ISG membrane coating a titanium metal gave rise to ~41897 Ω. Opposing, copper showed very small resistance, producing higher currents for the redox couple Fe(II)/Fe(III), as may be seen in Figure 3.6. The emerging resistance was too small to be measured under the conditions selected for testing all solid-contacts. This good feature is however undissociated from the poor chemically stability of copper. Under specific voltammetric conditions, electrodes with ISG membranes/copper showed several peaks on CV voltamograms, with only two of them being correlated to the Fe(II)/Fe(III) redox couple. The other peaks correspond to oxidized and reduced forms of cupper itself. On the whole, copper was a highly conductive material but easily oxidized while titanium displayed an inert pattern but a high charge transfer resistance. Aluminium based electrodes showed very high charge transfer resistances as may be seen from the absence of redox peaks on the CV voltamograms and the very high –Z'' values obtained in the EIS assays. These features justified the small correlation coefficients of the calibration curves (Table 3.1). Their calibrations were indeed close to a titration, as may be seen in Figure 3.4.

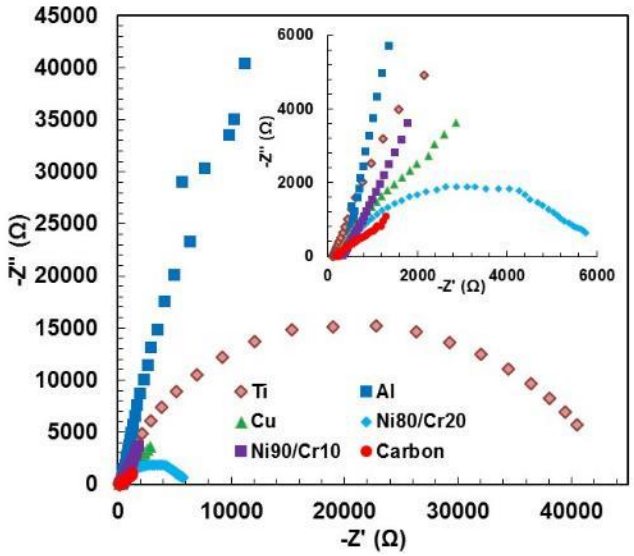

Figure 3.6 – Electrochemical impedance spectroscopy for different conductive supports, in 10^{-3} M of PIPES buffer (pH 6.5) with 5 mM $[Fe(CN)_6]^{3-/4-}$.

In general, Ni/Cr alloys and carbon displayed the smaller resistance to charge transfer (Figure 3.6). Only Ni/Cr alloy (90:10) showed measurable resistances in EIS studies, with the other materials having almost linear responses (Figure 3.6). Their conductivity ability followed this order: Ni/Cr (90:10) < Ni/Cr (80:20) < carbon. This may be easily seen on the CV voltamogram (Figure 3.5). Overall, ISEs/carbon electrodes exhibited a much higher sensitivity than those relying on nickel/chromium alloys and offered a much higher potential stability.

The potential drift observed for the ISG membranes applied on Ni/Cr alloys seemed to corroborate with the formation of an aqueous layer at the interface of the sensing membrane/alloy. Since the composition of this aqueous layer was not controllable, the emf changed in an unpredicted manner (Buck, 1978; Hauser et al., 1995). In general, considering both signal stability and sensitivity data of all electrodes, the electrode of carbon solid contact showed much better operating features for the intended purposes and was selected for the following studies.

3.3.5 Selectivity against inorganic compounds

According to 307/2008 Portuguese Decree-Law the most relevant ions controlled in waters for human consumption are Al^{3+}, NH_4^+, Cl^-, Mg^{2+}, Mn^{2+}, Na^+, and SO_4^{2-}. Thus the selectivity of the chemical sensor was tested against these species. Their maximum admitted levels were used as maximum interfering concentrations because it is highly unlikely their presence in environmental waters above these limits. These were 200 µg L^{-1}, 500 µg L^{-1}, 250 mg L^{-1}, 50 µg L^{-1}, 50 mg L^{-1}, 200 mg L^{-1} and 250 mg L^{-1}, respectively.

The potentiometric selectivity coefficients (K_{IJ}^{pot}) for a main ion (I) against a foreign one (J) were assessed by the MPM, first reported by (Gadzepko and Christian, 1984). This method is applicable to almost any sensor and does not require that a Nernstian response is observed (Horvai, 1997). The values of K_{IJ}^{pot} were obtained by following equation 3.1 where a_j is the interfering concentration required to give the same potential jump as the concentration of aI (both added over a common background of I).

$$K_{IJ}^{pot} = \frac{\Delta_{aI}^{(1)}}{a_J(IJ)^{(2)}} \quad (3.1)$$

Almost none of the tested species was able to provide the potential change of the primary ion solution, indicating that the electrodes displayed a very high selectivity for MC-LR. Only chloride managed to change the potential suitably. The corresponding average log ($K_{MC\text{-}LR,Cl}^{pot}$) was -2.57, indicating that the response for MC-LR prevailed (chloride was in much higher concentration than MC-LR when the emf matched that of the main ion). Thus, the electrodes offered very good selectivity properties for MC-LR, indicating that these are suitable for the analysis of environmental waters.

3.3.6 Response time and lifetime

The time required to achieve a steady potential response (± 0.5 mV) using the proposed sensors in 2.00 to 0.37 µg L^{-1} MC-LR concentration solutions with a rapid increase in concentration was established in 2 minutes. Replicate calibrations for equal electrodes indicated a small potential drift and confirmed their high reproducibility.

Detection limits, response times, linear ranges and calibration slopes were reproducible of their original values for at least 4 weeks when sensors were stored out of water and on dry atmosphere. The selected conditions for this have been resumed in Table 3.2.

Table 3.2 - Parametric data for Microcystin-LR selective electrodes.

Parameter	Studied range	Selected
pH	6.5-9.4	6.5
Buffer	PIPES, PBS, Borax	PIPES
Hydrolysis time (min.)	30-240	180
Template extraction time (h)	3-6	3
Sol-gel chemical stability(week)	–	4

3.3.7 Binding constant

A selective ISG material requires the formation of stable complexes between the template and the polymeric matrix. The higher the stability of these complexes, the higher the probability of reaching higher levels of complexation between the ISG guest sites and the analyte. This being a molecular-level occurrence sensed by an ISE, the MC-LR/guest site complexation affects both selectivity and sensitivity. Thus, this binding constant was established on the surface of the proposed sensors, having carbon as the solid contact material. The sandwich method earlier proposed by Mi and Bakker, (1999) was selected for this purpose. It is based on the transient membrane potential measurements taken on two-layer sandwich membranes. The following equation was used for this purpose,

$$\beta_{IL_n} = \left(L_T - \frac{nRT}{Z_i}\right)^{-n} \exp\left(\frac{E_m Z_I F}{RT}\right), \quad (3.2)$$

where L_T is the total concentration of ISG guest sites in the membrane segment, RT is the concentration of the lipophilic ionic site, *n* is the ion–ionophore complex stoichiometry and R, T and F are the gas constant, absolute temperature and Faraday constant respectively, for an ion carrying a charge of Z_I. The obtained formation constant, βIL_n, was 1.14 $\times 10^8$, thus revealing a high affinity between guest sites and MC-LR under the potentiometric experimental conditions tested.

3.3.8 Application to environmental waters

In order to investigate the application of the present method to the analysis of environmental waters, spiked solutions were tested and the corresponding relative errors calculated. These assays were conducted in water (pH 6.5) with ISEs calibrated within 0.65-2.00 μg L^{-1} of MC-LR. The average recoveries of two spiked solutions were 101.2±5.5 %, corresponding to average relative errors of 1.18 % and thus confirming the accuracy of the analytical data (*n* = 2 for two ISEs).

3.4 Conclusions

Portable potenciometric sensors were developed for the direct and *in-situ* determination of MC-LR in environmental waters. The selective membrane was of ISG material. It required an anionic lipophilic additive to control the charged response and a solid-contact made of carbon to produce stable/sensitive, and reproducible responses. The solid contact sensor and performed the best result in terms of sensitivity was carbon made. The limit of detection found for the best ISG sensor was of about 0.73 μg L^{-1}, in PIPES buffer (pH 6.5). The sensors displayed high selectivity properties for the most common ions (Al^{3+}, NH_4^+, Cl^-, Mg^{2+}, Mn^{2+}, Na^+, and SO_4^{2-}) in environmental waters and offered simplicity in designing and analysis. Also they requires short measurement times of about 2 minutes, good precision and high accuracy.

Overall, the proposed method was proven suitable for the routine screening of MC-LR, essentially because this method allowed in-situ real-time monitoring of MC-LR in several water media and decreased significantly the time between the sampling and the analytical result.

References

Amemiya, S. 2007. Potentiometric Ion-Selective Electrodes, in: Zoski, C.G. (Ed.). Handbook of Electrochemistry. Elsevier Science, Amsterdam, The Netherlands, pp. 261-292.

Buck, R.P. 1978. Theory and principles of membrane electrodes, in: Freiser H. (Eds.). Ion Selective Electrodes in Analytical Chemistry. Plenum, New York, pp 1-141.

Campàs, M.; Marty, J.-L. 2007. Biosens. Bioelectron. 22, 1034–1040.

Gadzepko, V.P.Y.; Christian, G.D. 1984. Anal. Chim. Acta 164, 279–282.

Hauser, P.C.; Chiang, D.W.L.; Wright, G.A. 1995. Anal. Chim. Acta 302, 241-248.

Horvai, G. 1997. Sensor. Actuator. B-Chem 43, 94–98.

Law-Decree 307/2007 (Portuguese Law) of 2007, August 31st. Defines water quality for Human consumption, Annex I, Part 3 – Indicative parameters. Republic Journal 1st Serie, N. 164, 5747.

Li, T.; Wu, T.; Mazeas, L.; Toffin, L.; Guerquin, K.J.; Leblon, G.; Bouchez, T. 2008. Environ. Microbiol. 10, 580–588.

Lindner, P.; Molza, R.; Yacoub-George, E.; Dürkop, A.; Wolf, H. 2004. Anal.Chim. Acta 521, 37–44.

Mi, Y.; Bakker, E. 1999. Anal. Chem. 71, 5279-528.

Nagy, G.; Nagy, L. 2007. Anal. Lett. 40, 3-38.

Panosso, R.; Costa, I.A.S.; Souza, N.R.; Attayde, J.L.; Cunha, S.R.S.; Gomes, F.C.F.; 2007. Oecologia Brasiliensis 11, 337–56.

Schaller, U.; Bakker, E.; Splchiger, U.E.; Pretsch, E. 1994. Anal. Chem. 66, 391-398.

Trebbe, U.; Niggemann, M.; Cammann, K.; Fiaccabrino, G.C., Koudelka-Hep, M.; Dzyadevich, S.; Shulga, O.; Fresenius, J. 2001. Anal. Chem. 371, 734–739.

World Health Organization. 1998. Drinking-water quality guidelines for parameters of concern in agricultural drainage water - Annex 3, Technical Report, pp. 281–289.

This page was intentionally left blank

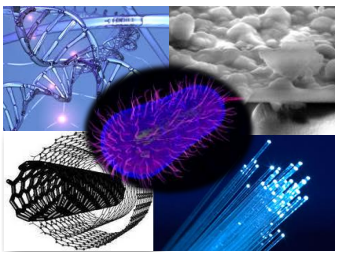

Chapter 4

Detection of microcystin-LR in water using molecular imprinted polymers on the wall of carbon nanotubes as sensory element

4.1 Introduction

The recent developments among nanomaterials, especially carbon nanostructures, trigered new expectations to the assembly of new affinity-based biorecognition elements. CNTs have been found to be promising materials in this context as they offer high electrical conductivity, chemical stability and mechanical strength, large length-to-diameter ratios, and easy chemical modification with almost any desired chemical or biological species to their surface (Balasubramanian and Burghard, 2006; Gooding et al., 2003; Merkoçi et al., 2005; Yang et al., 2007). They have been included in biosensors as biorecognition elements in different ways: as single probes (Ishikawa et al., 2009), as support of biomaterials (Mao et al., 2011; Moreira et al., 2011) or individually attached onto a proper transducing surface after synthesis (Li et al., 2005). They may also be used for surface modification or integrated in polymeric matrixes, in both oriented (vertically aligned) and non-oriented (random mixtures) configurations (Merkoçi et al., 2005). Several applications of these materials, as part of electrochemical platforms, have also been reported (Carrara et al., 2008; Lu et al., 2008; Pan et al., 2012; Poggi et al., 2002; Tang et al., 2008; Zhang et al., 2004).

Thus, the main target of the present work is to combine MI technology and nanomaterials (CNTs) within a low-cost recycled platform, enabling to carry out on-site analysis of an environmental contaminant. There are several kinds of environmental contaminants, including drugs and microbial cells and toxins.

Much attention has been paid to the tracking of drugs and microbial cells, while microbial toxins are in urgent need of novel and reliable methodologies for in-situ determinations. The most well known MC toxin is MC-LR. Its chronic toxicity potential was observed under the form of primary liver cancer, has led the WHO to establish a guideline of 1 μg L^{-1} as a maximum concentration of MC-LR in drinking water (WHO, 1998). MC-LR was also recently classified as a carcinogenic agent by the International Agency for Research on Cancer (Grosse et al., 2006). The search for fast-screening methods for rapid MCs control requires the development of methods that combine sensitive and selective recognition capabilities of low quantities of analyte.

Potentiometric sensors are attractive for practical applications, as they are associated with small size, portability and low energy consumption and cost. The development of solid contact ISEs along the years has led to major improvements of the LOD, increased range of applications, and simplification of the sensor construction, operation, and maintenance (Bakker and Pretsch, 2005 and 2007; Piletsky and Turner, 2002; Singh et al., 2012).

Herein, the design of a MIP for MC-LR on the surface of CNT and the integration of this material over a recycled screen-printed electrode (SPE) coupled to potentiometric transduction is presented. The ability of the sensory material to selectively recognize MC-LR and its cross-reactivity against other MC is shown, along with the overall analytical features of the device.

4.2 Materials and methods

4.2.1 Apparatus

All potential measurements were made by a Crison decimilivoltammeter, pH meter, GLP 21 (±0.1mV sensitivity) at room temperature and under constant stirring, see Figure 2.11.

The assembly of the potentiometric cell was: conductive solid support | MC-LR-selective membrane | buffered sample solution (10 mM 4-(2-hydroxyethyl)-1-piperazineethanesulfonic acid (HEPES), 150 mM of sodium chloride (NaCl), pH 6.6) || electrolyte solution, KCl | AgCl | Ag (s). The reference electrode was an Ag | AgCl | KCl saturated reference electrode from Crison Instrument, S.A. The selective electrode was prepared in a conventional configuration for batch mode evaluations. These devices had no internal reference solution and epoxy–graphite as solid contact (Kamel et al., 2009). The membrane was applied on the top of the carbon-paste electrodes. When necessary, the pH was measured by a Consort combined glass electrode connected to the Crison decimilivoltammeter, pH meter, GLP 21.

Polymeric film depositions over the metal contacts of the screen-printed electrode have been carried out by using an Autolab PGSTATION 128N computerized electrochemical instrument, controlled by dedicated NOVA 1.6 software (Ecochemie, Utrecht, The Netherlands). A 1×5 mm^2 silver electrode has been used as working electrode, while a glassy carbon rod and a pseudo silver electrode have been used as counter and reference electrode, respectively.

SEM images and Energy-dispersive X-ray spectroscopy (EDS) analysis were collected by a FEI Quanta 400FEG ESEM/EDAX Genesis X4M microscope. Raman experiments were performed using a JOBIN-YVON LABRAM spectrometer, and a He–Ne laser was used giving a monochromatic red light of 632.8 nm (at a power of 20 mW). Raman spectra were measured with a pin hole of 1000 μm and a slit of 100 μm. A 50X air objective lens of an Olympus optical microscope was used to focus the laser beam on the sample and also to collect the scattered radiation. A highly sensitive charge coupled device (CCD) camera was used to collect the Raman spectra. Extended scans from 100 cm^{-1} to 3500 cm^{-1} were performed on each sample.

4.2.2 Reagents and solutions

All chemicals were of analytical grade and double-deionized RNase free water (0.03 μS at 25 ºC) from ATS (Portugal) was used in the preparation of all solutions. PVC of high molecular weight, (vinylbenzyl)trimethylammonium chloride (VBTMA), potassium sulfate were purchased from Fluka, Europe, and tetrahydrofuran (THF) was obtained from Riedel-de-Häen, Germany.

TKClPB and o-nitrophenyl octyl ether (oNPOE) were obtained from Acros, Spain. MC-LR, multi-wall CNTs (CNTs, >7.5%, basis O.D.×L 7-15 nm × 0.5-10 μm), sodium 4-vinylbenzenesulfonate (VBSate), vinylbenzoate (VBate), tris(2-methoxyethoxy)vinylsilane (TMVS), benzoyl peroxide (BPO), vinylbenzene (VB), 3,4-ethylenedioxythiophene (EDOT), HEPES and divinylbenzene (DVB) were purchased from Sigma, Europe. Sodium chloride was purchased from Panreac, Spain. Chloroform was purchased by Carlo Erba, Europe. Iron III chloride 6-hydrate was purchased by Scharlau, Spain. Ammonium acetate was purchased by Analar, Portugal. Trichloroethylene (TCE) was obtained from Merck, Germany. The buffer used was 10 mM HEPES, 150 mM NaCl with a pH of 6.6.

4.2.3 Preparation of sensing membranes

The chemical structure of MC-LR has both polar and apolar regions. It contains three possible charged positions (2 carboxylic acids and 1 amine) and a side chain that may establish hydrophobic interactions. This hydrophobic side of the structure was used to adsorb MC-LR to the outer wall of the CNTs, while the eminent charged sites were used to attract charged monomers that, being involved in the subsequent polimerisation process, would create charged binding sites for MC-LR that were spatially distributed in complementary positions. Almost all chemical changes were carried out under mild conditions to ensure that the 3D arrangement and electrostatic environment of MC-LR were preserved.

To prepare the molecular imprinted carbon nanotubes (MI-CNTs), MC-LR (template, 3.5 μg in MeOH) was added to 2 mg of CNTs and let under continuous stirring for 4 hours (Figure 4.1A). Then, VBTMA (monomer, 1.5 g), VBSate (monomer, 0.72 g) and VBate (monomer, 0.52 g), all carrying charged organic functional groups, were added to this mixture and the mixture was again submitted to 4 hours of continuous stirring at ambient temperature (Figure 4.1B). Ionic interactions between these monomers and the charged groups of the adsorbed MC-LR were established here; the position of the vinyl groups in these monomers was conditioned by the charges of MC-LR and remained free to participate in the subsequent polimerisation step, responsible for imprinting the target molecule. After, the mixture was centrifuged and the supernatant removed. The solid material was let stand for 1 hour at 40 ºC to evaporate the remaining supernatant.

After that, 100 µL of TMVS was added to enable the link between the CNTs and the subsequent polymeric layer. Sol-gel chemistry ensured that the CNTs were covalently bounded to the silane group and the vinyl group remained free and capable of participating in the polimerisation step. CNTs contain hydroxyl, carbonyl and carboxylic groups at its surface enabling the formation of covalent bounds between these groups and CNTs. In particularly, hydroxyl groups act as binding sites in the silanization process (Kathi and Rhee, 2008; Luong et al., 2004; Scheibe et al., 2010). To ensure that the polymeric layer is covalently attached to CNTs is not necessary the full coverage of the entire CNTs surface but only a few anchor points.

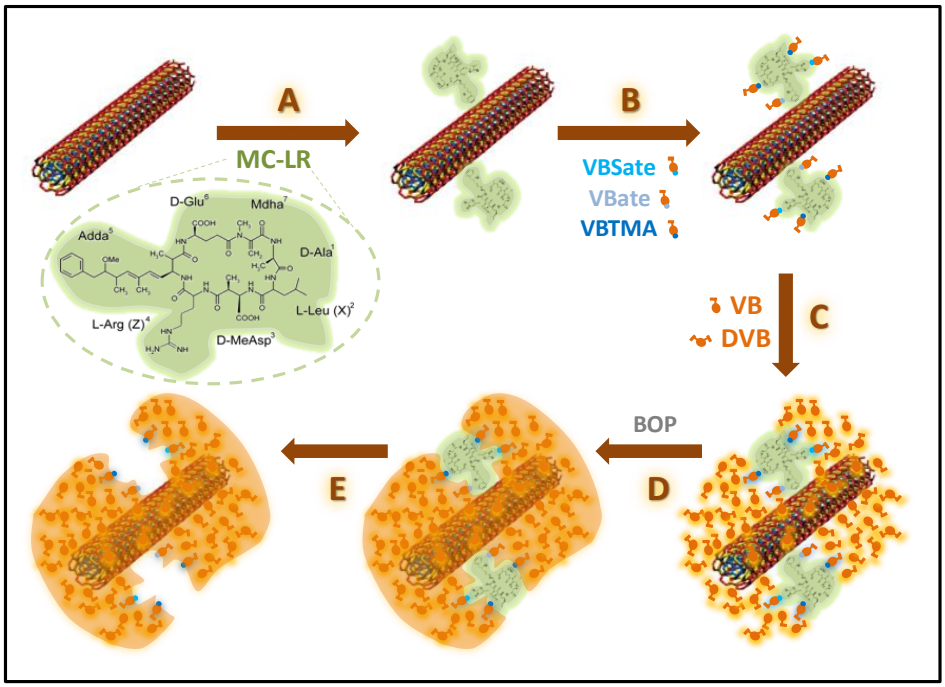

Figure 4.1 - Design of the carbon nanotubes imprinted polymers.

Next, BPO (radical initiator, 6 mg) was added, followed by the addition of VB (monomer, 50 µL) and DVB (cross-linker, 50 µL), kept under continuous stirring for 2 hours (Figure 4.1C and Figure 4.1D). These benzene derivative monomers have only phenyl radicals linked to the vinyl group. The presence of these phenyl groups was expected to increase the electron density of the polymer film, contributing to an easier polarization of this material. DVB acted as cross-linker because it carried two vinyl groups, leading to the formation of a reticulated and eventually rigid structure.

This polimerisation was carried out at room temperature for only 2 h, in order to avoid any alteration of the MC-LR conformation. Then, the mixture was centrifuged and the supernatant was removed. The mixture was then thoroughly washed with 3 cycles of centrifugation and re-suspension in fresh buffer solution to washout exceeding reactants and the template (Figure 4.1E). Finally, the solid material was dried overnight under nitrogen atmosphere inside a desiccator. Non-imprinted carbon nanotubes (NI-CNT) biomaterial was also prepared in parallel, by the same process but excluding the template from the overall process. In this case, the charged monomers do not interact with the template molecule (not present here) and the cavities are not form. The polymer form by VB, BPO and DVB is formed only around CNTs.

Five sensing membranes were prepared with the composition presented in Table 4.1. The core MC-LR selective membranes (Sensor I) were prepared by mixing MI-CNTs (ionophore, 0.50 mg) with PVC (polymer, 15.0 mg) and oNPOE (plasticizer, 30.0 mg). An additional membrane having also TKClPB (anionic additive, 0.25 mg) was also prepared (Sensor II). Three additional membranes were made in parallel as control: one had NI sensory material as ionophore (sensor III) and the other two had no ionophore (Sensor IV and V), with one of these including the additive (Sensor IV). Each of the above mixtures was stirred until the PVC was well moistened, and dispersed in 0.5 mL THF. These membranes were coated on carbon-electrodes and let to dry during 48 h. After drying, the electrodes were kept in buffer solution. The regeneration of the electrodes was made by washing the membranes in ultrapure water for 30 minutes between measurements.

Table 4.1 - Selective membrane composition and the corresponding analytical features in a buffer of 10 mM HEPES and 150 mM NaCl, pH 6.6 (n=3).

Sensor	Ionophore	Composition				Linear range	Slope	Detection limit	r^2
		Sensor (mg)	oNPOE (mg)	TKClPB (mg)	PVC (mg)	(µg L^{-1})	(mV $decade^{-1}$)	(µg L^{-1})	
I	MI	0.5	30	—	15	1.32 - 0.77	-62±4	0.69±0.028	0.998
II	MI + additive	0.5	30	0.25	15	1.21 - 0.74	-53±6	0.66±0.010	0.996
III	NI	0.5	30	—	15	1.28 - 0.72	29±5	0.53±0.010	0.981
IV	additive	—	30	0.25	15	—	—	—	—
V	blank	—	30	—	15	1.19 – 6.84	31±3	0.64±0.010	—

oNPOE: o-nitrophenyl octyl ether; TKClPB: tetrakis(4-chlorophenyl)borate; PVC: polyvinyl chloride ; MI: molecular imprinted membrane;
NI: non-imprinted membrane.

4.2.4 Potenciometric measurements

Several selective membranes were prepared, including MI and NI materials in plasticized PVC and casting the resulting solutions on solid-state carbon supports. Their overall composition was indicated in Table 4.1. Decreasing concentration levels of MC-LR were obtained by transferring increasing aliquots of buffer solution (from 1 to 5 mL), pH 6.6, to 5 mL of 2.0 $\mu g\ L^{-1}$ MC-LR solution. The range of concentrations studied was 0.46 to 2.0 $\mu g\ L^{-1}$.The potential readings of the stirred MC-LR solutions were measured at room temperature and recorded after stabilization to ± 1 mV, according to IUPAC - International Union of Pure and Applied Chemistry - recommendations (Buck and Cosofret, 1993).

4.2.5 Procedures for selectivity assays

Other species that are common in waters or expected as contaminant may interfere with the response of the potentiometric device. Selectivity studies followed MPM (Umezawa et al., 1995). The change in emf caused by the principal ion was measured for a MC-LR rise in concentration from 1.0 to 5.0 $\mu g\ L^{-1}$. Similarly, the emf of a 1.0 $\mu g\ L^{-1}$ MC-LR solution was measured and a solution of interfering species added until the same potential change was observed. Solutions of 500 mg L^{-1} NH_4^+, 250 mg L^{-1} Cl^-, 250 mg L^{-1} SO_4^{2-}, 200 µg L^{-1} Fe^{3+}, 200 mg L^{-1} Na^+, 100 µg L^{-1} chloroform and 10 µg L^{-1} of TCE were tested for this purpose, being these the main components/contaminants in waters by the Portuguese Law (Law-Decree 307/2007). All these interfering species solutions were prepared in buffer solution.

4.2.6 Analysis of environmental waters

Environmental water samples were collected in an artesian well and stored in amber glass bottles previously rinsed with double-deionized RNase free water. The pH and ionic strength of the water samples was adjusted by addition of buffer (50:50), and they were stored at 4 °C until analysis. The samples were finally spiked with MC-LR. These analyses were carried out in duplicate.

4.2.7 Recycling and designing the chips

Used SPEs were obtained from an old/non-reusable commercial screen-printed electrode carrying three silver contacts on a ceramic substrate (200×100 mm) and recycled in order to enable their application in the *in-situ* analysis of environmental waters, using only very low volume samples. The ceramic support was cut to remove the indicating, reference and counter electrode support material. The insulating polymer on top of these silver contacts was removed to expose the conductive silver and allow their use as conductive support. One of the sides of the ceramic was used as reference (RE) and working electrodes (WE), while the other side was used as electrical contact in the switch box where these screen-printed electrodes are routinely used. A 10^{-2} M $FeCl_3.6H_2O$ solution was deposited on the silver track acting as RE to allow the formation of a silver chloride on top of it. Each WE was first modified with a poly(EDOT) layer, by potentiostatic electropolimerisation of EDOT (monomer, 0.01 M), at a potential of +0.9 V during 240 s, in a supporting electrolyte of 0.1 M potassium chlorate ($KClO_3$). The deposited polymer was then reduced at −0.5V for 60 s in the same electrolyte solution and subsequently stabilized by cyclic voltammetry. For this purpose, five subsequent potential scans, from −0.5 to +0.5 V, at a potential scan rate of 0.05 Vs^{-1} were recorded in the same supporting electrolyte solution (Bello et al., 2007). The ceramic support was then let dry and the selective membranes casted on top of each WE track. These membranes were physically separated, an essential condition to obtain independent potentials.

4.3 Results and discussion

4.3.1 Scanning Electron Microscopy and Energy-Dispersive X-ray Spectroscopy analysis

SEM analysis was conducted over CNTs, MI-CNTs and NI-CNTs to confirm the formation of a polymeric layer around the nanotubes of carbon. The obtained images are shown in Figure 4.2, along with the corresponding EDS spectra. Plain CNTs were composed by carbon only, as indicated in the EDS spectra. The EDS analysis shows that polymers are formed around CNTs.

In the EDS analysis of CNTs only carbon (C) is observed, while in MI-CNTs and NI-CNTs other components due to the polymer formation around CNTs were observed. The tubes showed 8–20 nm thickness, being this wide range a consequence of using multi-wall nanotubes.

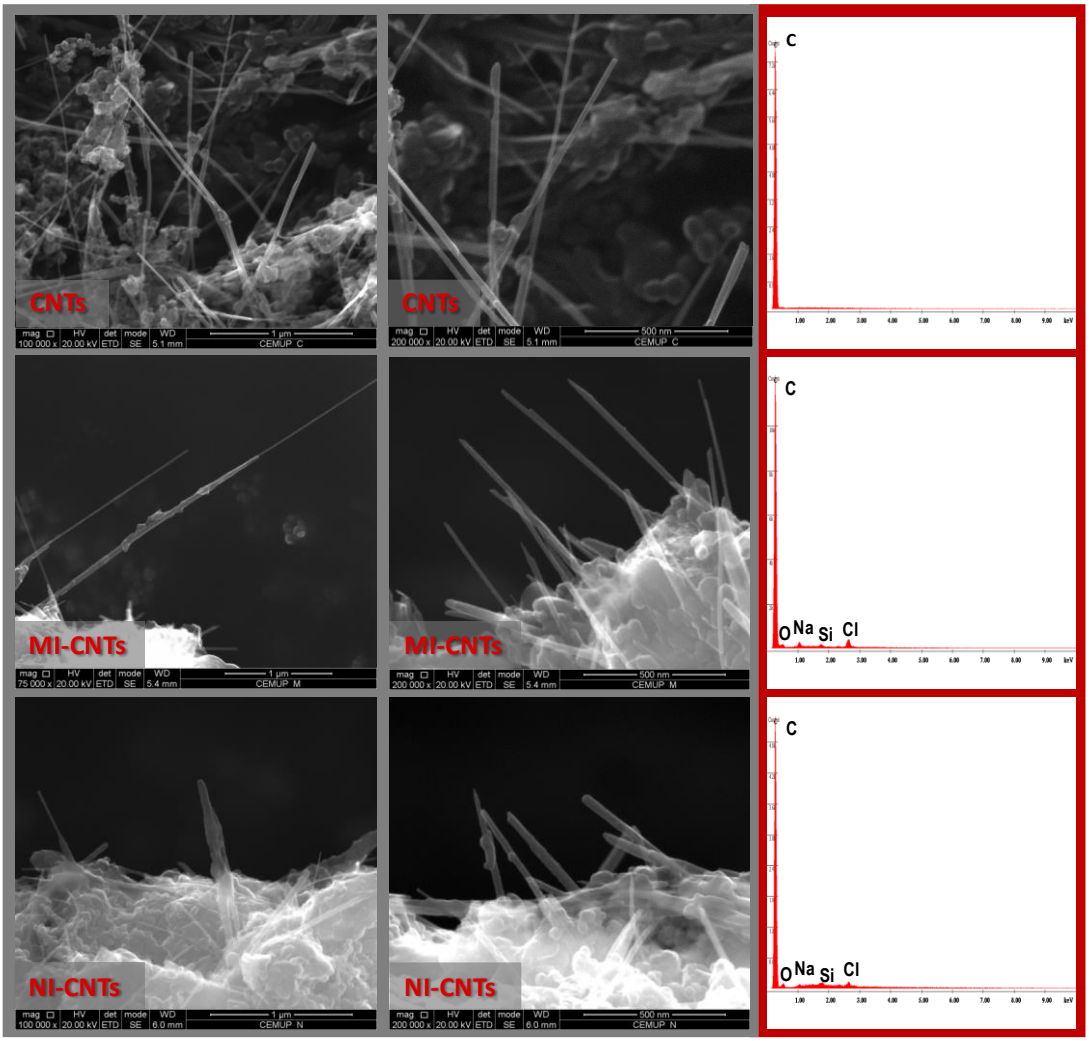

Figure 4.2 – Scanning electron microscopy (left) and energy-dispersive X-ray spectroscopy (right) analysis of carbon nanotubes (CNTs), molecular imprinted carbon nanotubes (MI-CNTs) and non-imprinted carbon nanotubes (NI-CNTs).

Modified CNTs (MI-CNTs or NI-CNTs) displayed thicker tubes, ranging within 18 and 40 nm (Figure 4.2). When compared to pure CNTs, the resolution of the SEM images of these materials under higher amplification (400000x), was reduced accounting for a decrease in the conductivity of this material. This observation supported the existence of organic carbon-based structures over the tubes of carbon. Technical differences between MIP and non-imprinted polymer (NIP) materials are however not clear under electron microscopy evaluations, with further studies being needed.

4.3.2 Raman analysis

The obtained Raman spectra for CNTs, MI-CNTs and NI-CNTs are shown in Figure 4.3. The spectra of CNTs showed three main peaks: (i) the D band at 1338 cm^{-1}, originated from the sp^3-hybridized carbons on the nanotubes; (ii) the G band at 1575 cm^{-1}, attributed to the a splitting of the E_{2g} stretching mode of graphite-like structures, which is relevant to vibration of the sp^2-bonded carbon atoms in a two-dimensional hexagonal lattice; and (iii) the 2D band at 2657 cm^{-1}, assigned to the overtone of the D band. The two most important of these bands were the G and the D band, which represented the sp^2 and sp^3 structures (Hsu et al., 2010). The G band corresponded to the E_{2g} modes which represented the movement in opposite directions of two neighbouring carbon atoms in a graphite sheet. The D band was attributed to the disorder present in the CNTs. The intensity ratio D/G band is often used to monitor the functionalization of CNTs (Gao et al., 2005; Linghao et al., 2012). In first-order Raman spectra, the positions of the bands D, G and D' (1100–1700 cm^{-1}) presented very similar behaviour, however the intensity ratio D/G ratio showed differed behaviours for each material which may be correlated to differences in their structural ordering and CNTs diameter (Antunes et al., 2006, 2007).

As can been seen in the Raman spectra (Figure 4.3), the intensity ratio of CNTs is higher (0.7) than the modified ones (MI-CNTs and NI-CNTs), which presented values of 0.31 and 0.32, respectively. The increase of tube diameter of the imprinted CNTs is the most probable responsible for the decrease on the ratio D/G observed on MI-CNTs and NI-CNT and may be correlated to a reduction on defect density. This is also the reason for the D/G ratio of unmodified CNTs is smaller. This corroborated well the presence of a polymeric layer on the overall CNTs structures.

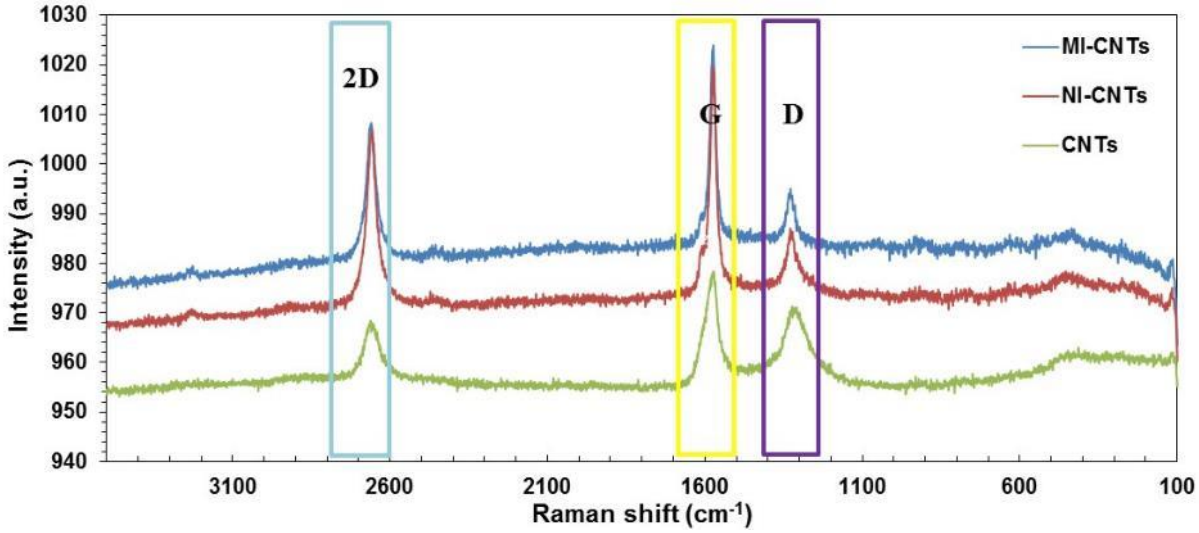

Figure 4.3 - Raman spectra of the carbon nanotubes (CNTs), molecular imprinted carbon nanotubes (MI-CNTs) and non-imprinted carbon nanotubes (NI-CNTs), with their typical 2D, G and D bands.

In addition, a small feature called G2 or D' near 1610 cm^{-1} was observed in the modified CNTs, characteristic of large diameter distribution of the CNTs (Zdrojek et al., 2004).

Full-width half-maximum (FWHM) in the Raman spectrum has been considered as a criterion in evaluating the structural disorder of CNTs, which arises from bond angle and bond length distortions (Casiraghi et al., 2005). The FWHM of the D-band (FWHM (D)) of modified CNTs (MI-CNTs and NI-CNTs) is narrowed than the CNTs. This is consistent with the introduction of a polymeric matrix which causes disorder bonds and amorphous carbon since FWHM (D) has the same tendency as the intensity ratio D/G (Antunes et al., 2007; Liu et al., 2010). Furthermore, D bands of modified CNTs appear with a significant shift to those of the CNTs; while the D band shifted 20 and 21 cm^{-1} in MI-CNTs and NI-CNTs materials, respectively, the G band shifted 4 and 3 cm^{-1}. In general, these shifts have been attributed to the structural changes introduced on the material organization by growing a polymeric layer over the CNTs.

Typical approaches to use Raman spectroscopy for assessment of purity have relied upon the intensity ratio of D/G. Recently, a report from DiLeo et al., was published where the ratio using the 2D band peak is shown to represent a more accurate alternative for measuring MWCNT quality and purity (DiLeo et al., 2007).

The results show that 2D band of the modified CNTs (MI-CNTs and NI-CNTs) was more intense than simple CNTs. This mode is known to be sensitive to increasing defect density. Second-order mode of 2D increases in intensity with increase in defects (Chakrapani et al., 2003), which can be consistent with the polymerisation around the CNTs materials. Overall, the obtained results confirmed the existence of slight structural differences between MI-CNTs and NI-CNTs materials and major differences between these and the CNTs.

4.3.3 Evaluation of standard curves

Several selective membranes were prepared by including MI-CNTs and NI-CNTs in plasticized PVC and casting the resulting solutions on solid-state carbon supports. Their overall composition was indicated in Table 4.1. The potentiometric response was evaluated by calibration in buffer (from 0.46 to 2.00 μg $L^{-1)}$.

The results showed that MI-CNTs and NI-CNTs presented opposite behaviour (Figure 4.4). Membranes with MI-CNTs (I and II) displayed negative slopes, while membranes with NI-CNTs (III) showed positive ones (Table 4.1). This opposite potential change against MC-LR concentration was attributed solely to the differences in the CNT modified materials, mostly because membranes (I) and (III) had only these materials acting as ionophores included in a plasticized PVC membrane. In addition, a blank membrane of plasticized PVC (V) was unable to provide a potentiometric response.

When a lipophilic anionic additive was included in MI-CNTs membranes (II), the slope kept its negative value. This additive was included in a small amount to increase the perm-selectivity of the membrane without governing the response of the electrode. This was not a good choice because the presence of the additive deteriorated the analytical features of the final device, exhibiting sub-Nernstian behaviour. This behaviour was consistent with the presence of charged sites within the imprinted cavities, not requiring additional charges to acquire a Nernstian response.

A membrane with only additive in plasticized PVC (V) was also prepared as control and was unable to produce a potentiometric response, at least within the concentration range studied.

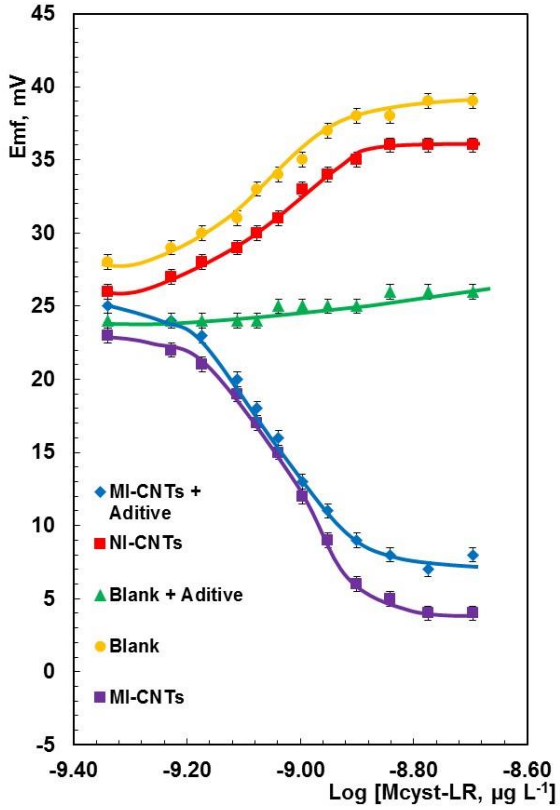

Figure 4.4 - Standard curves against microcystin-LR standards (emf was recorded at room temperature in the range 2.00 – 0.46 µg L^{-1} of microcystin-LR, in buffer, 10 mM HEPES, 150 mM NaCl, pH 6.6)

The biomimetic sensors presented low limits of detection of 0.66 and 0.69 µg L^{-1} for MI-CNTs membranes with and without additive. They show good sensitivity, for n=3, with slopes of -53 and -62 mV $decade^{-1}$ for MI-CNTs with and without additive, respectively, and they also showed fast response (t ≈ 20 s).

4.3.4 Selectivity against organic and inorganic compounds

Other species that are common in waters or expected as contaminant may interfere with the response of the potentiometric device. The most relevant ones include Fe^{3+}, NH_4^+, Cl^-, Na^+, and SO_4^{2-}, chloroform (as trihalomethane (THM)) and TCE (Law-Decree 307/2007). Thus, the selectivity of the sensors was tested against these species up to their maximum admitted levels, as their presence in environmental waters above these limits is highly unlikely. These were 0.5 mg L^{-1} of NH_4^+, 250 mg L^{-1} of Cl^-, 250 mg L^{-1} of SO_4^{2-}, 200 µg L^{-1} of Fe^{3+}, 200 mg L^{-1} of Na^+, 100 µg L^{-1} of chloroform and 10 µg L^{-1} of TCE. The values of (K_{IJ}^{pot}) were calculated from equation 3.1. Almost none of the tested species was able to provide the potential change of the primary ion solution, indicating that the electrodes displayed a very high selectivity for MC-LR. Only chloride and sodium managed to meet the desired potential change, but only when these were in much higher concentration than MC-LR. The average $\log(K_{Mcyst-LR,Cl}^{pot})$ and $\log(K_{Mcyst-LR,Na}^{pot})$ was -3.3 and -3.2, respectively, indicating that the response to MC-LR prevailed. Thus, the electrodes showed very good selectivity properties for MC-LR, indicating that these were suitable for the analysis of environmental waters.

4.3.5 Cross-response to others microcystins

There are several parent MCs in environmental waters that show close structural similarities. The cross-response of the sensor against these is therefore an important analytical parameter (Kawaguchi et al., 2007). This should provide some information about the way the analytical signal should be expressed: either the sensor turns out specific for MC-LR and all sample analytical data is attributed to its content in MC-LR; or it gives a similar response to most of the MCs and the resulting data must be interpreted as a combined result of all MCs expressed in terms of MC-LR standards.

The response of MI and NI sensors for MC-LR, MC-YR and MC-RR is presented in Figure 4.5. The results showed that all MCs had similar behaviour. Thus, the sensory material cannot discriminate different MCs, making the analytical response in environmental waters a measure of the total amount of MCs present.

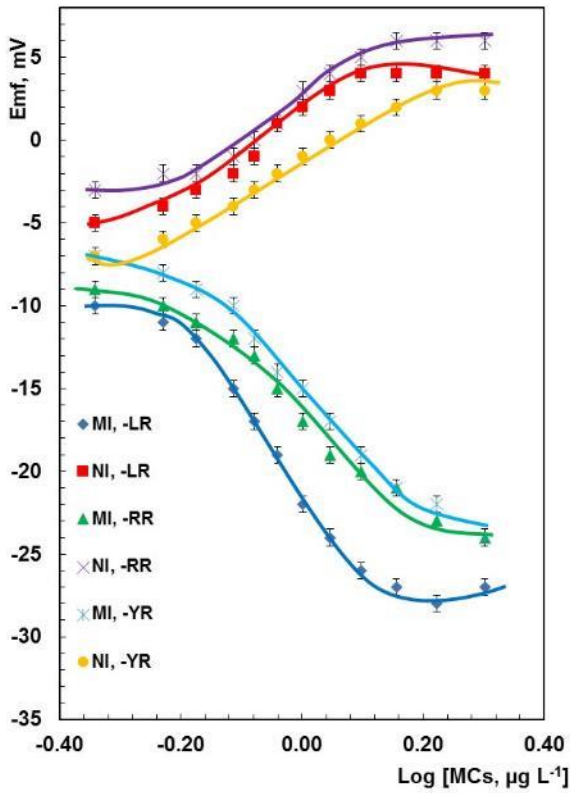

Figure 4.5 - Cross-reactivity against microcystins (microcystin-LR, microcystin-YR and microcystin-RR).

4.4.6 Analysis in a biparametric disposable chip for in-situ measurements

Used SPEs (Figure 4.6) were recycled in order to enable their application in the in-situ analysis of environmental waters, using only microvolummtric samples. Three independent conductive silver tracks were created. One served as reference, and was obtained by placing a small volume de ferric chloride on top of this track for a couple of hours. The other two served as indicating electrodes, and were prepared by electro-polymerizing a EDOT layer (independent from each other) and casting the membranes after on top of these (no electrical contact was enabled between these two).

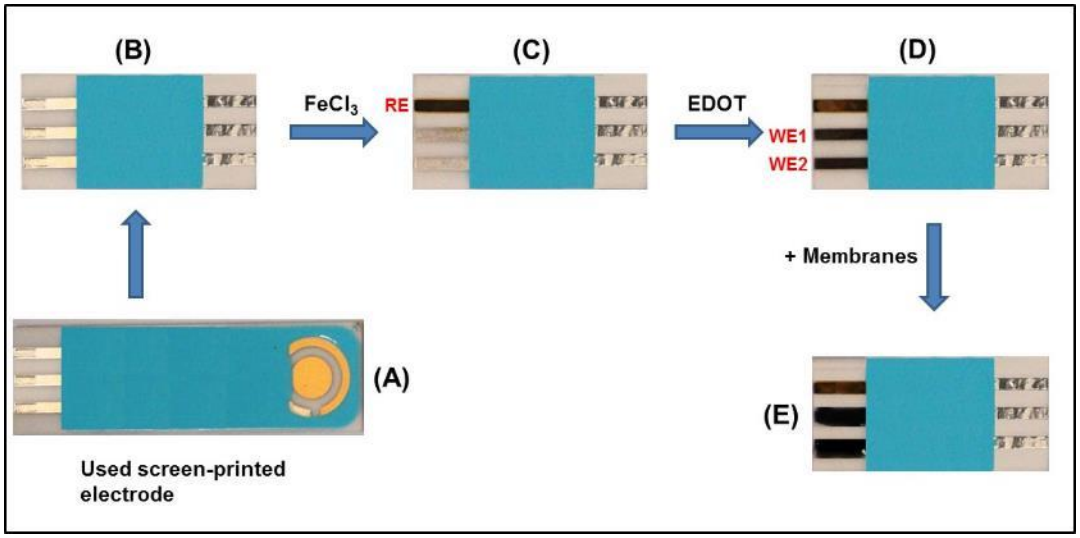

Figure 4.6 - Biparametric disposable chip construction; (A) used screen-printed electrode; (B) cutted screen-printed electrode and removal of the protective film; (C) formation of the silver chloride film over labelled reference electrode (RE); (D) 3,4-ethylenedioxythiophene (EDOT) electropolimerisation over labelled working electrodes (WE); (E) selective membrane application over working electrodes.

The potenciometric measurements were made in buffer. The chips presented a linear behaviour (squared correlation coefficients > 0.991) in the same range of concentration used previously and with the same positive/negative slopes. A significant difference was observed however, as the signal was amplified, up to slopes of -216 and 205 mV $decade^{-1}$ (n=2) for MI-CNTs and NI-CNTs, respectively. The use of these chips allowed simultaneous measurements of 2 different membranes but the concept can be easily extended to as many contacts are placed in the chip. The contacts are connected to a derivation box that read the signals individually without any interference between the signals. The use of these kinds of systems allows the reduction of the sample needed, up to 0.5 mL, and enable in situ analysis.

4.4.7 Application to environmental waters

In order to investigate the practical application of the present method, several waters were spiked and analysed, and the corresponding relative errors calculated. These assays were conducted in environmental waters (pH 6.5) with conventional sensors calibrated within 2.00 to 0.46 M of MC-LR.

The average recoveries of two spiked solutions was 102.4±1.7%, with an average relative error of -2.4%, thus confirming the accuracy of the analytical data (*n* = 2 for two sensors). The results were precise, with relative standard deviation < 6%.

4.4 Conclusions

A particularly successful surface imprinting approach was established to produce biomimetic materials for MC-LR used under potentiometric transduction, capable of differentiating imprinted from non-imprinted materials. The potentiometric results showed that MI-CNTs and NI-CNTs presented opposite behaviour being negative (slope) for membranes with MI-CNTs and positive for membranes with NI-CNTs. The biomimetic sensors presented good reproducibility for n=3, fast response (t ≈ 20 s) and low limits of detection, in all cases below the guideline value (1 μg L^{-1}) established by WHO, even in membranes without additive. The best imprinted sensor showed detection limits of about 0.66 μg L^{-1}.

The sensors offered good selectivity to some inorganic (Fe^{3+}, NH_4^+, Cl^-, Na^+, and SO_4^{2-}) and organic compounds (chloroform and TCE). The cross-reactivity analysis showed that sensors also respond to other types of MCs.

The biparametric disposable SPE allows the simultaneous measurement of multiple sensors, without signal interference, enabling *in situ* measurements. Further developments may be achieved by increasing the number of electrical contacts in the chip for more efficient multi-analyte performance.

References

Antunes, E.F.; Lobo, A.O.; Corat, E.J.; Trava-Airoldi, V.J. 2007. Carbon 45, 913–921.

Antunes, E.F.; Lobo, A.O.; Corat, E.J.; Trava-Airoldi, V.J.; Martin, A.A.; Veríssimo, C. 2006. Carbon 44, 2202–2211.

Bakker, E.; Pretsch, E. 2005. TrAC – Trends Anal. Chem 24, 199–207.

Bakker, E.; Pretsch, E. 2007. TrAC – Trends Anal. Chem. 27, 612–618.

Balasubramanian, K.; Burghard, M., 2006. Anal. Bioanal. Chem. 385, 452–468.

Bello, A.; Giannetto, M.; Mori, G.; Seeber, R.; Terzi, F.; Zanardi, C., 2007. Sensor. Actuator. B-Chem. 121, 430–435.

Buck, R.P.; Cosofret, V.V. 1993. Pure Appl. Chem. 65, 1849–1858.

Carrara, S.; Shumyantseva, V.V.; Archakov, A.I.; Samorì, B.; 2008. Biosens. Bioelectron. 24, 148–150.

Casiraghi, C.; Ferrari, A.C.; Robertson, J. 2005. Phys. Rev. B 72, 085401.

Chakrapani, N., Curran, S., Bingqing, W., Ajayan, P.M., Carrillo, A., Kane, R.S., 2003. J. Mater. Res. 18(10), 2515–21.

DiLeo, R.A., Landi, B.J., Raffaelle, R.P., 2007. J. Appl. Phys 101(6), 064301-1–5.

Gao, C., Jin, Y.Z., Kong, H., Whitby, R.L.D., Acquah, S.F.A., Chen, G.Y., Qian, H., Hartschuh, A., Silva, S.R.P., Henley, S., Fearon, P., 2005. J. Phys. Chem. B 109, 11925-11932.

Gooding, J.J.; Wibowo, R.; Liu, J.; Yang, W.; Losic, D.; Orbons, S.; Mearns, F.J.; Shapter, J.G.; Hibbert, D.B. 2003. J. Am. Chem. Soc. 125, 9006-9007.

Grosse, Y.; Baan, R.; Straif, K.; Secretan, B.; El Ghissassi, F.; Cogliano, V. 2006. Lancet Oncol. 7, 628−629.

Hsu, H.S.; Chung, P.Y., Zhang, J.H.; Sun, S.J.; Chou, H.; Su, H.C.; Lee, C.H.; Chen, J.; Huang, J.C.A. 2010. Appl. Phys. Lett. 97, 032503.

Ishikawa, F.N.; Stauffer, B.; Caron, D.A.; Zhou, C. 2009. Biosens. Bioelectron. 24, 2967–2972.

Kamel, A.H.; Sales, M.G.F.; Almeida, S.A.A.; Moreira, F.T.C. 2009. Anal. Sci. 25, 365–371.

Kathi, J.; Rhee, K.Y. 2008. J. Mater. Sci. 43, 33–37.

Kawaguchi, T.; Shankaran, D.R.; Kim, S.J.; Gobi, K.V.; Matsumoto, K.; Toko, K.; Miura, N. 2007. Talanta 72, 554–560.

Law-Decree 307/2007 (Portuguese Law) of 2007, August 31st. Defines water quality for Human consumption, Annex I, Part 3 – Indicative parameters. Republic Journal 1st Serie, N. 164, 5747.

Li, J.; Koehne, J.E.; Cassell, A.M.; Chen, H.; Tee, H.; Ye, Q.; Fan, W.; Han, J.; Meyyappan, M. 2005. Electroanal. 17, 15-27.

Linghao, He L.; Sun J.; Wang, X.; Fan, X.; Zhao, Q.; Cai, L.; Song, R.; Ma, Z.; Huang, W. 2012. Mater. Chem. Phys. 134, 1059–1066.

Liu, H.; Zhang, Y.; Li, R.; Sun, X.; Wang, F.; Ding, Z.; Mérel, P.; Desilets, S. 2010. Appl. Surf. Sci. 256, 4692–4696.

Lu, X.; Zhou, J.; Lu, W.; Liu, Q.; Li, J. 2008. Biosens. Bioelectron. 23, 1236–1243.

Luong, J.H.; Hrapovic, S.; Wang, D.; Bensebaa, F.; Simard, B. 2004. Electroanal. 16, 132–139.

Mao, Y.; Bao, Y.; Gana, S.; Li, F.; Niu, L. 2011. Biosens. Bioelectron. 28, 291–297.

Merkoçi¸ A.; Pumera, M.; Llopis, X.; Pérez, B.; del Valle, M.; Alegret, S.; 2005. TrAC – Trend. Anal. Chem. 24, 826-838.

Moreira, F.T.C.; Dutra, R.A.F.; Noronha, J.P.; Cunha, A.L.; Sales, M.G.F. 2011. Biosens. Bioelectron. 28, 243–250.

Pan, M.; Fang, G.; Duan, Z.; Kong, L.; Wang, S. 2012. Biosens. Bioelectron. 31, 11–16.

Piletsky, S.A.; Turner, A.P.F. 2002. Electroanal. 14, 317-323.

Poggi, M.A.; Bottomley, L.A.; Lillehei, P.T. 2002. Anal. Chem. 74, 2851-2862.

Scheibe, B.; Borowiak-Palen, E.; Kalenczuk, R.J. 2010. Mater. Charact. 61, 185-191.

Singh, S.; Srivastava, A.; Ohb, H.-M.; Ahnb, C.-Y.; Choib, G.-G.; Asthana, R.K. 2012. Toxicon 60(5), 878–894.

Tang, L.; Zhu, Y.; Yang, X.; Sun, J.; Li, C. 2008. Biosens. Bioelectron. 24, 319–323.

Umezawa, Y.; Umezawa, K.; Sat, H.; 1995. Pure Appl. Chem. 67, 507–518.

World Health Organization. 1998. Drinking-water quality guidelines for parameters of concern in agricultural drainage water - Annex 3, Technical Report, pp. 281–289.

Yang, W.; Thordarson, P.; Gooding, J.J.; Ringer, S.P.; Braet, F. 2007. Nanotechnol. 18, 412001 (12pp.).

Zhang, M.; Smith, A.; Gorski, W. 2004. Anal. Chem. 76, 5045-5050.

Zdrojek, M.; Gebicki, W.; Jastrzebski, C.; Melin, T.; Huczko, A.; 2004. Solid State Phenom. 99, 265-268.

This page was intentionally left blank

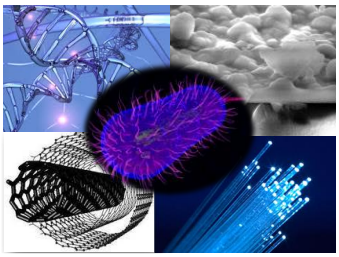

Chapter 5

Microcystin-LR detection in water by Fabry-Perot optical interferometry

5.1 Introduction

The search for alternative procedures for real-time bacteria control requires, as mentioned in chapters 3 and 4, the development of methods that combine sensitive and selective recognition capabilities of low quantities of analyte and sensory systems with rapid response and long term stability. A high sensitivity is fundamental since one must often detect only a few molecules (Li et al., 2008).

A suitable optical biosensor design could meet these criteria by employing an optical fibre interferometer (Jesus et al., 2009; Silva et al., 2008). For this purpose, the optical fibre tip must be covered with an element of recognition that enables a selective MC-LR detection. This may be achieved by coating the fibre with a compatible sensing material such as MC-LR imprinted sol-gel. Optical fibre interferometers are particularly suitable when very low concentrations should be detected in a regular fashion. The size of the sensitive element based on this principle can be as small as the diameter of the fibre (about 0.1 mm), presenting a high signal to noise ratio. Obviously, the selectivity here is attributed to the sensing membrane covering the optical fibre. This membrane is similar to the sensitive membrane developed and studied in chapter 3.

In this work, a FFPI sensing device with a MI sol-gel membrane at the cleaved end of an optical fibre is presented for detection of MC-LR (Figure 5.1). All the results were compared with those of a NISG obtained by removing the template from the sol-gel preparation.

5.2 Experimental

5.2.1 Apparatus

For the sensing head fabrication, a standard single-mode fibre SMF-28e, from Corning Inc., USA, was used, with 8.2 and 125 µm-diameters for the core and cladding, respectively. The fibre tip was cleaved with a cut machine FITEL S323 and dip-coated with a sol-gel based membrane in a home-made dip-coater. Figure 5.1 shows the experimental setup used to interrogate the FFPI sensing device. It consisted of a 100 nm broadband source in the 1550 nm spectral range, and an optical circulator to obtain the reflected channelled spectrum of the sensing head. The reflected Fabry–Perot signal was observed using an optical spectrum analyser (OSA), Ando AQ-6315B, with a maximum wavelength resolution 0.5 nm. The fusion splicer used was a Fujikura FSM 60S, and the fiber optic stripper was a Clauss CFS-2. The detail in Figure 5.1 shows the developed sensing head which is based on a standard single-mode fibre tip coated with MIP or NIP sol-gel material. The fibre Fabry-Perot cavity was then obtained by two interfering waves, one from the Fresnel reflection at the distal end of the fibre probe and the other from the reflected light at the end of the sensitive membrane deposited in the fibre tip. The preparation of sol-gel was done in a Yellow Line MST Basic C with temperature and stirring control. For the polimerization a Memmert TYP:U.10 was used.

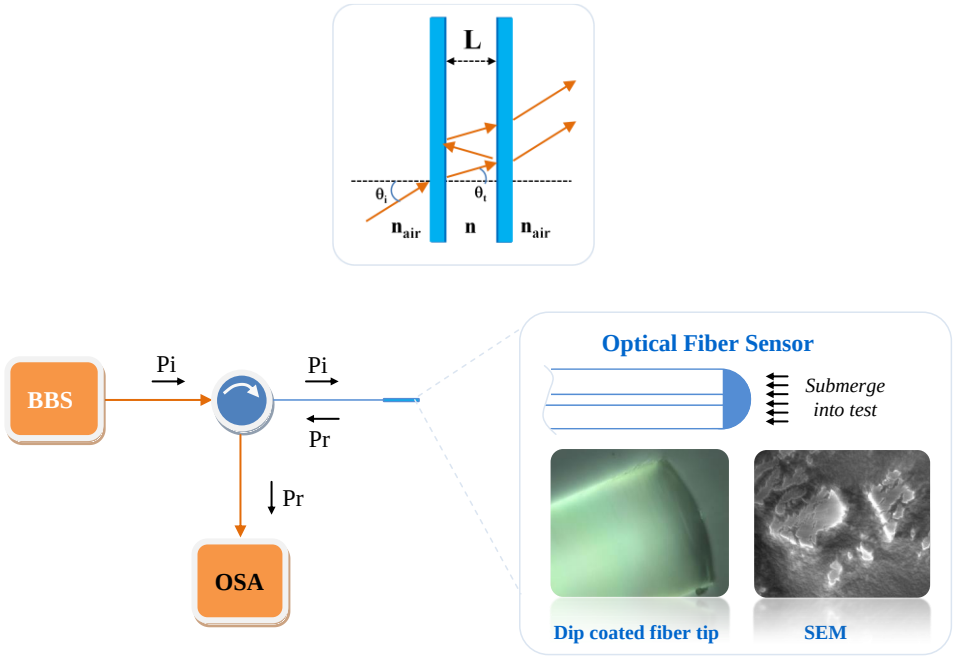

Figure 5.1 - Experimental setup with details of the sensing head, Scanning Electron Microscopy image, and scheme of the Fabry-Perot cavity. BBS: broadband source; OSA: optical spectrum analyser; P_i: incident power; P_r: reflected power; L: distance between mirrors; ϕ_i: incidence angle; ϕ_t: transmitted angle; n: refractive index.

5.2.2 Reagents and solutions

Deionized water was used throughout. MC-LR (Fluka), (3-aminopropyl)trimethoxysilane (APTMS, Fluka), DPDMS (ABCR), MeOH (Aldrich), TEOS (ABCR), HCl (Merck) and EtOH (Panreac), were pro-analysis grade and used without further purification. A stock solution of 10.0 µg L^{-1} MC-LR was prepared by diluting 10 µL of methanolic commercial standard (10.025 µg mL^{-1}) in deionised water. The decreased MC-LR concentrations were obtained by adding aliquots of the deionised water untill the desired concentration of MC-LR was achieved. The range of MC-LR concentrations studied was 0.29-2.00 µg L^{-1}.

5.2.3 Preparation of the microcystin-LR sol-gel membrane in a coated fibre

The ISG membrane was applied on the cleaved end of the single-mode fibre by dip-coating. The fibre was dipped in the gel for 2 minutes at 0.483 m s^{-1} and then the fibre was raised at the same velocity for drying during 2 minutes. This procedure was carried out 4 times. The membrane was obtained by mixing 10 µL of MC-LR with a selected sol-gel recipe composed of 3 mL of APTMS, 3 mL of DPDMS, and 10 mL of MeOH. This mixture was stirred at 60ºC for 30 minutes. Then, the resulting solution was hydrolyzed slowly with 1 mL of TEOS, 500 µL of HCl 0.1 M, 5 mL of EtOH and 1.5 mL of deionised water also at 60ºC. This was made under stirring until gel formation. The fibre tip was dip coated on the mixture and polymerized at 60ºC during 12 h. The template was removed by washing the MIP in deionised water for 3 h.

5.3 Results and discussion

5.3.1 Microcystin-LR sol-gel membrane

The process of sol-gel imprinting of MC-LR started by the addition of the template to the sol phase, then the mixture was hydrolysed and the matrix polymerized in a 3-D network. Finally the template was removed from the polymer, leaving vacant places behind. These places had suitable shape and functionalities for template rebinding. The NISG structured material was synthesized following the same procedure, but excluding the template from the formulation. The expected result was a similar membrane but without the cavities from MC-LR.

The sol-gel thin membrane was not hydrated prior to its first use. Hydration was avoided because it contributed to the instability of the analytical signal. Daily measures of the sol-gel fibre optic sensor were conducted at room temperature (unless specified otherwise) and on an acrylic homemade reactor of small capacity (50 mL), under continuous stirring. The sol-gel surface looked smooth and shiny and the initial SEM images were unable to capture the underlying surface. For this reason, the material was crashed, as may be seen in Figure 5.1.

The subsequent SEM images were not highly resolved due to the small conductivity of the material. They confirmed the existence of nanostructures, with dimensions lying within about 40 and 80 nm. In general, no significant differences were obtained between ISG and NISG membranes.

5.3.2 Optical spectra of imprinted sol-gel versus non-imprinted sol-gel sensors

The typical optical spectra of the FFPI signals obtained with MIP and NIP sensors are shown in Figure 5.2. Their periodicities were ~ 44.5 nm and 43.4 nm for the fibre tips with MIP and NIP membranes, respectively. These results indicate that in the central region of the membranes the optical thicknesses were ~19 μm. In general, the different special arrangements in ISG and NISG membranes caused different effective refractive indices which in turn were responsible by the different fringe amplitudes in the two cases.

It was expectable that the cavities in the sol-gel polymer would decrease the effective refractive index of the ISG membrane, therefore causing fringes with higher amplitude when compared to the fringes of the NISG membrane due to a higher mismatch with the fibre core refractive index.

5.3.3 Evidence of microcystin-LR binding

The interaction of the analyte with the sol–gel MC-LR membrane was evidenced by a strong influence in the phase of the FFPI. This was observed by the wavelength shift variation with the concentration of MC-LR. More intense shifts have been observed for imprinted sol-gel membranes. This difference was displayed for both wavelength shift and optical power, as may be seen in Figure 5.2.

The great difference observed between ISG and NISG sensors may result from the existence of a low number of conformational possibilities for MC-LR. Previous work reported that MC-LR in several solvents displayed only a single conformation (Trogen and Zdunek, 1996), thus contributing to the success of the molecular imprint.

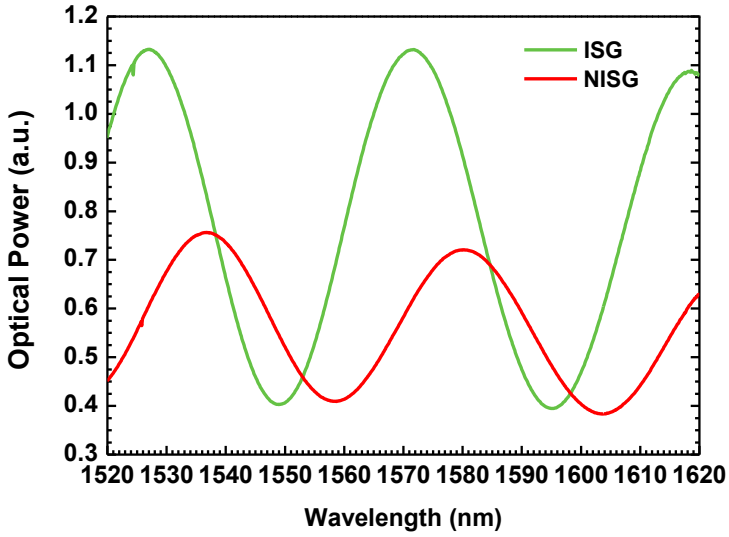

Figure 5.2 - Optical spectrum of the fibre Fabry-Perot interferometer with imprinted sol-gel (ISG) and non-imprinted sol-gel (NISG) membranes.

5.3.4 Thermal-cross sensitivity

The thermal cross-sensitivity was evaluated by immersing the sensing head in distilled water. The temperature was then increased from the room temperature up to 50 ºC with rising steps of 5 ºC. The wavelength deviation was then recorded for ISG and NISG sensors. The response of the FFPIs to temperature variation is shown in Figure 5.3. As it would be expected, the observed responses were non-linear. This behaviour was due to the thermo-optic coefficient variations of each sensing polymer. The FFPI with the ISG membrane displayed higher stability to temperature, which combined with its recognition binding capability indicating a great potential for MC-LR quantitative detection. The data presented was obtained reading with an OSA the shift of the FFPI channelled spectrum. This approach readily permitted to test the viability of this sensing structure. A dedicated interrogation unit to read with high sensitivity the cavity phase, with clear benefits considering the factors measurement resolution and cost, is now under development.

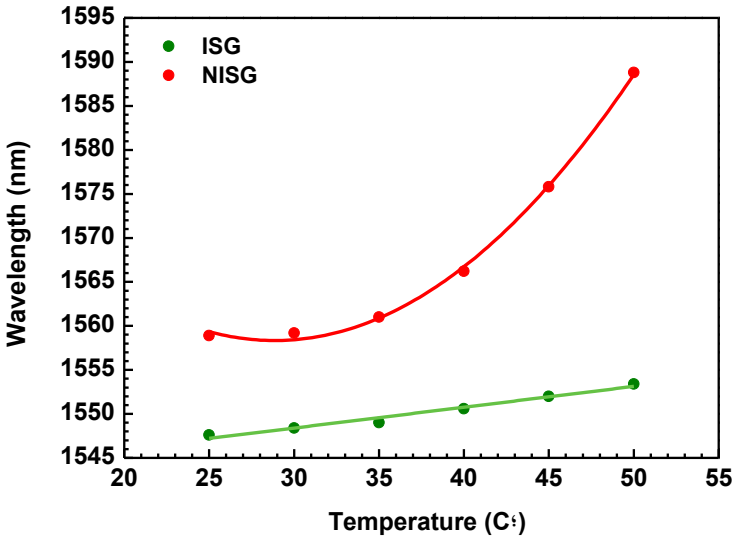

Figure 5.3 - Wavelength shift versus temperature variation for the fibre Fabry-Perot interferometer with imprinted sol-gel (ISG) and non-imprinted sol-gel (NISG) membranes.

The higher thermal stability of ISG sensor was attributed to the presence of MC-LR within its matrix, as this was the only difference between NISG and ISG membranes.

In general terms, the interactions between the positively charged groups among MC-LR and the negatively charged silicate matrix (Heller J. and Heller A., 1998) contributes to its integrity under increasing temperatures, up to 50 ºC. In opposite, the NISG material is expectedly more stable for higher temperatures, as any MC-LR molecule entrapped inside the sol-gel will be degraded. This was confirmed by differential scanning calorimetry assays indicating an endothermic alteration of MC-LR at 70 ºC, with an enthalpy of 118.5 J g^{-1}.

5.3.5 Sensor stability

It is a basic requirement of a chemical sensor to be able to maintain a fixed output over time when the sensor is exposed to a constant concentration of analyte (Mac-Craith et al., 1997). The perception of instability in interferometric readings with an OSA is not clear by the time of measure. The recorded signal was always a spectrum that had no perceptible correlation to the analytical signal change within time.

The relative standard deviation of consecutive readings was 2%, from standards ranging from 0.3 to 1.4 μg L^{-1}. Furthermore, the best fit for the calibration showed a correlation coefficient of 0.995, indicating that the method was suitable for an analytical application.

5.3.6 Response time

The response time of sol-gel sensors is generally associated with the diffusion time of the analyte through the sol-gel matrix. Long response times are observed when electrostatic interactions are established between the matrix and charged or polar site of the analyte (Mac-Craith et al., 1997). This was the case of MC-LR, carrying some ionization points within its structure. Standards of higher concentration took longer time to reach a stable response, always below 2 minutes. This was the maximum time taken to reach a steady wavelength of ± 1 nm. Thus a period of 2 minutes was set for each measure. This was the time required to ensure a homogeneous background of the measuring solution and close-to equilibrium conditions in the sensing layer. In addition, using a fixed period of time avoided subsequent problems associated to the low stability of the analytical signal.

5.3.7 Selectivity against organic and inorganic compounds

MIPs acting as host compounds may provide the means for selectivity enhancement because the “shape” of the template that is imprinted on it. The imprinted sites carry an induced molecular memory that should be capable of recognizing the previously imprinted molecules. They leave accessible binding sites with specific shape and functional group complementarily to the original printed molecule in the polymeric network.

However, non-specific interaction is established due to the existence of opposite polarities within the template and the imprinted site. Thus, a NIP is expected to display a response for MC-LR, although less sensitive than that of the MIP.

Table 5.1 - Interference effect from inorganic and organic species.

	Interfering species	Tolerance limit	Recovery percentage (%)
Inorganic	Al^{3+}	200 mg L^{-1}	100.1
	NH_4^+	500 mg L-1	100.7
	Cl^-	250 mg L^{-1}	100.5
	Fe^{3+}	200 mg L^{-1}	101.0
	Mg^{2+}	50 mg L^{-1}	98.5
	Mn^{2+}	50 mg L^{-1}	100.3
	Na^+	200 mg L^{-1}	100.8
	SO_4^{2-}	250 mg L^{-1}	101.6
Organic	Benzo(a)pyrene	0.010 mg L^{-1}	102.2
	Dichloroethene	3.0 mg L^{-1}	100.9
	Pesticide (r-cyhalothrin)	0.1 mg L-1	100.5
	PAH (Benzo(b)fluorenthene)	0.1 mg L-1	100.2
	TCE	10 mg L^{-1}	100.6
	THM (Chloroform)	100 mg L^{-1}	100.7
	EPA 610 PAH mix	0.1 mg L^{-1}	100.4

PAH: polycyclic aromatic hydrocarbons; TCE: trichloroethylene; THM: trihalomethane; EPA: Environmental Protection Agency.

Considering this non-specific interaction, the interfering effect of several concomitant species was tested. According to Portuguese Law (Law-Decree 307/2007), the most relevant ions tested on waters for human consumption are Al^{3+}, NH_4^+, Cl^-, Mg^{2+}, Mn^{2+}, Na^+, and SO_4^{2-}.

Thus the selectivity of the chemical sensor was tested against these species. Their maximum admitted levels (in Table 5.1) were used as maximum interfering concentration because it is highly unlikely that their presence in environmental waters above these limits. Using these concentrations, the recoveries of a 1 µg L^{-1} MC-LR solution ranged from 98.5 to 101.6%. These values pointed out negligible interference from other species.

Some organic compounds mentioned in law were also included in this study. Benzo(a)pyrene; dichloroethene (DCE); ρ-cyhalothrin as a pesticide; benzo(b)fluoranthene as a polyaromatic hydrocarbon (PAH) compound; chloroform as a THM compound, and TCE were considered for this purpose, tested at their maximum legal limits in waters.

Environmental Protection Agency (EPA) 610 PAH mix was also tested to assess the effect of combined PAH's. The results, also shown in Table 5.1, pointed out to recoveries from 100.2 to 102.2%.

5.3.8 Analytical behavior against concentration

Two analytical features were altered by the change in concentration: the wavelength and the visibility. Figure 5.4 and Figure 5.5 present the wavelength variation of both FFPIs for the MC-LR concentration range between 0.3 and 1.4 μg L^{-1} at a constant temperature of 18.3 ± 0.1 ºC. The results showed that, for the full concentration range, the wavelength variation of the FFPI with ISG membrane, was 16 nm, the double of the result found for FFPI with NISG membrane, 8 nm (Figure 5.6). Both MIP and NIP sensors showed a fairly linear response and sensitivities of -12.4 ± 0.7 nm L $μg^{-1}$ and -5.9 ± 0.2 nm L $μg^{-1}$, respectively (Table 5.2).

These results indicated that the presence of the analyte created a change in the effective index of the sensing membrane, introducing changes in the optical path of the cavity and, consequently, modifying the phase of the interferometric pattern. The results confirm that the adsorption capacities of ISG are larger than that of the NISG membrane, it was observed that ISG binding sites reached a near saturation state for higher MC-LR concentrations. In particular, it could be observed that, in the recommended limit range of MC-LR in drinking waters ≤ 1 μg L^{-1}, both FFPIs presented good linear behaviour.

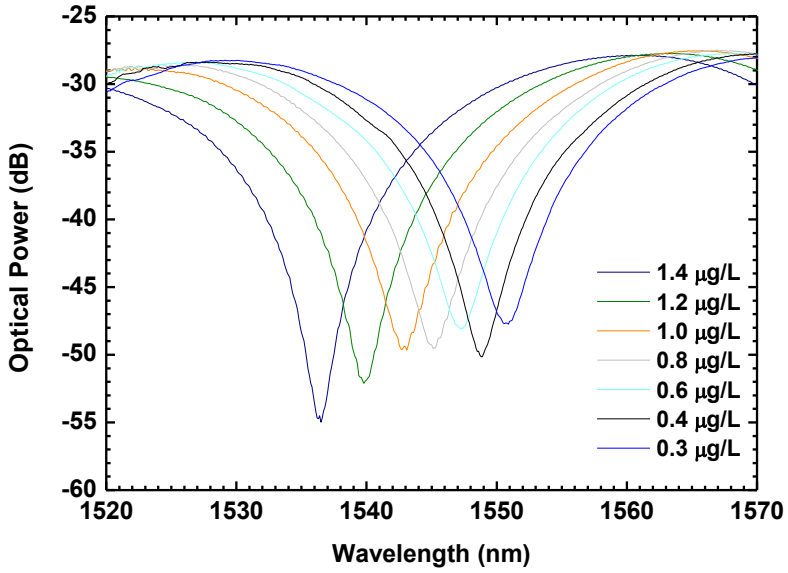

Figure 5.4 - Optical spectrum of the imprinted sol-gel fibre Fabry-Perot interfereometer with the concentration of microcystin-LR (0.3 – 1.4 µg L^{-1}).

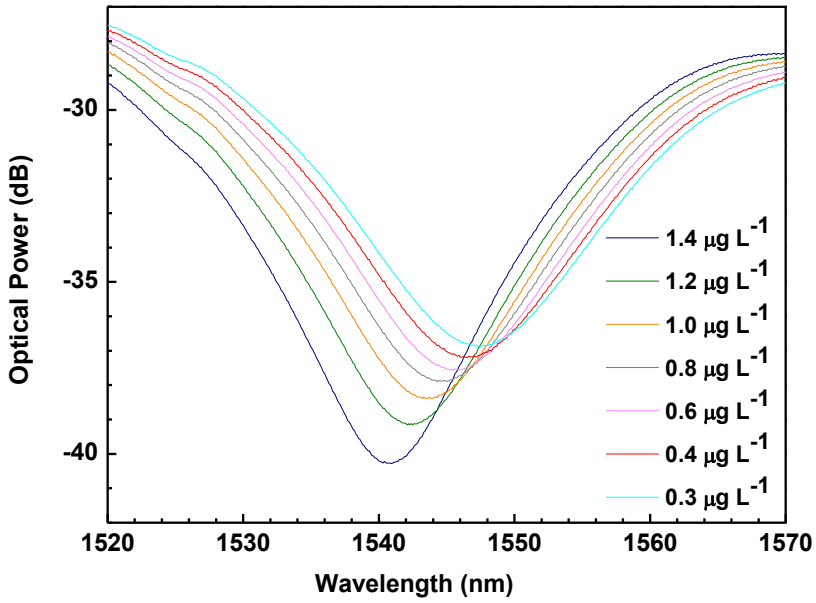

Figure 5.5 - Optical spectrum of the non-imprinted sol-gel fibre Fabry-Perot interfereometer with the concentration of microcystin-LR (0.3 – 1.4 µg L^{-1}).

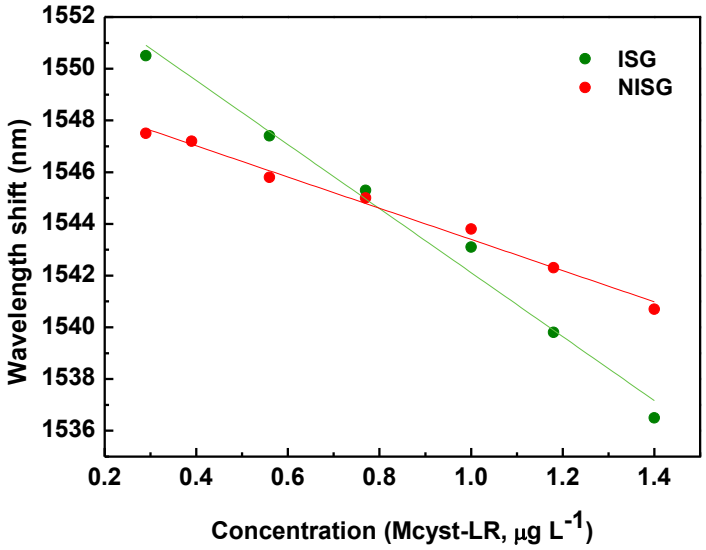

Figure 5.6 - Wavelength shift versus microcystin-LR concentration for imprinted (ISG) and non-imprinted (NISG) sol-gel membranes.

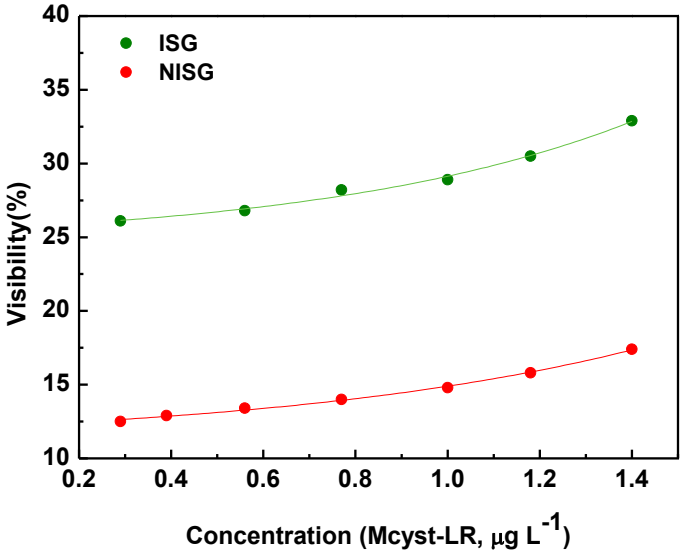

Figure 5.7 - Visibility change versus microcystin-LR concentration for imprinted (ISG) and non-imprinted (NISG) sol-gel membranes.

The results of dependence of the interferometric fringe visibility of both FFPIs (Figure 5.7), for the MC-LR concentration range between 0.3 and 1.4 μg L^{-1} showed that the fringe visibility for both FFPIs increased with the MC-LR concentration, meaning that this analyte changed the effective index of the sensing membranes. In the range studied, the total visibility variation was 6.6% and 4.8% for the FFPI with ISG and NISG membranes, respectively (Table 5.2). Again, the observed differences were due to the higher adsorption capacities of the ISG membrane, since the binding sites promptly reached a near saturation state for higher MC-LR concentrations.

Table 5.2 – Analytical features of imprinted sol-gel (ISG) and non-imprinted sol-gel (NISG) fibre Fabry-Perot interferometer for microcystin-LR concentration range between 0.3 and 1.4 μg L^{-1}.

Sensor	Wavelength shift variation (nm)	Visibility variation (%)	Linear range (μg L^{-1})	Sensitivity (nm L $μg^{-1}$)	LOD (μg L^{-1})
ISG	16	6.6	0.29 -1.40	-12.7±0.7	0.26
NISG	8	4.8	0.29-1.40	-5.9±0.2	0.26

In general, the results suggest that not only the ISG but also the NISG could adsorb MC-LR from aqueous solutions. However, the adsorption capacities of ISG seemed much larger than those of NISG. This feature suggests that the ISG sensor may be employed in the routine analysis of recreational or drinking waters.

5.3.9 Application to environmental waters

In order to investigate the application of the present method to the analysis of environmental waters, spiked water solutions were tested and the corresponding relative errors calculated. These assays were conducted within 0.3-1.4 μg L^{-1} of MC-LR. The average recoveries of two spiked solutions of 1.18 and 0.77 μg L^{-1} were 100.4 ± 0.6 % and 96.5 ± 2.9 % and corresponding to average relative errors of +0.57 % and -3.56 % thus confirming the accuracy of the analytical data (n = 2 for two FFPI sensor units).

5.4 Conclusions

An interferometric optical fibre sensor coated with sol–gel MC-LR imprinted membranes was a successful analytical tool for screening this dangerous toxin. Both ISG and NISG sensing membranes showed linear response to MC-LR concentrations in the range of concentrations required for the analysis of recreational or drinking waters. ISG sensor displayed higher sensitivity (double) and better detection capabilities than the corresponding NISG device. The detection limit found was of about 0.3 µg L^{-1}. The sensor are stable with a relative standard deviation of consecutive readings of about 2%. In terms of temperature stability, ISG sensor showed high stability up to temperature variation of 50 ºC.

The interfering effect of several organic contaminants species (Benzo(a)pyrene, DCE, ρ-cyhalothrin, benzo(b)fluoranthene, chloroform, EPA 610 PAH mix and TCE) and the most relevant ions (Al^{3+}, NH_4^+, Cl^-, Mg^{2+}, Mn^{2+}, Na^+, and SO_4^{2-}) was tested and none of them seem to interfere with the analysis.

The uses of synthetic materials for the sensing head in conjunction with standard single mode fibre and the easy fabrication and testing of the sensors contributes to the low-medium cost of the overall sensors and to the used of these units for the application *in situ* and in real time for the monitorization of MC-LR in environment waters.

References

Heller, J.; Heller, A.; 1998. J. Am. Chem. Soc. 120, 4586–4590.

Jesus, C.; Silva, S.F.O.; Castanheira, M.;. González-Aguilar, G.; Frazão, O.; Jorge, P.A.S.; Baptista, J.M. 2009. Meas. Sci. Tecnol. 20, 125201 (5pp).

Law-Decree 307/2007 (Portuguese Law) of 2007, August 31st. Defines water quality for Human consumption, Annex I, Part 3 – Indicative parameters. Republic Journal 1st Serie, N. 164, 5747.

Li, T.; Wu, T.-D.; Mazéas, L.; Toffin, L.; Guerkin-Kern, J.-L.; Leblon, G.; Bouchez, T. 2008. Environ. Microbiol. 10, 580–588.

Mac-Craith, B.D.; Mc Donagh, C.; Mcevoy, A.K.; Butler, T.; O'keeffe, G.; Murphy, V. 1997. J. Sol-Gel Sci. Technol. 8, 1053–1061.

Silva, S.F.O.; Frazão, O.; Caldas, P.; Santos, J.L.; Araújo, F.M.; Ferreira, L.A. 2008. Opt. Eng. 47(5), 054403.

Trogen, G.; Zdunek, J. 1996. Biochemistry 35, 3197-3205.

This page was intentionally left blank

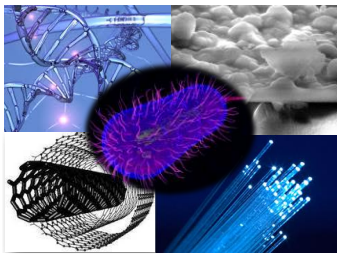

Chapter 6

Development of an aptamer-based biosensor for *Escherichia coli* outer membrane proteins detection in waters using Electrochemical Impedance Spectroscopy

6.1 Introduction

The consumption of contaminated water by *E. coli* bacteria can cause large and sometimes widely dispersed outbreaks. The rapid evolution of the symptoms caused by *E. coli* infections requires a rapid, sensitive and reliable monitoring of bacterial contamination. Biosensors can assume this role (Li et al., 2008; Turner, 2000), which in combination with electrochemical techniques for transduction of protein recognition can provide the simplicity and the speed required.

APTs are oligonucleotides, DNA or RNA molecules, which can interact with high specificity and affinity to their targets (Ellington and Szostak, 1990; Tombelli et al., 2005), due to its ability to fold into numerous tertiary conformations.

Despite several APT that have been developed to bind different targets, like proteins, small molecules, cells, antibiotics, and viruses (Stoltenburg et al., 2007), in various types of biodetection approaches from label-free (de-los-Santos-Álvarez et al., 2008) to self-reporting or labeling strategies (Miranda-Castro et al. 2009) using a variety of assay formats (Mascini et al., 2012), evolution of APTs against bacteria is an underexplored area.

Unlike conventional SELEX, the specific target is not usually known and a pool of aptamers against different targets is often found. This obliges to carry out further experiments in order to know the exact nature of the final target if desired. To avoid this cumbersome step, genetically modified bacteria to overexpress a certain protein is an alternative strategy to bias the selection of APTs against that specific protein (Torres-Chavolla and Alocilja 2009). Bruno et al. have recently evolved DNA APTs against EcOMPs (Bruno et al., 2010). The present work describes the use of two of these *E. coli* DNA APT (herein called ECA I and II) for the determination of EcOMPs in waters by the direct identification of EcOMPs electrochemically.

The electrochemical approach is cost-effective because it does not require expensive instrumentation (Dijksma et al., 2001; Kim et al., 2007) and would allow portability (Dorst et al., 2010). EIS transduction is especially well suited to detect changes that occur in the solution-electrode interface without the need of labels. This technique was one of the first used for electrochemical transduction of the aptamer-ligand recognition event for small molecules (Zayats et al. 2006), where the associated conformational change can be too small to cause a significant variation in a physical property of appropriate labels such as the case of antibiotics (de-los-Santos-Álvarez et al. 2007; González-Fernández et al. 2011). But it can also be used for the detection of large molecules (Rodriguez et al. 2005; Rohrbach et al. 2012; Xu et al. 2006) or whole cells (Labib et al. 2012). The analytical signal, the R_{et} of a redox probe, is related to the amount of protein bound to the aptamer immobilized on the electrode surface, which correlates with the concentration of proteins present in the sample.

Two *E. coli* DNA APT (ECA) candidate sequences raised against EcOMP containing 36 and 37 nucleotides were tested (Bruno et al., 2010). Both DNA sequences were also immobilized with and without the 6-mercapto-1-hexanol (MCH) to study if the nonspecific effects are reduced with the application of a bilayer.

The sensor interface plays a crucial role in the overall performance of electrochemical sensors. Nonspecific adsorption effects can be reduced by employing mixed self-assembled monolayers (SAMs) containing a thiol-derivatized capture probe DNA and a spacer thiol, mainly MCH (Steel et al., 1998). APT-based FIS biosensors could be a good alternative for the rapid, sensitive, and specific detection of *E. coli* species in environmental samples.

6.2 Experimental

6.2.1 Apparatus

All electrochemical measurements were performed with a standard three electrode cell controlled by an Autolab PGstat-12 potentiostat with NOVA software (EcoChemie, The Netherlands). A 0.5 mm diameter platinum wire acted as an auxiliary electrode and a 1.6 mm diameter gold electrode as a working electrode (Bioanalytical Systems, Inc.). The reference electrode used was an Ag|AgCl||KCl saturated reference electrode from Crison Instrument, S.A. see **Figure 6.1**.

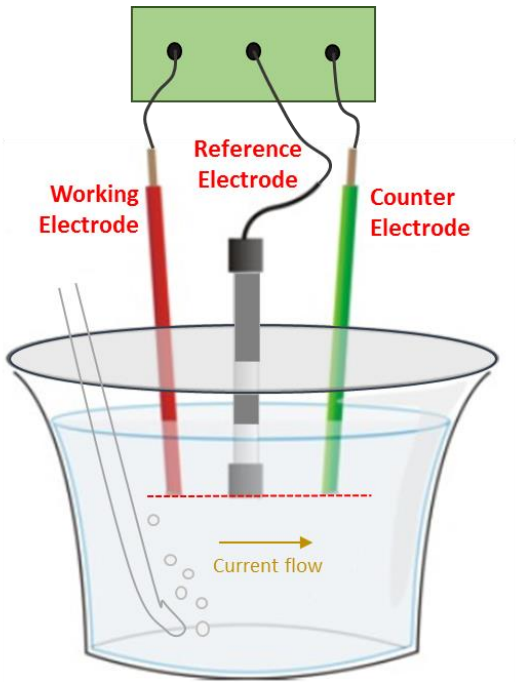

Figure 6.1 – Experimental setup scheme. The electrochemical cell was constituted by three electrodes and a nitrogen flow system (degassed).

6.2.2 Reagents and solutions

A lawn of E.coli ATCC® 8739™ was purchased in ATCC (USA). EcOMPs were extracted according to (Bruno et al., 2010). 36 mer (5'-SH-GTC TGC GAG CGG GGC GCG GGC CCG GCG GGG GATGCG C-3') (ECA I) and 37 mer (5'-SH-ACG GCG CTC CCA ACA GGC CTC TCC TTA CGG CAT ATT A-3') (ECA II) APTs were purchased from Sigma-Aldrich (Spain). The thiol-modified APTs were commercially supplied as the respective disulfides. Prior to use, these products were treated with dithiothreitol from Sigma-Aldrich and then purified by elution through a DNA gel filtration Ilustra NAP 25 columns with Sephadex G25 DNA grade used for DNA purification (GE Healthcare) with double-deionized RNAse free water 0.03 μS at 25 ºC from ATS (Portugal). Potassium hexacyanoferrate II and potassium hexacyanoferrate III were purchased from Sigma-Aldrich and Panreac, respectively. Hexaammineruthenium (III) chloride and MCH were purchased from Aldrich.

Salts for buffer solutions were prepared in double-deionized RNase free water. Magnesium chloride was purchased from Riedel-del-Häen (Germany), potassium chloride from Merck (Germany), sodium chloride and (tris(hydroxymethyl)aminomethane (TRIS) were obtained from Panreac, and SSPE buffer 20x concentrate (1X = 0.150 M sodium chloride, 0.010 M sodium phosphate, 0.001 M ethylenediamine tetraacetic acid (EDTA)) and bovine serum albumin (BSA) were obtained from Sigma. The buffers used in this work were: extraction buffer: phosphate buffer solution; Immobilization buffer: SSPE 1:10 (diluted from 20x SSPE); affinity buffer (50 mM TRIS/HCl pH 7.4, 250 mM NaCl, 5 mM $MgCl_2$) and measurement buffer (10 mM TRIS/HCl pH 7.4, 100 mM KCl, 5 mM $[Fe(CN)_6]^{3-/4-}$). Alumina slurries were prepared with MicroPolish deagglomerated alumina powders (1, 0.3, and 0.05 μm) purchased in Buehler (Germany). All the reagents were of analytical grade.

6.2.3 Experimental methods

6.2.3.1 Extraction and determination of *Escherichia coli* outer membrane proteins concentration

A lawn of *E. coli* ATCC® strain 8739™ (Crooks strain) was grown on a blood agar plate overnight at 37 °C. Bacteria were washed from the plate with the extraction buffer and transferred to 10 ml of cold 1.5 M $MgCl_2$ in sterile nuclease-free water.

The suspension of bacteria was left overnight at 4 °C to allow the chaotropic action of magnesium chloride ($MgCl_2$) to extract EcOMPs. The resultant pellet was washed again with buffer and centrifuged. The liquid was collected and the final concentration of EcOMPs was estimated spectrophotometrically at 280 nm (Bruno et al., 2010).

6.2.3.2 Electrode cleaning and pretreatment

The gold electrode was immersed in piranha solution [3 sulfuric acid (H_2SO_4):1 hydrogen peroxide (H_2O_2)] for 10 min. Then the electrode was polished in a cotton cloth sequentially with 1, 0.3 and 0.05 µm alumina slurries. After sonication in an ultrasound bath for 5 min, it was immersed in a 2 M potassium hydroxide (KOH) for 1 h at 60 ºC. Then the electrode was immersed in concentrated acids at room temperature for 10 min first in H_2SO_4 and after in nitric acid (HNO_3). Finally, the electrode was subjected to several potential cycles between 0 and 1.6 V in 0.1 M H_2SO_4 at 100 $mV.s^{-1}$ until a stable background was obtained. The electrodes were rinsed with double-deionized water between each step.

6.2.3.3 Aptamer immobilization and quantification

Each aptamer was immobilized onto a freshly cleaned electrode overnight. Unless otherwise stated, the electrode was immersed in 2.0×10^{-8} M ECA I or ECA II in the immobilization buffer at 4 ºC. After probe immobilization, the electrode surface was rinsed with double-deionized water to remove the weakly adsorbed aptamer. When preparing SAMs, the aptamer-modified electrode was subsequently immersed in 4.5 mM MCH in the same immobilization buffer for 30 min under stirring, in the dark, and then, rinsed with double-deionized water. The surface density of immobilized aptamer was determined by chronocoulometric measurements using hexaammineruthenium $[Ru(NH_3)_6]^{3+}$ as previously reported (Steel et al., 1998).

6.2.3.4 Electrochemical impedance spectroscopy measurements

The electrodes modified with single (ECA) and mixed (ECA-MCH) SAMs were incubated in varying concentrations of OMPs in the affinity buffer for 90 min, and after a brief washing step with water, it was transferred to the measurement solution to record the impedance spectrum at a bias potential of +0.225 V with a frequency range ranging from 0.1 to 10000 Hz and an alternating current amplitude of 5 mV. After measurement, the modified electrodes were washed with a 2 M HCl solution for 20 min, to regenerate the probe for re-use of the modified electrode. A schematic illustration of the modified electrode with the immobilized capture probes and the detection of the EcOMPs are presented in Figure 6.2.

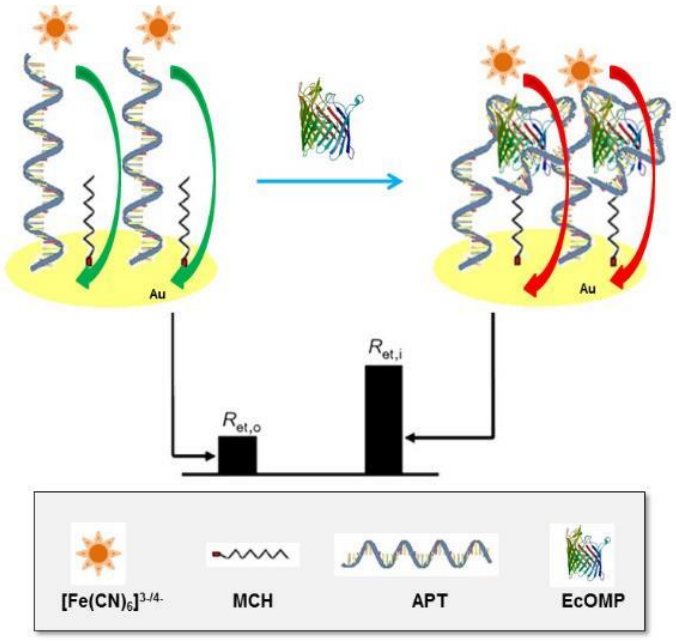

Figure 6.2 - Schematic illustration of the modified electrodes and the detection of *Escherichia coli* outer membrane proteins by electrochemical impedance spectroscopy.

6.3 Results and discussion

6.3.1 The principle of *Escherichia coli* aptamer impedimetric biosensor

The detailed principle of ECA impedimetric biosensor is illustrated in Figure 6.2.

Firstly, the aptamer functionalized with a thiol group at its 5' end was covalently attached on the Au surface. The modified electrode was then blocked with MCH to form a mixed SAM in order to effectively prevent the nonspecific adsorption of EcOMP on the electrode surface and also to align the APT to facilitate their interaction with the ligand, the OMPs. In the absence of OMPs, the added redox probe (ferrocyanide/ferricyanide) molecules can exchange electrons with the modified electrode surface but a certain resistance is observed. In the presence of EcOMP, the ECA folds around the proteins and forms an EcOMP-ECA complex. The formation of this complex blocks the electron transfer and consequently the R_{et} increases.

In Figure 6.3 to Figure 6.6, the variation of $(R_{et,1}-R_{et,0})/(R_{et,0})$ (normalized R_{et}), where $R_{et,1}$ is the R_{et} after incubation for a certain time and $R_{et,0}$ is the Ret before incubation with EcOMP (R_{et} for the sensing phase) with incubation time is shown for ECA I, ECA I-MCH, ECA II and ECA II-MCH. Normalized R_{et} increases rapidly with the increment of incubation time up to 90 min, and then gradually reaches a plateau, indicating that the affinity reaction reaches the equilibrium. Therefore, for further experiments 90 min of incubation was used.

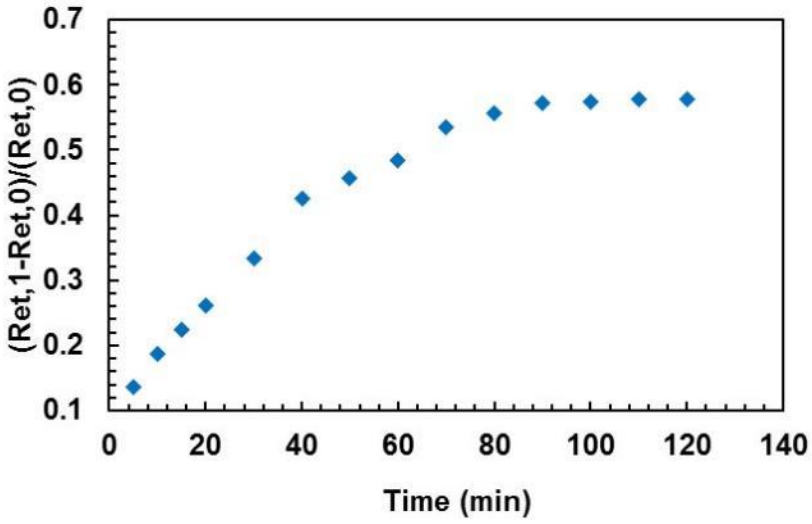

Figure 6.3 - Variation of normalized electron transfer resistance (Ret) with incubation time for ECA I.

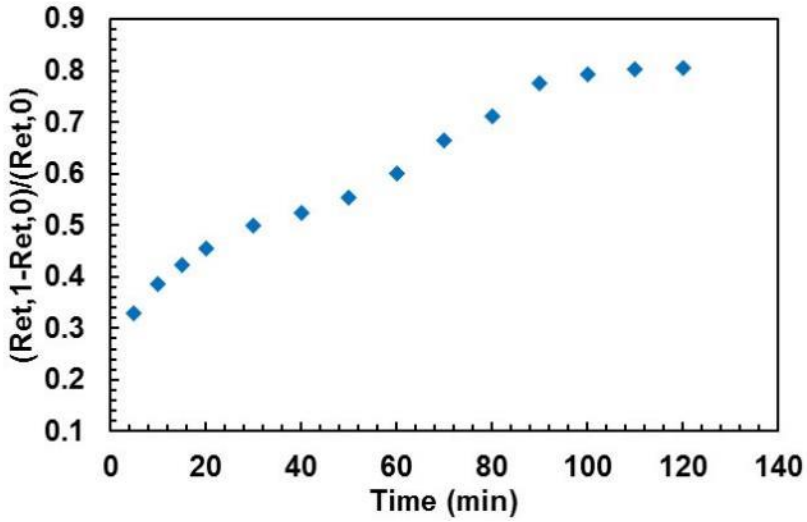

Figure 6.4 – Variation of normalized electron transfer resistance (Ret) with incubation time for ECA I-MCH.

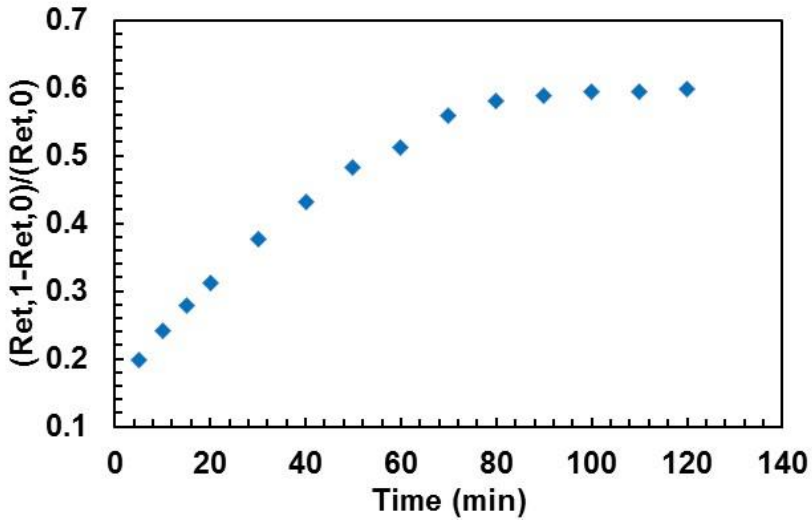

Figure 6.5 – Variation of normalized normalized electron transfer resistance (Ret) with incubation time for ECA II.

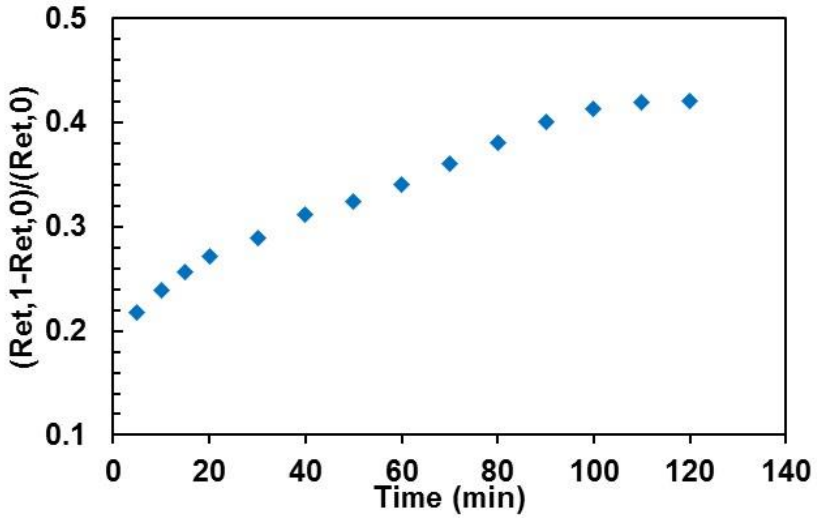

Figure 6.6 - Variation of normalized normalized electron transfer resistance (Ret) with incubation time for ECA II-MCH.

The amount of aptamer chemisorbed onto the gold electrode was estimated by chronocoulometry in SAMs prepared from 2.0×10^{-8} M aptamer solutions. A value of $(9.07\pm 0.03)\times10^{11}$ molecule cm^{-2} was obtained when ECA I was the only component of the SAM. After immersion in MCH solutions for 1 h, the amount of ECA I diminished to $(3.05\pm0.04)\times10^{11}$ molecule cm^{-2}, which is in good agreement with the well-known displacement effect of MCH on previously formed SAMs when used at mM concentrations. Higher concentrations of aptamer solutions up to 2.0×10^{-7} M did not increase the amount of aptamer attached onto the Au surface $(9.06\pm0.03)\times10^{11}$ molecule cm^{-2} and $(2.80\pm0.04)\times10^{11}$ molecule cm^{-2} for single and mixed monolayers, respectively), so a concentration of 2.0×10^{-8} M was selected for further experiments. Equivalent values were estimated from ECA II and ECA II-MCH monolayers.

6.3.2 Sensor performance

ECA I, ECA I-MCH, ECA II and ECA II-MCH capture probes were evaluated by testing the change in electron-transfer behavior before and after binding of EcOMP, Figure 6.7 to Figure 6.10. FIS measurements were conducted at room temperature in the measurement buffer. The experimental Nyquist plots were fitted by the electrochemical circle fit of NOVA 1.6 software using an electronic circuit based on the Randles theoretical model (Randles, 1947).

The bare Au electrode exhibits a very small semicircle domain, indicating a very low electron-transfer resistance as expected. The self-assembly of the ECA onto the electrode surface increases R_{et} in good agreement with the electrostatic repulsion between negative charges of the DNA APT backbone and the redox probe, $[Fe(CN)_6]^{3-/4-}$, which results in a barrier for the interfacial electron transfer. In mixed SAMs, after the immobilization of MCH layer, a decrease tendency of Ret is observed due to the displacement of some of aptamers from the surface of the gold electrode, as indicated above. Subsequently, the incubation of ECA with EcOMP of concentrations between 1.0×10^{-7} and 2.0×10^{-6} M in affinity buffer progressively increases R_{et} in the four modified surfaces tested because EcOMPs inhibit charge transfer between redox probe and the Au electrode.

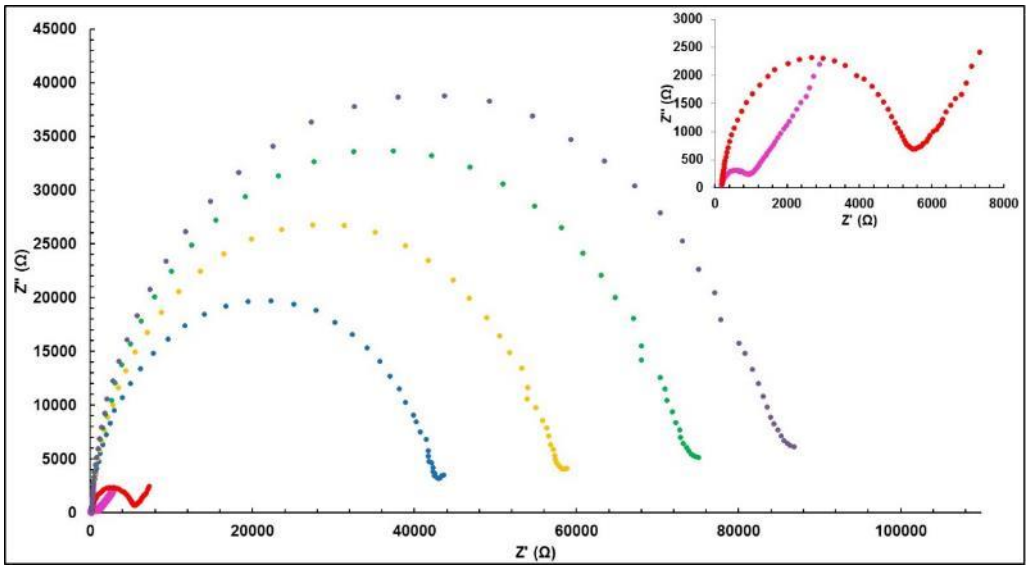

Figure 6.7 - Nyquist plots of the modified electrodes for ECA I. All steps of the detection system were recorded and displayed, (magenta) clean bare gold electrode, (red) after ECA I immobilization and after interaction with (blue) 1.0×10^{-7} M, (yellow) 3.0×10^{-7} M, (green) 9.0×10^{-7}M and (purple) 2.0×10^{-6} M *Escherichia coli* outer membrane proteins.

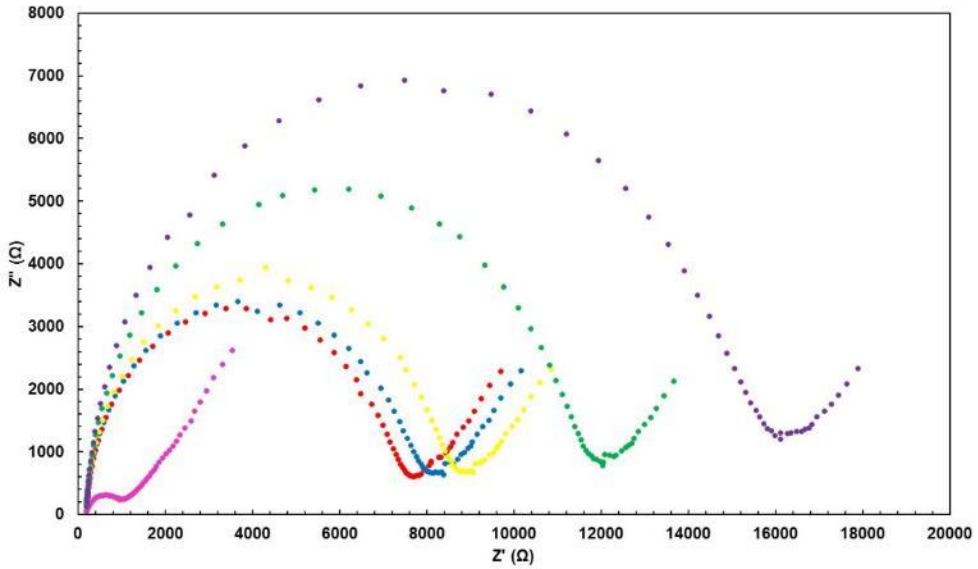

Figure 6.8 – Nyquist plots of the modified electrodes for ECA I-MCH. All steps of the detection system were recorded and displayed, (magenta) clean bare gold electrode, (red) after ECA I-MCH immobilization and after interaction with (blue) 1.0×10^{-7} M, (yellow) 3.0×10^{-7} M, (green) 9.0×10^{-7}M and (purple) 2.0×10^{-6} M *Escherichia coli* outer membrane proteins.

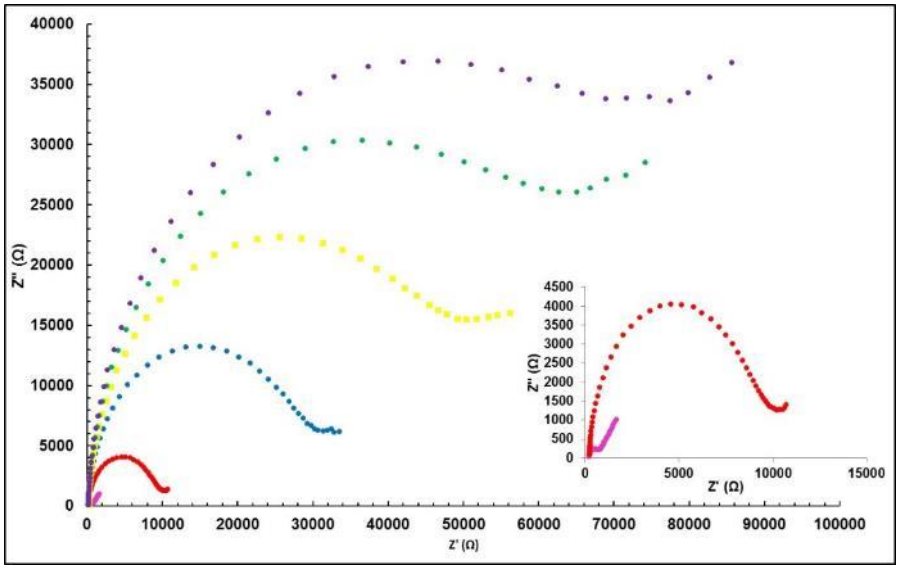

Figure 6.9 – Nyquist plots of the modified electrodes for ECA II. All steps of the detection system were recorded and displayed, (magenta) clean bare gold electrode, (red) after ECA II immobilization and after interaction with (blue) 1.0×10^{-7} M, (yellow) 3.0×10^{-7} M, (green) 9.0×10^{-7}M and (purple) 2.0×10^{-6} M *Escherichia coli* outer membrane proteins.

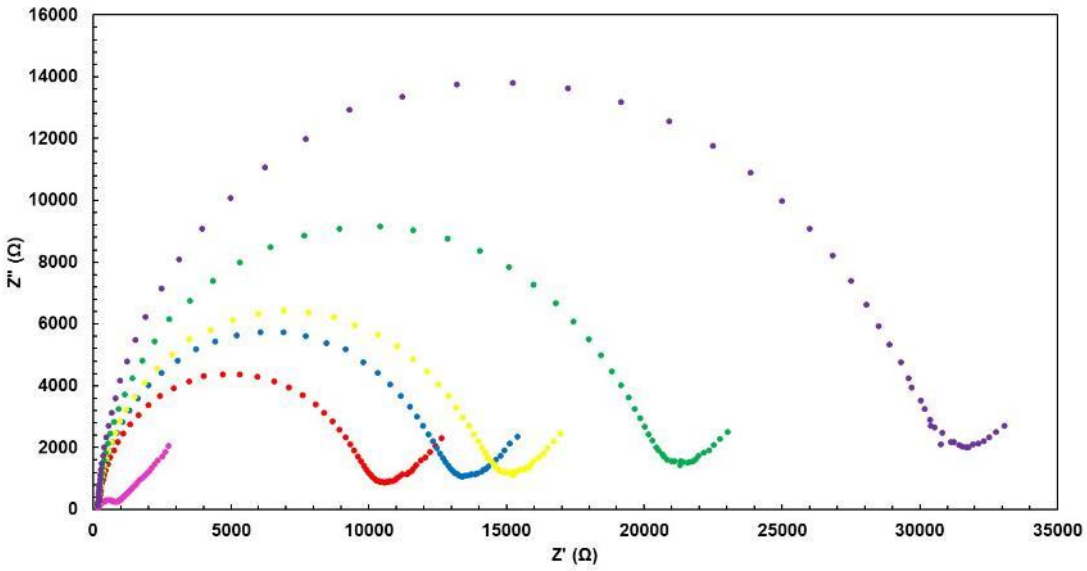

Figure 6.10 – Nyquist plots of the modified electrodes for ECA II-MCH. All steps of the detection system were recorded and displayed, (magenta) clean bare gold electrode, (red) after ECA II-MCH and after interaction with (blue) 1.0×10^{-7} M, (yellow) 3.0×10^{-7} M, (green) 9.0×10^{-7}M and (purple) 2.0×10^{-6} M *Escherichia coli* outer membrane proteins.

As shown in Table 6.1, there is a linear relationship between the normalized R_{et} and the target concentration in the range of 1.0×10^{-7} and 2.0×10^{-6} M for mixed SAMs. However, the interaction of ECA I and ECA II simple SAMs, with EcOMPs, presented a linear dependency with the logarithm of the EcOMPs concentration. This difference in behaviour is not due to unspecific adsorption on Au electrode. BSA was used as a control experiment. In all cases the incubation in increasing concentrations of BSA did not lead to a concentration-dependent increase in R_{et}. On the contrary, the R_{et} remained almost constant with BSA increasing concentration.

Table 6.1 - Regression parameters for the 4 different self-assembled monolayers evaluated.

	ECA I	**ECA I-MCH**	**ECA II**	**ECA II-MCH**
Regression equation	$(R_{et,1}-R_{et,0})/(R_{et,0})(\Omega)=$ (6.22 ± 0.07) log([EcOMP]/M) + (50.9 ± 0.4)	$(R_{et,1}-R_{et,0})/(R_{et,0})(\Omega)=$ $(5.89\pm0.02)\times10^{5}$[EcOMP]/M $+(0.016\pm0.002)$	$(R_{et,1}-R_{et,0})/(R_{et,0})(\Omega)=$ (4.6 ± 0.1) log([EcOMP]/M] + (34.5 ± 0.7)	$(R_{et,1}-R_{et,0})/(R_{et,0})(\Omega)=$ $(9.38\pm0.09)\times10^{5}$ [EcOMP]/M + (0.18 ± 0.01)
r^2	0.9998	0.9999	0.9990	0.9998

6.3.3 Cross-reactivity to other contaminants

To assess the non-specific binding of other molecules that could be present in water systems the different SAMs were incubated with $2.0x10^{-6}$ M EcOMPs, with 1 nM of MC-LR and with a mixture of both for 90 minutes in the affinity buffer. This MC-LR concentration is the recommended maximum level of MC-LR in waters established by (WHO, 1998).

The electron-transfer resistance of the complexes ECA I-EcOMPs and ECAII-EcOMPs for both types of sensing phases (single or mixed monolayers) presented a much higher value than after incubating in MC-LR solution (Figure 6.11). In the case of the mixture EcOMPs-MC-LR the R_{et} presented a similar value to the complexes ECA I-EcOMPs and ECA II-EcOMPS. These results showed the specificity of EcOMPs binding to the aptamer on the electrode even in the presence of potential interferences, and that FIS successfully detected this binding event.

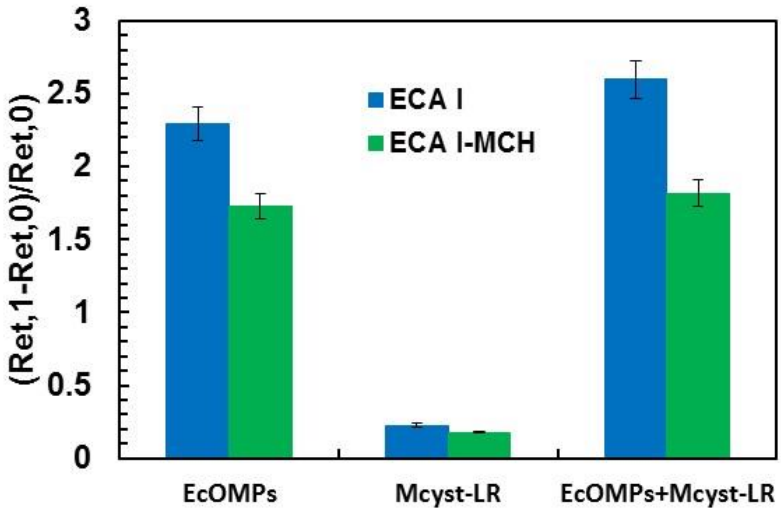

Figure 6.11 - Binding specificity of aptamers to *Escherichia coli* outer membrane proteins. Variation of normalized R_{et} of aptamers functionalized electrodes upon exposure to 2.0×10^{-6} M *Escherichia coli* outer membrane proteins, 1.0×10^{-9} M microcystin-LR, and the mixture of both, for ECA I and ECA I-MCH.

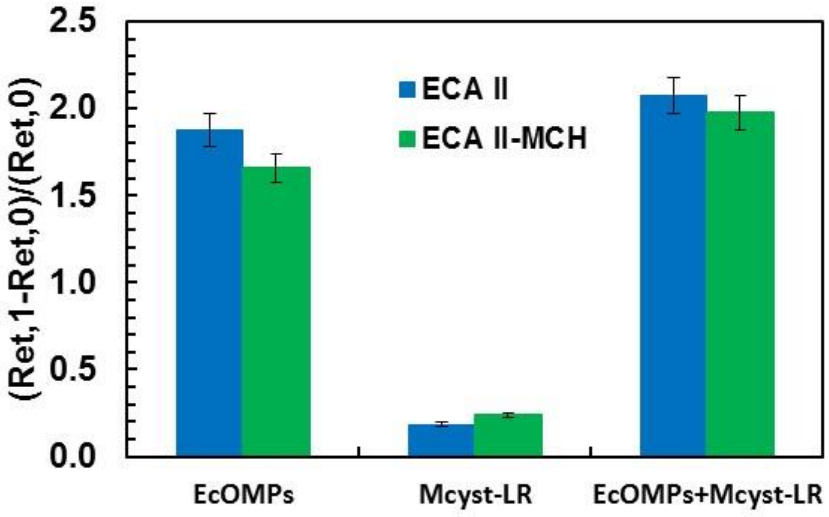

Figure 6.12 - Binding specificity of aptamers to *Escherichia coli* outer membrane proteins. Variation of normalized R_{et} of aptamers functionalized electrodes upon exposure to 2.0×10^{-6} M *Escherichia coli* outer membrane proteins, 1.0×10^{-9} M microcystin-LR, and the mixture of both, for ECA II and ECA II-MCH.

6.3.4 Regeneration of sensing phase

The regeneration of the sensing phase was tested by carrying out consecutive binding and washing steps. First, impedimetric measurements of the clean Au electrode surface, aptamer capture probe and immobilized EcOMPs (2.0×10^{-6} M) were performed. Then, several regeneration solutions (urea, TRIS-HCl-NaCl, glycine, HNO_3, HCl and tween 20) were used to regenerate the sensing phase. Although the signal decreased in some cases, it did not reach the baseline level and only HCl at 2 M presented a suitable result. As can be seen in Figure 6.13, for single SAMs, ECA I and ECA II, the surface is entirely regenerated after 20 min and capable of detecting OMPs again with the same sensitivity. In the case of mixed SAMs, ECA I-MCH and ECA II-MCH the regeneration is not as effective, presenting a regeneration of about 15 and 45 %, respectively. Even though, these capture probes are also capable of detecting EcOMPs in a second binding event, indicating that the biosensor has good stability and regeneration.

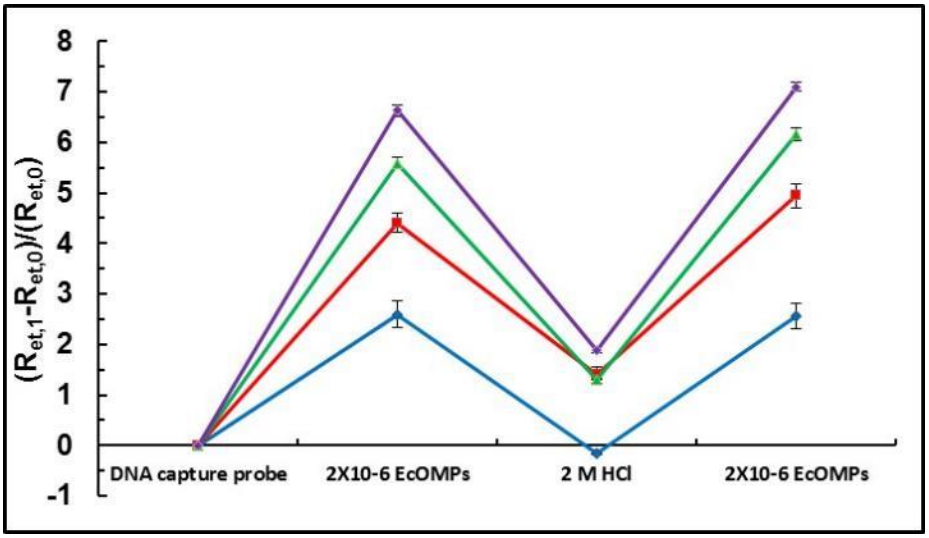

Figure 6.13 - Normalized Ret values for the several steps of binding and regeneration for (blue) ECA I, (red) ECA I-MCH, (green) ECA II, and (purple) ECA II-MCH sensing phases studied.

6.3.5 Detection of *Escherichia coli* outer membrane proteins in environmental water samples

In order to investigate the application of the present method to the analysis of environmental waters (pH 6.5), spiked waters were tested and the corresponding relative errors calculated. Environmental water samples were collected in an artesian well and stored in amber glass bottles previously rinsed with double-deionized RNase free water. The pH and ionic strength of the water samples were adjusted by addition of affinity buffer (50:50), and they were stored at 4 °C until analysis. *E. coli* bacteria were cultured in blood agar; thereafter the membrane of cells was destroyed and proteins extracted, according to point 2.3.1. After quantifying the concentration of EcOMPs by UV at 280 nm, environmental water samples were doped with these proteins solution for the final concentrations of 2.0, 5.0 and 7.0 ($\times 10^{-7}$ M). EcOMPs is achieved. These assays were carried out with sensors calibrated within 1×10-7 to 2.0×10-6 M of EcOMPs. The average recoveries of three spiked solutions for ECA I, ECA I-MCH, ECA II and ECA II-MCH were 80.2±13.5, 88.8±29.8, 85.6±18.1 and 138.9±36.8 %, corresponding to average relative errors of 19.8, 11.2, 14.4 and 38.9%, respectively and thus confirming the accuracy of the analytical data. Thus, this biosensor held promise as a sensitive and viable technique for EcOMPs detection in real samples.

6.4 Conclusions

A signal-on electrochemical aptasensor for the detection of EcOMPs based on the specific recognition between an immobilized aptamer capture probe onto a gold electrode and bacterial proteins, using the couple ferricyanide/ferrocyanide as a redox probe for EIS measurements. In general terms, both single and mixed monolayers showed a concentration-dependence behaviour. Single aptamer monolayers presented higher affinity for EcOMPs than mixed ones in terms of electron transfer resistance variation. Furthermore, this type of sensing phase was almost completely regenerated (under low pH conditions) and the deviation of the subsequent detection was less than 5 %. Also, both single and mixed monolayers are specific for EcOMPs even in the presence of other water contaminants.

These analytical features, as well as its fabrication easiness and operational convenience, make it a promising method to be involved into biochip fabrication allowing the real-time detection of *E. coli*.

With the identification of new APTs structures for specific bacterial targets, the aptamer-based biosensor approach may find its place in the market to favorably compete with the rather expensive antibody/antigen methods, which is the main commercial rapid method used at the present time.

References

Bruno, J.G.; Carrillo, M.P.; Phillips, T.; Andrews, C.J. 2010. J. Fluoresc. 20, 1211–1223.

de-los-Santos-Álvarez, N.; Lobo-Castañón, M.J.; Miranda-Ordieres, A.J.; Tuñón-Blanco, P. 2008. TrAC – Trend. Anal. Chem. 27(5), 437-446.

de-los-Santos-Álvarez, N.; Lobo-Castañón, M.J.; Miranda-Ordieres, A.J.; Tuñón-Blanco, P. 2007. J. Am. Chem. Soc. 129(13), 3808-3809.

Dijksma, M.; Kamp, B.; Hoogvliet, J.C.; van Bennekom, W.P. 2001. Anal. Chem. 73, 901-907.

Dorst, B.V.; Mehta, J.; Bekaert, K.; Martina, E.R.; Coen, W.D.; Dubruel, P.; Blust, R.; Robbens, J. 2010. Biosens. Bioelectron. 26, 1178–1194.

Ellington, A.D.; Szostak, J.W. 1990. Nature 346, 818–822.

González-Fernández, E.; de-los-Santos-Álvarez, N.; Lobo-Castañón, M.J.; Miranda-Ordieres, A.J.; Tuñón-Blanco, P. 2011. Electroanal. 23(1), 43-49.

Kim, Y.S.; Jung, H.S.; Matsuura, T.; Lee, H.Y.; Kawai, T.; Gua, M.B. 2007. Biosens. Bioelectron. 22, 2525–2531.

Labib, M.; Zamay, A.S.; Muharemagic, D.; Chechik, A.V.; Bell, J.C.; Berezoyski, M.V.; 2012. Anal. Chem. 84(4), 1813-1816.

Li, X.; Shen, L.; Zhang, D.; Qi, H.; Gao, Q.; Ma, F.; Zhang, C. 2008. Biosens. Bioelectron. 23, 1624-1630.

Mascini, M.; Palchetti, I.; Tombelli, S. 2012. Angew. Chem. Int. Ed. 51, 1316 – 1332.

Miranda-Castro, R.; de-los-Santos-Álvarez, N.; Lobo-Castañón, M.J.; Miranda-Ordieres, A.J.; Tuñón-Blanco, P. 2009. Electroanal. 21(19), 2077-2090.

Randles, J.E.B. 1947. Discuss. Faraday Soc. 1, 11–19.

Rodriguez, M.C.; Kawde, A.N.; Wang, J. 2005. Chem. Commun. 34, 4267-4269.

Rohrbach, F.; Karadeniz, H.; Erdem, A.; Famulok, M.; Mayer, G. 2012. Anal. Biochem. 421(2), 454-459.

Steel, A.B.; Herne, T.M.; Tarlov, M.J. 1998. Anal. Chem. 70, 4670-4677.

Stoltenburg, R.; Reinemann, C.; Strehlitz, B. 2007. Biomol. Eng. 24, 381–403.

Tombelli, S.; Minunni, M.; Mascini, M. 2005. Biosens. Bioelectron. 20, 2424–2434.

Torres-Chavolla, E.; Alocilja, E.C. 2009. Biosens. Bioelectron. 24(11), 3175-3182.

Turner, A.P.F. 2000. Science 290, 1315–1317.

World Health Organization. 1998. Drinking-Water Quality Guidelines for Parameters of Concern in Agricultural Drainage Water—Annex 3, Technical Report, pp. 281–289.

Xu, Y.; Yang, L.; Ye, X.Y.; He, P.A.; Fang, Y.Z. 2006. Electroanal. 18(15), 1449-1456.

Zayats, M.; Huang, Y.; Gill, R.; Ma, C.A.; Willner, I. 2006. J. Am. Chem. Soc. 128(42), 13666-13667.

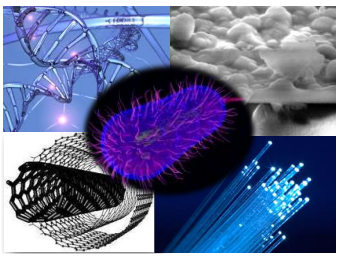

Chapter 7

Development of label-free aptamer-based long period grating biosensor for the detection of *Escherichia coli* outer membrane proteins

7.1 Introduction

The increasing need for devices capable of performing reliable, fast and in situ measurements in the field of biochemical detection is guiding researchers to look for new technologies (Baldini et al., 2012). One possibility is provided by optical refractometers, which measures the change in refractive index associated with a biochemical response. In the resulting sensors the crucial phenomenon is interaction, typically evanescent, of an optical signal with a sensitive layer which experiments a change on its own refractive index in the presence of an analyte. This variation will cause a change in light propagation conditions leading to a change in the properties of the signal (intensity, frequency, polarization or phase). In this case, the binding events cause an increase of the mass on the surface which results in an increase of the effective RI. Fiber optic refractometers are increasingly popular due to the versatility, relative ease of fabrication and high sensitivity of different evanescent wave configurations.

Among most popular fiber optic refractometric devices for biosensing application are side polished fibers (Slavík et al., 2002), fiber tapers (Beres et al., 2011), polished Fiber Bragg gratings (FBGs) (Chryssis et al., 2005) and LPG (Pilla et al., 2011). Among these, LPGs are the only ones where the physical integrity of the fiber is preserved thus increasing the robustness of the sensor and handling (Pilla et al., 2012). A LPG consists in a periodic modulation of the refractive index of the core of the fiber where the period (Λ) is in the range of hundreds of microns. This periodic perturbation satisfies the phase matching condition between the fundamental core mode and a forward propagating cladding mode of an optical fiber. Thereby, in an LPG, the core mode couples into the cladding modes of the fiber, resulting in several resonances centered at discrete wavelengths in the transmitted spectrum, where each one corresponds to the coupling to a different cladding mode (Bhatia et al., 1996). This mechanism provides evanescent interaction, which means that these devices are intrinsically sensitive to the SRI (Patrick et al., 1998). LPGs are among the most promising fiber optic-based refractive index transducers to be employed for unlabeled biochemical assays (Fan et al., 2008). The use of LPG is cost-effective because it does not require expensive instrumentation and may allow portability. Also, LPGs have been showing high performance and the resulting devices are, in terms of fabrication, easier and less expensive to obtain when compared with surface plasmon resonance-based fibre optic sensors, usually more sensitive. Moreover, they maintain fiber integrity (unlike other devices such as fiber tapers or etched FBGs) and probably represent the most popular device for label free sensing. They also present high sensitivity to refractive index measurement, which can be increased and tuned by using high refractive index overlays (Pilla et al., 2012).

In the latter work two APT candidate sequences were obtained and tested in an impedimetric assay. The present work describes the use of one *E. coli* DNA APT (herein called ECA) for the determination of *E. coli* in waters by the identification of EcOMP using a LPG as a refractometric platform. The APT raised against EcOMPs, containing 36 nucleotides, was immobilized using two different methods of immobilization: electrostatic (using PLL as cationic polymer) and covalent (using an organofunctional alkoxysilane molecule). The functionalization of the bare LPG by these two different methods of immobilization originate two different sensing heads that were characterized and tested against EcOMPs and applied to spiked environmental water samples.

7.2 Experimental

7.2.1 Apparatus

For the sensing heads fabrication, a standard single-mode fibre SMF-28 (Corning, inc., USA) was used, with 8.6 and 125 µm-diameters for the core and cladding, respectively. The sensing element was characterized using a FS 2200 Braggmeter from Fibersensing, SA (Portugal) working in the 1500-1600 nm range, with 1 pm of resolution, and modified to measure signals both in reflection and transmission modes in separate channels. A schematic illustration of the setup is presented in Figure 7.1.

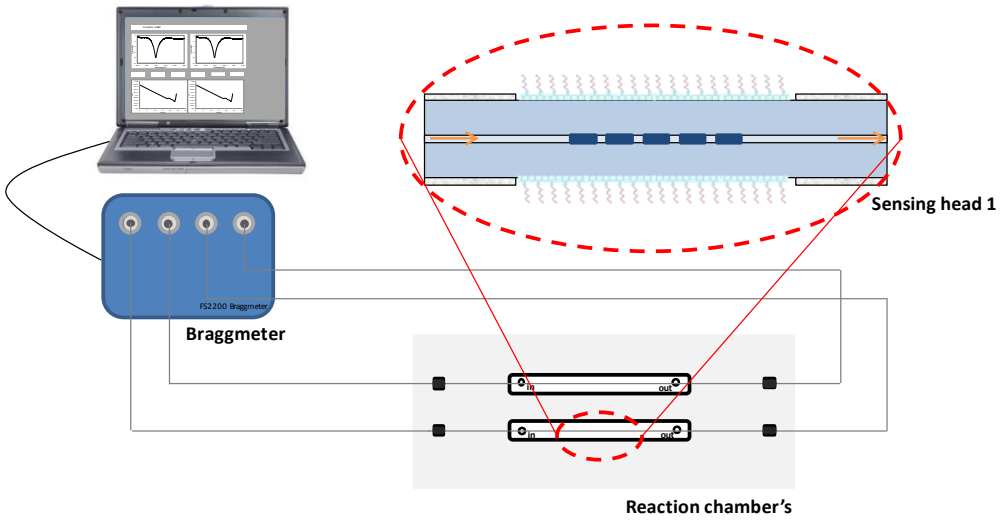

Figure 7.1 - Experimental setup with the detail of sensing head 1 (SH1) functionalized LPG. The setup was constituted by a Braggmeter (1500-1600 nm), 2 reaction chambers that operate in continuous mode and simultaneously and a laptop that receives and processes the readout information.

7.2.2 Reagents and solutions

A lawn of *Escherichia coli* ATCC® 8739™ was purchased in ATCC (USA) and EcOMP were extracted according to Bruno et al., 2010. 36 mer DNA oligo (5'-amine-GTC TGC GAG CGG GGC GCG GGC CCG GCG GGG GAT GCG-3') synthesis scale: 0.2 µM, purification HPLC, 5' modification-amine was purchased from Sigma-Aldrich (Spain).

Salts for buffer solutions were prepared in double-deionized water, < 2 MΩ-cm at 25 ºC from ELGASTAT-UHQ (UK). HCl and magnesium chloride were purchased from Panreac (Spain), TRIS were obtained from Fluka (Germany), APTES was obtained from ABCR (Germany), 0.1% (W/V) PLL), dimethyl suberimidate (DMS), KCl, NaCl, SSPE buffer 20x concentrate, TRIS-EDTA (TE) (10 mM TRIS pH 7.5-8.0; 1 mM EDTA) MC-LR were obtained from Sigma (Germany). The buffers used in this work were: ressuspension buffer: TE; immobilization buffer: SSPE (1:10); affinity buffer (50 mM TRIS/HCl pH 7.4, 250 mM NaCl, 5 mM MgCl2) and washing and measurement buffer (10 mM TRIS/HCl pH 7.4, 100 mM KCl). All the reagents were of analytical grade.

7.2.3 Experimental methods

7.2.3.1 Long period gratings fabrication and characterization

A detailed description of LPG fabrication by the electric arc discharge technique is presented in Figure 7.2. A stripped fiber was placed between the electrodes with a gap between 0.9 and 1.0 mm. The electrodes had 2 mm of diameter and were made in tungsten rods and are mounted on a x,y,z translation stage to position the fiber relatively to the electrode in such way that the electric discharge engages the fiber homogeneously. This operation was executed with the help of an optical microscope. The high voltage power supply was a BICC AFS3100 fusion splicer machine. The fiber was aligned and held in the same position with the help of a set of V-grooves with two clamp arms. One end of the fiber was clamped in a fiber holder on top of the translation stage, controlled with the precision of 0.1 µm. At the other end a mass is attached to keep the fiber under a constant axial tension (5 - 40 g). An arc discharge is then produced with an electric current of 8.5 - 10.0 mA for 0.5 s. As a result, a short portion of the fiber length was exposed. Afterwards, the fiber was translated by a distance which is equal to the grating period. The fiber is illuminated with a white light source and the spectrum was monitored in real time by using an OSA, Ando AQ-6315B, with a maximum wavelength resolution of 0.5 nm. The analysis was focused on the spectral range 1500-1600 nm.The sequence arc discharge/fiber displacement was repeated several times until a required attenuation value for the resonance peak (monitored with the OSA) was obtained (Rego et al., 2001).

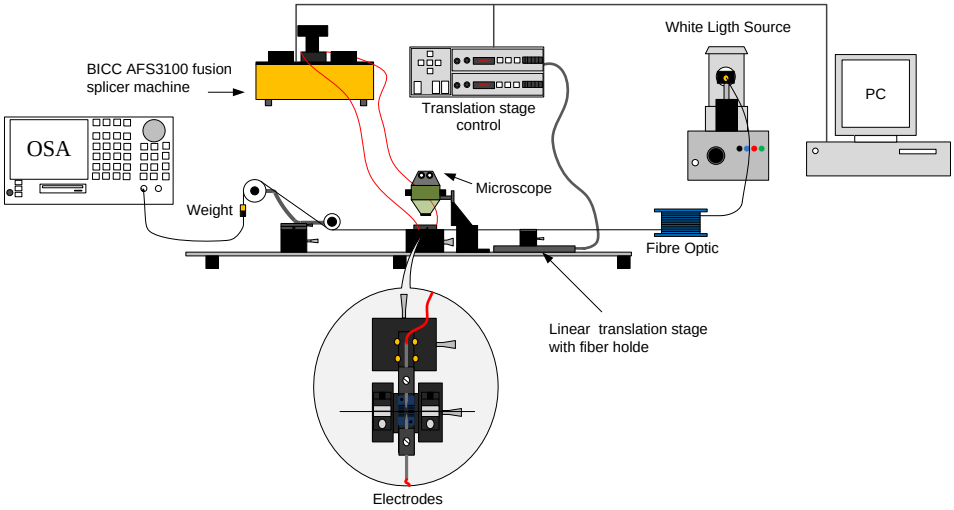

Figure 7.2 - Setup of the long period grating fabrication by electric arc discharge technique (Caldas, 2011). OSA: Optical spectrum analyser.

Figure 7.3 shows the growth of the resonance peak of the LPG with the increment of the number of periods. Several spectra are presented to elucidate the formation of the resonance band during the fabrication of the LPG. As the electrical discharges are being made the resonance peak increases in depth and becomes narrower until a maximum loss is reached.

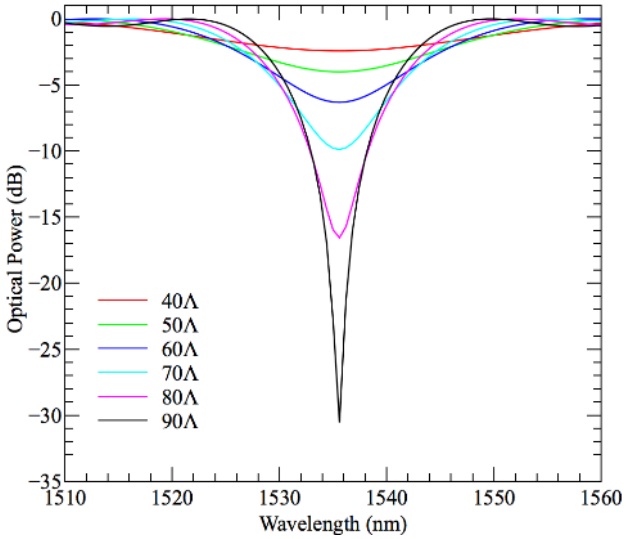

Figure 7.3 - Long period resonance peak growth as a function of the number of periods.

The sensitivity of an LPG is typically defined as a shift of the λ_R induced by a measurand. The characteristic sensitivity of a bare LPG to SRI depends on several factors including the fiber diameter, and changes with an increasing (in modulus) non-linear monotone trend. The result is that the maximum sensitivity is achieved when the external index is close to the cladding index while for lower refractive indices (around 1.33) the LPG is scarcely sensitive (Shu et al., 2001). The behavior changes when a sub-wavelength thin layer (few hundreds of nanometers) and with higher refractive index than that of the cladding is deposited thereon (Pilla et al., 2012). The high refractive index overlay draws the optical field towards the external medium extending its evanescent penetration. As a result there is an increased sensitivity of the device to the SRI. The field enhancement in the overlay depends strongly on the overlay thickness and refractive index. This technique allows the coupling of the optical design and sensitivity optimization of the device, together with the functionalization. High order cladding modes that strongly penetrate the external medium, on the other hand, offers higher sensitivity, and obviously these are the most desirable for sensing purposes. An increase in the order of the coupled cladding mode is obtained by decreasing the grating period (Shu et al., 2001). The careful design by means of the proper choice of the grating period, the overlay refractive index and a very controlled deposition method, together with the integration on the high refractive index of sensitive materials or biological active agents, provide a powerful platform for advanced optical label free biochemical sensing.

Figure 7.4 shows the resonance wavelengths versus grating periods for the cladding modes 1 to 8 (Baptista, 2009). Based on simulations and previous experiments, in order to excite the 6^{th} order cladding mode in the wavelength ~1550 nm, a period of around 395 μm must be used. It is the shortest period that can be achieved with the fabrication setup described, and as it was explained before, to acquire higher sensitivity, shorter periods should be used. The length of the used LPG is around 40 mm depending on the number of periods which was between 80 and 90. From this point forward, whenever LPG resonance will be referred, it will be relatively to the 6^{th} order cladding mode.

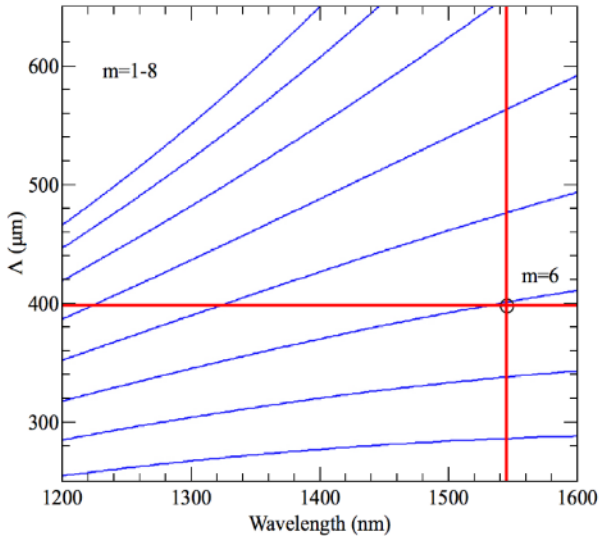

Figure 7.4 - Theoretical determination of the cladding mode considering the period (Λ) use in the fabrication of the long period grating and the resonance wavelength (λ_R) (Baptista, 2009).

The sensitivity of the LPG to the SRI was also studied for the range between 1.335 – 1.375 RIU, which is the range of interest for biological measurements (Zibaii et al., 2010). The LPG was characterized in terms of SRI and its transmission spectra for different SRIs were recorded. The SRI was changed by using solutions of distilled water with different percentages of ethylene glycol at constant temperature (25 ºC). Each liquid sample had its refractive index previously characterized with an Abbe refractometer using the sodium D line (589 nm). The necessary adjustments, considering the sensing head operation at 1550 nm, can be made using the Cauchy equation with the respective coefficients (Pereira et al., 2004). Figure 7.5 shows the spectral position of the resonance related to the 6th cladding mode for the LPG, for three different SRI. It is clear that with the increment of the external index, the resonance shifts to shorter wavelengths as expected. From this data a calibration was established and it is shown in Figure 7.6. The sensitivity of the device for the studied resonance is around 100 nm/RIU (Gouveia, 2008).

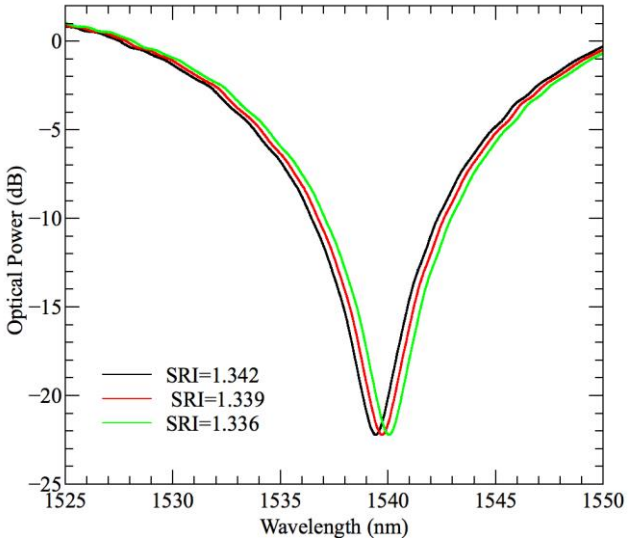

Figure 7.5 - LPG spectral characterization to surrounding refractive index (SRI) changes for the 6th order cladding mode resonance (Gouveia, 2008).

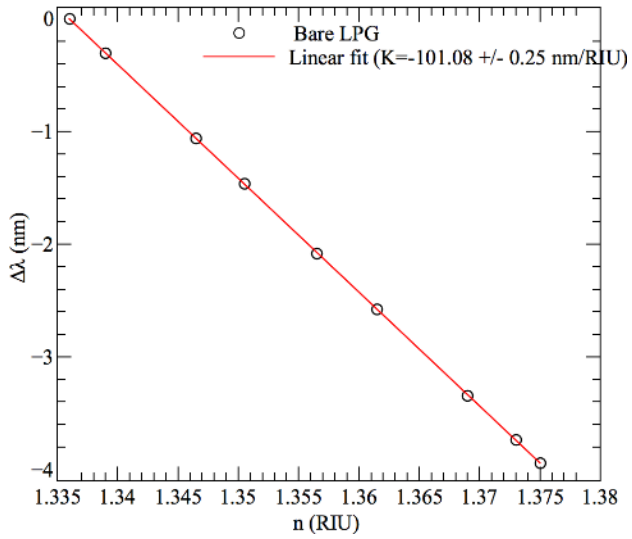

Figure 7.6 – Long period gratings response to surrounding refractive index in the range between 1.336 – 1.380 (adapted from Gouveia, 2008).

7.2.3.3 Sensing heads assembly

The LPG surface were functionalized using two different processes; an electrostatic method, using PLL as cationic polymer and a covalent method, using APTES.

Prior to functionalization of the LPG, these were cleaned by immersion in 5 M HCl for 30 min at room temperature, followed by rinsing in DD water and with washing buffer. SH1 were coated with 0.1 % PLL for 30 min at room temperature and then were washed with buffer. The silanization of the LPG surface, for the assembly of sensing head 2 (SH2), was performed by immersing the cleaned grating sample in fresh 10% APTES (in ethanol) for 1 h, also at room temperature. For activation of the fiber surface, the silanized LPGs were immersed in 25 mM DMS for 30 min at room temperature. The activated sensors were rinsed with washing buffer. Both sensing heads were incubated with 200 nM of ECA during the night at 4 ºC. The sensing heads were finally washed with buffer.

7.2.3.4 *Escherichia coli* outer membrane proteins detection assay

The sensing heads were incubated with several varying concentrations of EcOMP, in the affinity buffer for 1 h. EcOMPs were produced similarly to that performed in Chapter 6. The concentration ranged from 1.0×10^{-10} M to 3.0×10^{-8} M. Between all concentration steps the sensing heads were washed with buffer and then the wavelength shift of the resonance peak was recorded with the Braggmetter while in the measurement buffer. For a proper comparison, all the recorded spectra were made with the sensing probes immersed in the same buffer solution – the measurement buffer. After a complete assay the sensing heads were washed with a 2 M HCl solution for 1 h, to regenerate the probe for re-use.

7.3 Results and discussion

7.3.1 Scanning Electron Microscopy and Atomic Force Microscopy analysis

SEM and AFM analysis were conducted over both sensing heads at the different steps of the functionalization and the assembling process. The obtained images of SEM (left) and AFM (right) are shown in Figure 7.7 and Figure 7.8 for SH1 and SH2, respectively. In both Figures, Figure 7.7a) and Figure 7.8a), a roughened surface is observed resulting from the washing with HCl, for the activation of the surface.

After the functionalization with PLL of SH1 the surface became smooth as can be seen in Figure 7.7b). The effect of the functionalization of SH2 in the surface of the LPGs is presented in Figure 7.8 b) and c). It was observed that the surface is smoothed by application of the aminosilane but it does not appear as smooth as the surface functionalized with PLL. Figure 7.8c) shows that the immobilization of the DMS is not uniform, and that the layer is quite thick, about 10 nm. After the immobilization of the ECA, Figure 7.7c) and Figure 7.8d), it could be observed that the AFM images of each type of sensing heads surface were quite different. The surface of SH2 is more heterogeneous than the SH1. A possible explanation may be that the previous layer of DMS, was not evenly distributed, causing a heterogeneous layer of ECA. Regarding the immobilization of EcOMPs, Figure 7.7d) and Figure 7.8e), it could be observed that SH1 surface is granular while SH2 is flatter. Also, it seems that some bacterial membrane residues remain in EcOMPs solution and that could eventually interfere on the assay due to the comparatively large mass and proximity to the surface.

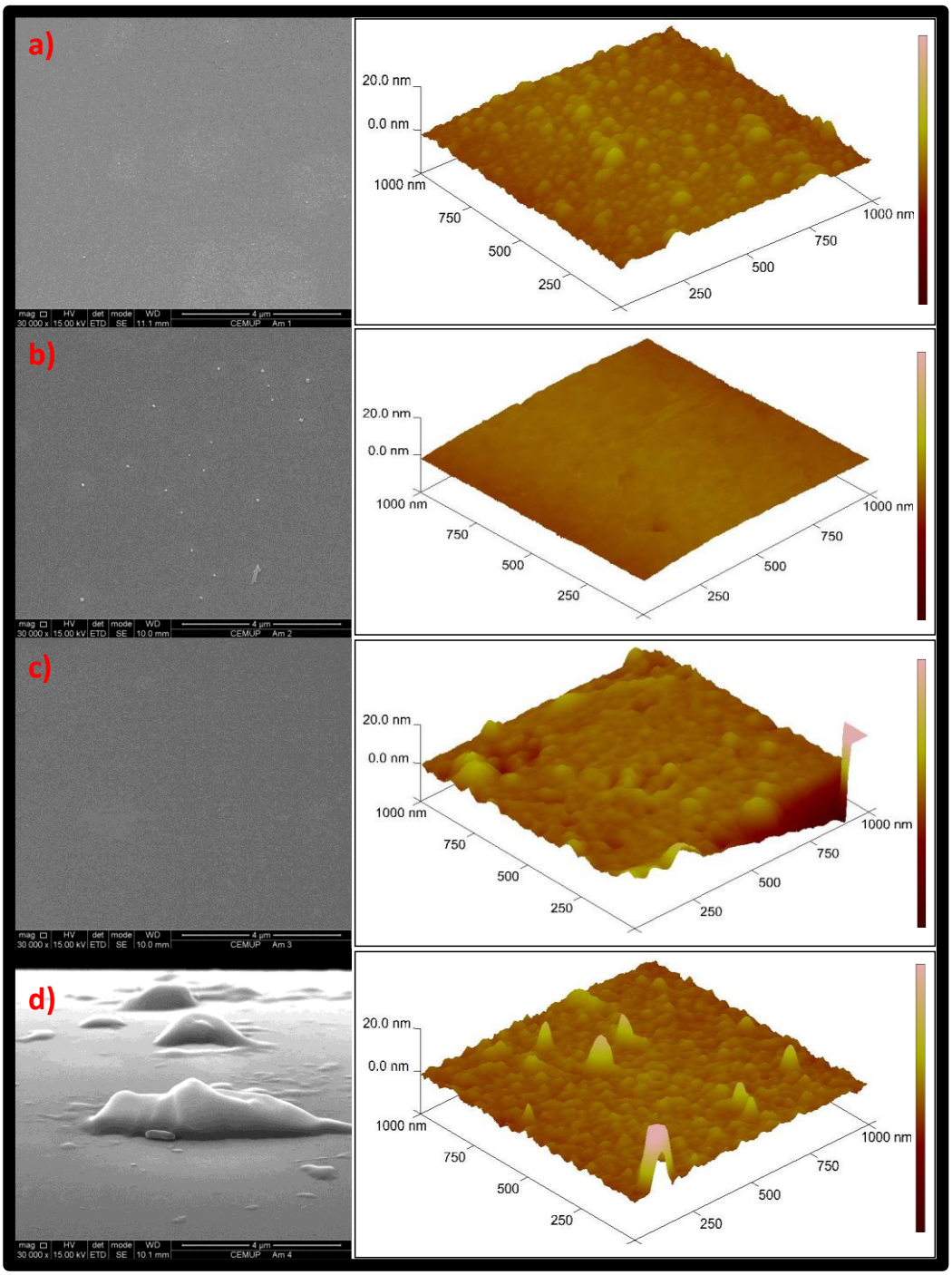

Figure 7.7 – Scanning electron microscopy (left) and 3-Dimensional Atomic force microscopy (right) images of sensing head 1 for a) after wash with hydrochloric acid; b) functionalization with poly-L-lysine; c) immobilization of 1.0×10^{-6} M of *Escherichia coli* aptamer; d) immobilization of 1.19×10^{-6} M of *Escherichia coli* outer membrane proteins.

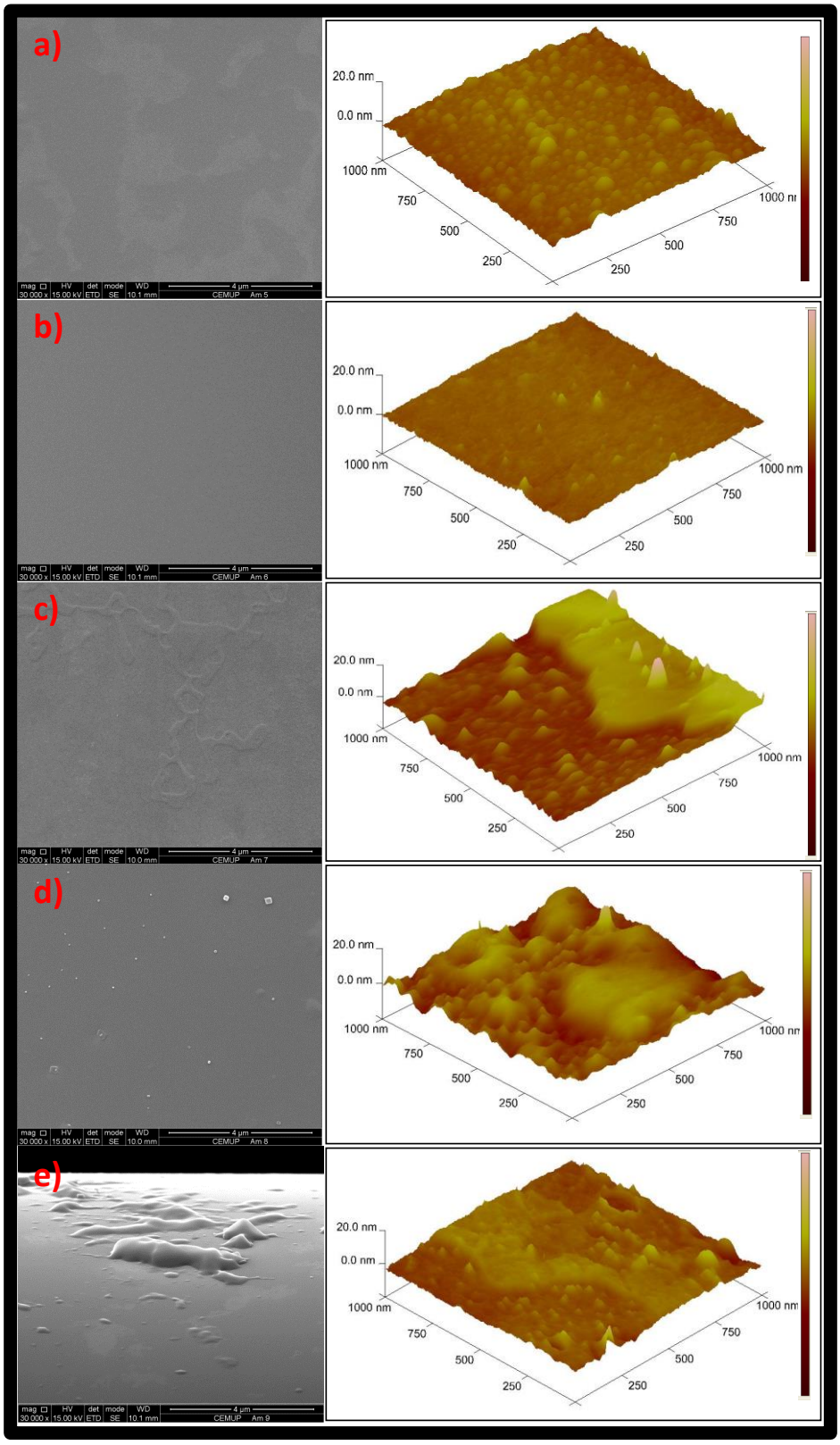

Figure 7.8 - Scanning electron microscopy (left) and 3-Dimensional Atomic force microscopy (right) images of sensing head 2 for a) after wash with hydrochloric acid; b) functionalization with 10% aminophenyltriethoxysilane; c) functionalization with 25 mM dimethyl sulfoxide; d) immobilization of 1.0×10^{-6} M of *Escherichia coli* aptamer; e) immobilization of 1.19×10^{-6} M of *Escherichia coli* outer membrane proteins.

7.3.2 Principle of *Escherichia coli* aptamer long period grating biosensor

The detailed principle of ECA LPG biosensor is illustrated in Figure 7.9, using SH1 as an example. For the measurements, a Braggmeter that works in the 1500-1600 nm range, in both reflection and transmission modes, was used. The sensing heads were connected to the unit in transmission mode. The optical signal launched to the single mode fibre by the unit is guided by the core, untill it reaches the grating region. In the LPG, the core mode couples into the cladding modes of the fibre, resulting in attenuation bands centred at specific wavelengths in the transmitted spectrum. A small fraction of the cladding mode, also known as evanescent field, travels outside of the optical fibre, interacting with the external medium; any variations in the refractive index of the outer region will affect the effective refractive index of the cladding modes and, thus, will change λ_R. The LPG sensing principle primarily relies on measuring the shift in λ_R, due to the changes in the refractive index. The changes in λ_R are monitored in real time by the unit and from step-to-step, the spectrum is also recorded. The fibres were properly fixed with fibre clamps in both sides, and a small tension was applied with a translation stage to avoid strain/curvature cross sensitivity. The functionalized APT with an amine group at its 5' end was bind to an optical fibre with an inscribed LPG (Λ= 395-398 µm) that was modified using two different processes. SH1 was modified with a cationic polymer - PLL (electrostatic interaction) and SH2 was modified by silanization using APTES and DMS (covalent bind). The polycationic nature of the PLL leads to its electrostatic attraction onto a negatively charged surface in an aqueous environment at neutral pH.

In covalent binding to a silica surface, SH2, a chemical bond has to be formed between a functional group of biomolecules and the amino group of the linker. Herein DMS was used. It is a water soluble and membrane permeable cross-linking agent to convert the amino groups into reactive imidoester (Hermanson, 1996). The imidoester functional group is a specific acylating group accessible for the modification of primary amines and has minimal cross reactivity to other nucleophilic groups in proteins (Mattson et al., 1993). Both, activated sensing heads were then incubated with 200 nM of ECA.

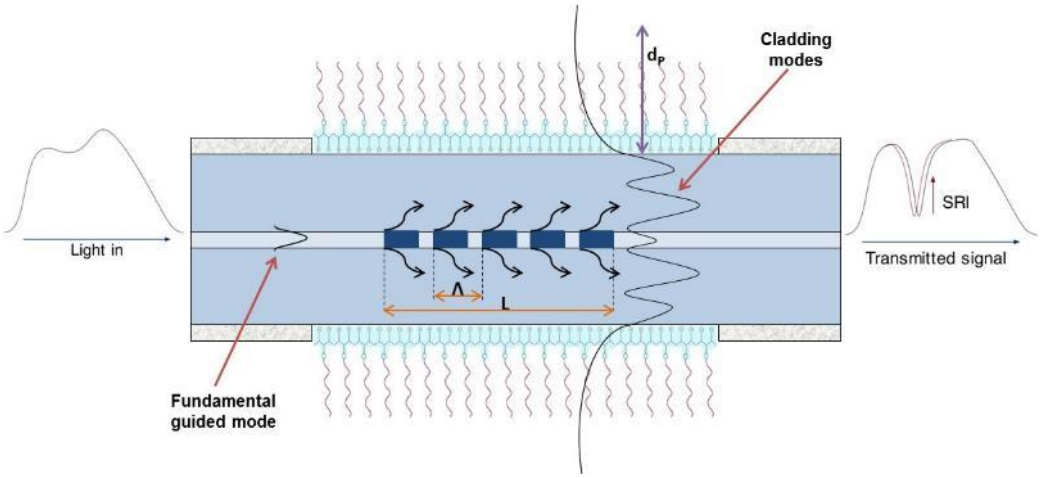

Figure 7.9 - Scheme of long period grating structure with the description of the mode coupling and spectra of incoming light and of transmitted light at the output of the long period grating; also the shift of the resonance peak for increasing surrounding refractive index (SRI) and the penetration depth (d_P) of the wavelength field are schematically represented.

Afterward, the sensing heads were incubated with varying concentrations of EcOMP. Between all these steps the shift of the resonance was measured. In the presence of EcOMP, the ECA folds around the proteins and forms an EcOMP-ECA complex. The formation of this complex causes an increase in the effective refractive index of the cladding and consequently a decrease of the wavelength of the resonance. Figure 7.10 and Figure 7.11 present the transmission spectra of the LPG reporting the resonance wavelength shift during the immobilization procedure and following the affinity-assay for SH1 and SH2, respectively.

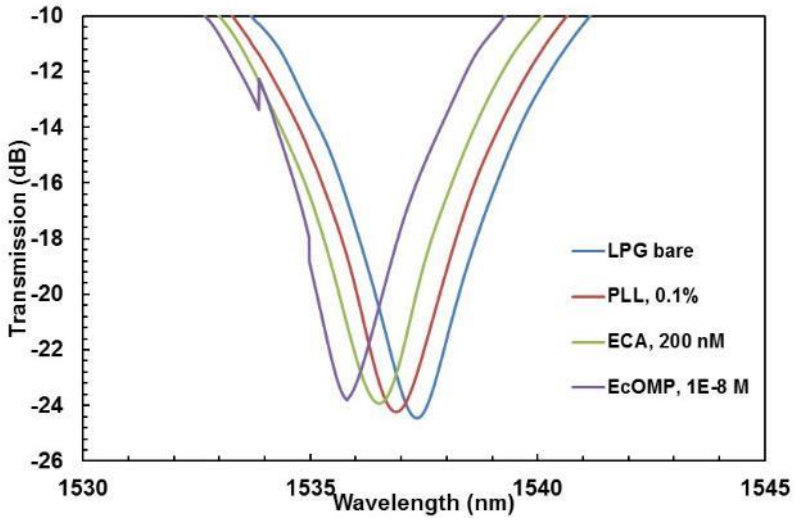

Figure 7.10 - Transmission spectra of the long period grating reporting the wavelength shift of the resonance during the immobilization procedure with poly-L-lysine and following affinity-assay (*Escherichia coli* aptamer- *Escherichia coli* outer membrane proteins) for sensing head 1.

The wavelength shift observed is of about 1.6±0.4 nm from the bare LPG to the affinity-assay between ECA and EcOMP for SH1 while for SH2 the difference is of about 0.48±0.3 nm, for *n*=5. In this case, the immobilization of the DMS creates a wavelength shift with opposite signal. These results show lack of experimental reproducibility. There are several aspects to take in consideration. The reproducibility of the LPG by electric arc is a critical issue, since it is quite difficult to write gratings with the same exact characteristics such as, length, resonance wavelength and strength. The resonance sharpness affects the resolution as well the wavelength, because the evanescent field is proportional to the wavelength. And the length of the device is, by itself, important due to the exposed sensing area. LPG are also highly sensitive to temperature, and the experiments were not made in a temperature-controlled environment, a topic that will be discussed later. On the other hand, small differences in the early steps of the functionalization process can cause substancial differences in the end. SEM and AFM results did show that the covalent process seems to result in less uniform functionalized surfaces. In the literature we did not find any information about reproducibility in biosensing with LPGs. It is therefore an open issue worth of investigation.

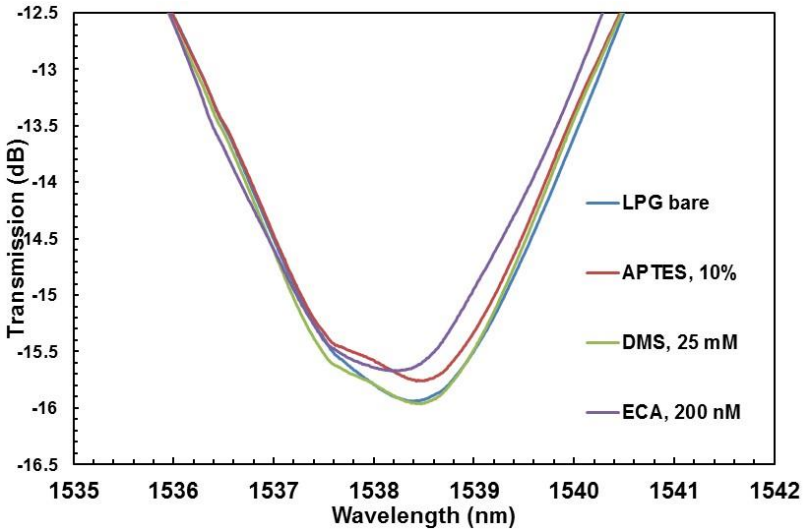

Figure 7.11 - Transmission spectra of the long period grating reporting the wavelength shift of the resonance during the immobilization procedure with aminopropyltriethoxysilane and dimethyl sulfoxide and following affinity-assay (*Escherichia coli* aptamer- *Escherichia coli* outer membrane proteins) for sensing head 2.

7.3.3 Sensor performance against *Escherichia coli* outer membrane proteins

The self-assembly of the ECA and consecutively EcOMPs, onto the bare LPG surface, increases the effective index of the LPG cladding mode resulting in a shift of the resonance as a function of the surface mass (which is also increasing). The sensor performance was tested by the evaluation of SH1 and SH2 against increasing concentrations of EcOMPs. Figure 7.12 to Figure 7.15 present the LPG sensorgrams and the calibration plots relative to the wavelength shift of the resonance during the affinity-assay of the complex ECA-EcOMP ranging from 1.0×10^{-10} M to 3.0×10^{-8} M of EcOMPs for SH1 and SH2, respectively.

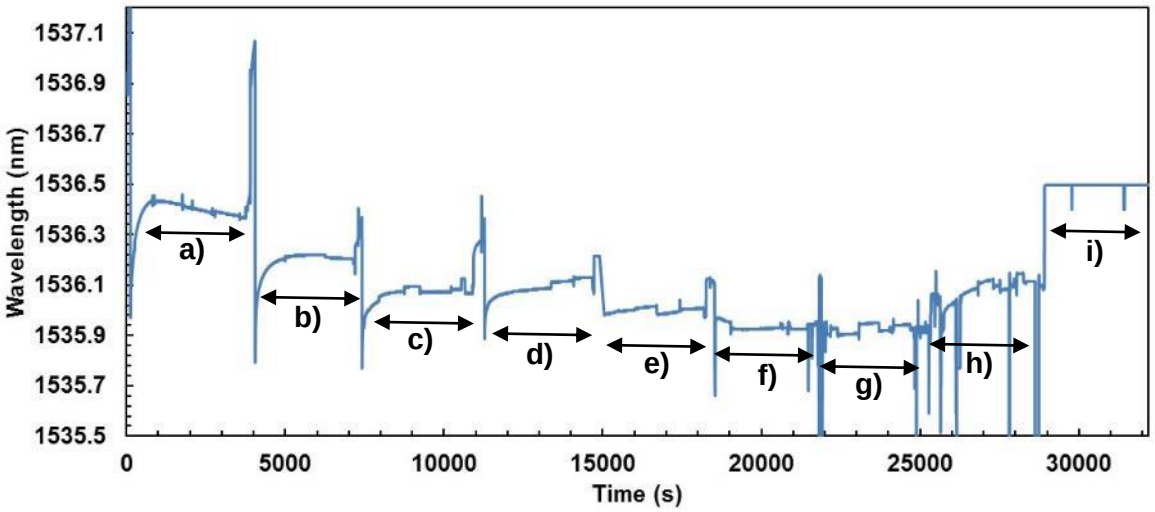

Figure 7.12 – Long period grating sensorgram reporting the resonance wavelength shift during the affinity-assay of the complex *Escherichia coli* aptamer (200 nM)-*Escherichia coli* outer membrane proteins ranging from 1×10^{-10} M to 3×10^{-8} M of *Escherichia coli* outer membrane proteins; measurements in buffer at room temperature for sensing head 1; a) 200 nM *Escherichia coli* aptamer, b) 1.0×10^{-10} M, c) 3.0×10^{-10} M, d) 1.0×10^{-9} M, e) 3.0×10^{-9} M, f) 6.0×10^{-9} M, g) 1.0×10^{-10} M, h) 3.0×10^{-10} M of *Escherichia coli* outer membrane proteins, and i) 2M hydrochloric acid.

As can be seen in Figure 7.12 and Figure 7.14 the interaction between ECA and the EcOMP were much faster during the first periods of the calibration and decrease along the time with the increase of the EcOMP concentration. This behaviour can mean that the surface of the sensing heads becomes covered and the linkage of arriving EcOMP to the surface is increasingly difficult. In the first periods of analysis, 60 min is enough time for the complete interaction between ECA and EcOMP, but, after the 5th period the interaction time should be increased to assure the complete affinity between the sensing heads and the EcOMP.

The incubation of ECA with EcOMP for concentrations between 1.0×10^{-10} and 1.0×10^{-8} M in affinity buffer progressively increased the SRI of the LPG surface and subsequently shifted the resonance for shorter wavelengths. For both sensing heads, a logarithmic relationship was verified between the resonance wavelength and the EcOMP concentration, as may be seen in the inset picture of Figure 7.13 and Figure 7.15.

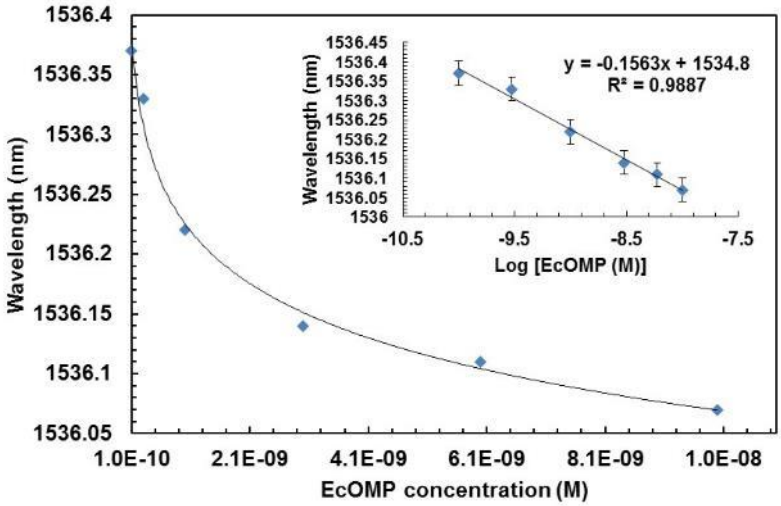

Figure 7.13 - Calibration plot of sensing head 1 for the affinity assay of the complex *Escherichia coli* aptamer-*Escherichia coli* outer membrane proteins ranging from 1.0×10^{-10} M to 1.0×10^{-8} M of *Escherichia coli* outer membrane proteins; measurements in buffer at room temperature; inset: linearization of calibration plot.

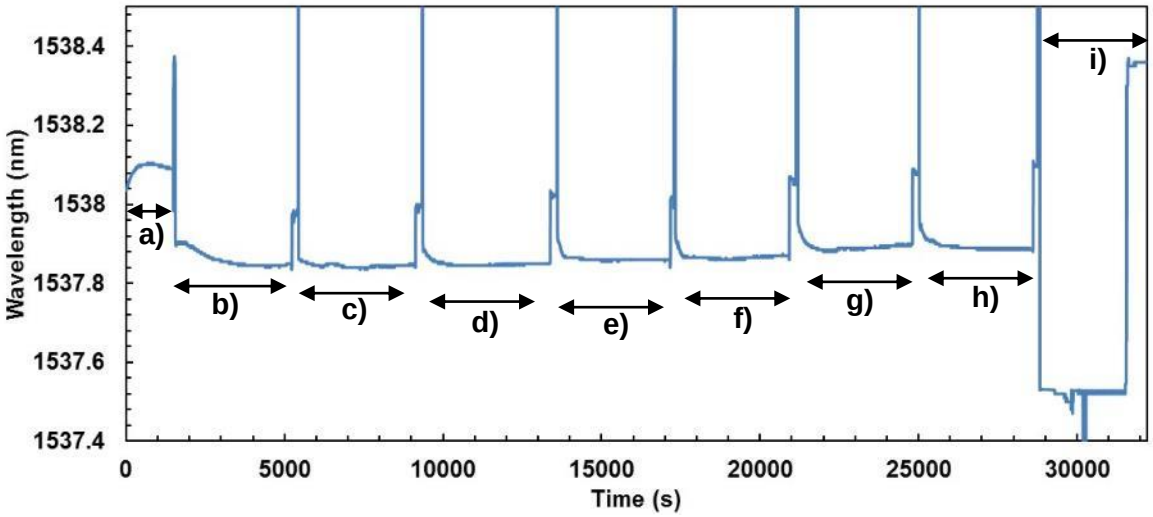

Figure 7.14 - Long period grating sensorgram reporting the resonance wavelength shift during the affinity-assay of the complex *Escherichia coli* aptamer (200 nM)-*Escherichia coli* outer membrane proteins ranging from 1×10^{-10} M to 3×10^{-8} M of *Escherichia coli* outer membrane proteins; measurements in buffer at room temperature for sensing head 2; a) 200 nM *Escherichia coli* aptamer, b) 1.0×10^{-10} M, c) 3.0×10^{-10} M, d) 1.0×10^{-9} M, e) 3.0×10^{-9} M, f) 6.0×10^{-9} M, g) 1.0×10^{-10} M, h) 3.0×10^{-10} M of *Escherichia coli* outer membrane proteins, and i) 2M hydrochloric acid.

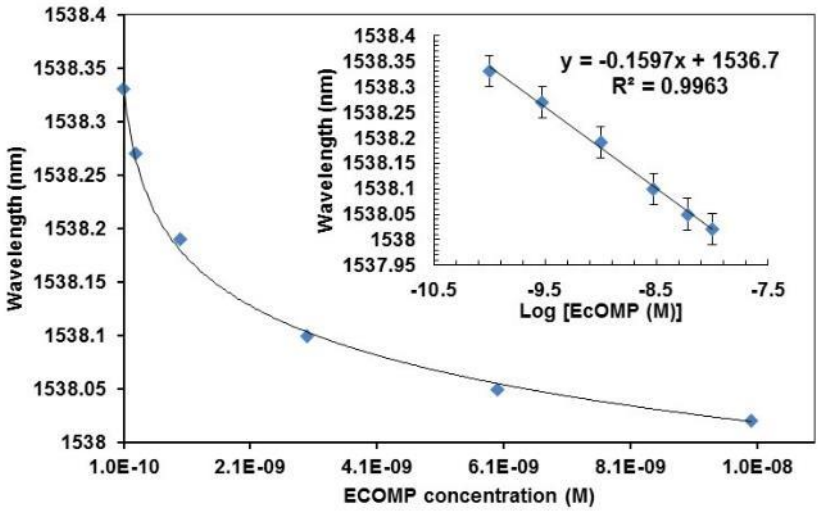

Figure 7.15 - Calibration plot of sensing head 2 for the affinity assay of the complex *Escherichia coli* aptamer-*Escherichia coli* outer membrane proteins ranging from 1.0×10^{-10} M to 1.0×10^{-8} M of *Escherichia coli* outer membrane proteins; measurements in buffer at room temperature; inset: linearization of calibration plot.

7.3.4 Regeneration of sensing heads

As referred in Chapter 6, the regeneration of the sensing heads can be achieved by using 2 M HCl. The regeneration of the sensing head was tested by carrying out consecutive binding and washing steps. The shift of the resonance was measured before and after the functionalization of the sensing heads, after the immobilization of the ECA and after the incubation of 200 nM ECA with 1.0×10^{-8} M EcOMP. Then, sensing heads were washed with a 2 M HCl solution for 30 min, to regenerate the probe for re-use and re-incubate with 1.0×10^{-8} M EcOMP. According to the LPG working principles the removal of the EcOMPs decreased the SRI and consequently the λ_R shifts to higher wavelengths, as can be seen in Figure 7.16 and Figure 7.17.

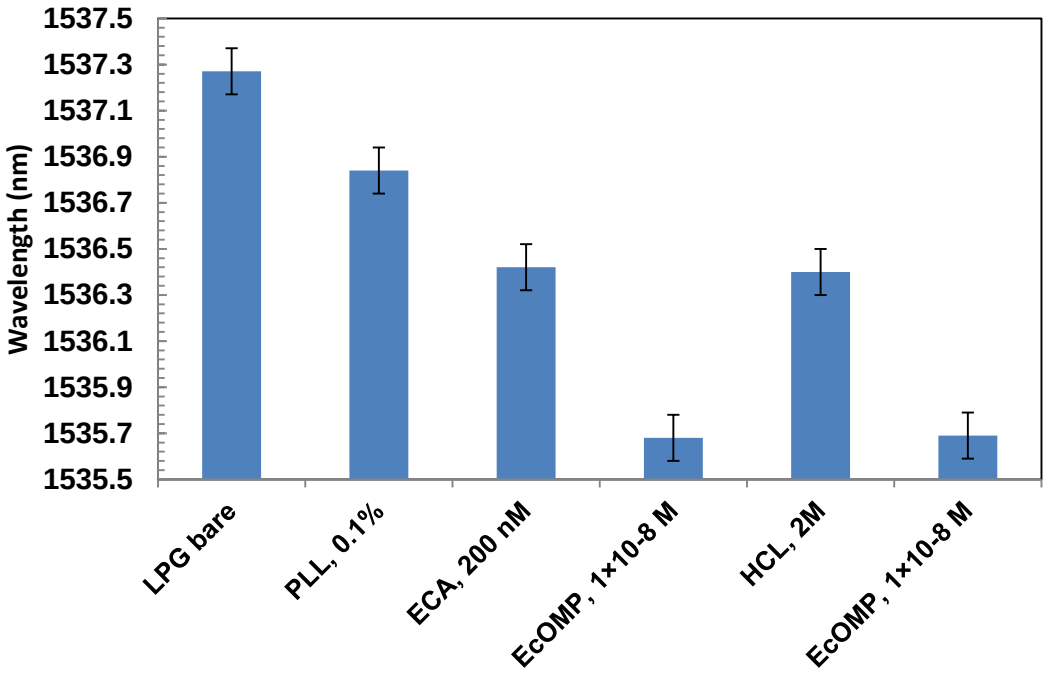

Figure 7.16 - Regeneration of sensing head 1; functionalization of bare long period grating follow by immobilization of *Escherichia coli* aptamer, binding with *Escherichia coli* outer membrane proteins washing with hydrochloric acid and rebinding of *Escherichia coli* outer membrane proteins.

As can be seen, the wavelength increases with the removal of the EcOMPs and decreases again after the immobilization of the EcOMPs, which demonstrates the surface is entirely regenerated after 20 min and is capable of detecting EcOMPs again with the same sensitivity. This assay was performed for both sensing heads and the same behavior was verified. Sensing heads show good stability and regeneration due to their ability of detect EcOMPs in successive binding and washing events.

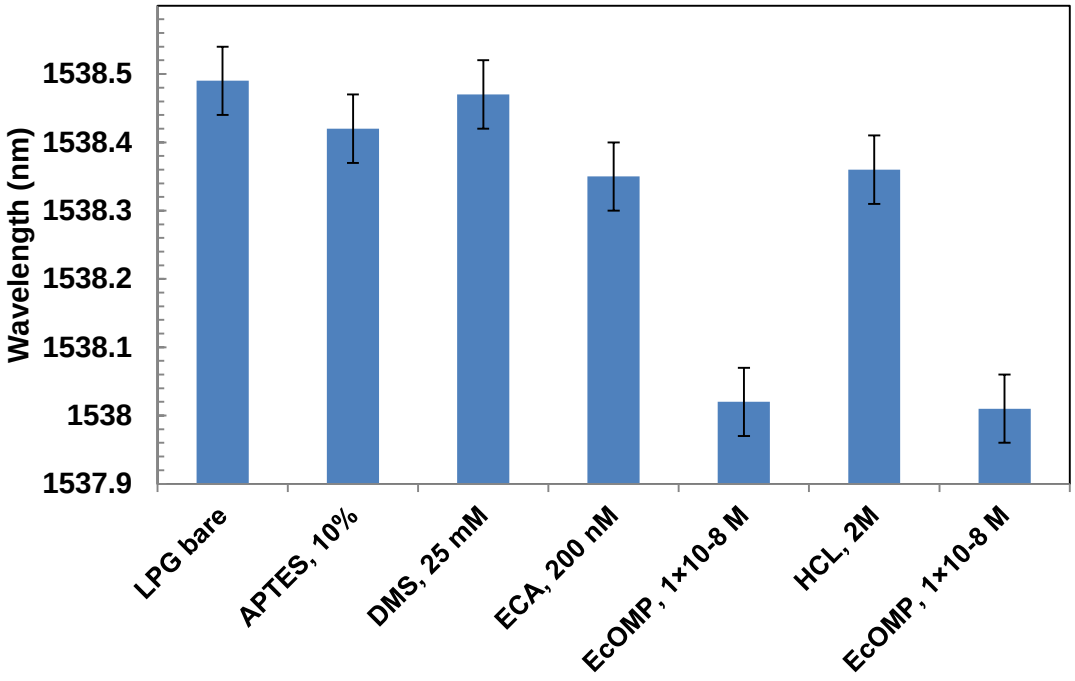

Figure 7.17 - Regeneration of sensing head 2; functionalization of bare long period grating follow by immobilization of *Escherichia coli* aptamer, binding with *Escherichia coli* outer membrane proteins washing with hydrochloric acid and rebinding of *Escherichia coli* outer membrane proteins.

7.3.5 Temperature dependence

As referred in section 7.3.2, LPGs are highly sensitive to temperature and all the measurements were made at room temperature. Considering that assays can take up to 8 consecutive hours and that the room temperature variation during one assay can vary 2.0±0.5 ºC, a FBG was introduced in series with the LPG inside the reaction chamber. The reflected peak of the FBG was recorded in real time for the temperature compensation during the assay.

The wavelength variation of the LPG depends on temperature and refractive index while wavelength variation of the FBG only depends on temperature (assuming strain applied to both sensors is constant), as equations 7.1 and 7.2 show, respectively.

$$\Delta\lambda_{LPG} = K_{T\,LPG}\Delta T + K_{n\,LPG}\Delta_n \tag{7.1}$$

$$\Delta\lambda_{FBG} = K_{T\,FBG}\Delta T\ , \tag{7.2}$$

where $K_{T,LPG}$ and $K_{T,FBG}$ are temperature sensitivity coefficients of the LPG and FBG respectively and $K_{n,LPG}$ is the refractive index sensitivity coefficient. All these coefficients are the slopes of the calibration curves previously obtained. Replacing equation 7.2, in order to ΔT, in equation 7.1 it gives,

$$\Delta\lambda_{LPG} = \frac{K_{T\,LPG}}{K_{T\,FBG}}\Delta\lambda_{FBG} + K_{n\,LPG}\Delta_n \quad (7.3)$$

Knowing the spectral position of the FBG peak, which is only temperature dependent, the $\Delta\lambda_{LPG}$ only depends on refractive index changes. It should be noted that Δn also is temperature dependent (dn/dT ~10^{-4} RIU/ºC). Although in a real application this effect must be taken into account, it is much smaller than the effect of temperature on the LPG itself. So in this first evaluation this effect was not considered.

Figure 7.18 represents a sensorgram of a sensing head during the affinity-assay between the ECA and EcOMP (1.0×10^{-10} M – 3.0×10^{-8} M) and the sensorgram of the sensing head with the correction of the temperature variation using equation 7.3.

As can be seen, In Figure 7.18, the FBG indicates that the temperature decreases at the first 2 stages and then slowly increases until the end of the assay. This is in disagreement with the temperature variation along the day and the assay, which increases during the morning and decreases during afternoon. Also, with the increase of temperature, the shift of the resonance is on the opposite direction than the shift of the resonance with the increase of effective refractive index. This way, the corrected signal should display a larger shift of the resonance as compared to the uncorrected signal. However, this is not the case of the present experiment. On the other hand, in periods where the temperature is apparently decreasing, the shift values of the corrected signal should be smaller than the uncorrected shift. In the calculation of the resonance total shift variation between the beginning and the end of the assay, it was verified that the corrected value was about twice as large of the uncorrected. Also, it was always larger than the temperature induced variation predicted by equation 7.3.

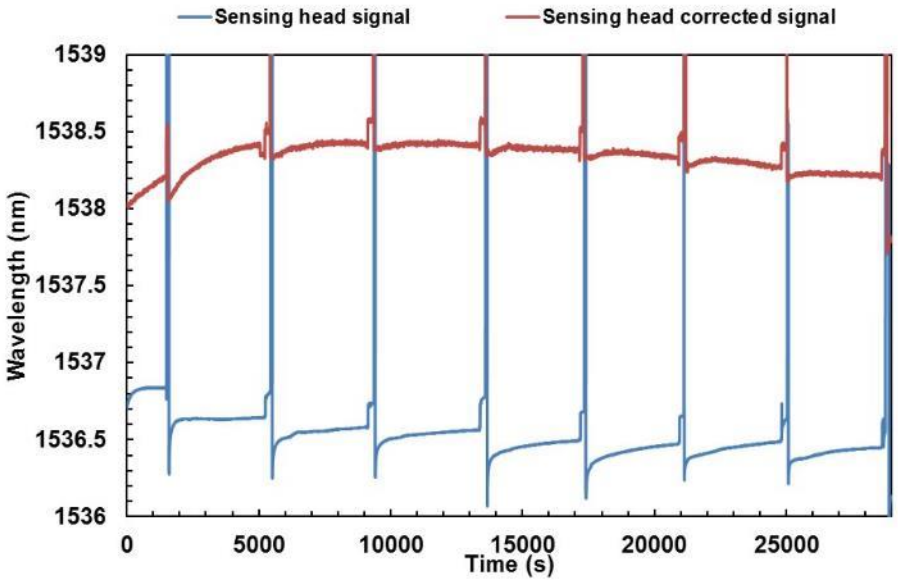

Figure 7.18 - Sensorgram of a sensing head, of the corrected output signal of the sensing head and of the fiber Bragg grating during the affinity-assay between *Escherichia coli* aptamers and *Escherichia coli* outer membrane proteins.

In a test performed with water at 40 ºC, at injection point, which was allowed to cool down to room temperature (Figure 7.19) it can be seen that, for the FBG, the wavelength values decreased during the cooling and remained constant after the room temperature was reached. But, concerning to the corrected signal of the sensing head, the wavelength values started to increase slowly after the room temperature was reached, indicating that there is an overcompensation of the real temperature effect.

This behaviour suggests that the effect of temperature is more complex than initially considered. Further studies should be performed in order to assess why this overcompensation is happening. Several aspects must be taken into consideration. First, the gratings are under mechanical tension and it is known that LPG are slightly sensitive to strain and FBG are highly sensitive to strain. In both of cases, with the increment of temperature or strain the resonance shifts to longer wavelengths. As referred in the section 7.3.2, in this experiment the fibre is fixed with fibre clamps and these are fixed to an aluminium slab. It is possible that the variations in the temperature also affected the aluminium slab, increasing the distance between the points of fixation and thereby increasing the tension applied. This would shift the resonance of the FBG (and also the LPG but with much lower sensitivity).

Thus, the resonance of the FBG is not just being subjected to temperature changes but also to strain changes that are caused by temperature. As long as the shifts are in the same direction, this can be a cause of the overcompensation. In this case the equation 7.3 is not valid for temperature compensation. One solution could be the use a FBG in parallel to the LPG, that is free and thus, not sensitive to strain. A more sophisticated alternative would be to use a second LPG functionalized with non-specific DNA that would serve both as a reference for temperature, strain, and bulk refractive index.

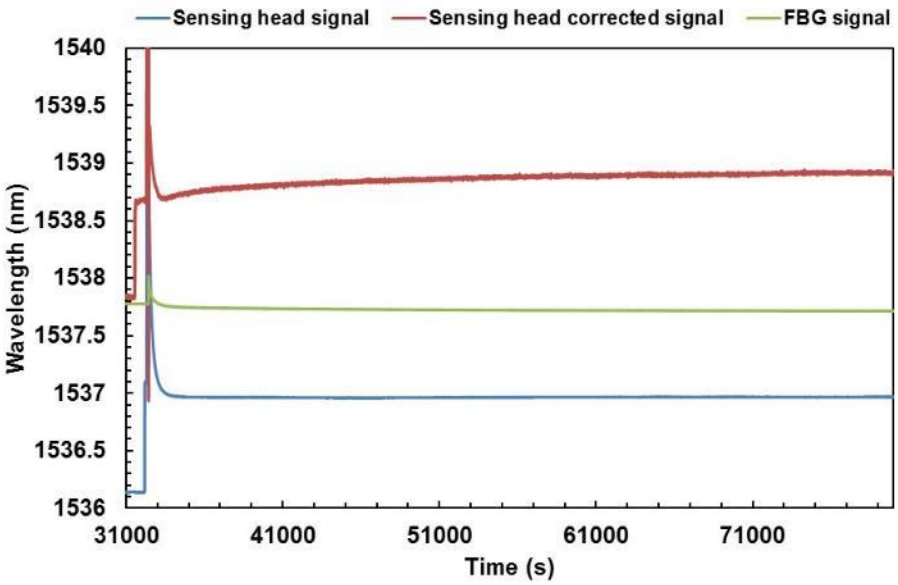

Figure 7.19 - Sensorgram of a sensing head, of the corrected signal of the sensing head and of the fibre Bragg grating during the cooling of 40 ºC double de-ionized water to room temperature.

7.3.6 Cross-reactivity to other molecules

To assess the non-specific binding of other molecules that could be present in water systems the different sensing heads were incubated with $1.0x10^{-9}$ M OMPs and with $1.0x10^{-9}$ M of MC-LR and with a mixture of both for 60 minutes in the affinity buffer. This MC-LR concentration is the recommended maximum level of MC-LR in waters established by (WHO, 1998). The shift of λ_R induced by the complex ECA-EcOMPs for both types of sensing heads was much higher than the shift obtained when incubating in MC-LR solution alone (Figure 7.20 and Figure 7.21).

In the case of the mixture EcOMPs-MC-LR, the shift of the λ_R presented a similar value to the complexes ECA-EcOMPs. These results showed that EcOMPs bound to the APT on the LPG with high selectivity, even in the presence of a potential interference such as MC-LR.

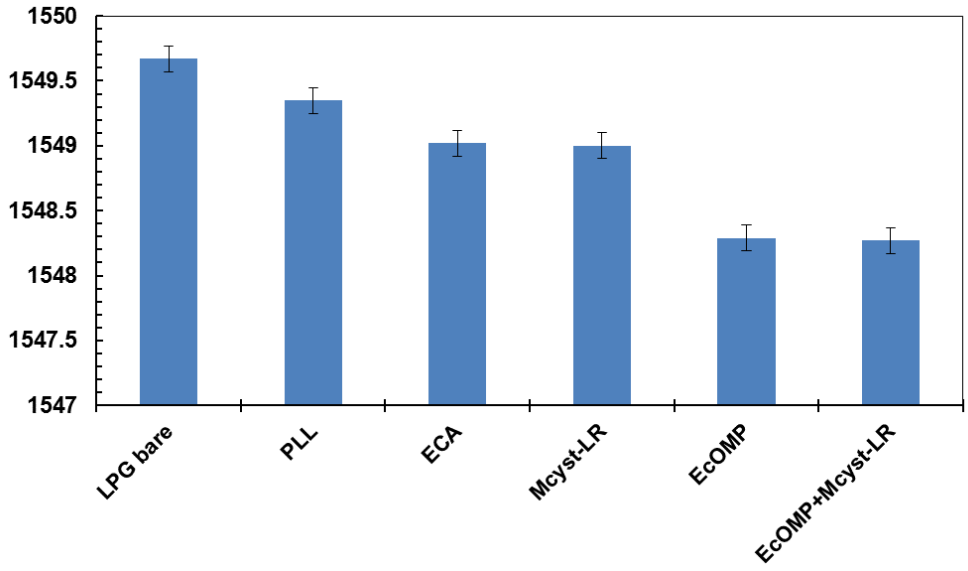

Figure 7.20 - Binding specificity of *Escherichia coli* aptamers to *Escherichia coli* outer membrane proteins. Wavelength shift of 6th order cladding mode resonance upon exposure to 1.0×10^{-9} M *Escherichia coli* outer membrane proteins, 1.0×10^{-9} M microcystin-LR, and the mixture of both for sensing head 1.

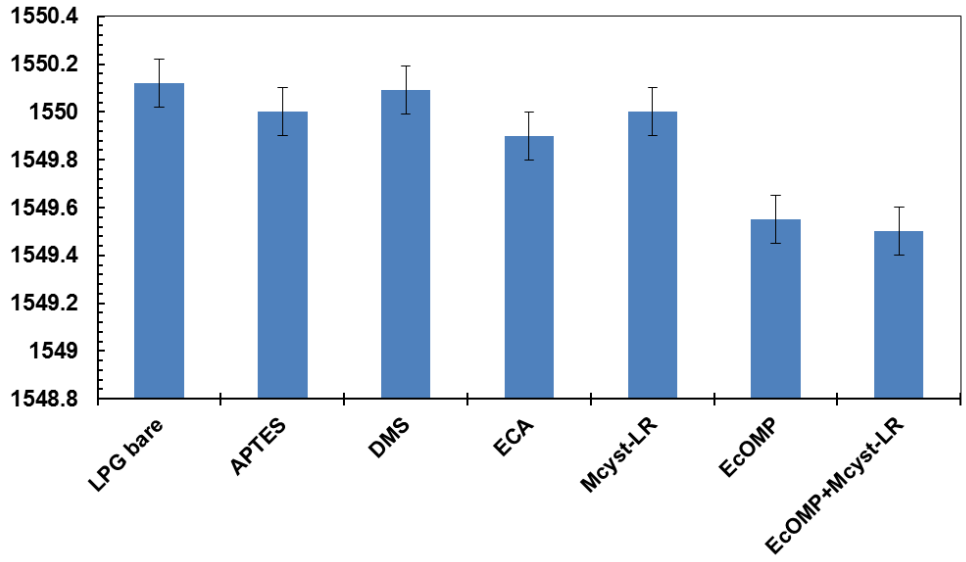

Figure 7.21 - Binding specificity of *Escherichia coli* aptamers to *Escherichia coli* outer membrane proteins. Wavelength shift of 6th order cladding mode resonance upon exposure to 1.0×10^{-9} M *Escherichia coli* outer membrane proteins, 1.0×10^{-9} M microcystin-LR, and the mixture of both for sensing head 2.

7.3.7 Detection of *Escherichia coli* outer membrane proteins in environmental water samples

In order to investigate the application of the present method to the analysis of environmental waters (pH 6.5), spiked waters were tested and the corresponding relative errors calculated. Environmental water samples were collected in a well and stored in amber glass bottles previously rinsed with double-deionized water. The pH and ionic strength of the water samples were adjusted by addition of affinity buffer (50:50), and they were stored at 4 °C until analysis. These assays were carried out with sensors calibrated within 1.0×10^{-10} M to 3.0×10^{-8} M of EcOMPs. The average recoveries of three spiked solutions for SH1 and SH2 were 123.39±11.26 % and 106.06±18.95 %, respectively. These sensors showed an error of about 23.39 % for SH1 and 6.06 % for SH2. Although SH2 seem promising devices for a successful analytical application, these biosensors require more studies and optimization in order to come to be used in real samples.

7.4 Conclusions

A label free biosensor using a LPG as a refractometric platform for the detection of EcOMPs based on the specific recognition between an APT capture probe and bacteria proteins was proposed. In general terms, two sensing heads were obtained by electrostatic interaction or covalent binding and both showed a concentration-dependence behavior. The detection limit found was of 1.0×10^{-10} M of EcOMPs. In terms of shift of the resonant loss SH1 presented a shift 3 times larger than SH2. The sensing heads were regenerated (under low pH conditions) and the deviation of the subsequent detection was less than 0.1 %. The sensors displayed high selectivity to MC-LR (a common toxin in environmental waters) and offered simplicity in designing and analysis as well as low limit of detection. The temperature control of the system still required further optimization due to the overcompensation of the signal correction. These analytical features, as well as its fabrication easiness and operational convenience, make it a promising method for the detection of *E. coli* in waters.

References

Baldini, F.; Brenci, M.; Chiavaioli, F., Giannetti, A.; Trono, C. 2012. Anal. Bioanal. Chem. 402, 109–116.

Baptista, D. 2009. Simulação do Comportamento Espectral de Redes de Período Longo em Fibra Óptica. Msc thesis, Centro de Ciências Exactas e da Engenharia, Universidade da Madeira, Portugal.

Beres, C.; de Nazaré, F.V.; de Souza, N.C.; Miguel, M.A.; Werneck, M.M. 2001. Biosens. Bioelectron. 30(1), 328-332.

Bhatia, V., Vengsarkar, A.M. 1996. Opt. Lett. 21, 692–694.

Bruno, J.G.; Carrillo, M.P.; Phillips, T.; Andrews, C.J. 2010. J. Fluoresc. 20, 1211–1223.

Caldas, P. 2011. Fiber optic sensing by evanescent field interaction. PhD thesis, Faculdade de Ciências da Universidade do Porto, Portugal, pp. 73-108.

Chryssis, A.N.; Saini, S.S.; Lee, S.M.; Yi, H.; Bentley, W.E.; Dagenais, M. 2005. IEEE J. Sel. Top. Quantum Electron. 11, 864-872.

Fan, X.; White, I.M.; Shopova, S.I.; Zhu, H.; Suter, J.D.; Sun, Y. 2008. Anal. Chim. Acta 620, 8–26.

Gouveia, C. 2008. Sensor em Fibra Óptica para Monitorização Ambiental. Msc thesis, Departamento de Matemáticas e Engenharias, Universidade da Madeira, Portugal.

Hermanson, G.T. 1996. Bioconjugate Techniques, 1st ed. Academic Press, The Netherlands.

Mattson, G.; Conklin, E.; Desai, S.; Nielander, G.; Savage, D.; Morgensen, S. 1993. Mol. Biol. Rep. 17, 167-183.

Patrick, H.J.; Kersey, A.D.; Bucholtz, F. 1998. J. Lightwave Technol. 16, 1606-1998.

Pereira, D.; Frazão, O.; Santos, J. 2004. Opt. Eng. 43(2), 299–304.

Pilla, P.; Malachovská, V.; Borriello, A.; Buosciolo, A.; Giordano, M.; Ambrosio, L.; Cutolo, A.; Cusano, A. 2011. Opt. Express 19(2), 512-526.

Pilla, P.; Trono, C.; Baldini, F.; Chiavaioli, F.; Giordano, M.; Cusano, A. 2012. Opt. Lett. 37, 4152-4154.

Rego, G.; Okhotnikov, O., Dianov, E.; Sulimov, V. 2001. J Lightwave Technol. 19(10), 1574-1579.

Shu, X.; Zhang, L.; Bennion, I. 2001. Opt. Lett. 26, 1755–1757.

Slavík, R.; Homola, J.; Brynda, E. 2002. Biosens. Bioelectron. 17, 591-595.

World Health Organization, Drinking-Water Quality Guidelines for Parameters of Concern in Agricultural Drainage Water—Annex 3, Technical Report, 1998, pp. 281–289.

Zibaii, M.I.; Kazemi, A.; Latifi, H.; Azar, M.K.; Hosseini, S.M.; Ghezelaiagh, M.H. 2010. J. Photochem. & Photobiol. B: Biology 101(3), 313–320.

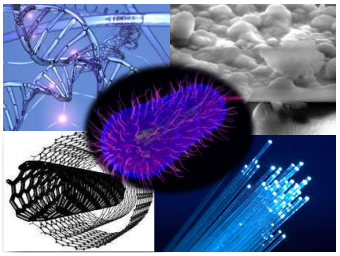

Chapter 8

Conclusions and Future work

8.1 Conclusions

The present work allowed the development of novel biosensors for the monitoring of bacterial contamination in water environments.

The use of sensors based on MIPs, both in sol-gel and polymeric matrices (using nanostructured carbon as support materials) originate sensing membranes with appropriate responses to the monitoring of MC-LR, particularly regarding to sensitivity and selectivity of action, being suitable for *in situ* control. The sensors fabricated bring some advantages such as relatively simple production and low cost, associated with good physical and chemical stability. The main disadvantage of MIPs materials is that large (stoichiometric) amounts of MC-LR are required to manufacture polymers. In our case this is of special interest because the analyte is very expensive.

The development of potentiometric ISEs is a very interesting field because it has a wide range of applications in species determination in waters. This technique is accurate, fast, economic and sensitive.

On the other hand, this technique presented some disadvantages such as the need for an ionic strength buffers and the necessity of having a reference electrode for the analysis. In addition the construction of carbon-paste electrodes can not be reproductible and are laborious to make. FFPI sensors are able to overcome these disadvantages.

Optical fibers have small size and weigth and do not request any type of reference control. These sensors also allow fast detection and quantification of the analyte of interest at the recommended level. Thus, it became evident that the combination of MIP with interferometry can be an advantageous alternative to the commonly used methods for the analysis of these compounds in real water samples.

The search for alternative affinity tools to overcome the handicaps of MIP led to development of a DNA-based aptamer for the monitoring of the well-know pathogenic bacterium *E. coli*. The developed DNA aptamer present an accurate and reliable molecular recognition of the EcOMP. Moreover, APTs are suitable for macromolecules detection as the case of EcOMPs. APT are more suitable for physiological applications unlike MIPs that work especially well in organic solvents instead of aqueous solutions. Concerning the analytical measurement systems, impedance measurements provide a complete description of an electrochemical reaction at the electrode/electrolyte interface. The use of this technique also allowed the study of the electrode surface functionalization, allowing the full study of the interactions between the diverse components of the SAM's. Besides the common advantages of the optical transducers over electrochemical, such as immunity towards electromagnetic interferences and the needless of using a reference cells, the integration of APTs in LPGs bring the advantage of high sensitivity, simple design and fabrication with low manufacturing costs. Like all other biosensors previously studied, this technique was also capable of detecting the analyte of interest to the desired level with the desired selectivity.

All the studied devices have introduced several technical innovations in the development of biosensors both in terms of the assembly of the recognition element and also in systems configuration. Both APT and MIP have shown to be tailor-made synthetic recognition elements provided with tuneable binding properties, well suited to biosensors applications. The used of FFPI sensors, by the monitoring of changes in the optical cavity, allows the studied of environmental factors such as concentration dependence with high accuracy and resolution. Electrochemical techniques are simple to handle and are able to provide analytical information in a real time.

EIS may be used for monitoring but is also consent the studied of many different processes that occur during electrochemical experiments, including adsorption of reactants and products as well as various reactions that either precede or follow the experiments, thereby changing the electrical characteristics of electrode/electrolyte interfaces.

The advantages presented by electrochemical and optical biosensors together with their sensitivity, selectivity and low cost, make them suitable for in situ and real-time environmental analysis, and an excellent complement to the expensive and time-consuming standard methods.

Considering all the proposal biosensors and the main characteristics that a biosensor should present for a successful application, a comparison was made regarding the detection of MC-LR and EcOMPs, see Table 8.1.

For the detection and quantification of MC-LR the analytical system based on Fabry-Perot optical interferometry using a sol-gel imprinted polymer and the potentiometric detection system using a surface imprinted polymer on the wall of carbon nanotubes presented the best analytical features. Both systems presented detection limits below the recommended value established by WHO for MC-LR, being the Fabry Perot system the one that presented the lowest value. About the response time of the sensors, the potentiometric system replies faster than the Fabry-Perot. Although this system requires less sample volume than the potentiometric system. In terms of cost of the system, the potentiometric systems is less expensive.

The biosensor that present the best analytical features for the detection and quatification of *E. coli* was the evanescent field system based on LPGs presenting the lower limit of detection, response time, and sample volume required for the analysis and also being the less expensive system as can be seen in Table 8.1.

Overall, the proposed biosensors shown to be a valuable tool, in fast screening and low cost monitoring of bacteria in waters.

Table 8.1 – Comparison between the developed biosensor proposals for the detection of Microcystin-LR and *Escherichia coli*.

Characteristics	BIOSENSORS				
	Proposal 1	**Proposal 2**	**Proposal 3**	**Proposal 1**	**Proposal 2**
Target	Microcystin-LR	Microcystin-LR	Microcystin-LR	*E. coli*	*E. coli*
Recog. Element	MIP sol-gel	MIP sol-gel	surface (CNTs) MIP	DNA aptamer	DNA aptamer
Transducer	Potenciometric	Fabry-Perot	Potenciometric	EIS	LPGs
Detection limit	0.73 µg L^{-1}	0.26 µg L^{-1}	0.69 µg L^{-1}	1×10^{-9} M	1.0×10^{-10} M
Linear range	0.77-1.67 µg L^{-1}	0.29-1.40 µg L^{-1}	0.77-1.32 µg L^{-1}	1×10^{-7} - 2 $\times10^{-6}$ M	1.0×10^{-10} -1.0×10^{-8} M
Selectivity	-	-	not differentiate other MCs	to Mcyst-LR	to Mcyst-LR
Regeneration	yes	yes	yes	yes	yes
Response time	2 minutes	2 minutes	20 s	90 minutes	60 minutes
Volume sample	3 mL	200 µL	500 µL	3 mL	1 mL
Cost	Low	High	Low	High	Medium

8.2 Future work

This research aimed the development of biosensors using new concepts in terms of the affinity tools and its integration in different and promising analytical systems giving indications of topics that require further investigation. In this PhD programme a large number of topics were investigated and therefore, some might require in fact a more detailed study. Some research topics that emerged within this work and require further investigation are the following:

- Optimization of sol-gel matrix, to extent the lifetime of sensor and to prevent more effectively the cracking of the membranes due to its consecutive use;
- Explore the possibility of made simultaneous measurements with different MI membranes and different APT sensing heads, both in electrochemical or optical measurements, thus eliminating possible interferences caused by the sample matrix;
- Test selectivity of all MC-LR MIPs sensors against other MCs and other cyanotoxins with different structure configurations as well as different water contaminants;
- Design new potenciometric devices to improve the attachment of membranes and to prevent water entry between the membrane and the solid support;
- In terms of APTs, try other assemblies approaches for the monolayers to avoid non-specific adsorption of proteins to electrodes surface;
- Optimization of the temperature control in LPG devices;
- Test multiparametric devices for all the analytical devices used allowing the measurement of multiplie analytes at once and the possibility of real-time monitoring of water contamination.

This page was intentionally left blank